

Modern Atomic and Optical Physics II

Lectures by M.D. Lukin
Notes taken and typed by L. Childress

Fall Semester 2005

Contents

Table of Contents	1
1 Preface: Quantum mechanics and atomic physics review	6
1.1 Introduction	6
1.2 Review of quantum mechanics	7
1.2.1 States	7
1.2.2 Superpositions - Interference	7
1.2.3 Observables	7
1.2.4 Uncertainty principle	8
1.2.5 Time evolution: Schrodinger's picture	8
1.2.6 Time evolution: Heisenberg picture	9
1.3 Basic Atomic Physics	9
1.3.1 Example: the hydrogen atom	9
1.3.2 Level degeneracies	10
1.3.3 Corrections to the hydrogen atom hamiltonian: lifting of the L degeneracy	11
1.3.4 Fine structure: lifting of the J degeneracy	11
1.3.5 Hyperfine interaction	13
1.3.6 Interaction with static external magnetic fields	14
1.3.7 Interaction with optical fields	15
2 Basic processes in AMO physics and quantum optics	19
2.1 Atomic Transitions	19
2.1.1 The Two-Level Atom	19
2.2 Bound to Continuum Transitions	29
2.3 Quantized electromagnetic fields	32
2.3.1 Quantization	32
2.3.2 Atomic interactions with the quantized field	35
2.3.3 Remarks about quantization	36
2.3.4 Wigner-Weisskopf theory of spontaneous emission	37

3	Mathematical methods for open systems	42
3.1	The density operator	43
3.2	System and environment	45
3.3	The dynamics of an open system	46
3.3.1	General formalism	47
3.3.2	Properties of the environment	48
3.3.3	Density operator method for a Markovian reservoir	50
3.4	The master equation	57
3.4.1	Remarks on the generalized master equation	57
3.4.2	Example: The two-level atom	59
3.4.3	Atomic response to a resonant field	60
4	Propagation of light in a resonant medium	63
4.1	The slowly-varying envelope approximation	64
4.2	Linear optical propagation	67
4.2.1	Absorption and refraction	68
4.2.2	Dispersion	69
4.2.3	Two level systems	69
4.2.4	Line-broadening mechanisms	71
4.3	Nonlinear atomic response	73
4.3.1	Saturation spectroscopy	77
5	Coherent interactions in multi-level systems	81
5.1	Raman transitions in the Λ level configuration	82
5.1.1	The Schrodinger equation approach	82
5.1.2	The density matrix approach	84
5.1.3	The stochastic wavefunction method	85
5.1.4	Large detuning Δ , weak Ω_1	87
5.1.5	Large Δ , arbitrary Ω_1 : Two-photon Rabi oscillations	89
5.1.6	Remarks	89
5.2	Resonant excitation: Electromagnetically induced transparency	91
5.2.1	The dark resonance	91
5.3	Parametric Processes	96
5.3.1	Example: the cascade system	96
5.3.2	Sum frequency generation	98
6	Stochastic Wavefunctions	105
6.1	Formalism	106
6.2	Example: Decay of a two-level atom	109

6.3	Non-Hermitian evolution: Summary	110
7	Adiabatic Processes	112
7.1	The adiabatic theorem for time-dependent Hamiltonians	112
7.1.1	The condition for adiabaticity	113
7.2	Adiabaticity for the two-level system	114
7.2.1	Rapid adiabatic passage	115
7.2.2	Adiabaticity condition for the two-level system	116
7.3	Adiabatic processes in multi-level systems	118
7.3.1	Stimulated Raman adiabatic passage (STIRAP)	119
7.3.2	Four-level systems	122
7.4	Analysis of STIRAP: The condition for adiabatic following	123
7.4.1	Remarks	128
8	Atomic motion in laser light	133
8.1	Incorporating center of mass motion into atom-light interactions	133
8.2	Semiclassical description	135
8.3	Doppler Cooling	140
8.4	Dissipation and quantum noise: the Heisenberg-Langevin approach	145
8.4.1	Brownian motion	145
8.4.2	The Heisenberg-Langevin approach	148
8.5	The Heisenberg-Langevin formalism applied to Doppler cooling	153
8.5.1	Momentum diffusion in laser cooling of a two-level atom	153
8.5.2	The Doppler cooling limit	155
8.5.3	Corrections for a dense sample	156
8.6	Sub-Doppler cooling	157
8.6.1	Experimental Observations	157
8.6.2	Sisyphus Cooling	158
8.6.3	Quantitative analysis of sub-Doppler cooling	160
8.6.4	The Sisyphus cooling limit	165
9	Quantum properties of light interacting with matter	168
9.1	Basic properties of quantum fields	168
9.1.1	Thermal states	169
9.1.2	Coherent states	170
9.2	Interactions between a single-mode radiation field and a two-level atom	176
9.2.1	The Jaynes-Cummings model	176
9.2.2	Initial vacuum field: vacuum Rabi oscillations	178

9.3	The effects of dissipation on quantum fields	183
9.3.1	Dynamics of a single mode field in a lossy cavity	183
9.3.2	Quantum mechanical treatment of the cavity mode	186
9.3.3	Cavity quantum electrodynamics	190
9.4	Quantum dynamics in non-linear mixing processes	199
9.4.1	Nonlinear amplification	200
9.4.2	Squeezed states	205
9.4.3	Effects of loss	206
10	Trapped ions: quantum state engineering	216
10.1	Ion traps	216
10.2	Model: An ion in a harmonic trap	218
10.2.1	The harmonic oscillator potential	219
10.2.2	Internal energy levels	220
10.2.3	Ion-laser interactions	220
10.2.4	Sideband cooling	225
10.3	Quantum state engineering	225
10.3.1	Preparation of an arbitrary motional quantum state	225
10.4	Ion trap quantum computation	227
10.4.1	Two ions in a linear trap	227
10.4.2	Quantum gates	229
11	Quantum dynamics of atomic matter waves	233
11.1	Introduction	233
11.1.1	Bose-Einstein statistics	234
11.1.2	BEC in an ideal gas	235
11.2	Experimental History	235
11.3	Experimental techniques used in Bose condensation of atoms	237
11.3.1	Atom-surface interactions	237
11.3.2	Trap depths	239
11.3.3	Initial Cooling	240
11.3.4	Optical and Magnetic traps	241
11.3.5	Evaporative cooling	242
11.3.6	The theory of evaporative cooling	245
11.3.7	Probing atomic ensembles	248
11.4	Atomic interactions	249
11.4.1	The van der Waals potential	250
11.4.2	Basic scattering theory	251
11.4.3	<i>S</i> -wave scattering	255
11.4.4	Particle statistics	259

11.4.5	Scattering off an atomic ensemble	259
11.4.6	Resonances	260
11.4.7	Quantum theory of an interacting Bose gas	265
11.5	Excitations in a Bose condensate	271
11.5.1	The Bogoliubov approximation	271
11.5.2	BEC with attractive interactions	275
11.5.3	Observation of BEC	276
11.6	First-order coherence of Bose condensates	276
11.6.1	Interference of two atomic clouds	277
11.6.2	Spontaneous symmetry breaking	278
11.7	Higher-order coherence of atomic matter waves	278
11.7.1	Toy model: cold, interacting atoms in a double-well potential	280
11.7.2	Optical lattice potentials	282
11.8	Cold atoms in an optical lattice	282
11.8.1	Atoms in a periodic potential	283
11.8.2	The physics of the Bose-Hubbard model	286

Chapter 1

Preface: Quantum mechanics and atomic physics review

1.1 Introduction

In this course, we will approach the field of atomic physics by presenting a unified picture of coherent evolution and environmental decoherence and dissipation. The course will develop around three themes: firstly, we will elucidate theoretical techniques for simultaneously treating both coherent and dissipative processes. We will also consider experimental methods for studying atomic systems, including, for example discussion of high resolution spectroscopy, laser trapping and cooling and preparation of quantum states of ions. Finally, we will incorporate examples which illustrate how these experimental and theoretical techniques find application in current research.

The basic philosophy of the course is to develop a theoretical understanding of "simple" systems first, that is systems where only a few states, a few particles, or a few quanta are relevant. This will lead us to explore some non-trivial quantum dynamics and study the possibility of controlling realistic quantum systems, including imperfections in "real world" experiments. Once these basic building blocks are mastered, we will consider more complex systems by combining elements we already understand at a basic physical level. To understand the dynamics of the systems we will study in this course, we will need to treat both dissipation and coherent quantum evolution on an equal footing.

1.2 Review of quantum mechanics

1.2.1 States

We briefly review basic quantum mechanics and some elementary results of atomic physics.

The most complete knowledge of the system is contained in the state vector $|\psi\rangle$, which is an element of a Hilbert space \mathcal{H} . We can expand the state vector $|\psi\rangle$ in any orthonormal basis $\{|n\rangle\}$ of the Hilbert space,

$$|\psi\rangle = \sum_n |n\rangle \langle n| \psi \rangle. \quad (1.1)$$

For convenience, we write $c_n = \langle n| \psi \rangle$ for the projection of the state $|\psi\rangle$ on the basis state $|n\rangle$, which gives us the expansion coefficients of the state $|\psi\rangle$ in the basis $\{|n\rangle\}$. The probability of finding the system in the state $|n\rangle$ is then $P_n = |c_n|^2$.

1.2.2 Superpositions - Interference

Quantum mechanics allows for superpositions of states, in particular, for two states

$$|\psi_1\rangle = \sum_n c_n^{(1)} |n\rangle \text{ and} \quad (1.2)$$

$$|\psi_2\rangle = \sum_n c_n^{(2)} |n\rangle, \quad (1.3)$$

their superposition $\frac{1}{\sqrt{2}}(|\psi_1\rangle + |\psi_2\rangle)$ has the unique property that the probability of being in state $|n\rangle$ is not in general given by the sum of probabilities. Instead it is given by the absolute value of the sum of *amplitudes*

$$P_n = \frac{1}{2} \left| c_n^{(1)} + c_n^{(2)} \right|^2 \neq \frac{1}{2} (P_n^{(1)} + P_n^{(2)}) \quad (1.4)$$

This inequality occurs as a result of the interference term between the two components of state vector, given in this case by $c_n^{(1)*} c_n^{(2)}$.

1.2.3 Observables

Observables in quantum mechanics are represented by Hermitian operators acting on states of the Hilbert space. An operator \hat{O} is Hermitian when for any two states $|\psi_{1,2}\rangle$ in the Hilbert space, we have

$$\langle \psi_1 | \hat{O} | \psi_2 \rangle = (\langle \psi_2 | \hat{O} | \psi_1 \rangle)^*. \quad (1.5)$$

The expectation value of the observable \hat{O} when the system is in state $|\psi\rangle$ is

$$\langle \hat{O} \rangle = \langle \psi | \hat{O} | \psi \rangle. \quad (1.6)$$

When the operator \hat{O} is diagonal in the basis $\{|n\rangle\}$, we have

$$\hat{O}|n\rangle = \mathcal{O}_n|n\rangle \quad (1.7)$$

$$\Rightarrow \langle \hat{O} \rangle = \sum_n \mathcal{O}_n |c_n|^2 = \sum_n \mathcal{O}_n p_n \quad (1.8)$$

where \mathcal{O}_n denotes the n^{th} eigenvalue of the operator \hat{O} . Note that if the system is in an eigenstate of \hat{O} , we always get the same result upon repeated measurements of the observable \hat{O} .

1.2.4 Uncertainty principle

In general operators do no commute, i.e.

$$[\hat{A}, \hat{B}] = i\hat{C} \quad (1.9)$$

so that for $\hat{C} \neq 0$, the operators \hat{A} and \hat{B} do not have the same eigenstates.

Heisenberg's uncertainty principle states that for any two operators \hat{A} and \hat{B} , we have

$$\Delta A \cdot \Delta B \geq \frac{1}{2} \langle [\hat{A}, \hat{B}] \rangle \quad (1.10)$$

where $\Delta A = \sqrt{\langle (\hat{A} - \langle \hat{A} \rangle)^2 \rangle}$.

1.2.5 Time evolution: Schrodinger's picture

In non-relativistic quantum mechanics, the dynamics of the system is described by Schrodinger's equation: in Schrodinger's picture the state vector describing the state of the system evolves in time, while the operators describing the observables corresponding to possible measurements on the system are stationary.

The state vector evolves in time according to

$$i\hbar \frac{d}{dt} |\psi\rangle = \hat{H} |\psi\rangle \quad (1.11)$$

where \hat{H} is the Hamiltonian of the system. The stationary solutions of Schrodinger's equation are given by $|E_n\rangle$ where $\hat{H}|E_n\rangle = E_n|E_n\rangle$. Any

state can be expanded in the basis of eigenstates of \hat{H} , and in that basis the time evolution of the state vector takes a particularly simple form, namely

$$|\psi(t)\rangle = \sum_n e^{-iE_n t/\hbar} c_n |E_n\rangle \quad (1.12)$$

corresponding to the initial state $|\psi(0)\rangle$ with expansion coefficients $c_n = \langle E_n | \psi(0) \rangle$. In the basis of its eigenstates, the Hamiltonian is diagonal $\hat{H} = \sum_n |E_n\rangle E_n \langle E_n|$. The time evolution equation can also be formally integrated to yield the time evolved state $|\psi(t)\rangle = \exp[-i\hat{H}t/\hbar]|\psi(0)\rangle = \hat{U}(t)|\psi(0)\rangle$, where $\hat{U}(t)$ is the time evolution operator.

1.2.6 Time evolution: Heisenberg picture

In Heisenberg's picture, the state vector describing the initial state of the system does not evolve in time, rather the observables describing possible measurements on the system at time t , depend explicitly on time and evolve according to Heisenberg's equation of motion

$$i\hbar \frac{d}{dt} \hat{O}(t) = [\hat{O}, \hat{H}] + i\hbar \frac{\partial \hat{O}}{\partial t}. \quad (1.13)$$

1.3 Basic Atomic Physics

The physical systems associated with atomic physics include neutral atoms, ions, and molecules as well as more modern “artificial atoms” such as quantum dots fabricated in semiconductor heterostructures. The structure of these systems determines their interaction with applied fields, whether they be electric, magnetic, oscillating, static, classical, or quantum. These interactions allow us to manipulate the system via applied fields, or, conversely, use matter to control the electromagnetic fields. Such techniques are at the heart of atomic physics, but to apply them we must understand the physical structure of the system under consideration.

1.3.1 Example: the hydrogen atom

One of the simplest systems to consider is hydrogen, which consists of one electron bound by the Coulomb force to a proton. The energy of the system is given by

$$\hat{H} = \frac{\hat{p}^2}{2m} - \frac{e^2}{\hat{r}}, \quad (1.14)$$

where \hat{p} represents the (operator-valued) electronic momentum and \hat{r} represents the distance between the electron and the proton.

The stationary solutions of Schrodinger's equation for this system are of two types. There is an infinite set of discrete bound states with energies $E_n = -\frac{R_\infty}{n^2}$ and a continuum set of unbound states with energies $E > 0$. The constant R_∞ is called Rydberg's constant; while its numerical value can be found in any textbook on quantum mechanics, it is a good exercise to know how to derive an expression for it from basic principles.

To estimate the binding energy R_∞ , we note that in the ground state Heisenberg's inequality is approximately obeyed as an equality. In particular, the uncertainty in momentum Δp and the uncertainty in position Δr obey $\Delta p \cdot \Delta r \sim \hbar$. Since the mean value of the momentum must be zero for a bound state, we can replace $\langle p^2 \rangle$ by $\Delta p^2 \sim (\hbar/\Delta r)^2$ in the Hamiltonian. Similarly, the average distance $\langle r \rangle$ should also be approximately Δr , yielding an average energy

$$E = \frac{\hbar^2}{2m\Delta r^2} - \frac{e^2}{\Delta r} \quad (1.15)$$

Minimizing the energy with respect to Δr , we find $\Delta r \sim \frac{\hbar^2}{me^2}$, so that the ground state energy is approximately given by

$$E_0 = -R_\infty \sim -\frac{me^4}{2\hbar^2}. \quad (1.16)$$

In fact, this turns out to be equal to the exact ground state energy for an infinitely heavy nucleus.

1.3.2 Level degeneracies

Although we have enumerated the energies of the bound states in hydrogen, we have not addressed whether or not these states are degenerate. In particular, suppose that there is an operator \hat{A} which commutes with the Hamiltonian \hat{H} , i.e. $[\hat{A}, \hat{H}] = 0$. We can then find a common set of eigenvectors $|E_n, A_l\rangle$ such that

$$\hat{A}|E_n, A_l\rangle = A_l|E_n, A_l\rangle \quad (1.17)$$

$$\hat{H}|E_n, A_l\rangle = E_n|E_n, A_l\rangle. \quad (1.18)$$

The energy E_n is the same for all states $|E_n, A_l\rangle$, and it does not depend on A_l . This level degeneracy is associated with the underlying symmetry which renders A invariant under Hamiltonian evolution. Consider the effect

of the transformation $\hat{S}(a) = e^{i\hat{A}a}$ on the eigenstates of \hat{H} . If $[\hat{A}, \hat{H}] = 0$, the energy levels are invariant under the transformation $\hat{S}(a)$. Thus we see that there is a relation between degeneracies and symmetries of the system, i.e. invariance under some set of unitary transformations.

For the hydrogen atom, the Hamiltonian Eq. (1.14) commutes with the total angular momentum \hat{L}^2 and the z-component of angular momentum \hat{L}_z , as well as with the electron spin angular momentum \hat{S}^2 and \hat{S}_z , and also with the nuclear spin angular momentum \hat{I}^2 and \hat{I}_z .

The energies depend only on the principal quantum number n , and all angular momentum states $l = 0, \dots, n-1$ with the same principal quantum number have n are allowed and have the same energy. Similarly, all states with eigenvalues of the z-component \hat{L}_z of angular momentum $l_z = -l, \dots, l$ and electron spin and nuclear spin sublevels have the same energy.

Degeneracies are removed, however, in the real hydrogen atom due to corrections to the Hamiltonian.

1.3.3 Corrections to the hydrogen atom hamiltonian: lifting of the L degeneracy

Deviations of the potential from $1/r$ result in a lifting of the degeneracy with respect to l . In multi-electron atoms, inner shell electrons tend to screen the nuclear charge, so that for fixed principal quantum number n , large l states of the valence electrons are less deeply bound than small l states (since electronic states further from the nucleus experience a greater screening effect). For example in alkali atoms such as Na, with shell structure $(1s)^2(2s)^2(2p)^6(3s)$, the Hamiltonian can be written as $\hat{H} = \frac{p^2}{2m} - \frac{e^2}{r} + V'(r)$, where $V'(r) \rightarrow 0$ as $r \rightarrow \infty$ but $V'(r) \neq 0$ as $r \rightarrow 0$. The energy is now a function of both the principal quantum number and the total angular momentum $E = E(n, l)$.

It is worth noting, however, that (for a given valence shell configuration) the effect of the inner electrons decreases as the principal quantum n number increases. Consequently large- n states have a reduced the energy splitting between different l states. Very large n states, known as “Rydberg states”, exhibit nearly hydrogen-like spectra.

1.3.4 Fine structure: lifting of the J degeneracy

Relativistic corrections result in the so-called fine structure splitting of the energy levels of the hydrogen atom. There are three contributions to the fine structure, and their net effect on an energy level depends only on its associ-

ated total electronic angular momentum $J = L + S$. Therefore, relativistic effects break the degeneracy of each principal level n such that different J values have different energies.

The first contribution to the fine structure is a relativistic correction to the kinetic energy. The second contribution is referred to as the spin-orbit term and physically represents the interaction between the intrinsic magnetic dipole of the electron (i.e., the electron's spin) and the internal magnetic field of the atom which is related to the orbital angular momentum of the electron. The final correction is referred to as the Darwin term, and is a relativistic correction to the potential energy. The Darwin term acts only at the origin and thus is only nonzero for $L = 0$ states.

To illustrate how such relativistic effects can result in the splitting of levels with different J , we examine the spin-orbit coupling below. For details on the kinetic energy and Darwin term, one can refer to any introductory quantum mechanics text.

The interaction energy of the spin-orbit effect is:

$$V_{SL} = A\hat{S} \cdot \hat{L}. \quad (1.19)$$

V_{SL} commutes with S^2, L^2, J^2 and J_z , where $\hat{J} = \hat{S} + \hat{L}$, so we now label atomic states by J^2 and J_z rather than by L_z and S_z (which do not commute with V_{SL} and are thus not good quantum numbers). As an example, consider sodium (Na). The ground state of Na has zero orbital angular momentum ($|\hat{L}| \equiv L = 0$), and therefore no fine structure since $J = S$ can only take on one value. For the first excited state ($L = 1$), $J = 1 + 1/2 = 3/2$ or $J = 1 - 1/2 = 1/2$. What is the energy splitting between the $J = 1/2$ and $J = 3/2$ states? Using the fact that

$$\hat{J} \cdot \hat{J} = J^2 = L^2 + S^2 + 2\hat{S} \cdot \hat{L} \quad (1.20)$$

$$\Rightarrow \hat{S} \cdot L = J^2 - L^2 - S^2, \quad (1.21)$$

we have

$$V_{SL} = A\hat{S} \cdot \hat{L} = (A/2)(J^2 - L^2 - S^2) \quad (1.22)$$

This implies that the energy splitting between the $J = 3/2$ and $J = 1/2$ state is given by

$$\Delta E_{3/2} - \Delta E_{1/2} = \frac{A}{2}[(9/4 - 1/4 - 1) - (1/4 - 1/4 - 1)] = \frac{A}{2} \cdot 2 = A. \quad (1.23)$$

Traditionally, the transition from the ${}^3S_{1/2}$ ground state of Na to the ${}^3P_{1/2}$ excited state is called the D1 line whereas the transition from the ${}^3S_{1/2}$ ground state of Na to the ${}^3P_{3/2}$ excited state is called the D2 line.

Remark concerning the wavefunctions of hydrogen-like atoms

The wavefunction of a hydrogen-like atom can be written as $\psi_{nlm}(\rho, \theta, \phi) = R_{nl}(\rho)Y_{lm}(\theta, \phi)$ where $R_{nl}(\rho)$ contains the radial dependence, and the angular dependence is contained in the spherical harmonics

$$Y_{lm}(\theta, \phi) = P_l^m(\cos \theta)e^{im\phi}, \quad (1.24)$$

where $P_l^m(\cos \theta)$ is the associated Legendre polynomial of degree l and order m . It is important to remember: (1) as $\rho \rightarrow 0$, $R_{nl} \sim \rho^l$, which vanishes unless $l = 0$, and (2) under the parity transformation ($\hat{r} \rightarrow -\hat{r}$, i.e., $\phi \rightarrow \phi + \pi$, $\theta \rightarrow \pi - \theta$), $Y_{lm}(\pi - \theta, \phi + \pi) = (-1)^l Y_{lm}(\theta, \phi)$. From this and the fact that the radial function $R_{nl}(\rho)$ is insensitive to the parity transformation, we see that the parity of the ψ_{nlm} wavefunctions is $(-1)^l$.

1.3.5 Hyperfine interaction

The interaction of the magnetic dipole of the valence electron with the nuclear spin \hat{I} is referred to as the hyperfine interaction. The magnetic field produced by a nucleus with magnetic moment \mathbf{m}_N is given by

$$\mathbf{B}(\mathbf{R}) = \frac{\mu_0}{4\pi} \left(\frac{3\mathbf{n}(\mathbf{n} \cdot \mathbf{m}_N) - \mathbf{m}_N}{R^3} + \frac{8\pi}{3}\mathbf{m}_N\delta(\mathbf{R}) \right), \quad (1.25)$$

where \mathbf{R} is the vector distance from the nucleus and \mathbf{n} is the unit vector in the direction of \mathbf{R} . The second term is a strong contact term which is non-zero only for $l = 0$ states, whereas the first term is a weaker long-range ($\sim 1/R^3$) term which is non-zero for all other l . The result is that the hyperfine interaction is generally strongest for S states with small r . The interaction energy may be approximated as

$$V_{HFS} = A_{HFS}\hat{I} \cdot \hat{J} \quad (1.26)$$

Taking into account both the fine and hyperfine interactions, the appropriate conserved quantum number is the total angular momentum \hat{F} given by

$$\hat{F} = \hat{I} + \hat{S} + \hat{L}. \quad (1.27)$$

Structure of the alkali ground state

As an example, consider the ground state of hydrogen for which $L = 0$, $I = 1/2$, and $S = 1/2$. Since $L = 0$, $F^2 = I^2 + S^2 + 2\hat{S} \cdot \hat{I}$, and $H_{HFS} = (A_{HFS}/2)(F^2 - I^2 - S^2)$. Allowed values of $F = 0, 1$ lead to hyperfine shifts

$H_{HFS}(F = 1, F = 0) = (A_{HFS}/4, -A_{HFS}/4)$. The hydrogen ground state thus has two levels split in energy by $A_{HFS}/2$, with $F = 0$ and 1. Similarly, one can calculate that the ground states of ^{23}Na and ^{87}Rb (for which $L = 0$, $I = 3/2$, and $S = 1/2$) consist of two levels $F = 1$ and $F = 2$ separated by $3A_{HFS}/2$.

1.3.6 Interaction with static external magnetic fields

In the presence of a static external magnetic field, the energy levels shift in a manner referred to as the Zeeman effect. In the $L = 0$ case, the shift can be calculated exactly, whereas for $L \neq 0$ states, approximations are required. The interaction of a magnetic moment μ in a constant magnetic field \mathbf{B} is given by

$$H = -\mu \cdot \mathbf{B}, \quad (1.28)$$

where this formula applies to both the electron and the nucleus. If we assume that the magnetic field is in the \hat{z} direction, we have

$$H = -\mu_z B_z. \quad (1.29)$$

Therefore, for a static field in the \hat{z} direction, the energy (Zeeman) shift of an $L = 0$ state is given by

$$H_Z = -\mu_e S_Z B_Z - \mu_N I_Z B_Z, \quad (1.30)$$

where $\mu_e = -g_J \mu_B$, $\mu_N = g_I \mu_B$, g_J is the Lande g-factor associated with electron spin for an electron bound to a nucleus, g_I is the Lande g-factor associated with nuclear spin, μ_B is the Bohr magneton, and $\mu_e \gg \mu_N$.

We can distinguish two cases: (1) strong field in which m_S , and m_I are good quantum numbers, and (2) weak field in which case F and m_F are good quantum numbers. In general, we can relate two bases ($|J, m_J\rangle$ and $|j_1, j_2\rangle$, where $\hat{J} = \hat{J}_1 + \hat{J}_2$ and $[J_1, J_2] = 0$) with so-called Clebsch-Gordan coefficients $C(J_1, J_2, J; j_1, j_2, m_J)$ defined by the following equation

$$|J, m_J\rangle = \sum_{j_1, j_2} \langle J_1 J_2 j_1 j_2 | J m_J \rangle |J_1 J_2 j_1 j_2\rangle \quad (1.31)$$

$$\equiv \sum_{j_1, j_2} C(J_1, J_2, J; j_1, j_2, m_J) |J_1 J_2 j_1 j_2\rangle. \quad (1.32)$$

The Clebsch-Gordan coefficients can be used to relate the $|F, m_F\rangle$ basis to the $|I, S; m_I, m_S\rangle$ basis (abbreviated as the $|m_I, m_S\rangle$). For example,

letting $J_1 = S = 1/2$, $J_2 = I = 1/2$, and $J = J_1 + J_2 = F$ (we're assuming $L = 0$), we have

$$|1, 1\rangle = |1/2, 1/2\rangle \quad (1.33)$$

$$|1, 0\rangle = \frac{1}{\sqrt{2}}(|1/2, -1/2\rangle + |-1/2, 1/2\rangle) \quad (1.34)$$

$$|0, 0\rangle = \frac{1}{\sqrt{2}}(|1/2, -1/2\rangle - |-1/2, 1/2\rangle) \quad (1.35)$$

$$|1, -1\rangle = |-1/2, -1/2\rangle \quad (1.36)$$

We will primarily be concerned with low values of the magnetic field, where the Zeeman effect can be treated as a perturbation to the fine and hyperfine interactions. In this case, we use the $|F, m_F\rangle$ basis as our zero-order wavefunctions, and the Zeeman shift ΔE_Z can be shown to be proportional to the applied magnetic field according to the relation

$$\Delta E_Z = g_F \mu_B m_F B_z, \quad (1.37)$$

where μ_B is the Bohr magneton, g_F is the Lande g-factor in the presence of nuclear spin given by

$$g_F = g_J \frac{F(F+1) + J(J+1) - I(I+1)}{2F(F+1)}. \quad (1.38)$$

Similarly, g_J is the Lande g-factor without considering nuclear spin given by

$$g_J = 1 + \frac{J(J+1) + S(S+1) - L(L+1)}{2J(J+1)}. \quad (1.39)$$

Note: A good reference on these topics is Vanier and Audoin, "Quantum Physics of Atomic Frequency Standards."

1.3.7 Interaction with optical fields

In this section we consider the interaction of isolated neutral atoms with optical fields. Such atoms alone have no net charge and no permanent electric dipole moment. In the presence of a static electric field \mathbf{E} , however, the atoms do develop an electric dipole moment \mathbf{d} which can then interact with the electric field with an interaction energy U given by

$$U = -\mathbf{d} \cdot \mathbf{E}. \quad (1.40)$$

In our semi-classical treatment of this interaction, we treat the atom quantum mechanically and therefore consider \hat{d} as an operator, but treat the electromagnetic field classically and so consider \mathbf{E} as a vector of complex numbers. This dipole interaction has two effects: (1) when the field is off-resonant with the atomic transitions, the dominant effect is that the atomic energy levels undergo an energy shift ($\sim E^2$), (2) when the field is near-resonant with an atomic transition, the dominant effect is transitions between atomic levels.

Selection rules

The Hamiltonian for the dipole interaction interaction, can be written in terms of a complete basis of states $\{|a\rangle\}$ for the atom:

$$\hat{H} = -\hat{\mathbf{d}} \cdot \mathbf{E} \quad (1.41)$$

$$= \sum_{aa'} |a'\rangle \langle a| \langle a'|\hat{\mathbf{d}}|a\rangle \cdot \mathbf{E}. \quad (1.42)$$

Note that the quantum state $|a\rangle$ is shorthand for a complete description in terms of quantum numbers n_a, l_a, s_a , etc. Transitions are possible between states $|a\rangle$ and $|b\rangle$ only when the matrix element

$$\mu_{a'a} \equiv \langle a'|\hat{\mathbf{d}}|a\rangle \neq 0. \quad (1.43)$$

There are many restrictions on the states $|a\rangle, |a'\rangle$ for which $\mu_{a'a} \neq 0$; these are referred to as selection rules. For example, parity arguments restrict the possible L values between which transitions are allowed. Since the scalar quantity

$$\mu_{a'a} \propto \int \psi_{L'} r \psi_L dV \quad (1.44)$$

is invariant under the parity operation $r \rightarrow -r, \psi_L \rightarrow (-1)^L \psi_L$, μ is nonzero only if $(-1)^{L+L'+1} = 1$, leading to the selection rule

$$\Delta L = \pm 1. \quad (1.45)$$

Of course, this argument really only implies that ΔL is odd. To prove that it must be specifically ± 1 , one can take the matrix element of both sides of equation

$$[L^2, [L^2, \hat{r}]] = 2\hbar^2(\hat{r}L^2 + L^2\hat{r}) \quad (1.46)$$

between $\langle \alpha', L', m'_L |$ and $|\alpha, L, m_L \rangle$. One can then derive the requirement $\Delta L = \pm 1$.

The spin argument is simple: since the dipole operator $\hat{d} = e\hat{r}$ contains no spin degrees of freedom, we must have

$$\Delta S = 0. \quad (1.47)$$

The rules for J and F are given by

$$\Delta J = \pm 1, 0 \quad (1.48)$$

$$\Delta F = \pm 1, 0. \quad (1.49)$$

The exception to these rules is that $J = 0 \rightarrow J' = 0$ transitions and $F = 0 \rightarrow F' = 0$ transitions are forbidden, because these transitions imply that $\Delta L = 0$ as a necessary consequence.

Before moving on to the selection rules for magnetic quantum numbers, it is useful to consider some practical notes concerning transitions strengths. In general,

$$\hat{\epsilon}_q \cdot \hat{r} = \sqrt{\frac{4\pi}{3}} \rho Y_{1q}(\theta, \phi), \quad (1.50)$$

where $\rho = |r|$. Therefore

$$\langle a | \hat{\epsilon}_q \cdot \hat{r} | a' \rangle = \text{radial part} \cdot \text{angular part}, \quad (1.51)$$

where the radial part $\bar{\rho}$ sets the size scale and the angular part can be evaluated using the Wigner-Eckart theorem (see e.g. Sakurai, "Modern Quantum Mechanics"). For example, the radial component for a hydrogen-like atom undergoing a $1S \rightarrow 2P$ transition is

$$\bar{\rho} = \int R_{nl}\rho R_{n'l+1} dV \quad (1.52)$$

$$\Rightarrow \bar{\rho} = 1.3 a_B (1S \rightarrow 2P) \quad (1.53)$$

where a_B is the Bohr radius.

In an atom with no fine or hyperfine structure, the angular part of the transition matrix element is given by

$$\langle L', m'_L | Y_{1q} | L, m_L \rangle = \langle Y_{L'm'_L} | Y_{1q} | Y_{L,m_L} \rangle, \quad (1.54)$$

which can be expressed in terms of what are referred to as 3j symbols (see Vanier or Metcalf), which themselves are related to the Clebsch-Gordan coefficients. To determine the angular part for atoms with fine and hyperfine structure requires the use of Clebsch-Gordan coefficients. For the fine structure, the energy levels are split by the spin-orbit interaction and so L is no

longer a good quantum number but is replaced by J . However, the optical field still couples only to the orbital angular momentum L of the states. To calculate the angular matrix element then one must use the Clebsch-Gordan coefficients to express the $|J, m_J\rangle$ states in terms of $|L, m_L\rangle |S, m_S\rangle$ states. One must use a similar procedure (twice) for atoms with hyperfine structure for which F is the good quantum number (see Metcalf and van der Straten, "Laser Cooling and Trapping", for example).

Now we move on to the selection rules for the magnetic quantum numbers which are related to the polarization of the incident electric field. We can write the electric field as a sum of linearly polarized components

$$\mathbf{E} = \hat{\epsilon}_x \mathbf{E}_x + \hat{\epsilon}_y \mathbf{E}_y + \hat{\epsilon}_z \mathbf{E}_z, \quad (1.55)$$

or as a sum of right and left circularly polarized and \hat{z} linearly polarized components

$$\mathbf{E} = \hat{\epsilon}_+ \mathbf{E}_+ + \hat{\epsilon}_- \mathbf{E}_- + \hat{\epsilon}_z \mathbf{E}_z, \quad (1.56)$$

where

$$\hat{\epsilon}_{\pm} = \mp(\hat{\epsilon}_x \pm i\hat{\epsilon}_y)/\sqrt{2}. \quad (1.57)$$

From Eq. 1.54 and knowledge of spherical harmonics, one immediately sees that the m_L selection rules are given by

$$\sigma^+ \text{ light } (\Rightarrow q = +1) \Rightarrow \Delta m_L = +1 \quad (1.58)$$

$$\sigma^- \text{ light } (\Rightarrow q = -1) \Rightarrow \Delta m_L = -1 \quad (1.59)$$

$$\hat{z} \text{ light } (\Rightarrow q = 0) \Rightarrow \Delta m_L = 0, \quad (1.60)$$

The same selection rules apply as well for m_J and m_F with an additional restriction. For $J = J'$, $\Delta m_J = 0$ with $m_J = 0$ is forbidden, because

$$\langle J, m_J | z | J, m_J \rangle \sim m_J \quad (1.61)$$

(where J here can stand for J or F). Note that Eq. 1.61 is true because all the functions in this matrix element are symmetric about z .

Chapter 2

Basic processes in AMO physics and quantum optics

2.1 Atomic Transitions

In the introductory lecture we have reviewed the somewhat complex level structure of hydrogenic atoms. Selection rules and energy conservation allow us to pick a subset of transitions, so that only a few energy levels are involved in the relevant dynamics. In this lecture we will focus in detail on the simplest atom-field system, namely that in which only two atomic energy levels interact with an applied laser field.

2.1.1 The Two-Level Atom

It is valid to approximate an atom as a two-level system when the external field is weak and nearly on resonance with a single atomic transition. In this case only the ground state and the near-resonant excited level will have appreciable probability of occupation. We will label these states $|1\rangle$ and $|2\rangle$ and designate their energy differency by $\hbar\omega$.

We consider the evolution of this system when illuminated by a nearly-monochromatic classical electromagnetic field

$$\mathbf{E}(\mathbf{r}, t) = \mathcal{E}(\mathbf{r}, t)e^{-i(\nu t - \mathbf{k} \cdot \mathbf{r})} + \mathcal{E}(\mathbf{r}, t)^* e^{i(\nu t - \mathbf{k} \cdot \mathbf{r})}, \quad (2.1)$$

where the slowly-varying envelope $\mathcal{E}(\mathbf{r}, t)$ varies on a timescale much slower than the optical frequency $\nu \approx \omega$ and a length scale much larger than the optical wavelength $2\pi/|\mathbf{k}|$. This electric field interacts with the atomic dipole, given by an operator $\hat{d} = e\hat{\mathbf{r}}$, which may be conveniently represented

in terms of the atomic eigenstates and the dipole matrix elements $\mu_{a,b} = \langle a|\hat{d}|b\rangle$:

$$\begin{aligned}\hat{d} &= \sum_{n,n'} |n'\rangle\langle n| \mu_{n',n} \\ &= |1\rangle\langle 2|\mu_{1,2} + |2\rangle\langle 1|\mu_{2,1}.\end{aligned}$$

In the latter expression, we have truncated the sum to include only the two relevant levels, and have assumed that the atomic eigenstates $|1\rangle$ and $|2\rangle$ do not have an associated permanent electric dipole, i.e. $\langle 1|\hat{d}|1\rangle = \langle 2|\hat{d}|2\rangle = 0$. This is the case for an isolated atomic system which retains its rotational symmetry.

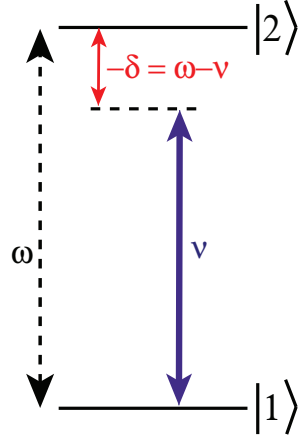


Figure 2.1: The structure of the two-level system. The applied classical field has angular frequency ν , while the atomic levels are separated by energy $\hbar\omega$.

The dynamics of the system are governed by the full Hamiltonian for the two level atom and classical field:

$$\hat{H} = \hbar\omega|2\rangle\langle 2| - (|1\rangle\langle 2|\mu_{1,2} + |2\rangle\langle 1|\mu_{2,1}) \cdot (\mathcal{E}e^{-i\nu t} + \mathcal{E}^*e^{i\nu t}). \quad (2.2)$$

To obtain the time dependent atomic state, we express the wavefunction in the basis of the eigenstates of the free Hamiltonian

$$|\psi\rangle = c_1(t)|1\rangle + c_2(t)|2\rangle. \quad (2.3)$$

Note that the atomic eigenstates are time independent, so the full time dependence of $|\psi\rangle$ is encapsulated by the probability amplitudes $c_1(t), c_2(t)$.

From the Schrödinger equation

$$i\hbar \frac{d}{dt} |\psi\rangle = \hat{H} |\psi\rangle, \quad (2.4)$$

we obtain coupled differential equations for the probability amplitudes:

$$\begin{aligned} \langle 2 | i\hbar \frac{d}{dt} |\psi\rangle &= \langle 2 | \hat{H} |\psi\rangle \Rightarrow i\hbar \dot{c}_2(t) = \hbar\omega c_2(t) - (\mathcal{E} e^{-i\nu t} + \mathcal{E}^* e^{i\nu t}) \mu_{21} c_1(t) \\ \langle 1 | i\hbar \frac{d}{dt} |\psi\rangle &= \langle 1 | \hat{H} |\psi\rangle \Rightarrow i\hbar \dot{c}_1(t) = -(\mathcal{E} e^{-i\nu t} + \mathcal{E}^* e^{i\nu t}) \mu_{12} c_2(t). \end{aligned}$$

These probability amplitudes $c_1(t)$ and $c_2(t)$ have a time dependent relative phase which evolves quickly in time. By transforming to an appropriate rotating frame, we can eliminate the explicitly time dependent terms in the equations of motion. In particular, we will rewrite the above equations by defining a slowly varying amplitude $\tilde{c}_2(t)$,

$$c_2(t) = \tilde{c}_2(t) e^{-i\nu t}, \quad (2.5)$$

so that

$$i\hbar \dot{\tilde{c}}_2(t) = -\hbar\delta \tilde{c}_2(t) - (\mathcal{E} + \mathcal{E}^* e^{2i\nu t}) \mu c_1(t) \quad (2.6)$$

$$i\hbar \dot{c}_1(t) = -(\mathcal{E} e^{-2i\nu t} + \mathcal{E}^*) \mu^* \tilde{c}_2(t), \quad (2.7)$$

where $\mu = \mu_{21}$ and $\delta = \nu - \omega$. These equations can be solved numerically, but are quite difficult to treat analytically. Nevertheless, these equations can be further simplified when we are interested in dynamics on timescales long compared to the optical frequency ν . This is nearly always true for optical fields, where $\nu \sim \text{THz}$; in other situations one must be more careful.

The dynamics we are concerned with occur at frequencies which scale with the Rabi frequency,

$$\Omega = \mathcal{E}\mu/\hbar, \quad (2.8)$$

and it makes intuitive sense that the terms which oscillate rapidly would on average have little effect on the atomic populations. More quantitatively, we may make the rotating wave approximation (RWA) and neglect the terms $\propto e^{\pm 2i\nu t}$ under the following circumstances:

- (a) The field is near resonance : $\delta \ll \nu, \omega$
- (b) The field is weak : $\Omega \ll \nu$

As we remarked earlier these requirements can be often satisfied for realistic experimental conditions but certainly not always.

In the RWA, the slowly varying amplitudes then satisfy

$$\dot{\tilde{c}}_2(t) = i\delta\tilde{c}_2(t) + i\Omega c_1(t) \quad (2.10)$$

$$\dot{c}_1(t) = i\Omega^*\tilde{c}_2(t). \quad (2.11)$$

These equations may be solved exactly, but much insight can be obtained by examining the solutions for two special cases: fields precisely on resonance, and fields far detuned from resonance.

Resonant field $\delta = 0$

The equations of motion take an especially simple form for $\delta = 0$:

$$\ddot{c}_1(t) = -|\Omega|^2 c_1(t), \quad \ddot{\tilde{c}}_2(t) = -|\Omega|^2 \tilde{c}_2(t), \quad (2.12)$$

so the amplitudes evolve as sines and cosines. For an atom initially in the $|1\rangle$ state, the population oscillates between the two levels at frequency Ω , with

$$c_1(t) = \cos |\Omega|t \quad (2.13)$$

$$\tilde{c}_2(t) = i\frac{\Omega}{|\Omega|} \sin |\Omega|t. \quad (2.14)$$

Physically, the absolute values of the amplitudes correspond to the populations of the two levels $p_{1,2} = |c_{1,2}|^2$, which oscillate out of phase. These “Rabi oscillations” correspond to the periodic absorption and stimulated emission of radiation.

Not all quantities of interest vary as slowly as the atomic populations. For example, the instantaneous polarization of the atom may be obtained from the expectation of the dipole moment operator,

$$\langle \hat{d} \rangle = c_1(t)^* c_2(t) \mu^* + c_1(t) c_2(t)^* \mu. \quad (2.15)$$

The polarization varies both on the fast timescale ν at which $c_2(t)$ evolves, and the slower timescale Ω on which the populations evolve. Note also that there is a phase shift between Ω and $\langle \hat{d} \rangle$; this will become important when we study the propagation of light in an atomic medium.

The system also has a simple solution even when the applied field amplitude $|\Omega(t)|$ varies with time. In this case, the amplitudes depend on the total area under the applied field. This can be seen by renormalizing the time $d\tau = |\Omega(t)|dt$ or $\tau = \int |\Omega| dt$:

$$\frac{d}{dt} \tilde{c}_2(t) = i\Omega c_1(t) \rightarrow \frac{d}{d\tau} \tilde{c}_2(\tau) = i(\Omega/|\Omega|) c_1(\tau) \quad (2.16)$$

$$\frac{d}{dt} c_1(t) = i\Omega^* \tilde{c}_2(t) \rightarrow \frac{d}{d\tau} c_1(\tau) = i(\Omega^*/|\Omega|) \tilde{c}_2(\tau). \quad (2.17)$$

Provided that the pulse is not chirped (so that $\Omega/|\Omega|$ is constant) these equations can be easily solved to find

$$c_1(t) = \cos\left(\int |\Omega| dt\right) \quad (2.18)$$

$$\tilde{c}_2(t) = i\frac{\Omega}{|\Omega|} \sin\left(\int |\Omega| dt\right). \quad (2.19)$$

Far-detuned field $\nu \gg \delta \gg \Omega$: adiabatic elimination

The equations of motion may be solved exactly for arbitrary detuning (provided that the RWA is still valid, $\nu \gg \delta$). Nevertheless, it is useful to develop approximation techniques which will prove indispensable as we consider more and more complex systems. Here we will introduce a technique known as “adiabatic elimination”.

Our physical intuition tells us that a field very far from resonance will hardly ever cause transitions to the excited state, i.e. $|c_1(t)| \approx 1, |c_2(t)| \ll 1$. To lowest order, we might consider setting $c_1(t) = 1$, so that

$$\dot{\tilde{c}}_2 = i\delta\tilde{c}_2 + i\Omega \Rightarrow \tilde{c}_2(t) = \int_0^t i\Omega e^{i\delta(t-t')} dt' \quad (2.20)$$

$$= -\frac{\Omega}{\delta} \left(1 - e^{i\delta t}\right). \quad (2.21)$$

We will see that this is not the best approximation we can make in this situation, but it does give us a sense of the structure of $c_2(t)$. In particular, one term is constant while the other oscillates very rapidly with the (large) detuning δ . Over timescales $t > 1/\delta$ the effect of the rapidly oscillating term should average to zero, so to understand the relevant, slowly evolving dynamics we need only consider the constant term.

The above exercise motivates the concept of adiabatic elimination, in which we disregard the time-varying portion of the amplitude $c_2(t)$ to find the relevant slowly-varying dynamics. More precisely, we are trying to solve the equation $\dot{\tilde{c}}_2 = i\delta\tilde{c}_2 + i\Omega c_1$ for \tilde{c}_2 in terms of c_1 . Since $i\delta\tilde{c}_2$ is very large, the time-varying part of \tilde{c}_2 will be dominated by fast oscillations which average to zero, and we can set $\dot{\tilde{c}}_2 \approx 0$. This yields a solution \tilde{c}_2 which adiabatically follows the amplitude c_1 according to $\tilde{c}_2 = -(\Omega/\delta)c_1$. After substituting the expression for c_2 into Eq. (2.10), we find $\dot{c}_1 = -i(|\Omega|^2/\delta)c_1$,¹ so

$$c_1(t) \approx c_1(0)e^{-i|\Omega|^2 t/\delta}. \quad (2.22)$$

¹The corrections to this adiabatic following can be obtained by substituting this solution into (2.10), resulting in $\tilde{c}_2 = -(\Omega/\delta)c_1 + (i/\delta)d/dt((\Omega/\delta)c_1) + \dots$. This procedure is sometimes called an adiabatic expansion.

The lower state amplitude evolves as if the state energy were shifted by $|\Omega|^2/\delta$, an effect known as the AC Stark shift or the “light shift”. [Note that because we assumed $c_2(t) \approx 0$, we cannot obtain the upper population energy shift from this calculation; to do so requires a similar calculation starting from initial conditions $c_2(0) = 1, c_1(0) = 0$.]

The far off resonant field induces a correction to the energy (and the eigenstates) which scales as $|\Omega|^2/\delta^2$. Consequently our perturbative treatment can only be valid when $\Omega \ll \delta$. This observation offers insight into the second requirement for the validity of the RWA, because the neglected terms act like applied fields detuned $\pm 2\nu$ from the atomic transition frequency. Inclusion of these terms would lead to corrections scaling as $|\Omega|^2/(2\nu)^2$, so to ignore them we require $|\Omega| \ll \nu$.

Dressed States

An elegant interpretation of the quantum dynamics just described is possible in the basis of the so-called “dressed” atomic states. Such states are important especially in the situations involving the interaction of light with complex systems, where simple solutions are no longer available.

The equations of motion for the slowly varying amplitudes (2.10,2.11) can be viewed as resulting from the effective Hamiltonian

$$\tilde{H} = -\hbar\delta|\tilde{2}\rangle\langle\tilde{2}| - \hbar(\Omega|\tilde{2}\rangle\langle 1| + \Omega^*|1\rangle\langle\tilde{2}|), \quad (2.23)$$

which has no explicit time dependence. This corresponds to the original Hamiltonian after making the RWA, written in the rotating frame. This Hamiltonian can be easily diagonalized. The eigenvectors $|\pm\rangle$ are mixtures of the bare atomic states $|1, 2\rangle$, and are known as dressed states; the corresponding eigenenergies are

$$\epsilon_{\pm} = \hbar \left(-\frac{\delta}{2} \mp \sqrt{\left(\frac{\delta}{2}\right)^2 + |\Omega|^2} \right). \quad (2.24)$$

In a resonant field $\delta = 0$, the dressed states are symmetric and antisymmetric combinations of the bare atomic states, $|\pm\rangle = (|\tilde{1}\rangle \pm |\tilde{2}\rangle)/\sqrt{2}$, where $|\tilde{1}\rangle = (|\Omega|/\Omega)|1\rangle$. Their energy separation is twice the Rabi frequency, $2|\Omega|$. The quantum dynamics on resonance can be easily understood in terms of dressed state picture. Specifically, the state $|1\rangle$ is a symmetric superposition of the split states $|\pm\rangle$. As the system evolves in time, the phases of $|\pm\rangle$ rotate in opposing directions, and after a time $t = \pi/2\Omega$, the system is in

the antisymmetric superposition of states $|\pm\rangle$ which corresponds exactly to the bare state $|\tilde{2}\rangle$.

A far off resonant field $\delta \gg \Omega$ leads to dressed states which bear a strong resemblance to the original atomic states, having only a small admixture of the other state. The energies and eigenstates

$$\epsilon_- = \frac{|\Omega|^2}{\delta} \quad |-\rangle = |1\rangle - \frac{\Omega}{\delta} |\tilde{2}\rangle \quad (2.25)$$

$$\epsilon_+ = -\delta - \frac{|\Omega|^2}{\delta} \quad |+\rangle = |\tilde{2}\rangle + \frac{\Omega^*}{\delta} |1\rangle \quad (2.26)$$

are also close to the bare energies and eigenstates.

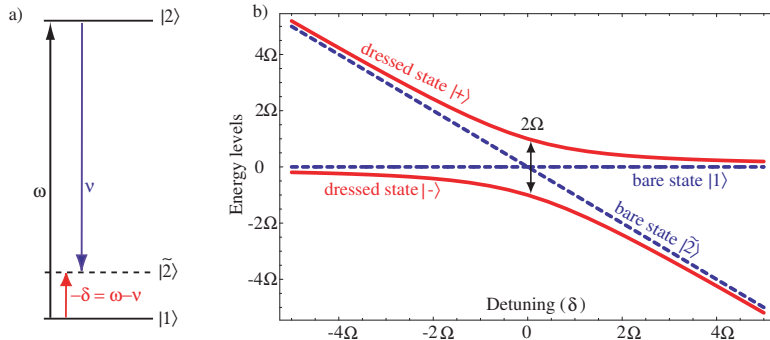


Figure 2.2: (a) Pictorial representation of moving to the rotating frame. In the absence of an applied field, the two atomic levels are split by atomic transition frequency ω . Upon application of a classical field with frequency v , we move to a frame rotating at frequency v , in which the state $|\tilde{2}\rangle$ has energy $-\delta = \omega - v$. In the rotating wave approximation, these states $|1\rangle$ and $|\tilde{2}\rangle$ are coupled by a static mixing term Ω . (b) The dressed state energy levels (red) are shown as a function of detuning. For reference, the bare state energy levels (dashed, blue) are also shown. The bare states are the eigenstates of the system when no applied field is present ($\Omega = 0$).

The Bloch sphere picture

We have thus far represented our two-level atom in terms of two complex numbers, c_1 and c_2 , satisfying $|c_1|^2 + |c_2|^2 = 1$. Alternately, the state of the two-level system can be represented as a vector on the unit sphere (see Figure 2.3). A vector pointing in the positive \hat{z} direction is identified with the state $|2\rangle$, while a vector pointing in the negative \hat{z} direction

represents the state $|1\rangle$. Vectors in the $\hat{x} - \hat{y}$ plane are superposition states $(|1\rangle + e^{i\phi}|2\rangle)/\sqrt{2}$. In the Bloch sphere picture, the rotating frame has a particularly nice interpretation: we view the vector from a reference frame which is rotating around the \hat{z} axis at the optical frequency ν .

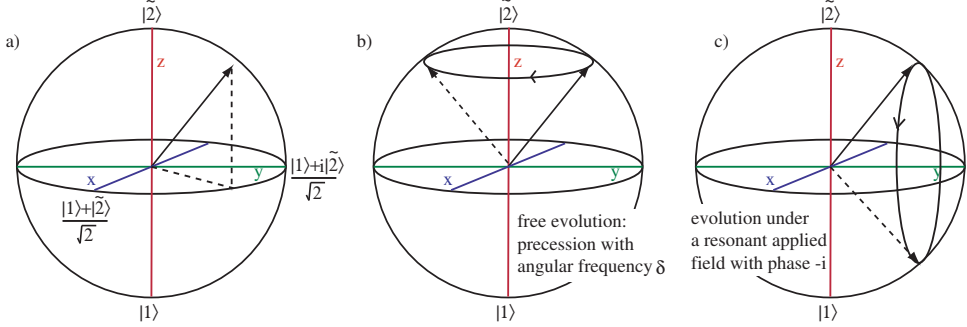


Figure 2.3: (a) An arbitrary state of a two-level system can be represented as a vector on the unit sphere. Here we are working in the rotating frame. (b) When no external fields are applied, the system precesses at the energy difference (in the rotating frame) between the two states. c) In the presence of a resonant applied field, the state precesses around an axis in the x - y plane whose azimuthal angle is determined by the phase of the applied field.

Interpreting this vector as a magnetic dipole, the dynamics of the system can be seen as resulting from precession around effective magnetic fields. In particular, suppose that $\Omega = 0$. In the bare frame, the vector precesses around the \hat{z} axis at frequency ω . Identifying a “spin” $\{c_1, c_2\}$ with associated spin operators

$$\hat{S}_z = |2\rangle\langle 2| - |1\rangle\langle 1| \quad (2.27)$$

$$\hat{S}_x = |1\rangle\langle 2| + |2\rangle\langle 1| \quad (2.28)$$

$$\hat{S}_y = -i|2\rangle\langle 1| + i|1\rangle\langle 2|, \quad (2.29)$$

we can rewrite the Hamiltonian as an effective magnetic field:

$$\hat{H} = \hbar\omega|2\rangle\langle 2| \rightarrow \frac{\hbar\omega}{2} \left(1 + \hat{S}_z \right). \quad (2.30)$$

Moving to the rotating frame,

$$\hat{H} = -\hbar\delta|\tilde{2}\rangle\langle\tilde{2}| \rightarrow -\frac{\hbar\delta}{2} \left(\hat{S}_z + 1 \right). \quad (2.31)$$

We can also understand an applied field Ω as an effective magnetic field. In particular, the effective Hamiltonian of Eq. (2.23) becomes

$$\hat{H} = -\frac{\hbar\delta}{2} (\hat{S}_z + 1) - \hbar(\text{Re } \Omega) \hat{\tilde{S}}_x - \hbar(\text{Im } \Omega^*) \hat{\tilde{S}}_y, \quad (2.32)$$

where $\hat{\tilde{S}}_{x,y}$ is the \hat{x}, \hat{y} component of the spin in the rotating frame. The constant term of Eq. (2.32) can be ignored since it contributes only an overall phase to the system. Working then in the Heisenberg picture, it is a useful exercise to show that the Hamiltonian of Eq. (2.32) leads to the equations of motion

$$\frac{d}{dt} \tilde{\mathbf{S}} = \boldsymbol{\Omega}(t) \times \tilde{\mathbf{S}}, \quad (2.33)$$

where the vector $\tilde{\mathbf{S}} = \{\tilde{S}_x, \tilde{S}_y, \tilde{S}_z\}$ and $\boldsymbol{\Omega}(t) = \{-2 \text{Re } \Omega(t), -2 \text{Im } \Omega^*(t), -\delta\}$. Eq. (2.33) resembles the equation of motion of a magnetic dipole in a magnetic field, and leads to a nice visualization of the dynamics of a two-level system, as illustrated in Fig. 2.3. This Bloch picture remains convenient even when processes like spontaneous emission and dephasing are included in the two-level dynamics.

Generalization to Multistate Systems

The techniques for treating the two level atom are also applicable to multi-state systems where each atomic transition has at most one slowly varying field near resonance. To illustrate how to extend the two-level calculation to multiple levels, we consider an atom with a single ground state $|1\rangle$ and many excited states $|k\rangle$. Each excited state is coupled to $|1\rangle$ by a field with amplitude \mathcal{E}_k and frequency ν_k , while the dipole matrix element for the k^{th} transition is $\hat{d}_{k,1} = \mu_k |k\rangle \langle 1| + \mu_k^* |1\rangle \langle k|$. The interaction between the dipole and field will have four terms, which we truncate to two by applying the RWA to obtain the Hamiltonian

$$\hat{H}_{RWA} = \sum_k \hbar\omega_k |k\rangle \langle k| - \hbar \sum_k (\Omega_k e^{-i\nu_k t} |k\rangle \langle 1| + \Omega_k^* e^{i\nu_k t} |1\rangle \langle k|) \quad (2.34)$$

where ω_k is the energy of the k^{th} transition and $\Omega_k = \mathcal{E}_k \mu_k / \hbar$.

Although each excited state has a different fast phase evolution, we may nonetheless remove the explicit time dependence from the Hamiltonian by making a unitary transformation represented by the operator

$$\hat{U} = e^{-i \sum_k \nu_k t |k\rangle \langle k|}. \quad (2.35)$$

The state vector $|\psi\rangle$ is expressed in a new basis defined by $\hat{U}|\tilde{\psi}\rangle = |\psi\rangle$. Because $\hat{U}(t)$ depends on time, it will introduce new terms in the Hamiltonian when we move to this new basis. Replacing $|\psi\rangle$ by $\hat{U}|\tilde{\psi}\rangle$ in the Schrödinger equation and expanding the time derivative yields

$$i\hbar \frac{d}{dt} (\hat{U}|\tilde{\psi}\rangle) = i\hbar \left(\hat{U} \frac{d}{dt} |\tilde{\psi}\rangle + \left(\frac{dU}{dt} \right) |\tilde{\psi}\rangle \right) = \hat{H}\hat{U}|\tilde{\psi}\rangle. \quad (2.36)$$

This expression may be written in the familiar form

$$i\hbar \frac{d}{dt} |\tilde{\psi}\rangle = \tilde{H}|\tilde{\psi}\rangle \quad (2.37)$$

by defining the Hamiltonian in the rotating frame,

$$\tilde{H} = \hat{U}^{-1} \hat{H} \hat{U} - i\hbar \hat{U}^{-1} \frac{dU}{dt}. \quad (2.38)$$

For the system under consideration, the second term is just $\sum_k \hbar \nu_k |\tilde{k}\rangle \langle \tilde{k}|$, so the new Hamiltonian may be easily found:

$$\tilde{H} = \sum_k \hbar(\omega_k - \nu_k) |\tilde{k}\rangle \langle \tilde{k}| - \hbar \sum_k \left(\Omega_k |\tilde{k}\rangle \langle \tilde{1}| + \Omega_k^* |\tilde{1}\rangle \langle \tilde{k}| \right). \quad (2.39)$$

By applying RWA and moving to the frame where each atomic state rotates at the associated optical frequency, we have found a basis where the Hamiltonian is time independent. The same approach will work for multilevel systems with many ground states and many excited states, so long as no atomic transition is linked by more than one applied field. In subsequent calculations, we will usually work in the rotating frame, so for notational convenience the tilde may be dropped.

These techniques break down when two fields are near resonance with a single transition. If we transform to the frame rotating with the frequency of the first field, the Hamiltonian will retain a time dependence associated with the second field. For example, suppose the two level system considered earlier now experiences two applied fields with Rabi frequencies Ω_a and Ω_b and optical frequencies ν_a and ν_b . The equations of motion (in the RWA and rotating frame) now include a term which oscillates with the beatnote frequency $\Delta = \nu_a - \nu_b$:

$$i\hbar \dot{\tilde{c}}_2(t) = -\hbar \delta \tilde{c}_2(t) - \hbar (\Omega_a + \Omega_b e^{i\Delta t}) c_1(t) \quad (2.40)$$

$$i\hbar \dot{c}_1(t) = -\hbar (\Omega_a^* + \Omega_b^* e^{-i\Delta t}) \tilde{c}_2(t). \quad (2.41)$$

To solve these equations requires expanding the probability amplitudes in a Fourier series $c_i = \sum_n c_i^{(n)} e^{in\Delta t}$, also known as the “Floquet basis”. The different Fourier components are all coupled to each other, so the probability amplitudes evolve with the beatnote and all of its higher harmonics. This simple example illustrates a mechanism underlying nonlinear optics.

2.2 Bound to Continuum Transitions

The complete basis of states for atomic systems includes not only the discrete bound energy states but also a continuum of higher energy unbound states. Photons with frequency at or above the photo-ionization threshold can induce transitions to this continuum, while even sub-threshold interactions can be influenced by energetically proximal unbound states. Examples of bound to continuum transitions include photoionization of atoms and photodissociation of ultracold molecules. It is important to understand the contribution of the continuum states to atom-field dynamics because their effects are qualitatively different from the Rabi oscillations characteristic of discrete states.

Mathematically, a continuum of states can be difficult to treat, so we discretize the unbound states by considering an atom in a box of volume L^3 . As the size of the box approaches infinity, the discrete energy levels approach the continuum. Here we consider only a single bound state and a generic continuum of unbound states, denoting the ground state by $|1\rangle$ and the excited states by $|k\rangle$, each with energy $\hbar\omega_k$. An applied field of frequency ν couples each bound state $|k\rangle$ to the bound state $|1\rangle$ with Rabi frequency Ω_k . The Hamiltonian (in the RWA and rotating frame) is thus

$$\hat{H} = \sum_k \hbar(\omega_k - \hbar\nu) |k\rangle\langle k| - \hbar \sum_k (\Omega_k |k\rangle\langle 1| + \Omega_k^* |1\rangle\langle k|). \quad (2.42)$$

We will investigate the dynamics using a trial wavefunction, similar to how we approached the two-level atom. Expanding the wavefunction in terms of the ground state and continuum states,

$$|\psi\rangle = c_1|1\rangle + \sum_k c_k|k\rangle \quad (2.43)$$

and substituting into the Schroedinger equation, we obtain the now familiar equations of motion

$$\dot{c}_1 = i \sum_k \Omega_k^* c_k \quad (2.44)$$

$$\dot{c}_k = i\delta_k c_k + i\Omega_k c_1 \quad (2.45)$$

where $\delta_k = \nu - \omega_k$.

These equations are formidable, and cannot be solved for an arbitrary set of states $|k\rangle$. We will proceed by formally integrating the second equation, then making a series of approximations which are valid for a densely spaced continuum of states spread over a large range of energies. For an atomic system which starts out in the ground state, $c_1 = 1$ and $c_k = 0$, formal integration of the second equation gives

$$c_k(t) = i\Omega_k \int_0^t c_1(t') e^{-i\delta_k(t'-t)} dt'. \quad (2.46)$$

Substitution into the first equation yields a nonlocal integral equation involving only the ground state amplitude,

$$\dot{c}_1(t) = - \sum_k |\Omega_k|^2 \int_0^t c_1(t') e^{-i\delta_k(t'-t)} dt'. \quad (2.47)$$

Since the detunings δ_k are summed over, the exponential will only be appreciably different from zero when $t = t'$. To lowest order (assuming that the probability amplitude $c_1(t)$ is slowly varying), we may set $c_1(t') = c_1(t)$ and pull it out of the integral. The remaining integral may then be evaluated by adding an infinitesimal imaginary part to δ_k ,

$$\lim_{\epsilon \rightarrow 0} \int_0^t e^{-i(\delta_k - i\epsilon)(t'-t)} dt' = \lim_{\epsilon \rightarrow 0} \frac{i(1 - e^{(i\delta_k - \epsilon)t})}{\delta_k + i\epsilon} \quad (2.48)$$

and taking the long time limit, so the second term in the numerator vanishes. Using an identity from complex analysis, the integral becomes

$$\lim_{\epsilon \rightarrow 0} \frac{i}{\delta_k + i\epsilon} = \pi\delta(\delta_k) + i\mathcal{P}\frac{1}{\delta_k}, \quad (2.49)$$

where \mathcal{P} indicates that the principal value should be taken when integrating over δ_k .²

The resulting equation of motion for the ground state probability amplitude includes a population decay at rate γ , and an energy shift Δ_{Stark} :

$$\dot{c}_1 = -c_1 \underbrace{\left(\pi \sum_k |\Omega_k|^2 \delta(\nu - \omega_k) - i \sum_k |\Omega_k|^2 \mathcal{P} \frac{1}{\nu - \omega_k} \right)}_{\gamma/2} \underbrace{- i \sum_k |\Omega_k|^2 \mathcal{P} \frac{1}{\nu - \omega_k}}_{\Delta_{Stark}}. \quad (2.50)$$

²For example, $\mathcal{P} \int_{-|a|}^{|b|} \frac{1}{x} dx = \lim_{\epsilon \rightarrow 0} \left(\int_{-|a|}^{-\epsilon} \frac{1}{x} dx + \int_{\epsilon}^{|b|} \frac{1}{x} dx \right)$

The amplitude for the ground state evolves simply as $c_1(t) = c_1(0)e^{-\gamma t/2+i\Delta_{Stark}t}$, so the population decays as $p_1(t) = p_1(0)e^{-\gamma t}$.

Note that the expression for γ ,

$$\gamma = 2\pi \sum_k |\Omega_k|^2 \delta(\nu - \omega_k), \quad (2.51)$$

is precisely the population decay rate one would obtain using Fermi's Golden Rule. Despite this apparent similarity, the relationship between the two derivations is rather subtle, since Fermi's Golden Rule arises from first order perturbation theory whereas our procedure explicitly involves a long time limit. The resolution to this lies in the fact that setting $t = t'$ in Eq. (2.47) implies that the continuum states have an effect on the ground state which is local in time, so the unbound states have no "memory" of earlier configurations. In particular, the decay rate for all times must be constant, so the value at early times (as calculated by e.g. Fermi's Golden Rule) sets the decay rate for the system. Furthermore, the perturbative approach is valid in the sense that the probability to excite any one of the continuum states is very small, although the ground state population of course changes dramatically.

The energy shift,

$$\Delta_{Stark} = \sum_k |\Omega_k|^2 \mathcal{P} \frac{1}{\nu - \omega_k} \quad (2.52)$$

is due to the AC Stark effect associated with continuum states. The relative importance of the decay and the energy shift depends on the precise system under consideration. For applied field frequencies below the photoionization threshold, the decay vanishes $\gamma = 0$, but the continuum states will still have an effect through the AC Stark shift. Photon frequencies above threshold lead to decay; moreover, the sign of the AC Stark effect changes with the sign of the detuning, so the contributions from above and below $\delta_k = 0$ will in large part cancel each other. Thus we expect that the energy shift is most important for sub-threshold illumination whereas the decay terms dominate above threshold.

For practical problems Δ_{Stark} is a very sensitive function of the precise nature of the continuum states, and in many cases it is not explicitly included in the analysis of the system. In some important practical cases, such as the interaction of an atom with the vacuum field considered below, it is a constant (e.g. Lamb shift) that simply leads to an appropriate renormalization of the atomic energy levels.

Disregarding the energy shift (or incorporating it into a renormalized atomic frequency), the excited state amplitudes c_k are given by

$$c_k(t) = i\Omega_k \int_0^t e^{-\gamma t'/2} e^{-i\delta_k(t'-t)} dt' \quad (2.53)$$

$$= i \frac{\Omega_k}{\gamma/2 + i\delta_k} (1 - e^{-(\gamma/2+i\delta_k)t}) e^{i\delta_k t}. \quad (2.54)$$

In the large time limit, the c_k approach the value $i\Omega_k e^{i\delta_k t}/(\gamma/2+i\delta_k)$. Physically, the system has been excited into a superposition of continuum states $\sum_k c_k |k\rangle$ which form an outgoing wavepacket propagating away from the atom. This seemingly irreversible behavior is qualitatively different from the Rabi oscillations studied previously, illustrating a mechanism by which an electron may leave the atom, converted to a freely propagating wavepacket. It is important to note, however, that the formalism presented above does not preclude reversing the dynamics. In fact, we should be able to time-reverse the dynamics, since our analysis thus far involves only wavefunctions undergoing unitary evolution. For example, starting with an initial wavepacket one could calculate the probability of capture into an atomic bound state. Such calculations are not possible with perturbation theory, and illustrate the flexibility of this approach (see e.g. homework problem 5).

2.3 Quantized electromagnetic fields

Thus far we have considered atomic absorption and emission processes stimulated by the presence of a classical field. However, practical experience tells us that real atoms will decay from an excited state even in the absence of any applied field. Such spontaneous emission processes result from the atom interaction with the vacuum modes of the field; to describe them requires a quantum mechanical treatment of the electromagnetic field.

2.3.1 Quantization

We will use a quantization procedure (following e.g. Meystre and Sargent “Elements of Quantum Optics”) which starts with Maxwell’s equations for a free field, i.e. in the absence of any sources. For a free field, Maxwell’s equations can be converted to wave equations for the electric and magnetic fields. Since the wave equation describes classical evolution of a harmonic oscillator, we will quantize the electric field in a manner precisely analogous

to the quantization of the harmonic oscillator. In particular, the electric field satisfies the wave equation

$$\nabla^2 \mathbf{E} = \frac{1}{c^2} \frac{\partial^2 \mathbf{E}}{\partial t^2}, \quad (2.55)$$

and the associated magnetic field can be found using

$$\nabla \times \mathbf{B} = \frac{1}{c^2} \frac{\partial \mathbf{E}}{\partial t}. \quad (2.56)$$

Note that these formulae and those that follow are written in S.I. units.

Our approach considers a field contained in a large cavity of length L and volume V with periodic boundary conditions. The eigenmodes of such a system are running waves $\propto e^{i\mathbf{k}\cdot\mathbf{r}}$, with allowed wavevectors

$$k_{\alpha,j} L_\alpha = 2\pi j_\alpha \text{ where } \alpha = \{x, y, z\} \text{ and } j_\alpha = \{\dots, -2, -1, 1, 2, \dots\}. \quad (2.57)$$

Each \mathbf{k} -vector can have two possible modes corresponding to the two polarizations orthogonal to \mathbf{k} . For notational convenience, we will assume that \mathbf{k}_j has an index j which includes both the mode number and the polarization of the wave. Note that it is possible to expand in terms of any complete set of mode functions. For example, a large cavity with vanishing electric field at the boundary would support sinusoidal modes; for examining laser beam propagation, Hermite-Gaussian modes may be more appropriate.

An arbitrary excitation may be expanded in terms of these spatial modes. In the case of the running wave modes, an \hat{x} -polarized field propagating along the \hat{z} axis may be written

$$E_x(z, t) = \sum_j \underbrace{\sqrt{\frac{\nu_i^2}{\epsilon_0 V}}}_{A_j} q_j(t) e^{ik_j z}, \quad (2.58)$$

where the time dependence is contained in $q_j(t)$, and A_j is chosen such that q_j will correspond to the position coordinate of a harmonic oscillator. The associated magnetic field is

$$B_y = \frac{1}{c^2} \sum_j \frac{\dot{q}_j(t)}{k_j} A_j e^{ik_j z}. \quad (2.59)$$

If we had instead chosen to expand in terms of standing waves, the electric and magnetic fields corresponding to an \hat{x} -polarized field with $\mathbf{k} \parallel \hat{\mathbf{z}}$ could be

written

$$E_x(z, t) = \sum_j \underbrace{\sqrt{\frac{2\nu_j^2}{\epsilon_0 V}}}_{\mathcal{A}_j} q_j \sin k_j z \quad (2.60)$$

$$B_y(z, t) = \frac{1}{c^2} \sum_j \frac{\dot{q}_j}{k_j} \mathcal{A}_j \cos k_j z. \quad (2.61)$$

Note that a slightly different proportionality factor $\mathcal{A}_j \neq A_j$ arises from the normalization of the mode functions.

The quantum mechanical Hamiltonian corresponds to the classical energy within the cavity,

$$H = \frac{1}{2} \int dV \left(\epsilon_0 E^2 + \frac{1}{\mu_0} B^2 \right) \quad (2.62)$$

$$= \sum_j \frac{\nu_j^2 q_j^2}{2} + \frac{\dot{q}_j^2}{2}. \quad (2.63)$$

There are no cross product terms $q_j \dot{q}_j$ because we expanded in the appropriate eigenbasis; our normalization choice for A_j yields a Hamiltonian analogous to that for a set of harmonic oscillators with position q_j , frequency ν_j and unit mass. Consequently the quantization procedure is identical to the familiar harmonic oscillator quantization, where we identify q_j and \dot{q}_j with non-commuting operators:

$$q_j \rightarrow \hat{q}_j \quad \dot{q}_j \rightarrow \hat{p}_j \quad (2.64)$$

$$[\hat{q}_j, \hat{p}_{j'}] = i\hbar\delta_{j,j'}. \quad (2.65)$$

We may also define creation and annihilation operators for excitations of each mode and polarization j ,

$$\hat{a}_j = \frac{1}{\sqrt{2\hbar\nu_j}} (\nu_j \hat{q}_j + i\hat{p}_j) \quad \hat{q}_j = \sqrt{\frac{\hbar}{2\nu_j}} (\hat{a}_j + \hat{a}_j^\dagger) \quad (2.66)$$

$$\hat{a}_j^\dagger = \frac{1}{\sqrt{2\hbar\nu_j}} (\nu_j \hat{q}_j - i\hat{p}_j) \quad \hat{p}_j = -i\sqrt{\frac{\hbar\nu_j}{2}} (\hat{a}_j - \hat{a}_j^\dagger). \quad (2.67)$$

The Hamiltonian may thereby be written in a much simpler form

$$\hat{H} = \frac{1}{2} \sum_j (\nu_j^2 \hat{q}_j^2 + \hat{p}_j^2) \quad (2.68)$$

$$= \sum_j \hbar\nu_j \left(\hat{a}_j^\dagger \hat{a}_j + \frac{1}{2} \right). \quad (2.69)$$

In subsequent calculations, we will need to express other operators in terms of the creation and annihilation operators. For example, an electric field with polarization vector ϵ_α may be expanded in terms of running-wave excitations³ as

$$\hat{E}_\alpha = \epsilon_\alpha \sum_j \underbrace{A_j \sqrt{\frac{\hbar}{\nu_j}}}_{\bar{\mathcal{E}}_j} \frac{(\hat{a}_j e^{i\mathbf{k}_j \cdot \mathbf{r}} + \hat{a}_j^\dagger e^{-i\mathbf{k}_j \cdot \mathbf{r}})}{\sqrt{2}}. \quad (2.70)$$

An important quantity has emerged from these calculations: $\bar{\mathcal{E}}_j$ is the electric field associated with a single photon of frequency ν_j .

$$\bar{\mathcal{E}}_j = \sqrt{\frac{\hbar\nu_j}{\epsilon_0 V}} \quad (2.71)$$

is a figure of merit for any phenomena relying on atomic interactions with a vacuum field – for example, cavity quantum electrodynamics. In fact, $\bar{\mathcal{E}}_j$ may be estimated by equating the quantum mechanical energy of a photon $\hbar\nu_j$ with its classical energy $(1/2) \int dV (\epsilon_0 E^2 + B^2 / \mu_0) \approx \epsilon_0 E^2 V$. It is also convenient to divide the electric field into the positive and negative frequency components,

$$\hat{E}_\alpha = \hat{\mathcal{E}}_\alpha + \hat{\mathcal{E}}_\alpha^\dagger \quad (2.72)$$

$$\hat{\mathcal{E}}_\alpha = \epsilon_\alpha \sum_j \sqrt{\frac{\hbar\nu_j}{2\epsilon_0 V}} \hat{a}_j e^{i\mathbf{k}_j \cdot \mathbf{r}}. \quad (2.73)$$

2.3.2 Atomic interactions with the quantized field

The interaction between an atom and a quantized field appears much the same as the semiclassical interaction. Starting with the dipole Hamiltonian for a two-level atom, we replace E by the corresponding operator, obtaining

$$\hat{V}_{af} = -\hat{E} \cdot \hat{d} \quad (2.74)$$

$$= -\sum_\alpha (\hat{\mathcal{E}}_\alpha + \hat{\mathcal{E}}_\alpha^\dagger) \cdot (\mu_\alpha |2\rangle\langle 1| + \mu_\alpha^* |1\rangle\langle 2|). \quad (2.75)$$

³This treatment glosses over some subtlety associated with having complex-valued amplitudes for running waves – these complications also appear in the standing wave treatment if you allow for cosine-like as well as sine-like modes. Careful accounting for the real and imaginary parts of the amplitudes (or the sine and cosine amplitudes) yields the given form, where you will note that \hat{a}_j and \hat{a}_j^\dagger multiply waves traveling in opposite directions.

As in the semiclassical analysis, the Hamiltonian contains four terms, which now have a clearer physical picture:

- $\hat{a}^\dagger|1\rangle\langle 2| \Rightarrow$ Atom decays from $|2\rangle$ to $|1\rangle$ and emits a photon
- $\hat{a}|2\rangle\langle 1| \Rightarrow$ Atom is excited from $|1\rangle$ to $|2\rangle$ and absorbs a photon
- $\hat{a}^\dagger|2\rangle\langle 1| \Rightarrow$ Atom is excited from $|1\rangle$ to $|2\rangle$ and emits a photon
- $\hat{a}|1\rangle\langle 2| \Rightarrow$ Atom decays from $|2\rangle$ to $|1\rangle$ and absorbs a photon

For photons near resonance with the atomic transition, the first two processes conserve energy; the second two processes do not conserve energy, and intuition suggests that they may be neglected. In fact, there is a direct correspondence between the RWA and energy conservation: the second two processes are precisely those fast-rotating terms we disregarded previously. To clarify the analogy, consider the time dependence of the annihilation operator $\dot{\hat{a}}_j = -i[\hat{a}_j, \hat{H}]/\hbar = -i\nu_j \hat{a}_j \Rightarrow \hat{a}(t) = \hat{a}(0)e^{-i\nu_j t}$. The annihilation operator is thus identified with the term $\Omega e^{-i\nu t}$ in the semiclassical analysis. Consequently, we may neglect the second two terms under the same conditions for which the RWA is valid.

The explicit form for the energy conserving terms of the atom-field Hamiltonian is

$$\hat{V}_{af} = - \sum_{j,\alpha} \hbar g_{j,\alpha} |2\rangle\langle 1| \hat{a}_{j,\alpha} + \hbar g_{j,\alpha}^* |1\rangle\langle 2| \hat{a}_{j,\alpha}^\dagger. \quad (2.76)$$

The coupling constant (given in terms of the atomic dipole moment μ_α for electric field polarization α) is

$$g_{j,\alpha} = \frac{\mu_\alpha}{\hbar} \sqrt{\frac{\hbar\nu_j}{2\epsilon_0 V}} e^{i\mathbf{k}_j \cdot \mathbf{r}}. \quad (2.77)$$

and $g_{j,\alpha}$ is known as the “single-photon Rabi frequency” because it corresponds to the frequency at which an atom will spontaneously emit and reabsorb a single resonant photon of frequency ν_j . One interesting scenario arises for photons confined to standing wave modes of a cavity. The single photon Rabi frequency then has spatial dependence $\sin \mathbf{k}_j \cdot \mathbf{r}$, so the atom-field coupling constant depends on the position of the atom in the cavity.

2.3.3 Remarks about quantization

The quantization procedure and resulting interactions detailed above may appear quite general, but in fact we made an important assumption at the

very beginning which will limit their applicability: we considered only the situation with no sources, so we implicitly treated only transverse fields where $\nabla \cdot E = 0$. Longitudinal fields result from charge distributions ρ , with $E_L = -\nabla\phi$ and $\nabla^2\phi = 4\pi\rho$, and they do not satisfy a wave equation. For more information on this topic, see e.g. Cohen-Tannoudji *et al.*, "Atom-Photon Interactions".

By considering only transverse fields, however, we have further avoided the issue of gauge. Since a transverse electric field E_T satisfies the wave equation, we were able to directly quantize it without intermediate recourse to the vector potential A . Moreover, by starting with a dipole interaction Hamiltonian $\hat{E} \cdot \hat{d}$, we never needed A , and thus never encountered a choice of gauge. In fact, the procedure can be viewed as corresponding to an implicit choice of gauge $\phi = 0$, $\nabla \cdot A = 0$ in our initial decision to only treat transverse fields.

A more general approach may use the canonical Hamiltonian for a particle of mass m and charge q in an electromagnetic field. In this approach, the particle momentum \hat{p} is replaced by the canonical momentum $\hat{p} - q\hat{A}/c$, so the Hamiltonian contains terms like $(\hat{p} - qA/c)^2/2m$. For an appropriate choice of gauge, the $\hat{p} \cdot \hat{A}$ terms imply the dipole interaction $\hat{E} \cdot \hat{d}$. More information on this topic can be found in, for example, Scully and Zubairy "Quantum Optics."

2.3.4 Wigner-Weisskopf theory of spontaneous emission

Armed with the formalism for treating quantized radiation modes, we will now calculate the rate at which an atom spontaneously relaxes to a lower energy state while emitting a photon. In fact, we will find that this problem reduces to something we already know how to treat: the bound to continuum transition.

Suppose a two-level atom starts out in its excited state $|2\rangle$, and the radiation field with which it interacts starts out in the vacuum state $\hat{a}_j|n_j = 0\rangle = 0$. Note that the assumption of an initial vacuum state is not always valid, but it is a good approximation for optical frequencies. By interacting with the quantized electromagnetic field, the atom can make a transition to its ground state $|1\rangle$ while emitting a photon of frequency ν_k , so the field ends up in state $|1_k\rangle$. We need only consider final states of the form $|1\rangle|1_k\rangle = |1, 1_k\rangle$, so we can project the full Hamiltonian

$$\hat{H} = \hbar\omega|2\rangle\langle 2| + \sum_j \hbar\nu_j \left(\hat{a}_j^\dagger \hat{a}_j + \frac{1}{2} \right) - \sum_j \left(\hbar g_j |2\rangle\langle 1| \hat{a}_j + \hbar g_j^* |1\rangle\langle 2| \hat{a}_j^\dagger \right) \quad (2.78)$$

onto the relevant states $|2, 0\rangle$ and $|1, 1_k\rangle$ to obtain an effective Hamiltonian

$$\begin{aligned}\hat{H} = & \hbar\omega|2, 0\rangle\langle 2, 0| + \sum_k \hbar\nu_k|1, 1_k\rangle\langle 1, 1_k| \\ & - \sum_k (\hbar g_k|2, 0\rangle\langle 1, 1_k| + \hbar g_k^*|1, 1_k\rangle\langle 2, 0|).\end{aligned}\quad (2.79)$$

Mathematically, this effective Hamiltonian is obtained by taking the matrix elements of the Hamiltonian between the relevant states.

In the limit of closely spaced photon frequencies, the effective Hamiltonian corresponds precisely to a bound-to-continuum transition between the discrete state $|2, 0\rangle$ and the continuum of states $|1, 1_k\rangle$. We have already derived the results:

(1) There is a shift in the energy levels. In the case of atom-field interactions, it is known as the Lamb shift, and since it depends only on the coupling constants g_j , it is usually incorporated into a renormalization of the atomic transition frequency ω . The Lamb shift will change, however, if the atom is put into a different environment, for example a cavity, where the density of states and the g_j are different.

(2) The atom decays from the excited state $|2\rangle$ at a rate γ given by

$$\gamma = 2\pi \sum_{\mathbf{k}, \alpha} |g_{\mathbf{k}, \alpha}|^2 \delta(\nu_k - \omega). \quad (2.80)$$

To put this expression in more usable form, we convert the sum over k to an integral,

$$\gamma = \frac{V}{(2\pi)^2} \sum_{\alpha} \int k^2 dk \int d\phi \int \sin \theta d\theta |g_{\mathbf{k}, \alpha}|^2 \delta(\nu_k - \omega). \quad (2.81)$$

To evaluate the sum over polarizations, we will choose the \hat{z} axis of our integration coordinates to lie along the same direction as \hat{k} . In this choice of coordinates, the only allowed polarization vectors lie in the $\hat{x} - \hat{y}$ plane. In particular,

$$\sum_{\alpha} |g_{\mathbf{k}, \alpha}|^2 = \frac{\nu_k}{2\hbar\epsilon_0 V} \sum_{\alpha=x, y} |\mu \cdot \epsilon_{\alpha}|^2 \quad (2.82)$$

$$= \frac{\nu_k}{2\hbar\epsilon_0 V} (|\mu \sin \theta \cos \phi|^2 + |\mu \sin \theta \sin \phi|^2). \quad (2.83)$$

Consequently,

$$\sum_{\alpha} |g_{\mathbf{k}, \alpha}|^2 = |g_k|^2 \sin \theta^2, \quad (2.84)$$

where

$$g_k = \frac{\mu}{\hbar} \sqrt{\frac{\hbar\nu_k}{2\epsilon_0 V}}. \quad (2.85)$$

The angular integration thus yields

$$\int d\phi \int d\theta \sin \theta \sum_{\alpha} |g_{k,\alpha}|^2 = 2\pi |g_k|^2 \int d\theta \sin^3 \theta \quad (2.86)$$

$$= \frac{8\pi}{3} |g_k|^2. \quad (2.87)$$

Substituting back into Eq. (2.81),

$$\gamma = \frac{2V}{3\pi} \int_0^\infty k^2 dk |g_k|^2 \delta(\nu_k - \omega) = \frac{2\omega^2 V}{3\pi c^3} |g_{k=\omega/c}|^2. \quad (2.88)$$

Finally, we write the single photon Rabi frequency using Eq. (2.85) to obtain the usual expression for the spontaneous emission rate (also known as the Einstein A coefficient):

$$\gamma = \frac{\omega^3 |\mu|^2}{3\pi \epsilon_0 \hbar c^3}. \quad (2.89)$$

Note that the spontaneous emission rate is proportional to the square of the atomic dipole moment and the cube of the atomic transition frequency. Consequently transitions with big dipole moments and large energy splittings will decay most quickly.

The dynamics which result from the spontaneous emission process are very similar to those discussed for bound to continuum transitions. Unlike the previous situation, however, no transformation to the rotating frame is needed. Since the radiation field and atom are treated on equal footing (with photon energy incorporated into the Hamiltonian), the initial and final states are already near resonance. The transformation to the rotating frame is an artifact of treating the system classically.

We can also explicitly calculate the dynamics: if the system state is given by $|\psi\rangle = c_2|2,0\rangle + \sum_{k,\alpha} c_{k,\alpha}|1,1_{k,\alpha}\rangle$, the coefficients obey the equations of motion

$$\dot{c}_2 = -(\gamma/2)c_2 - i\omega c_2 \quad (2.90)$$

$$\dot{c}_{k,\alpha} = -i\nu_k c_{k,\alpha} + ig_{k,\alpha}c_2(t), \quad (2.91)$$

where ω and ν_k appear in equivalent positions for the two equations. As we found before, the amplitudes to be in a photon state with polarization α and wavevector k approach

$$\lim_{t \rightarrow \infty} c_{k,\alpha} = \frac{g_{k,\alpha}}{\nu_k - \omega + i\gamma/2} e^{-i\nu_k t} \quad (2.92)$$

in the long-time limit. Now consider an atom which starts out in a superposition of states, $|\psi_0\rangle = c_2^0|2, 0\rangle + c_1^0|1, 0\rangle$. Since $|1, 0\rangle$ does not interact with the field, at time t the system is in state $|\psi(t)\rangle = e^{-\gamma t/2}e^{-i\omega t}c_2^0|2, 0\rangle + c_1^0|1, 0\rangle + \sum_j c_j(t)|1, j\rangle$. In contrast to classical Rabi oscillations, the atomic dipole moment decays in time:

$$\langle\psi|\hat{d}|\psi\rangle = \mu\langle\psi|1\rangle\langle 2|\psi\rangle + \mu^*\langle\psi|2\rangle\langle 1|\psi\rangle \quad (2.93)$$

$$= e^{-\gamma t/2} (c_2^0 e^{-i\omega t} (c_1^0)^* \mu + c_1^0 (c_2^0 e^{-i\omega t})^* \mu^*) \quad (2.94)$$

Note that the single photon coefficients $c_j(t)$ do not contribute because the single photon state is orthogonal to the radiation vacuum state. Consequently the system undergoes transitions between atomic levels without an accompanying buildup of atomic coherences.

We can also describe the state of the radiation field generated by spontaneous emission of an atom. In the long time limit, the system state is

$$|\psi\rangle = |1\rangle \otimes \sum_{k,\alpha} \frac{g_{k,\alpha}}{\nu_k - \omega + i\gamma/2} e^{-i\nu_k t} |1_{k,\alpha}\rangle. \quad (2.95)$$

We would like to understand the physical photon wavepacket this state describes. Naively, one might try calculating the electric field expectation, but in fact it vanishes

$$\langle\psi|\hat{E}_\alpha|\psi\rangle = 0 \quad (2.96)$$

The single photon field $|\psi\rangle$ is not a classical field, so it need not be an eigenstate of the electric field operator. In fancier language, the single photon field does not have the “first order coherence” associated with laser light. Nevertheless, higher order operators such as $\langle\psi|\hat{\mathcal{E}}_\alpha^\dagger \hat{\mathcal{E}}_\alpha|\psi\rangle$ can be nonzero. In particular, when we introduce a complete set of states into the expectation value we find that only the $n = 0$ states contribute (since the positive frequency component $\hat{\mathcal{E}}_\alpha \propto \hat{a}$):

$$\langle\psi|\hat{\mathcal{E}}_\alpha^\dagger \hat{\mathcal{E}}_\alpha|\psi\rangle = \sum_n \langle\psi|\hat{\mathcal{E}}_\alpha^\dagger|n\rangle \langle n|\hat{\mathcal{E}}_\alpha|\psi\rangle \quad (2.97)$$

$$= \langle\psi|\hat{\mathcal{E}}_\alpha^\dagger|0\rangle \langle 0|\hat{\mathcal{E}}_\alpha|\psi\rangle. \quad (2.98)$$

We can thus identify⁴

$$\langle 0|\hat{\mathcal{E}}_\alpha|\psi\rangle = \sum_k \bar{\mathcal{E}}_k \frac{g_{k,\alpha}}{\nu_k - \omega + i\gamma/2} e^{i(kz - \nu_k t)} \quad (2.99)$$

$$\propto \frac{e^{-\gamma(t-z/c)/2}}{z} \Theta(t - z/c) \quad (2.100)$$

with a kind of “wavefunction” for the photon describing a wavepacket outgoing from the initial position of the atom at speed c .

⁴For simplicity, here we consider photons propagating in a one-dimensional system to avoid more complicated expressions involving the vector nature of \mathbf{k} and polarization vectors. The important point is that there is a pole in the complex lower half-plane in Eq. (2.99). To evaluate this integral, we close the contour in the lower half-plane for $t > z/c$ and in the upper half-plane for $t < z/c$, which gives us the step function in the following line. For a more rigorous derivation, see *Scully and Zubairy*, pp. 209-210.

Chapter 3

Mathematical methods for open systems

Our primary goal thus far has been to describe the interactions between light and matter. In previous lectures we have developed two different formalisms for atoms interacting with classical and quantum mechanical radiation fields. Even though the latter allowed us to solve the problem of spontaneous emission, the full quantum mechanical treatment is cumbersome at best, and in many cases unnecessary. We would like to describe both coherent phenomena (such as classical field Rabi oscillations) and incoherent processes (such as spontaneous emission) in a more efficient manner. By truncating our description to include only the few modes or atomic levels of interest, we can treat much more complicated systems.

In more formal language, we seek a quantum mechanical treatment of open systems. The “system” interacts not only with controllable classical signals, but also with a large number of degrees of freedom we call the “environment” or “reservoir”, and over which we have no control. If we do not care about the reservoir state, we would like to be able to describe the system without also calculating the reservoir dynamics. For instance, the system might be an atom interacting with both a controllable laser field and an environment composed of the vacuum modes of the electromagnetic field; by properly eliminating the radiation field degrees of freedom while retaining their effect on the atom, we can obtain a simpler but equally accurate picture of the atomic evolution.

3.1 The density operator

Although the state of a quantum mechanical system is represented by $|\psi\rangle$, a vector in Hilbert space, this description does not provide a useful picture for many practical situations, and certainly cannot treat macroscopic objects. Any quantum mechanical state can also be represented as a density operator; moreover, the density operator can describe classical ensembles as well.

Suppose our system can be in one of a number of quantum states $|\psi_\alpha\rangle$ and it occupies each state with some probability p_α . The density operator for the system is

$$\hat{\rho} = \sum_{\alpha} p_{\alpha} |\psi_{\alpha}\rangle\langle\psi_{\alpha}|. \quad (3.1)$$

If there exists a basis in which $\hat{\rho} = |\phi\rangle\langle\phi|$ for some state $|\phi\rangle$, the system is said to be in a “pure state”. If such a basis cannot be found, the system is in a “mixed state”, and has lost some of its purely quantum mechanical character. Finally, if the off-diagonal elements of the density operator vanish, the system can be described by a classical ensemble of basis states, and is called a “statistical mixture”.

From this definition, one can immediately derive several important properties which any density operator must satisfy:

- (1) $\hat{\rho} = \hat{\rho}^\dagger$
- (2) $\text{Tr}[\hat{\rho}] = \sum_n \langle n | \hat{\rho} | n \rangle = 1$ where $\{|n\rangle\}$ form an orthonormal basis
- (3) $\langle n | \hat{\rho}^2 | m \rangle \leq \langle n | \hat{\rho} | m \rangle$ where $|m\rangle$ and $|n\rangle$ are any pure states

The first is self evident, the second follows from conservation of probability, and the third is an equality only when the density operator describes a pure state.

Operator expectation values may be calculated directly from the density operator. If \hat{S} is a system observable, its expectation value should be calculated in all possible quantum states weighted by their probability of occupation:

$$\langle \hat{S} \rangle = \sum_{\alpha} p_{\alpha} \langle \psi_{\alpha} | \hat{S} | \psi_{\alpha} \rangle \quad (3.2)$$

$$= \sum_{\alpha, n} p_{\alpha} \langle \psi_{\alpha} | \hat{S} | n \rangle \langle n | \psi_{\alpha} \rangle \quad (3.3)$$

$$= \sum_n \langle n | \underbrace{\left(\sum_{\alpha} p_{\alpha} |\psi_{\alpha}\rangle\langle\psi_{\alpha}| \right)}_{\hat{\rho}} \hat{S} | n \rangle \quad (3.4)$$

$$= \text{Tr}[\hat{\rho} \hat{S}]. \quad (3.5)$$

By inserting a completeness relation $\sum_n |n\rangle\langle n| = 1$ and rearranging terms, a considerable simplification is obtained.

In this context, the mathematical meaning of the trace may be unclear. However, given a basis $\{|n\rangle\}$, we may write the operators \hat{S} and $\hat{\rho}$ as matrices, whereby their trace is the usual sum of diagonal elements. The so-called density matrix has elements $\rho_{n,n'}$ such that

$$\hat{\rho} = \sum_{n,n'} |n\rangle \underbrace{\langle n|\hat{\rho}|n'\rangle}_{\rho_{n,n'}} \langle n'|. \quad (3.6)$$

These elements have a physical meaning, and there are two cases worth distinguishing:

- (1) Diagonal elements $\rho_{nn} = \langle(|n\rangle\langle n|)\rangle$ correspond to the probability of occupying state $|n\rangle$.
- (2) Off-diagonal elements $\rho_{nm} = \langle(|n\rangle\langle m|)\rangle$ correspond to the expectation value of the coherence between level $|n\rangle$ and $|m\rangle$, e.g. the atomic dipole operator.

For example, the density operator for a two-level atom may be written as a 2x2 matrix,

$$\hat{\rho} = \rho_{11}|1\rangle\langle 1| + \rho_{12}|1\rangle\langle 2| + \rho_{21}|2\rangle\langle 1| + \rho_{22}|2\rangle\langle 2|. \quad (3.7)$$

A pure state $|\psi\rangle = c_1|\psi\rangle + c_2|\psi'\rangle$ then has a density matrix with $\rho_{ij} = c_i c_j^*$. Pure states thus satisfy

$$|\rho_{ij}|^2 = \rho_{ii}\rho_{jj}. \quad (3.8)$$

By considering the requirement $\rho^2 \leq \rho$, we see that an arbitrary mixed state only satisfies the inequality

$$|\rho_{ij}|^2 \leq \rho_{ii}\rho_{jj}. \quad (3.9)$$

Consequently, for a pure state we have the maximal allowed off-diagonal components, or the “maximal coherence.”

Example 1: Two-level atom in thermal equilibrium

One example of a mixed state is the two-level atom with transition frequency ω in thermal equilibrium. In the basis $\{|1\rangle, |2\rangle\}$ its density operator takes the form

$$\hat{\rho} = \frac{e^{-\hat{H}/k_B T}}{\text{Tr}[e^{-\hat{H}/k_B T}]} \quad (3.10)$$

$$= \frac{1}{1 + e^{-\hbar\omega/k_B T}} \begin{pmatrix} 1 & 0 \\ 0 & e^{-\hbar\omega/k_B T} \end{pmatrix} \quad (3.11)$$

$$= \frac{1}{2 \cosh \hbar\omega/2k_B T} \begin{pmatrix} e^{\hbar\omega/2k_B T} & 0 \\ 0 & e^{-\hbar\omega/2k_B T} \end{pmatrix}. \quad (3.12)$$

Clearly, the equilibrium population depends on the relative scale of the atomic transition frequency and the temperature. For instance, at room temperature $T = 300K$, $k_B T/(2\pi\hbar) \approx 6 \cdot 10^{12}$ Hz, which corresponds to a frequency between microwave and near-infrared. If the atomic transition frequency is well above this scale, the atom will be in its ground state in equilibrium; otherwise, it will be in a statistical mixture of ground and excited states.

Example 2: Radiation field in thermal equilibrium

The density matrix for a thermal radiation field illustrates how the density operator formalism connects up with statistical mechanics. A single mode with frequency ν_j has a density operator

$$\hat{\rho}^{(j)} = \frac{e^{-\hbar\nu_j \hat{a}_j^\dagger \hat{a}_j / k_B T}}{\text{Tr}[e^{-\hbar\nu_j \hat{a}_j^\dagger \hat{a}_j / k_B T}]} \quad (3.13)$$

with matrix elements between Fock states $|n\rangle, |m\rangle$

$$\hat{\rho}_{nm}^{(j)} = \delta_{nm} e^{-\hbar\nu_j n / k_B T} \left(1 - e^{-\hbar\nu_j / k_B T} \right). \quad (3.14)$$

Note that only the diagonal elements are nonzero since the field is a statistical mixture of photon number states. Consequently, the expectation value for the annihilation operator vanishes,

$$\langle \hat{a}_j \rangle = \sum_n \langle n | \hat{a}_j \hat{\rho} | n \rangle = \sum_n \rho_{n+1,n} \sqrt{n+1} = 0, \quad (3.15)$$

but the average photon number obeys the Bose-Einstein distribution,

$$\bar{n}_j = \langle \hat{a}_j^\dagger \hat{a}_j \rangle = \sum_n \rho_{nn} = \frac{1}{e^{(\hbar\nu_j / k_B T)} - 1}. \quad (3.16)$$

3.2 System and environment

The density operator formalism is well suited for treating a system composed of two parts when only one subsystem is relevant. For clarity, we will call the

total system the universe, and its component parts are the system and the environment. The universe can be described by a quantum state $|\psi\rangle$, with the corresponding density operator $\hat{\rho} = |\psi\rangle\langle\psi|$, and in principle we can solve for the dynamics of the system by first finding how the universe evolves. Since we are really only interested in the system, we would like to find a more efficient description which does not require us to calculate precisely what happens to the environment degrees of freedom.

We proceed by first expanding the total state vector in terms of a product basis $\{|n\rangle|e\rangle\}$ where $|n\rangle$ is a state of the system and $|e\rangle$ is a state of the environment, so that

$$|\psi\rangle = \sum_{\{n,e\}} |n\rangle|e\rangle\langle n, e|\psi\rangle. \quad (3.17)$$

Consider the expectation value in this state of an operator \hat{S} which acts only on the system degrees of freedom,

$$\langle\hat{S}\rangle = \sum_{n,e} \langle n, e|\hat{S}|\psi\rangle\langle\psi|n, e\rangle \quad (3.18)$$

$$= \sum_n \underbrace{\langle n|\hat{S}(\sum_e \langle e|\psi\rangle\langle\psi|e\rangle)|n\rangle}_{\hat{\rho}_S} \quad (3.19)$$

$$= \text{Tr}_S[\hat{S}\hat{\rho}_S]. \quad (3.20)$$

The subscript S (R) on the trace indicates that only the system (reservoir) states are included in the sum. The second line in the equation above is true because the operator \hat{S} operates only on the system, and thus $\langle e|$ can be moved past \hat{S} . Eq. (3.20) states that the expectation value of a system operator can always be found in terms of a reduced density operator

$$\hat{\rho}_S = \text{Tr}_R[\hat{\rho}]. \quad (3.21)$$

Note that $\hat{\rho}_S$ has all the properties of a density operator, and can be expressed as a probabilistic mixture of system states, $\hat{\rho}_S = \sum_\alpha p_\alpha |\psi_\alpha^S\rangle\langle\psi_\alpha^S|$. In general, however, $\hat{\rho}_S$ does not have to describe a pure state, and this reflects the fact that the system under consideration interacts with the environment, i.e. it is an open system.

3.3 The dynamics of an open system

We will use the density operator as a tool to aid derivation of an efficient description for an open system interacting with its environment. To under-

stand how the reduced density operator evolves in time, consider first its evolution with a Hamiltonian \hat{H}_S acting only on the system:

$$i\hbar\dot{\rho}_S = \sum_{\alpha} p_{\alpha} (\underbrace{i\hbar|\psi_{\alpha}^S\rangle\langle\dot{\psi}_{\alpha}^S|}_{\hat{H}_S|\psi_{\alpha}^S\rangle} + |\psi_{\alpha}^S\rangle\langle\dot{\psi}_{\alpha}^S|) - \underbrace{\langle\psi_{\alpha}^S|\hat{H}_S}_{-\langle\psi_{\alpha}^S|\hat{H}_S}) \quad (3.22)$$

$$= \frac{1}{i\hbar} [\hat{H}_S, \hat{\rho}_S]. \quad (3.23)$$

Suppose now that there is some coupling between the system and the environment described by an interaction Hamiltonian \hat{H}_{SR} . The dynamics will become quite a bit more involved, since even if the system and environment start out independent of one another, the initial product state $|\psi_S\rangle \otimes |\psi_R\rangle$ will evolve under the influence of \hat{H}_{SR} into a state which cannot in general be factored into independent system and environment states. The system and environment are then said to be entangled.

As an illustration we return to the example of an atom spontaneously emitting a photon into the vacuum. If the atom starts out in a superposition state, $|\psi_0\rangle = (c_1|1\rangle + c_2|2\rangle) \otimes |0\rangle$, at time t it will be in a state $|\psi(t)\rangle = c_1|1\rangle \otimes |0\rangle + c_2(t)|2\rangle \otimes |0\rangle + \sum_k c_k(t)|1\rangle \otimes |1_k\rangle$ which can no longer be written as a direct product of atomic and electromagnetic states. The elements of the atomic reduced density matrix can then be calculated in terms of the decay rate γ :

$$\hat{\rho}_S = \text{Tr}_R[|\psi(t)\rangle\langle\psi(t)|] \quad (3.24)$$

$$= \sum_{n=0}^{\infty} \sum_k \langle n_k | \psi(t) \rangle \langle \psi(t) | n_k \rangle \quad (3.25)$$

$$= \begin{pmatrix} 1 - \rho_{22}(0)e^{-\gamma t} & \rho_{12}(0)e^{-\gamma t/2} \\ \rho_{21}(0)e^{-\gamma t/2} & \rho_{22}(0)e^{-\gamma t} \end{pmatrix}, \quad (3.26)$$

where $|n_k\rangle$ is a n -photon Fock state in mode k . Note that the off-diagonal elements decay at half the rate of the excited state population. This is characteristic of interactions which conserve energy.

3.3.1 General formalism

The total Hamiltonian may be represented as a sum of three terms,

$$\hat{H} = \hat{H}_S + \hat{H}_R + \hat{H}_{SR}. \quad (3.27)$$

The first term only affects system degrees of freedom and the second only affects the reservoir while the third contains products of system operators

with reservoir operators. The total density matrix obeys the equation of motion

$$\dot{\hat{\rho}} = \frac{1}{i\hbar} [\hat{H}, \hat{\rho}] \quad (3.28)$$

$$= \frac{1}{i\hbar} [\hat{H}_S + \hat{H}_R + \hat{H}_{SR}, \hat{\rho}], \quad (3.29)$$

and we may trace over the reservoir degrees of freedom on both sides of the equation to obtain the evolution for the system reduced density operator:

$$\dot{\hat{\rho}}_S = \text{Tr}_R[\dot{\hat{\rho}}] \quad (3.30)$$

$$= \frac{1}{i\hbar} [\hat{H}_S, \hat{\rho}_S] + \frac{1}{i\hbar} \underbrace{\text{Tr}_R[[\hat{H}_R, \hat{\rho}]]}_{=0} + \frac{1}{i\hbar} \text{Tr}_R[[\hat{H}_{SR}, \hat{\rho}]]. \quad (3.31)$$

Each of the three terms contributes differently. The system Hamiltonian has the same effect it would have in the absence of the reservoir. The reservoir Hamiltonian has no net effect on $\hat{\rho}_S$ because the trace is invariant under cyclic permutations of the reservoir operators, so the commutator must vanish. The interaction Hamiltonian, however, involves both system and reservoir operators and requires special treatment. Although we have obtained the equation of motion as a general result, no further progress can be made without specifying at least some of the properties of the interaction Hamiltonian and the reservoir itself.

3.3.2 Properties of the environment

Different environments can have qualitatively different impacts on the system with which they interact. To illustrate typical reservoir properties, we consider the example of a spin in a fluctuating magnetic field, where the interaction Hamiltonian is

$$\hat{H}_{SR} = \hbar f(t) \hat{S}_z. \quad (3.32)$$

This Hamiltonian corresponds to an energy splitting $\hbar f(t)$ between the spin states $|1\rangle, |2\rangle$, where $\hat{S}_z = (|2\rangle\langle 2| - |1\rangle\langle 1|)/2$. We will consider the case when $f(t)$ represents a random field. This model is applicable to a variety of physical systems, for example an electron spin in a (randomly fluctuating) bath of nuclear spins. Starting from the Hamiltonian, we can formally derive the operator describing unitary evolution of the spin

$$\hat{U} = e^{i \int_0^t f(t') dt' \hat{S}_z}, \quad (3.33)$$

from which we can calculate the time dependence of any expectation value. In particular, we will be interested in $\langle \hat{S}_+ \rangle$, which corresponds to the off-diagonal element of the spin density matrix ($\hat{S}_+ = |2\rangle\langle 1|$). This operator picks up a phase from the energy splitting in the Hamiltonian, so its time dependence is

$$\langle \hat{S}_+ \rangle = \langle e^{i \int_0^t f(t') dt'} \hat{S}_+(0) \rangle, \quad (3.34)$$

which depends on the moments of the random variable $f(t)$.

Random variables

The fluctuating energy splitting $\hbar f(t)$ represents a time dependent random process, also known as a random variable. At each point in time, $f(t)$ is characterized by some probability distribution, and we need to know something about this probability distribution to predict the average effect that $f(t)$ has on the operator we are calculating. In particular, we will want to know the following properties of the probability distribution:

- (1) The first moment is the expectation value $\langle f(t) \rangle$. Typically, we will be interested in so-called “stationary processes”, for which $\langle f(t) \rangle = \langle f \rangle$ is constant. We can then define

$$f(t) = \langle f \rangle + \delta f(t), \quad (3.35)$$

where $\langle \delta f(t) \rangle = 0$.

- (2) The variance of the random process $\langle \delta f(t) \delta f(t') \rangle \neq 0$ describes the typical extent of the deviations of $f(t)$ from its average value.

- (3) The correlation time τ_c represents the timescale on which $f(t)$ changes. It is related to the time dependence of the variance; in particular, the variance $\langle \delta f(t) \delta f(t') \rangle$ is nearly constant for $|t - t'| < \tau_c$.

For arbitrary probability distributions, we would in principle need to specify an infinite number of higher order moments. However, in what follows we will typically deal with “Gaussian” probability distributions. For a Gaussian probability distribution, knowledge of the mean and the variance is sufficient to specify all higher order moments because they factorize pairwise:

$$\langle \delta f(t_1) \delta f(t_2) \dots \delta f(t_n) \rangle = \sum \langle \delta f(t_1) \delta f(t_2) \rangle \langle \delta f(t_3) \dots \rangle, \quad (3.36)$$

where the sum is taken over all distinct groupings into pairwise and single expectation values. In particular, we should notice that for $\langle \delta f \rangle = 0$, all odd-order moments vanish.

Correlation time

For the example we are considering (the spin in a fluctuating field $f(t)$), we will distinguish two important limits:

$$(1) t < \tau_c$$

In this case, we examine the system on timescales which are much shorter than the timescale over which the environment changes. Each time that we examine the system (for example, running an experiment on it), we will find that the spin precesses around the \hat{z} axis at a rate $f(t < \tau_c)$ which is random in value but fixed over the duration of the evolution. Every realization will have a different value of $f(t)$, so on average we would find that $\langle \hat{S}_+ \rangle = 0$. However, this dephasing is in some sense reversible. If you know what $f(t)$ is for each experiment, you can compensate for it. For example, you could perform a spin echo experiment, wherein you reverse the orientation of the spin halfway through its evolution, so that the net precession vanishes. Consequently we refer to this first situation as “reversible evolution.”

$$(2) t \gg \tau_c.$$

For times long compared to the correlation time, spin echo techniques fail. There is simply no way to recover a history of the evolution and undo the damage done by the fluctuating environment. The ensemble average $\langle \hat{S}_+ \rangle = 0$ again vanishes, but in a way that is fundamentally irreversible. This situation corresponds to a reservoir which has a short memory time. Such a reservoir is known as a “Markovian environment” because it can be described by a Markov process (a random process with an infinitely short correlation time). In atomic physics and quantum optics, most environments are nearly Markovian, so we will focus on techniques for understanding the effects of a Markovian reservoir.

3.3.3 Density operator method for a Markovian reservoir

By limiting the system and reservoir to certain kinds of interactions relevant to atomic physics and quantum optics, we can develop a framework for analyzing open systems. In particular, we will consider environments which have a very short correlation time, so that the system is only influenced by the instantaneous state of the reservoir.

Again, we will assume $\hat{H} = \hat{H}_S + \hat{H}_R + \hat{H}_{SR}$. The interaction term \hat{H}_{SR} is the most relevant part. To focus on it we will work in the interaction picture, which is found by transforming according to the unitary operator

$$\hat{U} = e^{i(\hat{H}_R + \hat{H}_S)t/\hbar}. \quad (3.37)$$

In the interaction picture (denoted by tildes), the relevant operators are

$$\tilde{\rho} = e^{i(\hat{H}_R + \hat{H}_S)t/\hbar}\hat{\rho}e^{-i(\hat{H}_R + \hat{H}_S)t/\hbar} \quad (3.38)$$

$$\tilde{H}_{SR} = e^{i(\hat{H}_R + \hat{H}_S)t/\hbar}\hat{H}_{SR}e^{-i(\hat{H}_R + \hat{H}_S)t/\hbar}. \quad (3.39)$$

The unitary transformation automatically accounts for the free evolution of the system and reservoir, so that the only remaining dynamics are due to the interactions, i.e.

$$\frac{d}{dt}\tilde{\rho} = \frac{1}{i\hbar}[\tilde{H}_{SR}, \tilde{\rho}]. \quad (3.40)$$

Our analysis requires that the interaction be a bilinear product of system and reservoir operators,

$$\hat{H}_{SR} = \hat{S}\hat{R}^\dagger + \hat{R}\hat{S}^\dagger, \quad (3.41)$$

where \hat{S} (\hat{R}) is a general system (reservoir) operator. In practice, the interaction Hamiltonian may have a sum over such terms: the analysis proceeds in exactly the same manner, and the effects may be accounted for by considering each term of the sum separately and summing at the end. In the interaction picture, we will represent the Hamiltonian by

$$\tilde{H}_{SR} = \hat{S}\hat{F}_R(t)^\dagger + \hat{F}_R(t)\hat{S}^\dagger, \quad (3.42)$$

where all the time dependence is explicitly included in the reservoir operator $\hat{F}_R(t)$.

For example, consider the Hamiltonian for a single atom interacting with the radiation field in the Schrodinger picture,

$$\hat{H}_{SR} = -\underbrace{\sum_j \hbar g_j \hat{a}_j}_{\hat{R}} \underbrace{|2\rangle\langle 1|}_{\hat{S}^\dagger} - \sum_j \hbar g_j^* \hat{a}_j^\dagger |1\rangle\langle 2|, \quad (3.43)$$

where we can identify the system and reservoir operators appropriate to our more general form of the interaction. Likewise, in the interaction picture

the Hamiltonian includes the phase factors associated with free evolution of the system and reservoir:

$$\tilde{H}_{SR} = \underbrace{-\sum_j \hbar g_j \hat{a}_j e^{-i(\nu_j - \omega)t}}_{\hat{F}_R(t)} \underbrace{|2\rangle\langle 1|}_{\hat{S}^\dagger} - \sum_j \hbar g_j^* \hat{a}_j^\dagger e^{i(\nu_j - \omega)t} |1\rangle\langle 2|, \quad (3.44)$$

and we incorporate these phase factors into the new reservoir operator $\hat{F}_R(t)$.

In addition to the specified form for the interaction given by Eq. (3.42), our analysis requires two assumptions regarding the nature of the reservoir itself, namely

- (1) The reservoir is large (so it is not affected by the system)
- (2) The reservoir has a broad bandwidth (so its correlation time is very short¹).

The first assumption indicates that the reservoir state is not significantly affected by its interaction with the system. Consequently for our analysis we may take the reservoir to be in a stationary (time-independent) state, for example a statistical mixture at some temperature T. The second assumption implies that the correlation time $\tau_c \sim (1/\text{bandwidth})$ for the reservoir is short; in particular, we require that τ_c be much smaller than the typical timescale τ_S on which the system evolves. These assumptions together constitute the “Born-Markov Approximation”, and a reservoir which satisfies them is called Markovian.

The effect of the reservoir on the system can be simplified by averaging over a timescale Δt which is in between the correlation time and characteristic system evolution time, $\tau_c \ll \Delta t \ll \tau_S$. This approach is akin to perturbation theory in τ_c/τ_S , and will provide equations of motion for the system reduced density operator which are valid for times greater than Δt .

Starting from Eq. (3.40), we can formally integrate to obtain the density operator at a later time,

$$\underbrace{\tilde{\rho}(t + \Delta t) - \tilde{\rho}(t)}_{\Delta\tilde{\rho}} = \frac{1}{i\hbar} \int_t^{t+\Delta t} dt' [\tilde{H}_{SR}(t'), \tilde{\rho}(t')]. \quad (3.45)$$

¹This relationship between bandwidth and correlation time of the reservoir is often, but not always, true. For example, if the system consists of an ensemble of atoms with spatial extent L larger than the optical wavelength λ_0 , and the environment consists of the electromagnetic field, the correlation time $\tau_c \sim L/c$ corresponds to the time it takes for a photon to leave the medium, since a photon released by one atom can be absorbed by another a time τ_c later.

Expanding

$$\tilde{\rho}(t') \approx \tilde{\rho}(t) + \frac{1}{i\hbar} \int_t^{t'} dt'' [\tilde{H}_{SR}(t''), \tilde{\rho}(t'')], \quad (3.46)$$

(which is valid since $t' - t < \Delta t$), we obtain

$$\begin{aligned} \Delta\tilde{\rho} = & \frac{1}{i\hbar} \int_t^{t+\Delta t} dt' [\tilde{H}_{SR}(t'), \tilde{\rho}(t)] \\ & + \frac{1}{(i\hbar)^2} \int_t^{t+\Delta t} dt' \int_t^{t'} dt'' [\tilde{H}_{SR}(t'), [\tilde{H}_{SR}(t''), \tilde{\rho}(t'')]]. \end{aligned} \quad (3.47)$$

Now we trace over the reservoir degrees of freedom to find the change in the system reduced density operator over time Δt ,

$$\begin{aligned} \Delta\tilde{\rho}_S = & \frac{1}{i\hbar} \int_t^{t+\Delta t} dt' \text{Tr}_R[\tilde{H}_{SR}(t'), \tilde{\rho}(t)] \\ & + \frac{1}{(i\hbar)^2} \int_t^{t+\Delta t} dt' \int_t^{t'} dt'' \text{Tr}_R[\tilde{H}_{SR}(t'), [\tilde{H}_{SR}(t''), \tilde{\rho}(t'')]]. \end{aligned} \quad (3.48)$$

To proceed we must now make yet another assumption: the initial state is factorizable,

$$\tilde{\rho}(t) = \tilde{\rho}_S(t) \otimes \tilde{\rho}_R(t). \quad (3.49)$$

For times shortly thereafter, $t < t' < t + \Delta t$, the total density operator is approximately factorizable with some small correction,

$$\tilde{\rho}(t') \approx \tilde{\rho}_S(t) \otimes \tilde{\rho}_R(t) + \tilde{\rho}_{corr}(t, t'). \quad (3.50)$$

Provided that $\Delta t \ll \tau_S$, we can neglect $\tilde{\rho}_{corr}$ in the RHS of Eq. (3.48) to leading order, replacing the total density operator by the product of a system and reservoir density operator.²

Using the explicit forms for $\tilde{H}_{SR}(t)$ and $\tilde{\rho}(t)$, we will now examine the two terms in Eq. (3.48). The first term, $\Delta\tilde{\rho}_S^{(1)}$, has a straightforward effect on the system,

$$\Delta\tilde{\rho}_S^{(1)} = \frac{1}{i\hbar} \int_t^{t+\Delta t} dt' \text{Tr}_R[\hat{S}\hat{F}_R(t')^\dagger + \hat{F}_R(t')\hat{S}^\dagger, \tilde{\rho}_S(t) \otimes \tilde{\rho}_R(t)] \quad (3.51)$$

$$= \frac{1}{i\hbar} \int_t^{t+\Delta t} dt' [\hat{S}, \tilde{\rho}_S(t)] \otimes \text{Tr}_R\{\hat{F}_R(t')^\dagger, \tilde{\rho}_R(t)\} - h.c. \quad (3.52)$$

$$= \frac{1}{i\hbar} \int_t^{t+\Delta t} dt' [\hat{S}, \tilde{\rho}_S(t)] \otimes \langle \hat{F}_R(t')^\dagger \rangle - h.c. \quad (3.53)$$

²The Born approximation is actually slightly stronger than this. It states that the reservoir is large enough that the assumption of factorizability is good at all times as far as calculating the system dynamics is concerned.

$$= \frac{1}{i\hbar} \int_t^{t+\Delta t} dt' \underbrace{[\hat{S}\langle \hat{F}_R(t')^\dagger \rangle + \hat{S}^\dagger \langle \hat{F}_R(t') \rangle, \tilde{\rho}_S(t)]}_{\hat{H}'_S}. \quad (3.54)$$

Since the reservoir is large and does not change much under the influence of the system, $\langle \hat{F}_R(t')^\dagger \rangle$ is essentially a constant. The effect of the first term may thereby be interpreted an addition to the system Hamiltonian, $\hat{H}_S + \hat{H}'_S$. In many cases including the atom-field interaction, $\langle \hat{F}_R(t')^\dagger \rangle = 0$, and the first term vanishes altogether.

The second term, $\Delta\tilde{\rho}_S^{(2)}$, is responsible for the nontrivial effects of the reservoir. Expanding out the commutators of the interaction Hamiltonian $\tilde{H}_{SR}(t) = \hat{F}_R(t)\hat{S}^\dagger + \hat{F}_R(t)^\dagger\hat{S}$, we find

$$\begin{aligned} \Delta\tilde{\rho}_S^{(2)} &= \frac{1}{(i\hbar)^2} \int_t^{t+\Delta t} dt' \int_t^{t'} dt'' \text{Tr}_R[\hat{F}_R(t')\hat{S}^\dagger + \hat{F}_R(t')^\dagger\hat{S}, \\ &\quad [\hat{F}_R(t'')\hat{S}^\dagger + \hat{F}_R(t'')^\dagger\hat{S}, \tilde{\rho}(t'')]] \end{aligned} \quad (3.55)$$

$$\begin{aligned} &\approx \frac{1}{(i\hbar)^2} \int_t^{t+\Delta t} dt' \int_t^{t'} dt'' \text{Tr}_R[\hat{F}_R(t')\hat{S}^\dagger + \hat{F}_R(t')^\dagger\hat{S}, \\ &\quad [\hat{F}_R(t'')\hat{S}^\dagger + \hat{F}_R(t'')^\dagger\hat{S}, \tilde{\rho}_S(t)\tilde{\rho}_R(t)]]. \end{aligned} \quad (3.56)$$

The integrand can be further expanded out to yield

$$\begin{aligned} &\text{Tr}_R \left\{ (\hat{F}_R(t')\hat{S}^\dagger + \hat{F}_R(t')^\dagger\hat{S}) (\hat{F}_R(t'')\hat{S}^\dagger + \hat{F}_R(t'')^\dagger\hat{S}) \tilde{\rho}_S(t)\tilde{\rho}_R(t) \right\} \\ &- \text{Tr}_R \left\{ (\hat{F}_R(t')\hat{S}^\dagger + \hat{F}_R(t')^\dagger\hat{S}) \tilde{\rho}_S(t)\tilde{\rho}_R(t) (\hat{F}_R(t'')\hat{S}^\dagger + \hat{F}_R(t'')^\dagger\hat{S}) \right\} \\ &- \text{Tr}_R \left\{ (\hat{F}_R(t'')\hat{S}^\dagger + \hat{F}_R(t'')^\dagger\hat{S}) \tilde{\rho}_S(t)\tilde{\rho}_R(t) (\hat{F}_R(t')\hat{S}^\dagger + \hat{F}_R(t')^\dagger\hat{S}) \right\} \\ &+ \text{Tr}_R \left\{ \tilde{\rho}_S(t)\tilde{\rho}_R(t) (\hat{F}_R(t'')\hat{S}^\dagger + \hat{F}_R(t'')^\dagger\hat{S}) (\hat{F}_R(t')\hat{S}^\dagger + \hat{F}_R(t')^\dagger\hat{S}) \right\} \end{aligned} \quad (3.57)$$

We will evaluate it in terms of two-time correlation functions of the reservoir operators, defined by

$$g^{--}(t', t'') = \text{Tr}_R[\hat{F}_R(t')\hat{F}_R(t'')\tilde{\rho}_R] = \text{Tr}_R[\hat{F}_R(t'')\tilde{\rho}_R\hat{F}_R(t')] \quad (3.58)$$

$$g^{+-}(t', t'') = \text{Tr}_R[\hat{F}_R(t')^\dagger\hat{F}_R(t'')\tilde{\rho}_R] = \text{Tr}_R[\hat{F}_R(t'')\tilde{\rho}_R\hat{F}_R(t')^\dagger] \quad (3.59)$$

$$g^{-+}(t', t'') = \text{Tr}_R[\hat{F}_R(t')\hat{F}_R(t'')^\dagger\tilde{\rho}_R] = \text{Tr}_R[\hat{F}_R(t'')^\dagger\tilde{\rho}_R\hat{F}_R(t')] \quad (3.60)$$

$$g^{++}(t', t'') = \text{Tr}_R[\hat{F}_R(t')^\dagger\hat{F}_R(t'')^\dagger\tilde{\rho}_R] = \text{Tr}_R[\hat{F}_R(t'')^\dagger\tilde{\rho}_R\hat{F}_R(t')^\dagger], \quad (3.61)$$

where the second line when we cyclically permute reservoir operators.

Expanding out the integrand 3.57, we obtain

$$\begin{aligned} & g^{--}(t', t'') \hat{S}^\dagger \hat{S}^\dagger \tilde{\rho}_S(t) + g^{-+}(t', t'') \hat{S}^\dagger \hat{S} \tilde{\rho}_S(t) + g^{+-}(t', t'') \hat{S} \hat{S}^\dagger \tilde{\rho}_S(t) + g^{++}(t', t'') \hat{S} \hat{S} \tilde{\rho}_S(t) \\ & - g^{--}(t'', t) \hat{S}^\dagger \tilde{\rho}_S(t) \hat{S}^\dagger - g^{-+}(t'', t') \hat{S} \tilde{\rho}_S(t) \hat{S}^\dagger - g^{+-}(t'', t') \hat{S}^\dagger \tilde{\rho}_S(t) \hat{S} - g^{++}(t'', t') \hat{S} \tilde{\rho}_S(t) \hat{S} \\ & - g^{--}(t', t'') \hat{S}^\dagger \tilde{\rho}_S(t) \hat{S}^\dagger - g^{-+}(t', t'') \hat{S} \tilde{\rho}_S(t) \hat{S}^\dagger - g^{+-}(t', t'') \hat{S}^\dagger \tilde{\rho}_S(t) \hat{S} - g^{++}(t', t'') \hat{S} \tilde{\rho}_S(t) \hat{S} \\ & + g^{--}(t'', t') \tilde{\rho}_S(t) \hat{S}^\dagger \hat{S}^\dagger + g^{-+}(t'', t') \tilde{\rho}_S(t) \hat{S}^\dagger \hat{S} + g^{+-}(t'', t') \tilde{\rho}_S(t) \hat{S} \hat{S}^\dagger + g^{++}(t'', t') \tilde{\rho}_S(t) \hat{S} \hat{S}. \end{aligned} \quad (3.62)$$

Noting that

$$g^{--}(t', t'')^* = \text{Tr}_R[\hat{F}_R(t') \hat{F}_R(t'') \tilde{\rho}_R]^\dagger \quad (3.63)$$

$$= \text{Tr}_R[\tilde{\rho}_R \hat{F}_R(t'')^\dagger \hat{F}_R(t')^\dagger] \quad (3.64)$$

$$= g^{++}(t'', t') \quad (3.65)$$

and similarly

$$g^{+-}(t', t'')^* = \text{Tr}_R[\hat{F}_R(t')^\dagger \hat{F}_R(t'') \tilde{\rho}_R]^\dagger \quad (3.66)$$

$$= \text{Tr}_R[\tilde{\rho}_R \hat{F}_R(t'')^\dagger \hat{F}_R(t')] \quad (3.67)$$

$$= g^{+-}(t'', t'), \quad (3.68)$$

we can write the integrand 3.62 in a much more compact form:

$$\begin{aligned} & g^{--}(t', t'') \left(\hat{S}^\dagger \hat{S}^\dagger \tilde{\rho}_S(t) - \hat{S}^\dagger \tilde{\rho}_S(t) \hat{S}^\dagger \right) + g^{-+}(t', t'') \left(\hat{S}^\dagger \hat{S} \tilde{\rho}_S(t) - \hat{S} \tilde{\rho}_S(t) \hat{S}^\dagger \right) \\ & + g^{+-}(t', t'') \left(\hat{S} \hat{S}^\dagger \tilde{\rho}_S(t) - \hat{S}^\dagger \tilde{\rho}_S(t) \hat{S} \right) + g^{++}(t', t'') \left(\hat{S} \hat{S} \tilde{\rho}_S(t) - \hat{S} \tilde{\rho}_S(t) \hat{S} \right) \\ & + h.c. \end{aligned} \quad (3.69)$$

This gives us the second term in our equation for $\Delta\tilde{\rho}_S$ in terms of the correlation functions:

$$\begin{aligned} \Delta\tilde{\rho}_S^{(2)} = & \frac{1}{(i\hbar)^2} \int_t^{t+\Delta t} dt' \int_t^{t'} dt'' \left(g^{--}(t', t'') \left(\hat{S}^\dagger \hat{S}^\dagger \tilde{\rho}_S(t) - \hat{S}^\dagger \tilde{\rho}_S(t) \hat{S}^\dagger \right) \right. \\ & + g^{-+}(t', t'') \left(\hat{S}^\dagger \hat{S} \tilde{\rho}_S(t) - \hat{S} \tilde{\rho}_S(t) \hat{S}^\dagger \right) + g^{+-}(t', t'') \left(\hat{S} \hat{S}^\dagger \tilde{\rho}_S(t) - \hat{S}^\dagger \tilde{\rho}_S(t) \hat{S} \right) \\ & \left. + g^{++}(t', t'') \left(\hat{S} \hat{S} \tilde{\rho}_S(t) - \hat{S} \tilde{\rho}_S(t) \hat{S} \right) + h.c. \right). \end{aligned} \quad (3.70)$$

As an example, we can explicitly evaluate one of these correlators for an environment formed by the radiation field, where

$$g^{+-}(t', t'') = \hbar^2 \sum_{j,k} g_j^* g_k \langle \hat{a}_j^\dagger \hat{a}_k \rangle e^{i(\nu_j - \omega)t' - i(\nu_k - \omega)t''}. \quad (3.71)$$

If the radiation field is in a thermal state, $\langle \hat{a}_j^\dagger \hat{a}_k \rangle = \delta_{jk} \bar{n}_j$, so the correlator becomes

$$g^{+-}(t', t'') = \hbar^2 \sum_j |g_j|^2 \bar{n}_j e^{i(\nu_j - \omega)(t' - t'')}. \quad (3.72)$$

The two time correlation function now depends only on the difference in time, $t'' - t' = \tau$, and it is a sharply peaked function of τ whose width corresponds to the reservoir correlation time τ_c . In the limit that the radiation field volume $V \rightarrow \infty$, $\tau_c \rightarrow 0$, we recover the Wigner-Weisskopf approximation for which the correlator is a delta function in time. Note that for the radiation field, $g^{--} = g^{++} = 0$, and g^{-+} is the same as g^{+-} with $\langle \hat{a}_j^\dagger \hat{a}_j \rangle$ replaced by $\langle \hat{a}_j \hat{a}_j^\dagger \rangle = \langle \hat{a}_j^\dagger \hat{a}_j \rangle + 1$. Expressed in terms of correlation functions, the second term becomes

$$\Delta\tilde{\rho}_S^{(2)} = \frac{1}{(i\hbar)^2} \int_t^{t+\Delta t} dt' \int_t^{t'} dt'' \left\{ g^{+-}(t', t'') \left(\hat{S}\hat{S}^\dagger \tilde{\rho}_S - \hat{S}^\dagger \tilde{\rho}_S \hat{S} \right) + g^{-+}(t', t'') \left(\hat{S}^\dagger \hat{S} \tilde{\rho}_S - \hat{S} \tilde{\rho}_S \hat{S}^\dagger \right) \right\} + h.c., \quad (3.73)$$

where we have neglected contributions from g^{--} and g^{++} . The only significant time dependence enters through the sharply-peaked correlation functions. In the case of the radiation field we may evaluate the inner integral using the same procedure performed in the Wigner Weisskopf approximation, obtaining

$$-\frac{1}{\hbar^2} \int_t^{t'} dt'' g^{+-}(t', t'') = -\sum_j \int_t^{t'} dt' |g_j|^2 \bar{n}_j e^{i(\omega - \nu_j)(t'' - t')} \quad (3.74)$$

$$= -\pi \sum_j |g_j|^2 \bar{n}_j \delta(\nu_j - \omega) \quad (3.75)$$

$$= -\frac{\gamma}{2} \bar{n}(\omega). \quad (3.76)$$

Here we have neglected the energy shift arising from the principal part of the integral, because that can be incorporated into the bare system Hamiltonian. As mentioned above, the calculation for g^{-+} proceeds in the same manner, yielding

$$-\frac{1}{\hbar^2} \int_t^{t'} dt'' g^{-+}(t', t'') = -\frac{\gamma}{2} (\bar{n}(\omega) + 1). \quad (3.77)$$

The remaining integral over t' may be approximated by Δt - integrand because Δt is now small compared to the time variation of the integrand. Dividing through by Δt , we obtain a time-averaged differential equation for $\tilde{\rho}_S$:

$$\frac{\Delta\tilde{\rho}_S}{\Delta t} = -\frac{\gamma}{2} \bar{n}(\omega) \left(\hat{S}\hat{S}^\dagger \tilde{\rho}_S - \hat{S}^\dagger \tilde{\rho}_S \hat{S} \right) - \frac{\gamma}{2} (\bar{n}(\omega) + 1) \left(\hat{S}^\dagger \hat{S} \tilde{\rho}_S - \hat{S} \tilde{\rho}_S \hat{S}^\dagger \right) + h.c. \quad (3.78)$$

This result is known as the “master equation”, and it provides an essential tool for studying the evolution of open systems coupled to Markovian reservoirs. This formalism provides a method to properly treat non-unitary behavior in the system of interest. It can be seen, for example, that Eq. (3.78) preserves the trace of the density matrix ($\text{Tr } \hat{\rho} = 0$). While Eq. (3.78) describes a two-level atom interacting with a thermal state of the electromagnetic field, we note that it is possible to derive master equations for other types of interactions as well, *e.g.*, a harmonic oscillator interacting with an environment of other harmonic oscillators.

3.4 The master equation

3.4.1 Remarks on the generalized master equation

In the previous lecture we derived the equation governing the evolution of an open system coupled to a Markovian reservoir. In the Schrodinger picture, this so-called master equation takes the form

$$\begin{aligned}\frac{\Delta\hat{\rho}_S}{\Delta t} &= -\sum_p \frac{\gamma_p}{2} \bar{n} \left(\hat{S}_p \hat{S}_p^\dagger \hat{\rho}_S - \hat{S}_p^\dagger \hat{\rho}_S \hat{S}_p \right) + h.c. \\ &\quad - \sum_p \frac{\gamma_p}{2} (\bar{n} + 1) \left(\hat{S}_p^\dagger \hat{S}_p \hat{\rho}_S - \hat{S}_p \hat{\rho}_S \hat{S}_p^\dagger \right) + h.c. \\ &\quad + \frac{1}{i\hbar} [\hat{H}_S, \hat{\rho}_S].\end{aligned}\quad (3.79)$$

The system time dependence is built into the last term, and we have included a sum over different interactions with the reservoir. Explicitly, the system-reservoir interaction takes the form $\hat{H}_{SR} = \sum_p \hat{S}_p \hat{R}_p^\dagger + h.c.$, and each term has its associated rate γ_p . In order to incorporate multiple system-reservoir interaction terms, we implicitly make an assumption that the different terms are incoherent, so that the interference between them vanishes. While this requirement is satisfied most of the time, one should bear in mind that there exist cases where such interference is important.

Although Eq. (3.79) allows us to efficiently account for the effects of the reservoir, this added information comes with a computational price. Suppose that we are interested in studying the dynamics of an isolated n -level system. In the wavefunction approach, evolution of this system is governed by n differential equations for the state amplitudes $\{c_i(t)\}$. When the effect of the environment is included, the system must be described by the $\mathcal{O}(n^2)$ differential equations comprising Eq. (3.79). The large number of equations can complicate the mathematics, and we will frequently need more sophisticated tools to extract a solution.

One more caveat deserves attention: In our previous derivation, we assumed that the state of the universe was factorizable, i.e.

$$\tilde{\rho}(t') \approx \tilde{\rho}_S(t) \otimes \tilde{\rho}_R(t), \quad (3.80)$$

where $t' - t \leq \Delta t$. We made this statement with little justification, but we will now show that our assumption is valid for a reservoir with no memory, $\tau_c = 0$.

Suppose that the system and reservoir do not interact until a time $t = t_i$, so that for all times prior to t_i the universe density operator is factorizable. At some time $t > t_i$, we may certainly write

$$\tilde{\rho}(t) = \tilde{\rho}_S(t_i) \otimes \tilde{\rho}_R(t_i) + \tilde{\rho}_{corr}(t_i, t) \quad (3.81)$$

where $\tilde{\rho}_{corr}(t_i, t)$ depends on the correlations built up between the system and the reservoir *prior* to the time interval $t \rightarrow t + \Delta t$ for which we calculated the correlations. We will use perturbation theory to estimate the contributions to $\Delta\tilde{\rho}_S = \tilde{\rho}_S(t + \Delta t) - \tilde{\rho}_S(t)$ which we neglected by setting $\tilde{\rho}_{corr}(t_i, t) = 0$. To leading order,

$$\tilde{\rho}_{corr}(t_i, t) \approx \frac{1}{i\hbar} \int_{t_i}^t [\tilde{H}_{SR}(t'), \tilde{\rho}_S(t_i) \otimes \tilde{\rho}_R(t_i)], \quad (3.82)$$

so that the neglected change in the system density operator is

$$\Delta\tilde{\rho}_S \propto \int_{t_i}^t dt' \int_t^{t+\Delta t} dt'' \underbrace{\langle \tilde{H}_{SR}(t'') \tilde{H}_{SR}(t') \rangle}_{\propto \delta(t'' - t')} \quad (3.83)$$

Recall that the time correlation function for a reservoir with no memory is a delta function; since the time intervals for integration do not overlap, the delta function is zero everywhere within the region of integration. The contributions to $\Delta\hat{\rho}_S$ due to $\tilde{\rho}_{corr}(t_i, t)$ thus vanish to leading order (and all higher orders) for $\tau_c = 0$. In fact, a more rigorous analysis shows that the corrections scale as τ_c^2 .

We have now shown that a reservoir with no memory has a local interaction with the system; that is, it immediately forgets about all previous correlations and depends only on the current state. This amnesia implies irreversibility since information is lost (so entropy must increase). For practical purposes, irreversible vs. reversible dynamics will provide our boundary between system and environment. Any part of the environment which exhibits time reversibility we will include in the system even if we are not explicitly interested in its evolution.

We have highlighted two situations where the master equation may not suffice: (1) when there is interference between different interaction terms and (2) when the reservoir interaction is reversible. A more thorough discussion of the assumptions and approximations implicit in the master equation may be found in, *e.g.*, Cohen-Tannoudji *et al.*, “Atom-Photon Interactions”.

3.4.2 Example: The two-level atom

The master equation is frequently used to describe the evolution of a driven two-level system coupled to a dissipative environment. The coherent interaction with the driving field takes the form

$$\hat{H}_S = -\hbar\delta|2\rangle\langle 2| + \hbar\Omega^*|1\rangle\langle 2| + \hbar\Omega|2\rangle\langle 1|, \quad (3.84)$$

while the reservoir effects enter the density matrix equation:

$$\begin{aligned} \frac{\Delta\hat{\rho}_S}{\Delta t} &= -\frac{\gamma}{2}(\bar{n}+1)(\sigma_{22}\hat{\rho}_S - \sigma_{12}\hat{\rho}_S\sigma_{21}) + h.c. \\ &\quad -\frac{\gamma}{2}\bar{n}(\sigma_{11}\hat{\rho}_S - \sigma_{21}\hat{\rho}_S\sigma_{12}) + h.c. \\ &\quad + \frac{1}{i\hbar}[\hat{H}_S, \hat{\rho}_S], \end{aligned} \quad (3.85)$$

where we have used $\hat{S} = |1\rangle\langle 2| = \sigma_{12}$ in Eq. (3.79), and $\sigma_{ij} = |i\rangle\langle j|$. Taking the matrix elements $\langle i|\frac{\Delta\hat{\rho}_S}{\Delta t}|j\rangle = \dot{\rho}_{ij}$ yields four differential equations for the components of the density matrix,

$$\dot{\rho}_{22} = -\gamma(\bar{n}+1)\rho_{22} + \gamma\bar{n}\rho_{11} + i\Omega^*\rho_{21} - i\Omega\rho_{12} \quad (3.86)$$

$$\dot{\rho}_{11} = \gamma(\bar{n}+1)\rho_{22} - \gamma\bar{n}\rho_{11} - i\Omega^*\rho_{21} + i\Omega\rho_{12} \quad (3.87)$$

$$\dot{\rho}_{12} = -\frac{\gamma}{2}(2\bar{n}+1)\rho_{12} - i\delta\rho_{12} - i\Omega^*(\rho_{22} - \rho_{11}) \quad (3.88)$$

$$\dot{\rho}_{21} = -\frac{\gamma}{2}(2\bar{n}+1)\rho_{21} + i\delta\rho_{21} + i\Omega(\rho_{22} - \rho_{11}). \quad (3.89)$$

These equations are known as the “optical Bloch equations.” Note that only two of these equations are independent, since the evolution equations must preserve probability, $\rho_{11} + \rho_{22} = \text{Tr}[\hat{\rho}_S] = 1$, and hermiticity, $\rho_{12} = \rho_{21}^*$.

Three types of processes contribute to the system evolution described by Eq. (3.89):

- (1) coherent driving $\propto \Omega$,
- (2) thermal photons $\propto \gamma\bar{n}$, and
- (3) spontaneous emission $\propto \gamma$.

Coherent interactions are characteristic of the ideal two-level system introduced in previous lectures, and come from the system Hamiltonian terms.

Thermal photons lead to incoherent transitions in *both* directions, whereas spontaneous emission only allows population in ρ_{22} to leak into ρ_{11} :

$$\dot{\rho}_{22} = \gamma\bar{n}(\rho_{11} - \rho_{22}) - \gamma\rho_{22} + \dots \quad (3.90)$$

$$\dot{\rho}_{11} = \gamma\bar{n}(\rho_{22} - \rho_{11}) + \gamma\rho_{22} + \dots \quad (3.91)$$

Although incoherent processes can increase and decrease the populations ρ_{11} and ρ_{22} , they only decrease the off-diagonal terms. The decay rate of the coherences γ_{12} (defined through $\dot{\rho}_{12} = -\gamma_{12}\rho_{12} + \dots$) is related to the rate of population decay out of state $|1\rangle$, $\gamma_1 = \gamma\bar{n}$, and $|2\rangle$, $\gamma_2 = \gamma(\bar{n} + 1)$, by

$$\gamma_{12} = \frac{\gamma_1 + \gamma_2}{2} = \frac{2\bar{n} + 1}{2}\gamma = \gamma_{21}. \quad (3.92)$$

For multi-level atoms, this relation holds for any two states and their associated coherence, and only depends on the rates out of the states, not into them.

While we see that there is a coherence decay rate associated with population decay, in general there also exist processes which decrease the coherences without affecting the populations. These are typically incorporated phenomenologically into the master equation by setting

$$\gamma_{12} = \gamma_{21} = \frac{\gamma_1 + \gamma_2}{2} + \gamma_d, \quad (3.93)$$

where γ_d is the so-called decoherence or dephasing rate. Such decoherence can result from a variety of sources including, for example, finite linewidth of an applied laser field or atom-atom interactions.

3.4.3 Atomic response to a resonant field

We will consider two special cases to gain physical insight into the dynamics of an atom as it undergoes simultaneous coherent and incoherent pumping.

Weak applied field

For sufficiently small applied fields Ω , the master equation can be treated perturbatively. Since the populations change by terms $\propto \Omega^2$, to lowest order we may set $\rho_{11} \approx \rho_{11}^{(0)} + O(\Omega^2)$, $\rho_{22} \approx \rho_{22}^{(0)} + O(\Omega^2)$, and consider only the evolution of the coherences,

$$\dot{\rho}_{21} \approx -(\gamma_{21} - i\delta)\rho_{21} + i\Omega(\rho_{22}^{(0)} - \rho_{11}^{(0)}). \quad (3.94)$$

Since this equation is now linear in Ω , we may solve it by taking the Fourier transform of ρ_{21} and Ω ,

$$\rho_{21}(t) = \int d(\delta\nu) e^{-i\delta\nu t} \rho_{12}(\delta\nu) \quad (3.95)$$

$$\Omega(t) = \int d(\delta\nu) e^{-i\delta\nu t} \Omega(\delta\nu). \quad (3.96)$$

With this substitution, we find that in the weak field limit the coherence at frequency $\delta\nu$ is a Lorentzian with effective detuning $\delta + \delta\nu$:

$$\rho_{21}(\delta\nu) = \Omega(\delta\nu) \frac{i(\rho_{22}^{(0)} - \rho_{11}^{(0)})}{\gamma_{21} - i(\delta + \delta\nu)}. \quad (3.97)$$

This approach may be generalized to multilevel atoms, so that

$$\rho_{ij}(\delta\nu) = \Omega_{ij}(\delta\nu) \frac{i(\rho_{ii}^{(0)} - \rho_{jj}^{(0)})}{\gamma_{ij} - i(\delta_{ij} + \delta\nu)}, \quad (3.98)$$

whenever the populations ρ_{ii} and ρ_{jj} are essentially frozen in time. For atoms approximately in the ground state ($\rho_{11}^{(0)} \approx 1, \rho_{22}^{(0)} \approx 0$), the atomic response resembles that of a classical dipole, as the atom acquires a dipole moment linear in the field strength. On the other hand, for sufficiently large Ω the quantized nature of the atom becomes important. In this case the population in the upper state cannot be neglected and leads to effects like non-linearity of the atomic response and saturation.

Continuous-wave fields of arbitrary strength

When the applied field is constant in time, we expect that the system will undergo Rabi oscillations which are damped by the reservoir interaction. The decay terms drive the system into an equilibrium state after a time $\propto 1/\gamma_{21}$, and a steady-state description of the system is easily found by setting the time derivative of its density matrix elements to zero. Solving for the coherence,

$$\dot{\rho}_{21} = 0 \Rightarrow \rho_{21} = \frac{i\Omega(\rho_{22} - \rho_{11})}{\gamma_{21} - i\delta} \quad (3.99)$$

we then find the steady state population (for $\bar{n} = 0$)

$$\rho_{22} = \frac{R_{opt}}{\gamma + 2R_{opt}}, \quad (3.100)$$

where

$$R_{opt} = 2\gamma_{21} \left| \frac{\Omega}{\Gamma_{21}} \right|^2 \quad (3.101)$$

and $\Gamma_{21} = \gamma_{21} - i\delta$. R_{opt} acts like an incoherent pumping rate associated with the applied (coherent) field.

The pumping rate R_{opt} determines two important limits:

$$R_{opt} \ll \gamma \Rightarrow \rho_{22} \rightarrow 0 \quad (3.102)$$

$$R_{opt} \gg \gamma \Rightarrow \rho_{22} \rightarrow \frac{1}{2}. \quad (3.103)$$

In the first case, the coherent field is weak, so that the atom ends up in the ground state with almost unit probability. More specifically it can be seen that the population in the excited state is proportional to the field intensity in this limit ($\rho_{22} \propto |\Omega|^2$), and the perturbative weak-field approach is valid. In the second case the applied field leaves the atom in a statistical mixture of the ground and excited states with equal weight, and the atomic response is said to be saturated.

Note that the weak-field limit is sufficient but not necessary to disregard evolution of the coherences (*i.e.*, to set $\dot{\rho}_{21} \approx 0$); it is only required that $|\Omega|^2 \ll \gamma_{21}^2 + \delta^2$. The solution to ρ_{21} given by Eq. (3.99) is analogous to making an adiabatic approximation that the coherences adiabatically follow the population difference. Another way of saying this is that in the limit $|\Omega|^2 \ll \gamma_{21}^2 + \delta^2$, the populations change on a time scale much slower than the natural decay/oscillation time of the coherence. The resulting equations for the populations,

$$\dot{\rho}_{22} = -\gamma\rho_{22} + R_{opt}(\rho_{11} - \rho_{22}) \quad \text{with} \quad \dot{\rho}_{11} = -\dot{\rho}_{22}, \quad (3.104)$$

are known as the “rate equations.” They apply in situations when a coherence ρ_{21} is present, but its dynamics are unimportant. For example, the rate equations can be used to describe an atom interacting with incoherent radiation, since γ_{21} is very large in this case due to dephasing.

Chapter 4

Propagation of light in a resonant medium

We have now developed a formalism to describe coherent and incoherent interactions between atoms and light. These techniques will prove useful in understanding how a resonant light beam propagates through an atomic cloud. In particular, we have previously derived how the applied field induces coherences and transitions in the atomic system; if the system is to be self-consistent, we must also consider the effect of the induced atomic dipole back on the field.

An atom influences the applied field through its dipole moment

$$\langle \hat{d} \rangle = \mu \rho_{21} + \mu^* \rho_{12}. \quad (4.1)$$

A single atom has a very weak effect on a classical field, but a large ensemble of atoms can drastically affect light propagation, so we might seek to identify a macroscopic polarization associated with N atoms in a volume V by

$$P = \frac{N}{V} (\mu \rho_{21} + \mu^* \rho_{12}), \quad (4.2)$$

and solve for the density matrix components using the single-atom optical Bloch equations. However, a large ensemble of atoms may only be treated using our single-atom formalism if the atoms evolve independently. The assumption of independent atoms is valid provided that

- (1) The atoms do not interact strongly on the timescales of the processes we wish to describe.
- (2) Each atom is damped by its own reservoir. More quantitatively, the atoms must be far enough apart $|r_i - r_j| > \lambda$ that we may neglect interference from two atoms interacting with the same mode of the reservoir.

(3) The applied field is classical.

Mathematically, atoms comprising an atomic ensemble are independent when the ensemble density matrix may be factorized into a direct product of individual atomic density matrices,

$$\hat{\rho}_{ensemble} = \prod_{j=1}^N \hat{\rho}^{(1)} \otimes \dots \otimes \hat{\rho}^{(N)}. \quad (4.3)$$

Since our fields may vary in space as well as time, it is convenient to define a macroscopic polarization,

$$P(r_i) = \frac{N_i}{V_i} \sum_{r_j \in V_i} (\mu \rho_{21}(r_j) + \mu^* \rho_{12}(r_j)), \quad (4.4)$$

which depends on the total dipole moment of the set of N_i atoms at positions $\{r_j\}$ within a small volume V_i centered at position r_i . Using the optical Bloch equations, we can calculate the polarization for a given field; self-consistency requires that this polarization then act as a source term in the Maxwell equations governing light propagation through the atomic cloud:

$$\nabla \times \mathbf{E} = -\frac{\partial \mathbf{B}}{\partial t} \quad (4.5)$$

$$\nabla \times \mathbf{B} = \frac{1}{c^2} \frac{\partial}{\partial t} \left(\mathbf{E} + \frac{1}{\epsilon_0} \mathbf{P} \right). \quad (4.6)$$

In principle, we could now self-consistently calculate the evolution of the atomic medium and applied light field. In practice, we will typically deal with nearly monochromatic light fields, for which a considerable simplification can be obtained by using the slowly-varying envelope approximation.

4.1 The slowly-varying envelope approximation

We can rewrite the Maxwell equations (in the absence of unbound charges and currents) as a wave equation for \mathbf{E} : ¹

$$\nabla^2 \mathbf{E} - \frac{1}{c^2} \frac{\partial^2 \mathbf{E}}{\partial t^2} = \frac{1}{\epsilon_0 c^2} \frac{\partial^2 \mathbf{P}}{\partial t^2}. \quad (4.10)$$

¹Using $\nabla \times (\nabla \times \mathbf{A}) = \nabla(\nabla \cdot \mathbf{A}) - \nabla^2 \mathbf{A}$ and the curl of Eq. (4.5) we get

$$\nabla \times (\nabla \times \mathbf{E}) = \nabla(\nabla \cdot \mathbf{E}) - \nabla^2 \mathbf{E} \quad (4.7)$$

$$= -\frac{1}{c^2} \frac{\partial^2}{\partial t^2} \left(\mathbf{E} + \frac{1}{\epsilon_0} \mathbf{P} \right). \quad (4.8)$$

The wave equation is second order in time and space, but application of the slowly varying envelope approximation can reduce it to first order. An electric field which is nearly monochromatic can be parameterized by an envelope function and its central frequency $\bar{\nu}$,

$$\mathbf{E}(r, t) = \mathcal{E}(r, t)e^{i\bar{k}z - i\bar{\nu}t} + c.c., \quad (4.11)$$

where \mathcal{E} varies slowly in z and t compared to the optical frequency $\bar{\nu}$ and wavevector $\bar{k} = \bar{\nu}/c$. We also introduce a slowly varying polarization amplitude,

$$\mathbf{P}(r, t) = \mathcal{P}(r, t)e^{i\bar{k}z - i\bar{\nu}t} + c.c. \quad (4.12)$$

Substituting these expressions into Eq. (4.10) and keeping only the lowest order derivatives of the envelopes, we find the evolution equation for the slowly varying amplitudes,

$$\frac{1}{2i\bar{k}}\nabla_{\perp}^2\mathcal{E} + \frac{\partial\mathcal{E}}{\partial z} + \frac{1}{c}\frac{\partial\mathcal{E}}{\partial t} = \frac{i\bar{k}}{2\epsilon_0}\mathcal{P} \quad (4.13)$$

The derivation of Eq. (4.13) governing the slowly varying amplitudes is straightforward. Using the derivatives of the electric field and polarization:

$$\nabla^2\mathbf{E} = \left(\nabla^2\mathcal{E} + 2i\bar{k}\frac{\partial}{\partial z}\mathcal{E} - \bar{k}^2\mathcal{E} \right) e^{i\bar{k}z - i\bar{\nu}t} + c.c. \quad (4.14)$$

$$\frac{\partial^2}{\partial t^2}\mathbf{E} = \left(\frac{\partial^2}{\partial t^2}\mathcal{E} - 2i\bar{\nu}\frac{\partial}{\partial t}\mathcal{E} - \bar{\nu}^2\mathcal{E} \right) e^{i\bar{k}z - i\bar{\nu}t} + c.c. \quad (4.15)$$

$$\frac{\partial^2}{\partial t^2}\mathbf{P} = \left(\frac{\partial^2}{\partial t^2}\mathcal{P} - 2i\bar{\nu}\frac{\partial}{\partial t}\mathcal{P} - \bar{\nu}^2\mathcal{P} \right) e^{i\bar{k}z - i\bar{\nu}t} + c.c. \quad (4.16)$$

we substitute into the wave equation to find

$$\nabla^2\mathcal{E} + 2i\bar{k}\frac{\partial}{\partial z}\mathcal{E} - \bar{k}^2\mathcal{E} - \frac{1}{c^2}\left(\frac{\partial^2}{\partial t^2}\mathcal{E} - 2i\bar{\nu}\frac{\partial}{\partial t}\mathcal{E} - \bar{\nu}^2\mathcal{E}\right) = \quad (4.17)$$

$$\frac{1}{\epsilon_0 c^2}\left(\frac{\partial^2}{\partial t^2}\mathcal{P} - 2i\bar{\nu}\frac{\partial}{\partial t}\mathcal{P} - \bar{\nu}^2\mathcal{P}\right). \quad (4.18)$$

In the absence of unbound charges, $\nabla \cdot \mathbf{E} = 0$, so we obtain the wave equation

$$\nabla^2\mathbf{E} - \frac{1}{c^2}\frac{\partial^2}{\partial t^2}\mathbf{E} = \frac{1}{\epsilon_0 c^2}\frac{\partial^2}{\partial t^2}\mathbf{P}. \quad (4.9)$$

Taking $\bar{\nu} = c\bar{k}$, and noting that in the slowly varying envelope approximation

$$|\bar{\nu}\mathcal{P}| \gg |\frac{\partial}{\partial t}\mathcal{P}| \quad (4.19)$$

$$|\bar{\nu}\mathcal{E}| \gg |\frac{\partial}{\partial t}\mathcal{E}| \quad (4.20)$$

$$|\bar{k}\mathcal{E}| \gg |\frac{\partial}{\partial z}\mathcal{E}|, \quad (4.21)$$

(4.22)

the relevant terms reduce to

$$\nabla_{\perp}^2\mathcal{E} + 2i\bar{k}\frac{\partial}{\partial z}\mathcal{E} + \frac{1}{c^2}2i\bar{\nu}\frac{\partial}{\partial t}\mathcal{E} = -\frac{1}{\epsilon_0 c^2}\bar{\nu}^2\mathcal{P}, \quad (4.23)$$

or

$$\frac{1}{2i\bar{k}}\nabla_{\perp}^2\mathcal{E} + \frac{\partial}{\partial z}\mathcal{E} + \frac{1}{c}\frac{\partial}{\partial t}\mathcal{E} = \frac{i\bar{k}}{2\epsilon_0}\mathcal{P}. \quad (4.24)$$

Two properties of this equation should be noted:

(1) In the first term, $\nabla_{\perp}^2 = \frac{\partial^2}{\partial x^2} + \frac{\partial^2}{\partial y^2}$ leads to transverse effects such as focussing or diffraction which cannot in general be neglected. However, for a plane wave there is no transverse spatial variation so the first term vanishes and we obtain

$$\frac{\partial}{\partial z}\mathcal{E} + \frac{1}{c}\frac{\partial}{\partial t}\mathcal{E} = \frac{i\bar{k}}{2\epsilon_0}\mathcal{P}. \quad (4.25)$$

(2) The slowly varying polarization \mathcal{P} is proportional to the positive-frequency component of the dipole operator in the rotating frame. For example, a two level atom leads to a polarization $\mathcal{P} = (N/V)\mu\rho_{21}(z)e^{-i\bar{k}z}$. (Note that $\rho_{21}(z)$ itself is driven by the local electric field, which contains a fast phase term $e^{i\bar{k}z}$ so that \mathcal{P} is in fact slowly varying in space.)

Generalizations of the SVEA

Our derivation of the slowly varying envelope approximation can be generalized to include multiple optical frequencies. To illustrate this idea, we will consider the example of atomic interactions with an optical frequency comb. This periodic train of short optical pulses can be represented in the Fourier domain by a comb of harmonics, so that the electric field may be written

$$E = \sum_n \mathcal{E}_n(z, t) e^{inkz - i\nu_n t}. \quad (4.26)$$

The spacing between harmonics $\nu_{n+1} - \nu_n$ determines the repetition rate of the pulses, while the bandwidth occupied by the set of harmonics determines

the duration of each pulse. Provided that each harmonic has an envelope $\mathcal{E}_n(z, t)$ which varies slowly in space and time, we can use an extension of the SVEA. Defining the polarization harmonics by

$$P = \sum_n \mathcal{P}_n(z, t) e^{inkz - i\nu_n t}, \quad (4.27)$$

the propagation equation becomes a set of equations for each harmonic component

$$\frac{1}{2ik} \nabla_{\perp}^2 \mathcal{E}_n + \frac{\partial}{\partial z} \mathcal{E}_n + \frac{1}{c} \frac{\partial}{\partial t} \mathcal{E}_n = \frac{i\bar{k}}{2\epsilon_0} \mathcal{P}_n. \quad (4.28)$$

This treatment applies to arbitrarily short pulses, since there is no restriction on the number of harmonics included. Note, however, that in general the atomic response will act to couple different harmonics, i.e. \mathcal{P}_n will depend on all components $\mathcal{E}_{n'}$, so the coupled Maxwell-Bloch equations may be quite complicated to solve.

4.2 Linear optical propagation

The simplest possible case of light propagation in a resonant field consists of an applied field sufficiently weak that the atoms only respond to it linearly. We found earlier that when the applied field is weak, perturbation theory may be used to solve exactly for the atomic density matrix components in the Fourier domain. We shall take a similar approach here, where the Fourier components of the polarization may be written in terms of the Fourier components of the off-diagonal elements of the (two-level) atomic density matrix,

$$\mathcal{P}(\delta\nu) = \frac{N}{V} \mu \rho_{21}(\delta\nu) e^{-i\bar{k}z}. \quad (4.29)$$

If the atoms respond linearly, the polarization must be proportional to the applied field. The proportionality constant defines the susceptibility,

$$\chi(\delta\nu) = \frac{\mathcal{P}(\delta\nu)}{\epsilon_0 \mathcal{E}(\delta\nu)}. \quad (4.30)$$

This quantity χ entirely characterizes the atom-photon interaction in the linear regime, and no further information is needed to find an exact solution.

For plane wave propagation (where transverse effects may be disregarded), the SVEA equation reduces to

$$\frac{\partial \mathcal{E}}{\partial z} + \frac{1}{c} \frac{\partial \mathcal{E}}{\partial t} = \frac{i\bar{k}}{2\epsilon_0} \mathcal{P}. \quad (4.31)$$

This first order equation may be trivially solved by moving to the Fourier domain,

$$\frac{\partial \mathcal{E}}{\partial z} = \frac{i\delta\nu}{c} \mathcal{E} + \frac{i\bar{k}}{2} \underbrace{\chi(\delta\nu)}_{\propto \mathcal{P}} \mathcal{E}, \quad (4.32)$$

where the frequency components of the electric field obey

$$\mathcal{E}(\delta\nu, z) = \mathcal{E}(\delta\nu, 0) e^{iz(\delta\nu/c + \bar{k}\chi(\delta\nu)/2)}. \quad (4.33)$$

By transforming back to the time domain, we obtain a general solution for linear propagation,

$$\mathcal{E}(t, z) = \int d(\delta\nu) e^{-i\delta\nu t} \mathcal{E}(\delta\nu, 0) e^{iz(\delta\nu/c + \bar{k}\chi(\delta\nu)/2)}. \quad (4.34)$$

This solution tells us that, given the spectrum of the field at some position in space, we can decompose the field into frequency components, propagate each frequency component separately, and then transform back to the time domain to obtain the full solution. Note that we only need $\chi(\delta\nu)$ to solve the linear propagation problem exactly. This expression encompasses three main effects:

- (1) Absorption arises from the imaginary part of the susceptibility.
- (2) Refraction is caused by the real part of the susceptibility.
- (3) Dispersion results from frequency dependence of the susceptibility.

4.2.1 Absorption and refraction

The effects of absorption and refraction can be illustrated by considering a resonant, continuous-wave field with a delta function frequency distribution, $\mathcal{E}(\delta\nu) \propto \delta(\delta\nu)$, so that

$$\mathcal{E}(t, z) = \mathcal{E} e^{i\bar{k}\chi(0)z/2}. \quad (4.35)$$

In general χ may be a complex quantity, and its real and imaginary parts have qualitatively different effects on the propagating field. In particular, $\text{Im}[\chi]$ leads to exponential attenuation or amplification of the beam intensity with distance at a rate

$$\alpha = \bar{k} \text{Im}[\chi(0)]. \quad (4.36)$$

The real component $\text{Re}[\chi]$ shifts the phase of the field linearly with distance, which can be understood as a modification of the wavevector $\bar{k} \rightarrow \bar{k} + \bar{k}\text{Re}[\chi]/2$, or a change in the index of refraction

$$n = 1 + \frac{\text{Re}[\chi(0)]}{2}. \quad (4.37)$$

Note that these formulae are only valid when the slowly varying envelope approximation holds, i.e. $|\text{Im}[\chi(0)]|, |\text{Re}[\chi(0)]| \ll 1$.

4.2.2 Dispersion

If the applied field has a finite bandwidth, the frequency dependence of the susceptibility begins to matter. For nearly monochromatic fields, the susceptibility may be expanded around its resonant value,

$$\chi(\delta\nu) \approx \chi(0) + \frac{d\chi}{d\nu}\delta\nu + \dots \quad (4.38)$$

Each term leads to different effects: the first corresponds to refraction, the second to group velocity, the third to group velocity dispersion, and so on. For example, if we keep only the second order terms, we find

$$\mathcal{E}(t, z) = \int d(\delta\nu) \mathcal{E}(\delta\nu, 0) e^{-i\delta\nu t} e^{iz(\delta\nu/c + \bar{k}(\chi(0) + \frac{d\chi}{d\nu}\delta\nu)/2)} \quad (4.39)$$

$$= e^{iz\bar{k}\chi(0)/2} \int d(\delta\nu) \mathcal{E}(\delta\nu, 0) e^{-i\delta\nu(t-z/v_g)} \quad (4.40)$$

$$= e^{iz\bar{k}\chi(0)/2} \mathcal{E}(t - z/v_g, z = 0), \quad (4.41)$$

so the envelope propagates at the so-called group velocity

$$v_g = \frac{c}{1 + \frac{\bar{\nu}}{2} \frac{d\chi}{d\nu}}. \quad (4.42)$$

4.2.3 Two level systems

Consider light propagation through a dilute gas of identical, noninteracting two-level atoms. In the steady state, we can solve the optical Bloch equations for the off-diagonal density matrix elements to obtain the polarization and thus the susceptibility,

$$\chi(\delta\nu) = i \frac{N}{V} \frac{\mu^2}{\hbar\epsilon_0} (\rho_{11}^0 - \rho_{22}^0) \frac{1}{\gamma_{12} - i\delta\nu}. \quad (4.43)$$

Clearly, the susceptibility exhibits a Lorentzian lineshape with linewidth γ_{12} . Identifying the dipole moment with the spontaneous emission rate ($\gamma = \frac{\mu^2 k_0^3}{3\pi\epsilon_0\hbar}$ and $k_0 = 2\pi/\lambda$), we can also express the susceptibility as

$$\chi(\delta\nu) = i \frac{3}{8\pi^2} \frac{N}{V} \lambda^3 (\rho_{11}^0 - \rho_{22}^0) \frac{\gamma}{\gamma_{12} - i\delta\nu}. \quad (4.44)$$

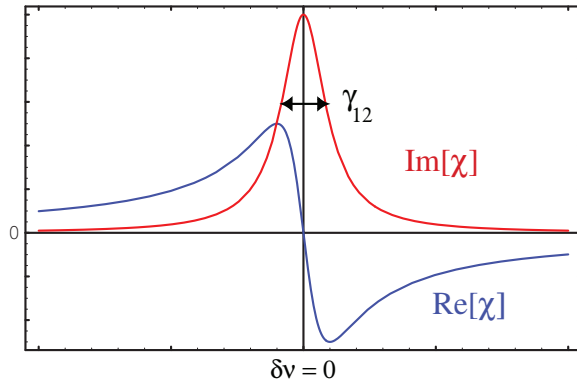


Figure 4.1: The real (refractive) and imaginary (absorptive) parts of the susceptibility for a two-level atom near resonance

Resonant fields

The magnitude of the susceptibility on resonance is

$$\chi(0) = i \frac{3}{8\pi^2} \frac{N}{V} \lambda^3 \frac{\gamma}{\gamma_{12}}. \quad (4.45)$$

Here we have set $\rho_{11}^0 = 1, \rho_{22}^0 = 0$, since it is in the regime where the upper state is negligibly populated that the atom responds linearly to the field. Since $\chi(0)$ is purely imaginary, there is no refraction on resonance, but there is absorption. The electric field amplitude propagates as

$$\mathcal{E}(z) = \mathcal{E}(0)e^{(-\text{Im}[\chi(0)] + i\text{Re}[\chi(0)])\bar{k}z/2} \quad (4.46)$$

and we define the corresponding intensity loss

$$I(z) = I(0)e^{-N\tilde{\sigma}z/V} \quad (4.47)$$

in terms of the absorption cross-section

$$\tilde{\sigma} = \frac{3}{4\pi} \lambda^2 \frac{\gamma}{\gamma_{12}} \quad (4.48)$$

$$\rightarrow \frac{3}{2\pi} \lambda^2 \text{ for purely radiative broadening.} \quad (4.49)$$

Surprisingly, in the case of radiative broadening the resonant cross section is independent of the atomic dipole moment and depends only on λ^2 ; this maximal absorption cross section is known as the “unitary limit”.

Far-detuned fields

Far from resonance, $\delta\nu \gg \gamma_{12}$, the imaginary (absorptive) component $\text{Im}[\chi] \propto 1/\delta\nu^2$ is much smaller than the real (reactive) component $\text{Re}[\chi] \propto 1/\delta\nu$, so the medium is almost entirely refractive and causes little absorption.

4.2.4 Line-broadening mechanisms

The existence of the unitary limit shows that different line broadening mechanisms (e.g. radiative vs non-radiative) can have different effects on the behavior of a system. It is particularly important to distinguish between processes which affects every atom equally and processes which broaden the linewidth of an ensemble but not its constituent atoms. The former “homogeneous” linewidth may not be visible in an ensemble exhibiting the latter “inhomogenous” broadening. Two important examples of systems exhibiting inhomogeneous broadening are

- (1) Optical emitters (e.g. color centers or quantum dots) in a solid state environment. Local fields have a strong influence on the optical transitions, so each emitter will exhibit different transition strengths and frequencies.
- (2) Atoms with a thermal velocity distribution. The Doppler effect shifts their resonant frequency, so each atom interacts differently with applied fields.

Doppler broadening

To illustrate how inhomogenous broadening affects linear optical propagation, we will examine the Doppler broadened atoms in more detail. In particular, we consider atoms in a thermal gas which are illuminated in the z direction by a field of frequency ν . Each atom experiences an apparent frequency $\nu - kv_z + \mathcal{O}(v^2)$ which is Doppler shifted due to the atomic velocity v_z . Equivalently, one can view this as a shift in the atomic resonance frequency $\omega \rightarrow \omega + kv_z$. For a Doppler-broadened medium an incident light beam will only be on resonance with a subset of atoms with the appropriate velocity class, but the absorption spectrum will be very broad, with width on order kv_T where v_T is the characteristic velocity corresponding to the atomic temperature. In order to calculate the susceptibility, we will determine the atomic response of each velocity class, and then sum over all velocity classes. The susceptibility is thus approximately

$$\chi(\delta\nu) \approx \int dv_z \frac{n(v_z)}{\gamma_{12} - i(\delta\nu - kv_z)} \quad (4.50)$$

where the thermal velocity distribution is

$$n(v_z) = \frac{N}{V} e^{-v_z^2/v_T^2} \frac{1}{\sqrt{\pi} v_T}. \quad (4.51)$$

The integral in Eq. (4.50) cannot be solved exactly, but we will consider two limiting cases where it can be approximately evaluated. For very cold atoms, $\gamma_{12} \gg kv_T$, there is no inhomogeneous broadening, and the observed ensemble absorption spectrum is Lorentzian, matching the intrinsic atomic linewidth. In the opposite limit, inhomogeneous broadening dominates, and the ensemble spectrum is Gaussian with width $\sim kv_T$. Note that inhomogeneous broadening also reduces the $\delta\nu = 0$ cross section by $\sim\gamma_{12}/kv_T$, so that

$$\sigma_{inhom.}(0) = \frac{3}{4\pi} \lambda^2 \frac{\sqrt{\pi}\gamma}{kv_T}. \quad (4.52)$$

As a quantitative example, atomic Rb at $T = 300\text{K}$ has an inhomogeneous linewidth of $\sim 500\text{MHz}$, which is far greater than its radiative linewidth of $\gamma \approx 5\text{MHz}$. For a Maxwell-Boltzmann thermal distribution of velocities, the Doppler width scales as the square root of the temperature. By laser cooling atoms (for example in a magneto-optical trap), it is possible to reduce the Doppler broadening to less than the radiative linewidth.

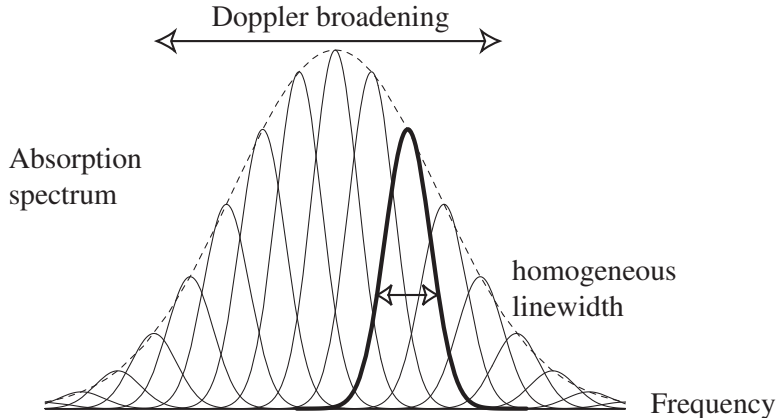


Figure 4.2: The absorption spectrum for a Doppler broadened ensemble of atoms is much broader than the absorption spectrum of a single velocity class, which has a linewidth set by the dephasing rate γ_{12} .

In general, however, it is impossible to tell whether an ensemble is homogeneously or inhomogeneously broadened with linear measurements. Such properties can be probed only by measuring the nonlinear response of the medium.

4.3 Nonlinear atomic response

The perturbative methods used in the linear regime cannot be used to treat strong applied fields. A general approach in the nonlinear regime requires a time-varying solution for the density matrix components as a function of the time-dependent applied field, $\Omega(t)$. As the system complexity increases, such solutions become increasingly difficult to obtain even numerically.

As a special case, we will consider only continuous-wave fields of fixed frequency, and look for the steady-state behavior of the system. To start with, consider a homogeneous ensemble of two-level atoms illuminated by photons with frequency detuned from atomic resonance by $\delta = \bar{\nu} - \omega$. Recall that the steady-state solution for the off-diagonal density matrix components is

$$\rho_{21} = -i \frac{\Omega}{\gamma_{12} - i\delta} (\rho_{11} - \rho_{22}). \quad (4.53)$$

For strong fields, we can no longer neglect changes in the atomic populations, so we should substitute (in the steady state)

$$\rho_{11} - \rho_{22} = \frac{\gamma}{\gamma + 2R_{opt}} \quad (4.54)$$

where

$$R_{opt} = \frac{2|\Omega|^2 \gamma_{12}}{\gamma_{12}^2 + \delta^2}. \quad (4.55)$$

We can use the steady state coherence to find the nonlinear susceptibility in the Fourier domain:

$$\chi_n(\delta) = \frac{\mathcal{P}(\delta)}{\epsilon_0 \mathcal{E}(\delta)} \quad (4.56)$$

$$= \frac{1}{\epsilon_0 \mathcal{E}(\delta)} \frac{N}{V} \mu \rho_{21}(\delta). \quad (4.57)$$

Proceeding in the same manner as before, we find that

$$\chi_n(\delta) = \frac{3}{8\pi^2} \frac{N}{V} \lambda^3 \frac{i\gamma}{\gamma_{12} - i\delta} \frac{\gamma}{\gamma + 2R_{opt}}. \quad (4.58)$$

Note that, whereas the linear susceptibility provided a complete solution to all time-dependent linearly propagating fields, the nonlinear susceptibility $\chi_n(\delta)$ we have just derived is applicable only to continuous wave, steady state solutions. For this special situation we are considering, the susceptibility determines the nonlinear propagation equation for the applied field. Since we are working with continuous wave fields, we may disregard the time derivatives in the wave equation, so the only remaining terms are

$$\frac{\partial \mathcal{E}}{\partial z} = i\bar{k}\chi_n(\delta)\mathcal{E} \quad (4.59)$$

$$= i\bar{k} \left(\frac{3}{8\pi^2} \frac{N}{V} \lambda^3 \frac{i\gamma}{\gamma_{12} - i\delta} \frac{\gamma}{\gamma + 2R_{opt}} \right) \mathcal{E}. \quad (4.60)$$

The nonlinear susceptibility is itself a function of the strength of the applied field $\Omega = \mu\mathcal{E}/\hbar$, which enters through R_{opt} . As the applied field grows, χ is diminished, an effect known as saturating absorption. In the limit of a weak field, $R_{opt} \ll \gamma$, this expression reduces to the linear susceptibility obtained earlier. We will now examine the nonlinear susceptibility in a few special cases.

Resonant fields

For a perfectly resonant field, $\delta = 0$, the real part of the susceptibility vanishes and the imaginary part becomes

$$\text{Im}[\chi_n(0)] = \frac{3}{8\pi^2} \frac{N}{V} \lambda^3 \frac{\gamma}{\gamma_{12}} \frac{1}{1+s} \quad (4.61)$$

where

$$s = \frac{4|\Omega|^2}{\gamma_{12}\gamma}. \quad (4.62)$$

When this saturation parameter s is large, $s \gg 1$, the applied field bleaches the medium, and the transmitted power grows nonlinearly as the incident intensity is increased. In this saturated regime, the spatial profile of absorption changes qualitatively from a linear decay in strong fields to the exponential decay characteristic of weak fields.

Far-detuned fields

It is possible to define a saturation parameter as a function of the detuning,

$$s = \frac{2R_{opt}}{\gamma}. \quad (4.63)$$

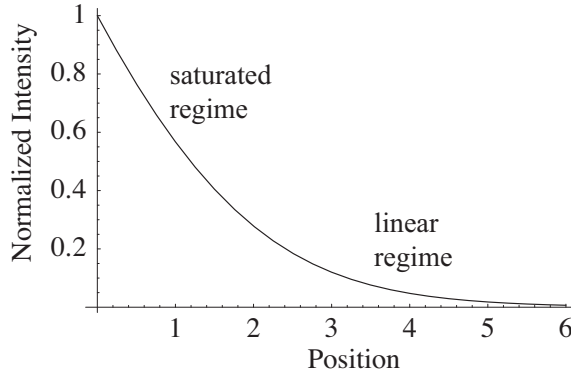


Figure 4.3: An incident field with intensity equal to the saturation intensity initially decays linearly with distance. Once the field is sufficiently weak that nonlinear effects are negligible, the intensity decays exponentially.

Since R_{opt} decreases as detuning increases, greater power is required to saturate an off-resonant transition. For very large detunings, $\delta \gg \Omega, \gamma$, the imaginary part of the susceptibility is negligible, with the real part given by

$$\chi_n \approx -\frac{3}{8\pi^2} \frac{N}{V} \lambda^3 \frac{\gamma}{\delta} \left(1 - \frac{4|\Omega|^2 \gamma_{12}}{\delta^2 \gamma} \right). \quad (4.64)$$

The refractive index of the medium is determined by $\text{Re}[\chi]$, and consequently depends on the intensity. The physics of an intensity dependent refractive index (known as the Kerr effect) may be captured by defining an index which is linear in intensity, $n = n_0 + n_2 I$. Such effects have important physical consequences, including intensity-dependent phase shifts which are often referred to as “self-phase modulation”. In addition, the medium will act as a lens for a beam with finite transverse extent, since the refractive index is a function of power and thus transverse position, leading to so-called self-focussing or de-focussing.

Weakly saturated regime

In some situations we will be working with relatively weak fields, and wish only to calculate the leading order corrections to linear propagation. In such cases, it is useful to expand the susceptibility

$$\chi_n = \chi + \chi^{(3)} |E|^2 + \dots, \quad (4.65)$$

where χ is the linear susceptibility and $\chi^{(3)}$ is the next order correction (at least for a system exhibiting inversion symmetry). In terms of the susceptibility for the two-level system, this expansion looks like:

$$\begin{aligned}\chi_n(\delta) &= \frac{3}{8\pi^2} \frac{N}{V} \lambda^3 \frac{i\gamma}{\gamma_{12} - i\delta} \frac{\gamma}{\gamma + 2R_{opt}} \\ &\approx \frac{3}{8\pi^2} \frac{N}{V} \lambda^3 \frac{i\gamma}{\gamma_{12} - i\delta} \left(1 - \frac{2R_{opt}}{\gamma}\right) \\ &\approx \frac{3}{8\pi^2} \frac{N}{V} \lambda^3 \frac{i\gamma}{\gamma_{12} - i\delta} - \left(\frac{3\lambda^3}{2\pi^2\hbar^2} \frac{N}{V} \frac{i}{\gamma_{12} - i\delta} \frac{|\mu|^2 \gamma_{12}}{\gamma_{12}^2 + \delta^2}\right) |E|^2,\end{aligned}$$

where we identify the first term as the linear susceptibility and the second term as the leading nonlinear correction.

Experimental considerations

For practical purposes, it is useful to estimate the intensity needed to saturate a transition at resonance. In a radiatively broadened system, $\gamma_{12} = \gamma/2$, $R_{opt} = 4|\Omega|^2/\gamma$, so the saturation threshold $s = 1$ corresponds to $8|\Omega|^2 \approx \gamma^2$, or an intensity of a few mW/cm² for the alkali atoms. In a Doppler broadened system, $k v_T \gg \gamma_{12}$, a much larger power is required, since an applied field satisfying $8|\Omega|^2 \approx \gamma^2$ will only saturate a velocity class of atoms. However, in this intermediate regime where a small subset of velocity groups are saturated, nonlinear spectroscopy such as pump-probe or hole-burning experiments may be performed with sub-Doppler resolution.

In practice, real systems can saturate much faster than these calculations would predict because the existence of other atomic levels means that the system doesn't necessarily decay back into its original state. For instance, consider an atom with two long-lived hyperfine levels and a third excited level. When a field is applied which is resonant with the transition from one of the hyperfine levels to the excited state, most of the atomic population will end up in the other hyperfine level, an effect known as optical pumping. Now saturation of the resonant transition only requires that R_{opt} exceed the (slow) decay between hyperfine levels, making it much easier to saturate. This example illustrates how the two-level model is often not a very good approximation, especially in situations related to nonlinear interactions of atoms with light.

4.3.1 Saturation spectroscopy

Saturation spectroscopy is an important example of incoherent nonlinear multi-photon interactions. It provides a simple method for probing the natural linewidth of an inhomogeneously broadened medium (unlike linear interactions which cannot distinguish between a homogeneously and inhomogeneously broadened resonance). Saturation spectroscopy is typically performed with two counterpropagating beams at the same frequency ν , near resonance with the atomic transition energy Δ . The beams create an electric field profile in the cloud of thermal atoms,

$$\mathbf{E} = \mathcal{E}_+ e^{-i\nu t + ikz} + \mathcal{E}_- e^{-i\nu t - ikz} + c.c, \quad (4.66)$$

where \mathcal{E}_+ represents a strong field in the forward direction and \mathcal{E}_- represents a weak field in the backward direction.

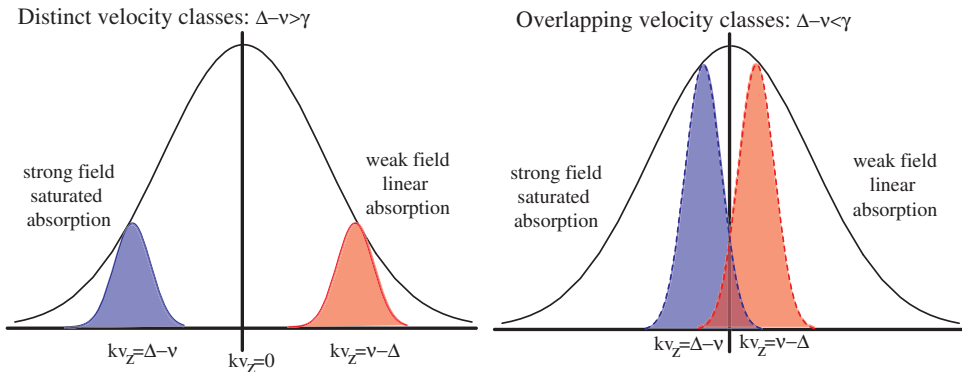


Figure 4.4: The forward and backward propagating beams interact with the velocity class of atoms for which they are resonant. The velocity classes begin to overlap as the optical frequency ν approaches the bare atomic resonance

Due to Doppler shifts in the thermal atoms, these two beams each interact with a certain velocity class. The strong field interacts with atoms satisfying $\nu = \Delta + kv_z$, saturating their transition, while the weak field interacts with atoms Doppler shifted by $\nu = \Delta - kv_z$. For generic detunings, $\nu \neq \Delta$, the two fields do not interact with the same group of atoms. As the frequency approaches the bare atomic resonance, however, $v_z \rightarrow 0$ and the two velocity classes begin to overlap. On resonance, both fields interact with stationary atoms. Consequently, we expect that the absorption

spectrum for the weak field \mathcal{E}_- will show sharp features near $\nu = \Delta$ due to stationary atoms saturated by the strong field.

Qualitative saturated absorption spectrum for the weak probe

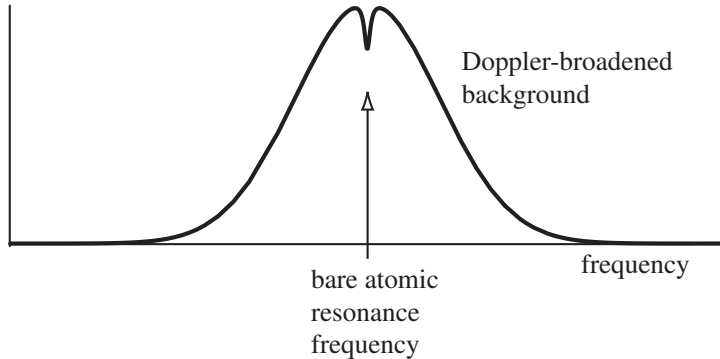


Figure 4.5: The absorption spectrum for the weak probe in the presence of a counterpropagating strong field of the same frequency.

The saturated absorption spectrum

The qualitative picture of saturated spectroscopy may be verified quantitatively by calculating the absorption coefficient for the probe beam, $\alpha_- = k\text{Im}[\chi_-] = k\text{Im}[P_-/\epsilon_0\mathcal{E}_-]$. To separate out the forward and backward propagating fields, we decompose the atomic polarization into two running waves in the $\pm\hat{z}$ direction,

$$P = P_+ e^{-i\nu t + ikz} + P_- e^{-i\nu t - ikz} + c.c. \quad (4.67)$$

In order to account for the inhomogenous Doppler broadening, this total polarization can be further broken down into contributions from atoms with different velocities. A particular velocity group v_z contributes a polarization $P^{(v_z)}$ proportional to the atomic coherence induced by the two counterpropagating beams,

$$\rho_{21}^{(v_z)} = \underbrace{\rho_{21}^{(v_z)+}}_{\sim\mathcal{E}_+} + \underbrace{\rho_{21}^{(v_z)-}}_{\sim\mathcal{E}_-}. \quad (4.68)$$

Once we have calculated the polarization for the appropriate density $n(v_z)$ of atoms, $P_{\pm}^{(v_z)} = n(v_z)\mu^*\rho_{21}^{(v_z)\pm}$, we can sum over velocity classes and divide by $\epsilon_0\mathcal{E}_{\pm}$ to obtain the probe beam susceptibility.

We can use our previous results from analysis of linear interactions to find this coherence $\rho_{21}^{(v_z)-}$ because the probe beam \mathcal{E}_- is weak. In particular, we find

$$\rho_{21}^{(v_z)-} \approx \frac{i\Omega_-(\rho_{11} - \rho_{22})^{(v_z)}}{\gamma_{12} - i(\delta + kv_z)}, \quad (4.69)$$

where $\Omega_{\pm} = \mu\mathcal{E}_{\pm}/\hbar$. Note that the detuning $\delta = \nu - \omega$ is Doppler shifted due to the atomic velocity along the axis of light propagation. Our previous linear analysis required no further calculations because the population distribution $\rho_{11} - \rho_{22}$ was independent of Ω_- for a sufficiently weak field. To accurately model the nonlinear aspects of saturated absorption spectroscopy, however, we must incorporate the effects of the strong field $|\Omega_+|^2$ on $\rho_{11} - \rho_{22}$. We saw earlier that strong, nonlinear interactions can saturate a transition by redistributing the atomic population:

$$(\rho_{11} - \rho_{22})^{(v_z)} = \frac{1}{1 + S(\delta - kv_z)}, \quad (4.70)$$

where the saturation parameter is

$$S(\delta - kv_z) = \frac{4|\Omega_+|^2(\gamma_{12}/\gamma)}{\gamma_{12}^2 + (\delta - kv_z)^2}. \quad (4.71)$$

Note that the sign of the Doppler shift is reversed for Ω_+ because it is propagating in the opposite direction to Ω_- . Substituting into Eq. (4.69), we obtain the backward-propagating coherence induced by Ω_+ and Ω_- in atoms with velocity v_z :

$$\rho_{21}^{(v_z)-} \approx \left(\frac{\gamma_{12}^2 + (\delta - kv_z)^2}{\gamma_{12}^2 + (\delta - kv_z)^2 + 4|\Omega_+|^2(\gamma_{12}/\gamma)} \right) \left(\frac{i\Omega_-}{\gamma_{12} - i(\delta + kv_z)} \right). \quad (4.72)$$

We are now prepared to calculate the absorption coefficient for the probe beam $\alpha_- = k \operatorname{Im}[\chi_-] = k \operatorname{Im}[P_-/\epsilon_0\mathcal{E}_-]$ by summing over contributions to the polarization from all atomic velocity classes,

$$P_- = \int dv_z \mu^* \rho_{21}^{(v_z)-} n(v_z), \quad (4.73)$$

where each velocity class is weighted by the thermal distribution $n(v_z)$.

$$\chi_- = \frac{|\mu|^2}{\epsilon_0\hbar} \int dv_z n(v_z) \frac{i}{\gamma_{12} - i(\delta + kv_z)} \left(1 - \frac{S(\delta - kv_z)}{1 + S(\delta - kv_z)} \right) \quad (4.74)$$

The first term describes the usual Doppler-broadened absorption of a weak probe; the second term describes the saturated effect we wish to calculate. By approximating the thermal velocity distribution as constant over the velocities which contribute to the saturated absorption dip, $n(v_z) = n$, we can calculate the integral of the second term in closed form. The resulting expression is rather convoluted, and to elucidate the effects of the strong field we will expand it to lowest order in Ω_+ :

$$\begin{aligned}\chi_- &\approx \frac{|\mu|^2}{\epsilon_0 \hbar} \int dv_z n(v_z) \frac{i}{\gamma_{12} - i(\delta + kv_z)} \left(1 - \frac{4|\Omega_+|^2(\gamma_{12}/\gamma)}{\gamma_{12}^2 + (\delta - kv_z)^2} \right) \\ &= \frac{|\mu|^2}{\epsilon_0 \hbar} \int dv_z n(v_z) \frac{i(\gamma_{12} + i(\delta + kv_z))}{\gamma_{12}^2 + (\delta + kv_z)^2} \left(1 - \frac{4|\Omega_+|^2(\gamma_{12}/\gamma)}{\gamma_{12}^2 + (\delta - kv_z)^2} \right)\end{aligned}$$

The saturated absorption feature is thus given by

$$\begin{aligned}\text{Im}[\chi_-]_{\text{sat}} &\approx -\frac{|\mu|^2}{\epsilon_0 \hbar} \int dv_z n \frac{\gamma_{12}}{\gamma_{12}^2 + (\delta + kv_z)^2} \frac{4|\Omega_+|^2(\gamma_{12}/\gamma)}{\gamma_{12}^2 + (\delta - kv_z)^2} \\ &= -\frac{|\mu|^2 n}{\epsilon_0 \hbar k} \frac{2\pi |\Omega_+|^2 (\gamma_{12}/\gamma)}{(\gamma_{12}^2 + \delta^2)},\end{aligned}\tag{4.75}$$

where we have used $n(v_z) = n$ and

$$\int_{-\infty}^{\infty} \frac{1}{1 + (x - a)^2} \frac{1}{1 + (x + a)^2} = \frac{\pi}{2(1 + a^2)}.\tag{4.76}$$

The expression for the saturated absorption feature, in the limit that Ω_+ is weak and $n(v_z)$ is slowly varying, indicates that we should see a sharp dip in the absorption with a characteristic width given by the Doppler-free linewidth γ_{12} .

Chapter 5

Coherent interactions in multi-level systems

In previous lectures we have concentrated on understanding the interaction of a two-level atom with a single quasi-monochromatic beam of light. We now turn to multi-level systems which interact with multiple optical fields. Such multi-photon processes can be roughly organized into three classes:

(1) Incoherent interactions: Atomic coherences (e.g. off-diagonal elements of the atomic reduced density matrix) are not important. One type of incoherent process which we have already seen is saturation spectroscopy, where one applied field modifies the atomic populations while the other field probes them.

(2) Coherent interactions: Atomic coherences are important, and two or more photons are required to generate them. A typical example of a coherent interaction is a Raman transition, where two photons can stimulate a dipole-forbidden transition via an excited state.

(3) Parametric interactions: No energy is exchanged between the light and the atoms, but the atoms mediate interactions between multiple light beams as in, for example, four-wave mixing.

In this chapter we will focus on the second type of multi-photon process, which involves the atomic coherences in addition to the atomic populations. By applying two or more fields, multi-photon interactions can drive dipole-forbidden transitions for which the associated atomic coherence has a very long lifetime. Typical configurations are illustrated in Figure 7.3.

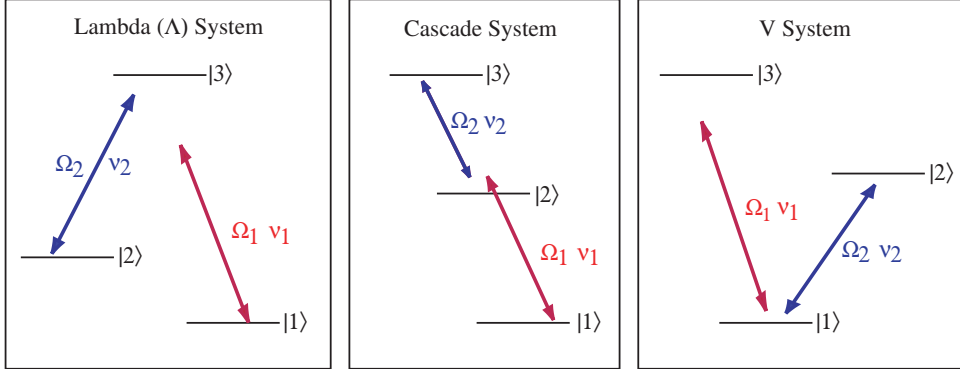


Figure 5.1: Examples of two photon Raman transitions for different configurations of energy levels and allowed transitions.

5.1 Raman transitions in the Λ level configuration

In the following discussion we will focus on the three-level Λ system illustrated in Figure 9.3, in which a single excited state mediates transitions between two lower-energy states. Since the transitions to the excited state are dipole allowed, radiative decay from the excited state must occur relatively quickly. However, transitions from $|2\rangle$ to $|1\rangle$ are dipole forbidden, so the metastable state $|2\rangle$ can have a very long lifetime. Although the radiative decay paths are much faster than the decay rate of the metastable state, it can be important to account for both types of decay to avoid spurious divergences.

5.1.1 The Schrodinger equation approach

By identifying the single-photon detunings Δ_1 and Δ_2 and the two-photon detuning $\delta = \Delta_1 - \Delta_2$, we can easily write down the Hamiltonian for this system in the appropriate rotating frame,

$$\hat{H} = -\Delta_1|3\rangle\langle 3| - \delta|2\rangle\langle 2| - (\Omega_1|3\rangle\langle 1| + \Omega_2|3\rangle\langle 2| + \Omega_1^*|1\rangle\langle 3| + \Omega_2^*|2\rangle\langle 3|), \quad (5.1)$$

where we have set the energy of $|1\rangle$ to zero. Neglecting decay terms for the moment, a general state of the form

$$|\psi\rangle = c_1(t)|1\rangle + c_2(t)|2\rangle + c_3(t)|3\rangle \quad (5.2)$$

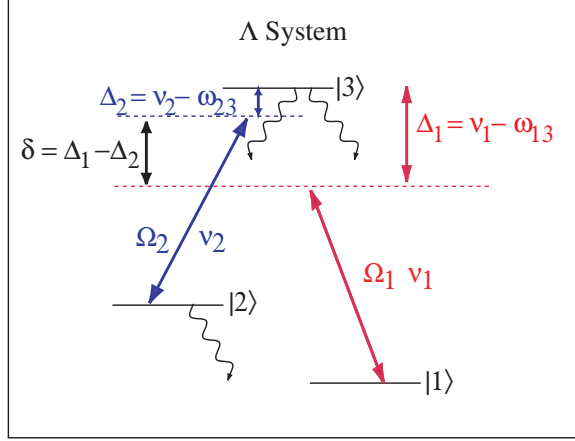


Figure 5.2: The Λ system under consideration, with the single- and two-photon detunings shown. Squiggly lines indicate possible decay paths

obeys the Schrodinger equation for the Hamiltonian, yielding equations of motion for the population amplitudes,

$$\dot{c}_1 = i\Omega_1^* c_3 \quad (5.3)$$

$$\dot{c}_2 = i\delta c_2 + i\Omega_2^* c_3 \quad (5.4)$$

$$\dot{c}_3 = i\Delta_1 c_3 + i\Omega_1 c_1 + i\Omega_2 c_2. \quad (5.5)$$

The Λ system has a particularly simple solution for large but similar single photon detunings $\Delta_1 \sim \Delta_2 = \Delta \gg \Omega_1, \Omega_2, \gamma_3, \delta$. Since Δ is much larger than all other time scales in the problem, to lowest order in $\Omega_{1,2}/\Delta$ the excited state amplitude will be constant, with

$$c_3 = -\frac{\Omega_1 c_1 + \Omega_2 c_2}{\Delta}. \quad (5.6)$$

Substituting c_3 back into the equations of motion, we obtain the evolution equations for the probability amplitudes of the lower two states:

$$\dot{c}_1 = -i\frac{|\Omega_1|^2}{\Delta}c_1 - i\frac{\Omega_2\Omega_1^*}{\Delta}c_2 \quad (5.7)$$

$$\dot{c}_2 = i(\delta - \frac{|\Omega_2|^2}{\Delta})c_2 - i\frac{\Omega_1\Omega_2^*}{\Delta}c_1. \quad (5.8)$$

This system behaves essentially as though the two levels $|1\rangle$ and $|2\rangle$ were coupled by a field with effective Rabi frequency

$$\Omega_{\text{eff}} = -\frac{\Omega_2^* \Omega_1}{\Delta}. \quad (5.9)$$

By absorbing a photon on transition ν_1 and emitting a photon of frequency ν_2 , population can be coherently transferred between the two ground states, leading to a large coherence $\rho_{21} = c_2 c_1^*$. Although we have neglected effects of the upper state decay, the excited state population is strongly suppressed by the large detuning Δ . Consequently, the probability for spontaneous emission is small, and the effective two-level description appears to be a good approximation.

The simple wavefunction approach has given us some intuition for two-photon transitions in an effective two-level system. In many situations, however, it will be necessary to account for the effects of dephasing and decay as well.

5.1.2 The density matrix approach

To meticulously account for decay and dephasing, we must resort to the density matrix method. The equation of motion is

$$\dot{\rho} = \mathcal{L}_{31}(\rho) + \mathcal{L}_{32}(\rho) + i[\hat{H}, \rho], \quad (5.10)$$

where the Louvillian operators which account separately for decays from $|3\rangle$ to $|2\rangle$ and from $|3\rangle$ to $|1\rangle$ are given by e.g.

$$\mathcal{L}_{31} = -\frac{\gamma_{3 \rightarrow 1}}{2} (\sigma_{31} \sigma_{13} \rho - \sigma_{13} \rho \sigma_{31} + h.c.). \quad (5.11)$$

Using the Hamiltonian for the three-level system, we can find the coherent evolution of the density matrix components. The Louvillian operators will account for from $|3\rangle$ to $|1\rangle$ at rate γ , from $|3\rangle$ to $|2\rangle$ at rate $\tilde{\gamma}$, and from $|2\rangle$ to $|1\rangle$ rate γ' . The total decay rate out of $|3\rangle$ is $\gamma_3 = \gamma + \tilde{\gamma}$ whereas the total decay rate out of $|2\rangle$ is $\gamma_2 = \gamma'$. Finally, we will incorporate nonradiative decoherence mechanisms by setting the decay rate of a coherence ρ_{ij} to γ_{ij} . (In the limit of radiative decoherence γ_{ij} will be equal to half the sum of the decay rates out of $|i\rangle$ and $|j\rangle$.) The density matrix equations of motion for the lambda system are then

$$\dot{\rho}_{11} = -i\Omega_1 \rho_{13} + i\Omega_1^* \rho_{31} + \gamma \rho_{33} + \gamma' \rho_{22} \quad (5.12)$$

$$\dot{\rho}_{22} = -i\Omega_2 \rho_{23} + i\Omega_2^* \rho_{32} - \gamma' \rho_{22} + \tilde{\gamma} \rho_{33} \quad (5.13)$$

$$\dot{\rho_{21}} = -(\gamma_{12} - i\delta)\rho_{21} + i\Omega_2^*\rho_{31} - i\Omega_1\rho_{23} \quad (5.14)$$

$$\dot{\rho_{31}} = -(\gamma_{13} - i\Delta)\rho_{31} + i\Omega_2\rho_{21} + i\Omega_1(\rho_{11} - \rho_{33}) \quad (5.15)$$

$$\dot{\rho_{32}} = -(\gamma_{23} - i(\Delta - \delta))\rho_{32} + i\Omega_2(\rho_{22} - \rho_{33}) + i\Omega_1\rho_{12}, \quad (5.16)$$

where $\Delta = \Delta_1$. Note that the remaining equations can be found using $\rho_{ji} = \rho_{ij}^*$ and $\rho_{11} + \rho_{22} + \rho_{33} = 1$. For notational convenience, we will frequently express the phase evolution and decay of the coherences in terms of a complex decay parameter

$$\Gamma_{12} = \gamma_{12} - i\delta \quad (5.17)$$

$$\Gamma_{13} = \gamma_{13} - i\Delta \quad (5.18)$$

$$\Gamma_{23} = \gamma_{23} - i(\Delta - \delta). \quad (5.19)$$

$$(5.20)$$

For far-detuned systems $\Delta \gg \Omega_{1,2}$, we can approach this system of equations by using adiabatic elimination to set $\rho_{32} = \rho_{31} = 0$. Nevertheless, the density matrix equations of motion are mathematically cumbersome.

5.1.3 The stochastic wavefunction method

The density matrix approach involves painful mathematics, but we can find a clever way around it by using the stochastic wavefunction method to incorporate decays without adding extra degrees of freedom. In particular, we will treat the system using a non-Hermitian Hamiltonian which adds two decay channels to the original Hermitian component,

$$\hat{H}_{\text{eff}} = \hat{H} - \frac{i\hbar\gamma_3}{2}|3\rangle\langle 3| - \frac{i\hbar\gamma_2}{2}|2\rangle\langle 2|. \quad (5.21)$$

We are free to use the Schrodinger equation $i\hbar|\psi\rangle = \hat{H}_{\text{eff}}|\psi\rangle$ so long as the probability for a quantum jump is small,

$$P_{\text{jump}} = \int dt (\gamma_2|c_2(t)|^2 + \gamma_3|c_3(t)|^2) \ll 1. \quad (5.22)$$

This constraint is satisfied in two important situations:

- (1) If the system starts out in $|1\rangle$ and the probe field is weak, $\Omega_1 \rightarrow 0$, the populations in states $|2\rangle$ and $|3\rangle$ are of order $|\Omega_1|^2$ or higher, so to lowest order in Ω_1 we may neglect quantum jumps.
- (2) If the system has finite population in both $|1\rangle$ and $|2\rangle$, quantum jumps are negligible provided that the decay from $|2\rangle$ is slow ($\gamma_2 \rightarrow 0$) and the excited state population is small ($\rho_{33} \rightarrow 0$).

The non-Hermitian Schrodinger equation yields the following equations of motion for the stochastic wavefunction amplitudes:

$$\dot{c}_1 = i\Omega_1^* c_3 \quad (5.23)$$

$$\dot{c}_2 = -\underbrace{\left(\frac{\gamma_2}{2} - i\delta\right)}_{\Gamma_{12}} c_2 + i\Omega_2^* c_3 \quad (5.24)$$

$$\dot{c}_3 = -\underbrace{\left(\frac{\gamma_3}{2} - i\Delta_1\right)}_{\Gamma_{13}} c_3 + i\Omega_1 c_1 + i\Omega_2 c_2. \quad (5.25)$$

These equations may be solved in different regimes using different methods. If Ω_1 is weak and Ω_2 is continuous wave, they may be solved exactly using Fourier transforms. If the applied fields have envelopes which vary slowly in time, adiabatic elimination provides a method for finding an approximate solution. Regardless of the precise mathematical manipulations employed, it is important to always check at the end that the probability for quantum jumps is indeed small.

We will now consider the behavior of the Λ system in a few special cases. For a weak probe field Ω_1 and a constant field Ω_2 of arbitrary strength, to zeroth order in Ω_1 a system which starts in $|1\rangle$ will remain in $|1\rangle$, so $c_1(t) \approx 1$. The remaining probability amplitudes can be found by Fourier transforming the equations of motion, so that

$$\underbrace{\left(\frac{\gamma_2}{2} - i(\delta - \omega)\right)}_{\Gamma_{12}} c_2 = i\Omega_2^* c_3 \quad (5.26)$$

$$\underbrace{\left(\frac{\gamma_3}{2} - i(\Delta_1 - \omega)\right)}_{\Gamma_{13}} c_3 = i\Omega_1 + i\Omega_2 c_2. \quad (5.27)$$

Note that the Fourier frequency ω enters in the same place as the detuning, so we will again make reference to the complex decay rates Γ_{12} and Γ_{13} , bearing in mind that the dependence on frequency is implied. The results for the density matrix components follow easily:

$$\rho_{11} = |c_1|^2 = 1 \quad (5.28)$$

$$\rho_{21} = c_1^* c_2 = -\frac{\Omega_1 \Omega_2^*}{\Gamma_{12} \Gamma_{13} + |\Omega_2|^2} \quad (5.29)$$

$$\rho_{31} = c_1^* c_3 = i\Omega_1 \frac{\Gamma_{12}}{\Gamma_{12} \Gamma_{13} + |\Omega_2|^2}. \quad (5.30)$$

All other density matrix elements are of order $|\Omega_1|^2$ or higher, and consequently may be disregarded. The same results may be obtained directly from the master equation, where in general the complex decay rates would include effects of dephasing as well as decay.

5.1.4 Large detuning Δ , weak Ω_1

The three-level system can be considerably simplified in the case of a large single-photon detuning Δ . When the probe is weak, we can characterize the response of the system by the linear susceptibility on the probe transition,

$$\chi_1 = \frac{|\mu|^2}{\hbar\epsilon_0} \frac{\rho_{31}}{\Omega_1}, \quad (5.31)$$

which is proportional to

$$\frac{\rho_{31}}{\Omega_1} = \frac{i}{\Gamma_{13}} \left(\frac{\Gamma_{12}}{\Gamma_{12} + |\Omega_2|^2/\Gamma_{13}} \right) \quad (5.32)$$

$$= \frac{i}{\Gamma_{13}} \left(1 - \frac{|\Omega_2|^2/\Gamma_{13}}{\Gamma_{12} + |\Omega_2|^2/\Gamma_{13}} \right). \quad (5.33)$$

The first term i/Γ_{13} contains the single photon physics for a two-level system of $|1\rangle$ and $|3\rangle$ coupled by Ω_1 , and appears as a broad resonance at $\nu_1 = \omega_{13}$ with linewidth γ_{13} . The second term deserves greater care since it describes the effects of two-photon transitions. In the limit that $\Delta \gg \gamma_{13}$, the complex decay rate $\Gamma_{13} \approx -i\Delta$, so the second term becomes

$$\frac{\rho_{31}}{\Omega_1} - \frac{i}{\Gamma_{13}} \approx \frac{i|\Omega_2|^2/\Delta^2}{\Gamma_{12} + (|\Omega_2|^2/\Delta^2)(\gamma_{13} + i\Delta)} \quad (5.34)$$

$$\approx \underbrace{\frac{i|\Omega_2|^2/\Delta^2}{(\gamma_{12}/2) + (\gamma_{13}/2)(|\Omega_2|^2/\Delta^2)}}_{\gamma_{\text{eff}}} - i \underbrace{\frac{(\delta - |\Omega_2|^2/\Delta)}{\delta'}}_{\delta'}. \quad (5.35)$$

The real and complex parts of the denominator correspond to the effective width and detuning of the two-photon resonance. Because we have included decay, the susceptibility remains finite even on resonance $\delta \rightarrow |\Omega_2|^2/\Delta$. The width of the two-photon resonance is set by both the metastable state decoherence γ_{12} and a term resulting from excited state decay, $\gamma_{13}|\Omega_2|^2/\Delta^2$, which is strongly suppressed by the large single-photon detuning.

Another important physical effect can be derived from our susceptibility calculation. For a system exactly on resonance, $\delta = |\Omega_2|^2/\Delta$, with no

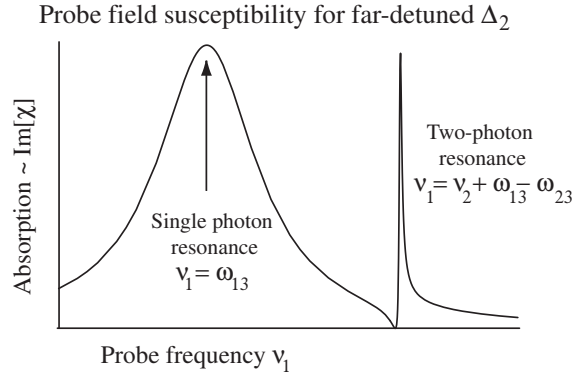


Figure 5.3: The imaginary part of the probe beam susceptibility as a function of the probe beam detuning. The absorption of Ω_1 exhibits a double resonance lineshape in the presence of a far-off resonant coupling beam Ω_2 . In this calculation, $\gamma_{12} = 0$, so the single-photon and two-photon resonances have the same peak value, but the linewidth of the two-photon peak is significantly narrower.

dephasing $\gamma_{12} = 0, \gamma_{13} = \gamma_3/2$, the susceptibility

$$\frac{\rho_{31}}{\Omega_1} \sim \frac{2i}{\gamma_3} \quad (5.36)$$

corresponds to that of a radiatively broadened system. Consequently the system is approaching the unitarity limit, and the cross-section is proportional to the wavelength λ^2 . In this regime, the two-photon peak has the same amplitude as the single-photon resonance.

Dressed state interpretation

We can obtain insight into the physical origin of this result by examining the system in the dressed state picture. The strong field Ω_2 “dresses” the bare three-level system, so that the eigenstates probed by Ω_1 contain a mixture of states $|2\rangle$ and $|3\rangle$,

$$|+\rangle \approx |3\rangle - \frac{\Omega_2^*}{\Delta}|2\rangle \quad (5.37)$$

$$|-\rangle \approx |2\rangle + \frac{\Omega_2}{\Delta}|3\rangle, \quad (5.38)$$

where we have only kept terms to lowest order in Ω_2/Δ because of the large detuning. The single photon resonance corresponds to transitions from the ground state to $|+\rangle$, which is very nearly the excited state $|3\rangle$, and consequently exhibits a linewidth close to the radiative width γ_3 . The observed two-photon Raman transition corresponds to the transition $|1\rangle \rightarrow |-\rangle$. Since $|1\rangle$ is the ground state, the linewidth of the transition is set by the dephasing rate of $|-\rangle$,

$$\gamma_- \approx \gamma_{12} + \frac{|\Omega_2|^2}{\Delta^2} \gamma_{13}, \quad (5.39)$$

which precisely corresponds to the result from our mathematical analysis.

5.1.5 Large Δ , arbitrary Ω_1 : Two-photon Rabi oscillations

Although the linear susceptibility analysis holds only for weak fields Ω_1 , it is possible to use the same stochastic Schrodinger equation to predict the effects of two strong fields Ω_1 and Ω_2 . Of course, to neglect the quantum jumps we must verify that their probability is small. In the far-detuned regime $\Delta \gg \Omega_{1,2}$, this requirement becomes

$$\frac{|\Omega_1|^2}{\Delta^2} \gamma_3 t, \frac{|\Omega_2|^2}{\Delta^2} \gamma_3 t \ll 1. \quad (5.40)$$

For large detunings the excited state can be eliminated, and the three-level system will behave as an effective two-level system coupled by a two-photon transition even when $\Omega_1 \sim \Omega_2$. In particular, the number of completed Rabi oscillations can be large

$$\left| \frac{\Omega_1 \Omega_2^*}{\Delta} \right| t \gg 1, \quad (5.41)$$

even for times short enough that a quantum jump is unlikely. Since the effective decoherence rate scales as $1/\Delta^2$ while the effective Rabi frequency scales as $1/\Delta$, in principle one can always find a detuning large enough that Rabi oscillations occur faster than dephasing.

5.1.6 Remarks

Generalization to many excited states

Our analysis may also be trivially generalized to include the effects of many excited states. For large detunings, the precise excited state energy levels are unimportant since they do not affect the two-photon detuning. Once we

have eliminated the excited states, the Λ system will again behave as a two level system with effective Rabi frequency

$$\Omega_{\text{eff}} = \sum_i \frac{\Omega_{1i}\Omega_{2i}^*}{\Delta_i}. \quad (5.42)$$

The Stark shifts and effective decay rates arising from multiple excited states may be calculated in a similar manner.

The influence of Doppler broadening

Until now, we have implicitly assumed that the three-level atoms under consideration are stationary. If they are free to move, we must incorporate the Doppler shift which results from the atomic velocity \mathbf{v} by changing the detunings

$$\Delta_1 \rightarrow \Delta_1 - \mathbf{k}_1 \cdot \mathbf{v} \quad (5.43)$$

$$\Delta_2 \rightarrow \Delta_2 - \mathbf{k}_2 \cdot \mathbf{v} \quad (5.44)$$

$$\delta \rightarrow \delta - (\mathbf{k}_1 - \mathbf{k}_2) \cdot \mathbf{v}. \quad (5.45)$$

Changes in the single photon detunings Δ_1, Δ_2 are unimportant for far-off resonant fields. Moreover, the two-photon detuning can be made almost insensitive to Doppler broadening if the two beams are nearly the same frequency, $\nu_1 \approx \nu_2$, and co-propagating, $\mathbf{k}_1 \parallel \mathbf{k}_2$, so that $\mathbf{k}_1 \approx \mathbf{k}_2$.

The Doppler-free two-photon resonance can be understood physically by considering the momentum kicks imparted to the atom. During the Raman process, an atom absorbs a photon ν_1 , acquiring momentum $\hbar\mathbf{k}_1$, and subsequently emits a photon ν_2 , losing momentum $\hbar\mathbf{k}_2$, so that the total momentum transfer is $\hbar(\mathbf{k}_1 - \mathbf{k}_2)$. Although $\nu_1 \neq \nu_2$, so $|k_1| \neq |k_2|$, their difference can be very small compared to optical frequencies. For example, Doppler effects contribute only \sim kHz to the linewidth for a copropagating two-photon transition between hyperfine levels in Rb.

Phase sensitivity

In the linear susceptibility analysis, we found that ρ_{31}/Ω_1 depended only on $|\Omega_2|^2$, and not on the relative phase of the two fields. This happens because the two-photon coherence ρ_{21} is free to follow the phase of the optical coherences. If the transition between $|1\rangle$ and $|2\rangle$ was dipole allowed, then the relative phase of the three fields coupling the three states would become important.

Cascade and V-type transitions

Other three-level configurations (see Figure 7.3) exhibit similar behavior for large single-photon detunings. To illustrate where differences can arise, we will examine a far-detuned cascade system. Although the cascade system will also exhibit two-photon resonance features, it differs from the Λ system in the following aspects:

- (1) The final state $|3\rangle$ often has dipole-allowed spontaneous emission, since transitions to the (lower) intermediate state $|2\rangle$ are dipole allowed. The two-photon resonances will thus typically be broader. A notable exception to this rule is the $1s \rightarrow 2p \rightarrow 2s$ transition in atomic Hydrogen, where the final state $2s$ is metastable and the fields typically applied for two-photon resonance are very far detuned from the $2p$ state.
- (2) The cascade atoms have different Doppler properties, since the Raman transition involves absorbing two photons rather than absorbing one and emitting the other. Consequently, the Doppler shifts cancel for counter-propagating beams, since the different frequency photons will impart momentum kicks in opposite directions to the atom.

5.2 Resonant excitation: Electromagnetically induced transparency

The Λ system examined above in the far-detuned regime exhibits a very different response to resonant excitation. As we bring the single photon detunings to zero $\Delta_1, \Delta_2 \rightarrow 0$, the two-photon resonance approaches the single-photon resonance and begins to broaden. Simultaneously, the AC Stark shifts increase. The overall effects, however, remain the same provided that $\Delta \gg \gamma_{13}, \Omega_{1,2}$. When this condition is no longer satisfied, the system response changes qualitatively (see Figure 5.4).

5.2.1 The dark resonance

Consider an experiment where we illuminate the three-level atom with an applied field Ω_2 which is precisely on resonance, $\Delta_2 = 0$. We then sweep the frequency of the probe beam $\Delta_1 = \delta$, and observe how the susceptibility changes as a function of Δ_1 . Using the expression we previously derived for the optical coherence on the ν_1 transition,

$$\frac{\rho_{31}}{\Omega_1} = \frac{i}{\Gamma_{13}} \left(1 - \frac{|\Omega_2|^2/\Gamma_{13}}{\Gamma_{12} + |\Omega_2|^2/\Gamma_{13}} \right), \quad (5.46)$$

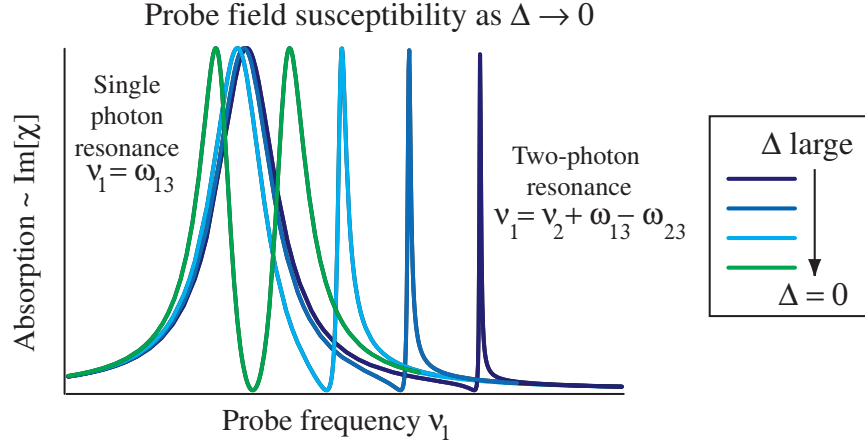


Figure 5.4: As the detuning Δ is reduced, the two-photon resonance moves towards the single-photon resonance and broadens. When the two resonances begin to overlap, the system no longer behaves like a far-detuned system, and qualitatively new effects appear.

we find that the absorption vanishes precisely on resonance $\delta = 0$ (for simplicity, here we ignore various factors of 2 arising from the equations):

$$\text{Im}\left[\frac{\rho_{31}}{\Omega_1}\right] = \frac{\gamma_{12}}{\gamma_{13}\gamma_{12} + |\Omega_2|^2} \rightarrow 0 \text{ as } \gamma_{12} \rightarrow 0. \quad (5.47)$$

For $\Omega_2 \ll \gamma_{13}$, the width of this absorption dip is $\gamma_{12} + |\Omega_2|^2/\gamma_{13}$, whereas for $\Omega_2 \gg \gamma_{13}$, the width is approximately $\gamma_{12} + |\Omega_2|$. Note that the width of the dip can be very narrow $\ll \gamma_{13}$; this is an indication that two-photon physics is essential to the so-called “dark resonance”. Although the optical coherence ρ_{31} vanishes at zero detuning, the coherence on the forbidden transition, $\rho_{21} \rightarrow -\Omega_1/\Omega_2$, remains finite, indicating that atomic coherence also plays a crucial role in this phenomenon. Far from the resonance condition, the usual far-detuned behavior applies, so we expect the probe to reveal a broad absorption peak with a narrow dark resonance in the center (see Figure 5.5).

Physical picture of the dark resonance

In the situation when $\Omega_2 \gg \Omega_1$, the dressed state interpretation provides a reasonable description of the physics behind the dark resonance. In this

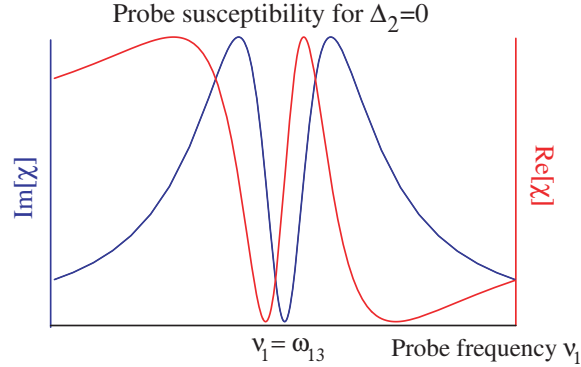


Figure 5.5: The real and imaginary part of the probe beam susceptibility are shown under resonant illumination by Ω_2 . The absorption dip at zero detuning is known as a dark resonance or electromagnetically induced transparency.

case, the strong resonant field Ω_2 creates two dressed states $|\pm\rangle \propto |2\rangle \pm |3\rangle$, separated in energy by $2\Omega_2$. The weaker probe Ω_1 should then exhibit two peaks corresponding to the transitions to the two dressed states. However, this picture does not provide a good explanation for why the absorption precisely vanishes when the probe field is tuned halfway between the dressed states, and it is not valid for arbitrary $\Omega_{1,2}$.

To gain further intuition for the physics behind the dark resonance, we shall examine the non-Hermitian effective Hamiltonian. If the metastable decoherence rate vanishes, $\gamma_{12} = 0$, and the applied fields are precisely on resonance, $\Delta = \delta = 0$, the effective Hamiltonian becomes

$$\hat{H}_{\text{eff}} = -\frac{i\hbar\gamma_3}{2}|3\rangle\langle 3| - (\Omega_1^*|1\rangle\langle 3| + \Omega_2^*|2\rangle\langle 3| + h.c.) \quad (5.48)$$

$$= -\frac{i\hbar\gamma_3}{2}|3\rangle\langle 3| - \underbrace{(\Omega_1^*|1\rangle + \Omega_2^*|2\rangle)}_{|B\rangle}\langle 3| - |3\rangle \underbrace{(\Omega_1\langle 1| + \Omega_2\langle 2|)}_{\langle B|}. \quad (5.49)$$

Note that the excited state $|3\rangle$ only couples to a particular superposition of the lower states, $|B\rangle$. Furthermore, if we can construct a state $|D\rangle$ such that $\langle D|B\rangle = 0$, this new orthogonal superposition will be decoupled from

the excited state and thus insensitive to its decay. This so-called dark state,

$$|D\rangle = \frac{\Omega_2|1\rangle - \Omega_1|2\rangle}{\sqrt{|\Omega_1|^2 + |\Omega_2|^2}} \quad (5.50)$$

is an eigenstate of the effective Hamiltonian with zero energy:

$$\hat{H}_{\text{eff}}|D\rangle = 0. \quad (5.51)$$

A system in state $|D\rangle$ has vanishing absorption and polarization on the $|1\rangle$ to $|3\rangle$ transition, but finite polarization on the forbidden transition. Quantitatively, the density matrix for the dark state,

$$\rho = |D\rangle\langle D|, \quad (5.52)$$

has off-diagonal elements

$$\rho_{21} = -\frac{\Omega_2^*\Omega_1}{|\Omega_1|^2 + |\Omega_2|^2}. \quad (5.53)$$

In the limit that $\Omega_1 \ll \Omega_2$, we reproduce our previous result. Consequently, we see that the vanishing absorption on resonance is associated with the production of dark states which are decoupled from both light beams. This can also be viewed as a quantum interference phenomenon, where simultaneous excitations of $|3\rangle$ by Ω_1 and Ω_2 destructively interfere, leaving the excited state unpopulated by the applied fields.

Dispersive properties of the dark resonance: "slow light"

Thus far we have considered only the imaginary part of the probe susceptibility in the vicinity of the dark resonance. The real part leads to dispersive effects, since for $\Delta_2 = 0$ and δ small

$$\text{Re}[\chi] \propto \text{Re}\left[\frac{\rho_{31}}{\Omega_1}\right] \approx \frac{\delta}{|\Omega_2|^2 + \gamma_{12}\gamma_{13}}. \quad (5.54)$$

In the situation relevant to the dark resonance, the slope of the refractive index $n \propto \text{Re}[\chi]$ can be controlled by changing the intensity of Ω_2 . In particular, this slope determines the group velocity since

$$v_g = \frac{d\omega}{dk} = \frac{c}{n(\omega) + \omega \frac{dn}{d\omega}} \quad (5.55)$$

(where $n(\omega)$ is the index of refraction) and $n(\omega) = 1 + \text{Re}[\chi]/2$. The slope $\frac{dn}{d\omega}$ diverges as $\gamma_{12} \rightarrow 0$ and $\Omega_2 \rightarrow 0$:

$$v_g \approx \frac{c}{1 + \frac{\gamma_{13}\bar{\nu}3\pi(N/V)(\lambda/2\pi)^3}{|\Omega_2|^2 + \gamma_{13}\gamma_{12}}} \quad (5.56)$$

so that the group velocity is reduced to zero as $\Omega_2 \rightarrow 0$ (see problem set 3 for a derivation of this formula). Simultaneously, the width Δw of the resonance also vanishes, since

$$\Delta w \approx \frac{|\Omega_2|^2}{\gamma_{13}} \rightarrow 0. \quad (5.57)$$

Note that when the linewidth is dynamically reduced while a pulse is travelling through the medium, careful considerations show that the spectrum of the pulse itself is also dynamically reduced. In particular, if the pulse spectrum fits inside the transparency window initially, it fits in the window at all times and no dissipation is taking place (see problem set 3 and references therein for further details).

Since the two-photon resonance can be much narrower than the single-photon linewidth, the group velocity of the probe pulse Ω_1 can be reduced substantially below the speed of light. As resonant probe light enters the medium it compresses by a factor v_g/c , then slowly propagates through the atomic cloud, dragging along a spin coherence associated with the dark state. Since absorption vanishes, virtually all of the probe light is transmitted, with a significant delay due to the slow group velocity. This phenomenon is known as “electro-magnetically induced transparency” or “slow light”.

Preparation of the dark state

Our discussion has not explained how the system is prepared in the dark state. In fact, if the probe light turns on slowly enough, the system will adiabatically follow from the initial state $|1\rangle$ to $|D\rangle$, in essence preparing itself. This phenomenon is an example of stimulated Raman adiabatic passage (STIRAP), whereby slowly varying applied fields can be used to efficiently and robustly manipulate the populations and atomic coherences of a system. Unlike π pulses based on Rabi oscillations, which are exquisitely sensitive to pulse amplitude and timing, STIRAP techniques do not depend on the details of pulse shape.

To understand the basic mechanism for dark state formation, consider the asymptotic behavior of the dark state under different applied powers:

$$\Omega_2 \rightarrow 0, \Omega_1 \text{ fixed} \Rightarrow |D\rangle = -|2\rangle \quad (5.58)$$

$$\Omega_1 \rightarrow 0, \Omega_2 \text{ fixed} \Rightarrow |D\rangle = |1\rangle. \quad (5.59)$$

The physics here is fairly obvious, since $|1\rangle$ does not couple to Ω_2 and vice versa. Consequently, if the system starts out in the state $|1\rangle$ illuminated only by Ω_2 , it is already in the dark state. By slowly decreasing Ω_2 while increasing Ω_1 , the atomic state will adiabatically follow the dark state, finally ending up in $|2\rangle$ when $\Omega_2 = 0$. Since the dark state contains no component of the excited state, and does not couple to the light, the atomic state will be free from dissipation or decoherence from the excited state. Such manipulation is known as a “counter-intuitive pulse sequence,” since the light is initially applied on the transition which is unpopulated.

5.3 Parametric Processes

Parametric processes represent an important category of coherent interactions between atoms and light. In such systems, we are interested primarily in the propagation and interaction of applied and generated light fields; the nonlinear atomic response is important only because it mediates interactions between optical fields. No energy is exchanged between photons and atoms, but atomic nonlinearities can lead to mixing between applied fields or even generation of fields at new frequencies. In practice, the nonlinear medium need not be atomic; in the most general treatment, optical fields impinge on a “nonlinear black box” which can give birth to higher frequency harmonics or sum and difference frequencies.

5.3.1 Example: the cascade system

We will first examine how parametric processes in the cascade level configuration can be used to generate higher-frequency fields. The situation we will consider has two fields \mathcal{E}_1 and \mathcal{E}_2 near resonance with the two-photon transition $\nu_1 + \nu_2 \approx \omega_{12}$. By driving this two-photon process, we hope to induce the atom to emit radiation at frequency $\nu_1 + \nu_2$.

From symmetry considerations, one might argue that the $|2\rangle \rightarrow |1\rangle$ transition is dipole forbidden if the two-photon process is dipole-allowed. Nevertheless, by breaking the associated symmetry (in this case, inversion symmetry), it is possible to have both single-photon and two-photon dipole allowed transitions between $|1\rangle$ and $|2\rangle$. Such symmetry breaking can be accomplished in a variety of ways. The hydrogen atom furnishes a particularly simple example: if we apply a static electric field to the hydrogen

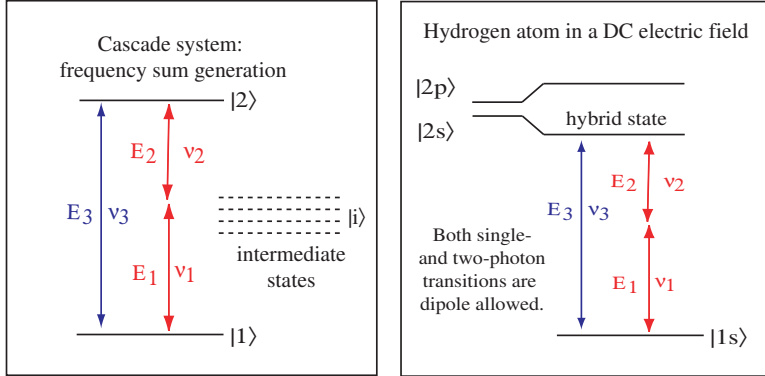


Figure 5.6: Left: The cascade level system used for sum-frequency generation. Right: A physical implementation of the cascade level system in the Hydrogen atom. A DC field mixes the $|2s\rangle$ and $|2p\rangle$ levels so that both the single- and two-photon transitions are dipole allowed. This DC Stark shift breaks the inversion symmetry of the Hydrogen atom, which makes second-order nonlinear processes possible.

atom, the linear Stark shift mixes the $|2s\rangle$ and $|2p\rangle$ levels so that the resulting hybrid state does not have a well-defined parity. Selection rules are thereby relaxed, so that a far-off-resonant two-photon transition can indeed induce single-photon transitions back to $|1s\rangle$.

Sum frequency generation has an intuitive semiclassical explanation. Suppose you drive the Stark-shifted Hydrogen atom with two fields with frequencies $\nu_1 + \nu_2 = \omega_{1s \rightarrow 2s}$. The resulting off-diagonal atomic coherence ρ_{12} leads to a polarization which oscillates at the sum frequency $\nu_1 + \nu_2$. From a semiclassical perspective, the oscillating polarization will emit radiation at the sum frequency. Note that the polarization is proportional to both applied fields

$$P_{\nu_1+\nu_2} \propto \mu_{12} \mathcal{E}_1 \mathcal{E}_2, \quad (5.60)$$

and we will introduce a nonlinear susceptibility as the proportionality constant

$$\chi^{(2)} = \frac{P_{\nu_1+\nu_2}}{\epsilon_0 \mathcal{E}_1 \mathcal{E}_2}. \quad (5.61)$$

Whenever a medium has $\chi^{(2)} \neq 0$, application of two fields can result in generation of the sum frequency.

Non-linear polarization in the cascade level configuration

We will now derive an expression for the nonlinear susceptibility in terms of atomic system parameters. Taking the limit when the two-photon transition is far-detuned from the intermediate states, the system can be effectively treated as a two-level system coupled by a field with Rabi frequency

$$\Omega_{\text{eff}} = \sum_i \frac{\Omega_{1i}\Omega_{2i}}{\Delta_i} = \sum_i \frac{\mu_{1i}\mu_{2i}}{\Delta_i \hbar^2} \mathcal{E}_1 \mathcal{E}_2. \quad (5.62)$$

The Stark shifts from the applied fields \mathcal{E}_1 and \mathcal{E}_2 can be incorporated into a renormalization of the two-photon detuning δ_{eff} . For $\Delta_i, \delta_{\text{eff}}$ large, the off-diagonal density matrix components are given by

$$\rho_{21} = -\frac{\Omega_{\text{eff}}}{\delta_{\text{eff}}}, \quad (5.63)$$

so we can immediately write down the polarization

$$P_3 = \frac{N}{V} \mu^* \rho_{21} = \frac{N}{V} \mu^* \frac{1}{\hbar^2} \sum_i \frac{\mu_{1i}\mu_{2i}}{\delta_{\text{eff}}\Delta_i} \mathcal{E}_1 \mathcal{E}_2. \quad (5.64)$$

The nonlinear susceptibility is thus

$$\chi^{(2)} = \frac{N}{V} \mu^* \frac{1}{\epsilon_0 \hbar^2} \sum_i \frac{\mu_{1i}\mu_{2i}}{\delta_{\text{eff}}\Delta_i}. \quad (5.65)$$

5.3.2 Sum frequency generation

The cascade system has provided an illustration of how a medium can generate a polarization oscillating at the sum frequency of two applied fields. We now seek to understand how this oscillating polarization gives birth to a new field. To simplify the analysis we will assume:

- (1) Both applied fields are continuous-wave.
- (2) All fields propagate along the \hat{z} direction.

We can thus write down the total electric field as a sum of three components, treating the third field on equal footing with the two applied fields:

$$\mathcal{E} = \mathcal{E}_1 e^{i(\nu_1 z/c - \nu_1 t)} + \mathcal{E}_2 e^{i(\nu_2 z/c - \nu_2 t)} + \mathcal{E}_3 e^{i(\nu_3 z/c - \nu_3 t)} + c.c. \quad (5.66)$$

Note that, in the spirit of the slowly-varying envelope approximation, we have factored out the rapidly oscillating terms. Using the generalized SVEA, we will find propagation equations for each of the three slowly-varying amplitudes.

The evolution equations for the slowly-varying amplitudes include both the normal linear response of the medium and the effects of the oscillating polarization P_3 . If \mathcal{E}_3 is sufficiently weak compared to the two applied fields \mathcal{E}_1 and \mathcal{E}_2 , then we might expect that the two applied fields will not be greatly depleted while generating \mathcal{E}_3 . This is known as the undepleted pump approximation, since \mathcal{E}_1 and \mathcal{E}_2 act as pump fields driving the creation of \mathcal{E}_3 . When we neglect the nonlinear terms associated with depletion of $\mathcal{E}_{1,2}$ by \mathcal{E}_3 , the evolution equations for \mathcal{E}_1 and \mathcal{E}_2 are the same as for a linear medium,

$$\frac{\partial}{\partial z} \mathcal{E}_{1,2} = \frac{i\nu_{1,2}}{2c} \chi_{1,2} \mathcal{E}_{1,2}, \quad (5.67)$$

where χ_i is the linear response of the medium to frequency ν_i .

The evolution equation for \mathcal{E}_3 must include both the linear and nonlinear response, since sum-frequency generation will occur even if $\mathcal{E}_3(0) = 0$, and this generated field will subsequently interact nearly linearly with the atoms. Consequently we find

$$\frac{\partial}{\partial z} \mathcal{E}_3 = \frac{i\nu_3}{2c} \chi^{(2)} \mathcal{E}_1 \mathcal{E}_2 + \frac{i\nu_3}{2c} \chi_3 \mathcal{E}_3. \quad (5.68)$$

For the far-detuned system under consideration, Δ_i large, we can identify the dominant terms in the linear susceptibilities:

$$\chi_{1,2} \approx \frac{N}{V} \frac{1}{\epsilon_0 \hbar} \sum_i \frac{|\mu_{1i,2i}|^2}{\Delta_i} \quad (5.69)$$

$$\chi_3 \approx \frac{N}{V} \frac{1}{\epsilon_0 \hbar} \frac{|\mu_{12}|^2}{\delta_{\text{eff}}} \quad (5.70)$$

$$(5.71)$$

In conjunction with the initial conditions $\mathcal{E}_1(0), \mathcal{E}_2(0) \neq 0, \mathcal{E}_3(0) = 0$, we now have a completely defined problem.

The evolution equations are most easily solved by introducing new variables $\tilde{\mathcal{E}}_i$ which absorb the linear terms,

$$\mathcal{E}_i = \tilde{\mathcal{E}}_i e^{i\nu_i \chi_i z / 2c} \quad (5.72)$$

so that the propagation equations become

$$\frac{\partial}{\partial z} \tilde{\mathcal{E}}_{1,2} = 0 \quad (5.73)$$

$$\frac{\partial}{\partial z} \tilde{\mathcal{E}}_3 = \frac{i\nu_3}{2c} \chi^{(2)} \tilde{\mathcal{E}}_1 \tilde{\mathcal{E}}_2 e^{i\Delta_k z}, \quad (5.74)$$

where

$$\Delta k = \frac{\nu_1 \chi_1}{2c} + \frac{\nu_2 \chi_2}{2c} - \frac{\nu_3 \chi_3}{2c}. \quad (5.75)$$

Since $\nu_i \chi_i / 2c = n_i \nu_i / c = k_i$ is just the wave-vector of the field \mathcal{E}_i inside the medium, $\Delta k = k_1 + k_2 - k_3$ is simply the difference of the total wavevectors of all three fields.

Phase-matching

In sum-frequency generation, Δk is the most important quantity determining the growth of \mathcal{E}_3 . The output field is

$$\tilde{\mathcal{E}}_3(L) = \int_0^L \frac{i\nu_3}{2c} \chi^{(2)} \tilde{\mathcal{E}}_1 \tilde{\mathcal{E}}_2 e^{i\Delta kz} = \left(\frac{e^{i\Delta k L} - 1}{i\Delta k} \right) \frac{i\nu_3}{2c} \chi^{(2)} \tilde{\mathcal{E}}_1 \tilde{\mathcal{E}}_2. \quad (5.76)$$

In the situation when $\Delta k = 0$, the system is said to satisfy the “phase-matching condition.” This is the most favorable configuration for sum frequency generation because the field grows linearly with distance,

$$\tilde{\mathcal{E}}_3(L) = \frac{i\nu_3}{2c} \chi^{(2)} \tilde{\mathcal{E}}_1 \tilde{\mathcal{E}}_2 L. \quad (5.77)$$

The physical interpretation for this linear field growth comes from examining the phase velocities of the generated field and the induced polarization. When $\Delta k = 0$, the phase velocity of the field \mathcal{E}_3 precisely matches the phase velocity of the polarization P_3 , so the polarization always contributes constructively to the generation of the new field. If the phase velocities are not matched, $\Delta k \neq 0$, the phase of the polarization slips out of alignment after a distance $\approx \pi/\Delta k$, producing a field which interferes destructively with the propagating field \mathcal{E}_3 .

An alternate interpretation for the phase-matching condition invokes momentum-conservation. The parametric up-conversion involves absorbing two photons and emitting one, and this process must conserve both energy $\nu_3 = \nu_1 + \nu_2$ and momentum, $k_3 = k_1 + k_2$. For a atomic cloud of finite length L , the momentum is uncertain to within $\approx \pi/L$, so for distances less than the coherence length, $\Delta k L \ll 1$ the system is phase-matched and the field grows linearly. Once the field has propagated far enough that $\Delta k L \gg 1$, momentum conservation is no longer satisfied, and destructive interference sets in.

Competing processes

Phase-matching provides an example of so-called competing processes which reduce the effects of nonlinearities. The linear susceptibility of the medium

Sum frequency generation: $\Delta k \neq 0$

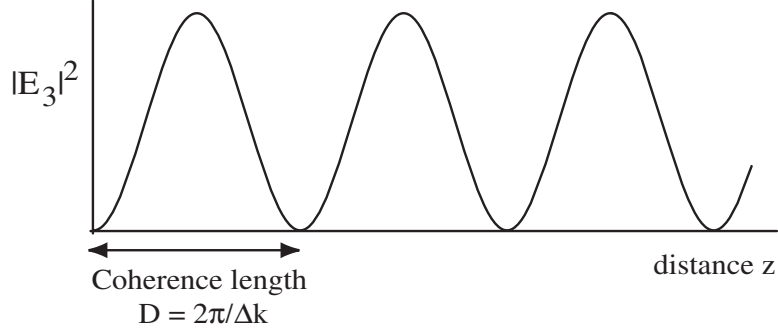


Figure 5.7: When the phase-matching condition is not satisfied, the sum-frequency field only grows for a distance $\sim \pi/\Delta k$ before destructive interference sets in.

competes with nonlinear generation, making the outcome for \mathcal{E}_3 much smaller than it could potentially be. Other effects such as absorption or beam breakup also diminish the net output nonlinear processes. These competing processes frequently overwhelm nonlinear effects, and in large part explain why nonlinearities in practical systems are often so small.

Sum-frequency generation in the cascade system

We will now apply our calculations for the general nonlinear system to the cascade level configuration, where we can express the output field in terms of known atomic quantities. By inspecting Eq. (5.76) with $\Delta k \neq 0$, we see that after a distance $z = \pi/\Delta k$, \mathcal{E}_3 achieves its maximal amplitude,

$$\tilde{\mathcal{E}}_3\left(\frac{\pi}{\Delta k}\right) = \frac{i\nu_3}{2c\Delta k} \chi^{(2)} \tilde{\mathcal{E}}_1 \tilde{\mathcal{E}}_2. \quad (5.78)$$

Since Δk is determined by the linear susceptibilities for the system, the strength of the generated field depends on the ratio of the nonlinear susceptibility to the linear susceptibilities. For the far-detuned two-photon transition (Δi large), the near-resonant susceptibility χ_3 dominates Δk . In this limit, we can easily express the maximal field amplitude in terms of

atomic dipole moments,

$$\tilde{\mathcal{E}}_3\left(\frac{\pi}{\Delta k}\right) = \overbrace{\mu_{12}^* \sum_i \frac{\mu_{1i}\mu_{2i}}{\delta_{\text{eff}}\Delta_i}}^{\sim\chi^{(2)}} \cdot \underbrace{\frac{\delta_{\text{eff}}}{\hbar|\mu_{12}|^2}}_{\sim 1/\chi_3}. \quad (5.79)$$

As we tune closer to two-photon resonance, $\delta_{\text{eff}} \rightarrow 0$, the nonlinear susceptibility grows, but this growth is perfectly balanced by corresponding growth in the linear susceptibility; indeed, the two-photon detuning drops out of the problem.

The overall size of the new field is very small when the system is not phase-matched. If we choose $\mathcal{E}_1 \sim \mathcal{E}_2 \sim \mathcal{E}$, the relative amplitude of the sum-frequency field is

$$\frac{\mathcal{E}_3(\pi/\Delta k)}{\mathcal{E}} \sim \sum_i \frac{\Omega_i}{\Delta_i} \ll 1. \quad (5.80)$$

Practical implementation of phase-matching

In view of this result, it is important to consider practical methods to achieve phase-matching. This goal requires engineering the linear dispersion so that polarization and sum-frequency field propagate in phase.

In atomic physics, phase-matching has been done by mixing two species of gas. One species provides the nonlinearity, while the other is introduced to provide the necessary dispersion to compensate any phase-mismatch. By carefully adjusting the ratios of the two atoms, phase matching may be achieved.

Another method frequently used in atomic physics engineers the dispersion by using strong nonperturbative fields. For example, EIT-like configurations can be used to eliminate the linear susceptibility, so that $\Delta k = 0$ precisely. A similar system has been used for second harmonic generation ($\nu_1 = \nu_2$) in hydrogen. The strong DC field couples the $2s$ and $2p$ levels, acting like a nonperturbative driving field, while the second harmonic \mathcal{E}_3 probes the $1s$ to $2p$ transition. The three-level system composed of $1s$, $2s$ and $2p$ thus takes on the Λ configuration, allowing EIT propagation for the second harmonic. [See K. Hakuta, L. Marmet, & B.P. Stoicheff, PRL 66, 596 (1991)]

While atomic systems are almost the sole source of coherent radiation in the UV and UUV spectral regions, most practical devices in the visible spectrum do not use atomics: nonlinear crystals are typically used

for sum-frequency generation. Similar phase-matching considerations apply, but other practical methods for achieving it are employed. For example, non-symmetric crystals can exhibit birefringence, where different polarizations can experience different linear susceptibilities which vary with temperature. Phase-matching can be engineered by carefully choosing the polarizations of the pump fields and appropriately heating the crystal. Angle tuning may also be employed, using the fact that Δk is in fact a vector sum of the wave-vectors.

Saturation

When phase-matching is achieved, Eq. (5.76) indicates that the sum-frequency field grows linearly without bound. From physical grounds, this prediction cannot be correct, since a finite quantity of power is pumped into the system by the applied fields \mathcal{E}_1 and \mathcal{E}_2 . In fact, as \mathcal{E}_3 grows, the undepleted pump approximation eventually breaks down. For parametric processes no energy is exchanged between the atoms and the optical fields, so (in a lossless system)

$$\frac{\partial}{\partial z} (|\mathcal{E}_1|^2 + |\mathcal{E}_2|^2 + |\mathcal{E}_3|^2) = 0. \quad (5.81)$$

Consequently we expect saturation of the generated field to occur when \mathcal{E}_3 begins to approach the amplitudes of the applied fields $\mathcal{E}_{1,2}$.

Generalization to other parametric processes

We have discussed one specific process in detail: parametric upconversion. The same physical and mathematical tools apply to other nonlinear parametric processes. For example, rather than applying two red fields which give birth to a sum-frequency blue field, one could consider generating lower frequency optical fields by applying a blue field and a red field to generate the difference frequency. The same evolution equations apply, and phase-matching considerations will again play an important role.

Third-order nonlinear processes

In all of our analysis, we have assumed non-vanishing dipole couplings on all transitions $\mu_{12}, \mu_{1i}, \mu_{2i} \neq 0$, and we noted that this situation arises when certain symmetries are violated. In fact, one can show that in systems with inversion symmetry, the second order nonlinear susceptibility vanishes, $\chi^{(2)} = 0$, so that the lowest order nonlinear susceptibility is $\chi^{(3)}$. The third

order susceptibility is defined by

$$\chi^{(3)} = \frac{P}{\epsilon_0 \mathcal{E}_1 \mathcal{E}_2 \mathcal{E}_3}, \quad (5.82)$$

where P is the polarization resulting from three applied fields $\mathcal{E}_{1,2,3}$. For example, the Kerr effect is a special case of a third-order nonlinear process where only one field is present, so $P \propto \mathcal{E}|\mathcal{E}|^2$. In addition, one can interpret the sum-frequency generation in hydrogen as a third-order process. Rather than invoking symmetry breaking caused by the DC field, one can treat this static field as the third applied field and use a third-order susceptibility to analyze the resulting sum-frequency generation.

Chapter 6

Stochastic Wavefunctions

The master equation is an essential tool for studying the dynamics of a system interacting with its surroundings. In some situations, however, the complexity of the system or the subtlety of interpretation has spurred development of more sophisticated techniques for solving the master equation. One such method makes use of random processes to simulate the system state. We will derive the equations governing the evolution of these stochastic or Monte Carlo wavefunctions, and discuss appropriate applications for this technique.

The Monte Carlo wavefunction was derived simultaneously in the 1990s by two groups interested in very different questions. A group of scientists in France, Dalibard, Castin, and Mølmer, wanted to simulate laser cooling of atoms quantum mechanically in three dimensions. Their numerical solution required discretizing space into a grid of 40x40x40 positions; to implement the master equation on such a space would have required a density matrix with $\mathcal{O}(40^6) \sim 10^9$ entries – such calculations are beyond the scope of even modern computers. However, simulating a wavefunction with $\mathcal{O}(40^3)$ entries is quite feasible. Consequently the group sought to convert the master equation to something more like the Schrodinger equation.

At the same time, Carmichael was interested in the effect that continuous monitoring would have on a system. For example, a two-level atom prepared in an equal superposition of states can decay by emitting a photon; if that photon is detected, the experimenter knows with certainty that the atom is in its ground state. But what happens 50% of the time when a photon is not detected? Certainly, after a long time has passed, the atom must be in its ground state, but how does that happen? To study these and similar questions, Carmichael wanted to incorporate the effects of continuous

monitoring, and understand how a measurement can cause the system state to suddenly jump into a different state.

6.1 Formalism

The description on which both groups converged begins with the most general form of the master equation,

$$\frac{d\hat{\rho}_S}{dt} = \frac{1}{i\hbar} [\hat{H}_S, \hat{\rho}_S] + \mathcal{L}(\hat{\rho}_S), \quad (6.1)$$

where the Liouvillian operator can be expressed as

$$\mathcal{L}(\hat{\rho}_S) = - \sum_k \frac{\gamma_k}{2} \left(\hat{c}_k^\dagger \hat{c}_k \hat{\rho}_S + \hat{\rho}_S \hat{c}_k^\dagger \hat{c}_k - 2 \hat{c}_k \hat{\rho}_S \hat{c}_k^\dagger \right). \quad (6.2)$$

It can be shown that Eq. (6.1) is the most general form for a master equation allowed by physics, and it has the added advantage that it is notationally compact. Since it is the most general form, it must contain the master equation we derived by assuming a certain kind of environment. To see this, identify the (in principle arbitrary) operators \hat{c}_k with

$$\hat{c}_{2k} = \sqrt{\bar{n} + 1} \hat{S}_k \quad (6.3)$$

$$\hat{c}_{2k+1} = \sqrt{\bar{n}} \hat{S}_k^\dagger, \quad (6.4)$$

in which case both the decay and absorption terms are included in Eq. (6.1).

Combining Eq. (6.1) with the definition for $\mathcal{L}(\hat{\rho}_S)$, and expanding $\hat{\rho}_S = \sum_\alpha p_\alpha |\psi_\alpha\rangle\langle\psi_\alpha|$, we can rewrite the master equation in a suggestive form:

$$\frac{d\hat{\rho}_S}{dt} = \frac{1}{i\hbar} [\hat{H}_S, \hat{\rho}_S] - \sum_k \frac{\gamma_k}{2} \left(\hat{c}_k^\dagger \hat{c}_k \hat{\rho}_S + \hat{\rho}_S \hat{c}_k^\dagger \hat{c}_k - 2 \hat{c}_k \hat{\rho}_S \hat{c}_k^\dagger \right) \quad (6.5)$$

$$\begin{aligned} &= \sum_\alpha \left\{ \frac{1}{i\hbar} \left(\hat{H}_S - i\hbar \sum_k \frac{\gamma_k}{2} \hat{c}_k^\dagger \hat{c}_k \right) p_\alpha |\psi_\alpha\rangle\langle\psi_\alpha| \right. \\ &\quad - \frac{1}{i\hbar} p_\alpha |\psi_\alpha\rangle\langle\psi_\alpha| \left(\hat{H}_S + i\hbar \sum_k \frac{\gamma_k}{2} \hat{c}_k^\dagger \hat{c}_k \right) \\ &\quad \left. + \sum_k p_\alpha \gamma_k \hat{c}_k |\psi_\alpha\rangle\langle\psi_\alpha| \hat{c}_k^\dagger \right\}. \end{aligned} \quad (6.6)$$

The first two terms can be rewritten in terms of an effective Hamiltonian,

$$\hat{H}_{\text{eff}} = \hat{H}_S - i\hbar \sum_k \frac{\gamma_k}{2} \hat{c}_k^\dagger \hat{c}_k, \quad (6.7)$$

so that the master equation now reads

$$\frac{d\hat{\rho}_S}{dt} = \sum_{\alpha} p_{\alpha} \left(\frac{1}{i\hbar} \left(\hat{H}_{\text{eff}} |\psi_{\alpha}\rangle\langle\psi_{\alpha}| - |\psi_{\alpha}\rangle\langle\psi_{\alpha}| \hat{H}_{\text{eff}}^{\dagger} \right) + \sum_k \gamma_k \hat{c}_k |\psi_{\alpha}\rangle\langle\psi_{\alpha}| \hat{c}_k^{\dagger} \right). \quad (6.8)$$

This form for the first two terms resembles the master equation for a pure state evolving according to \hat{H}_{eff} ; the final term we will interpret as a “quantum jump” operator which changes $|\psi_{\alpha}\rangle$ into another state $|\phi_{k,\alpha}\rangle = \hat{c}_k |\psi_{\alpha}\rangle$ with some probability.

The Schrodinger equation corresponding to the first two terms of Eq. (6.8) is

$$i\hbar \frac{d}{dt} |\psi_{\alpha}\rangle = \hat{H}_{\text{eff}} |\psi_{\alpha}\rangle, \quad (6.9)$$

and since we are interested in using Eq. (6.8) to describe a stochastic evolution, we will write it in discrete time,

$$|\psi_{\alpha}(t + \delta t)\rangle = \left(1 + \frac{\hat{H}_{\text{eff}} \delta t}{i\hbar} \right) |\psi_{\alpha}(t)\rangle. \quad (6.10)$$

Note that $|\tilde{\psi}_{\alpha}(t + \delta t)\rangle$ is not normalized because the effective Hamiltonian is not Hermitian. To lowest order in the small time δt ,

$$\langle \psi_{\alpha}(t + \delta t) | \psi_{\alpha}(t + \delta t) \rangle = \langle \psi_{\alpha} | \left(1 - \frac{\hat{H}_{\text{eff}}^{\dagger} \delta t}{i\hbar} \right) \left(1 + \frac{\hat{H}_{\text{eff}} \delta t}{i\hbar} \right) | \psi_{\alpha} \rangle \quad (6.11)$$

$$= \langle \psi_{\alpha} | \left(1 - \frac{\delta t}{i\hbar} (\hat{H}_{\text{eff}}^{\dagger} - \hat{H}_{\text{eff}}) \right) | \psi_{\alpha} \rangle \quad (6.12)$$

$$= \langle \psi_{\alpha} | \left(1 - \delta t \sum_k \gamma_k \hat{c}_k^{\dagger} \hat{c}_k \right) | \psi_{\alpha} \rangle. \quad (6.13)$$

To simplify notation, we define

$$\delta p_{k,\alpha} = \delta t \gamma_k \langle \psi_{\alpha} | \hat{c}_k^{\dagger} \hat{c}_k | \psi_{\alpha} \rangle \quad (6.14)$$

$$\delta p_{\alpha} = \delta t \sum_k \gamma_k \langle \psi_{\alpha} | \hat{c}_k^{\dagger} \hat{c}_k | \psi_{\alpha} \rangle, \quad (6.15)$$

so that the norm of the state becomes

$$\langle \psi_{\alpha}(t + \delta t) | \psi_{\alpha}(t + \delta t) \rangle = 1 - \sum_k \delta p_{k,\alpha} = 1 - \delta p_{\alpha}. \quad (6.16)$$

We now know the proper normalization for the state at time $t + \delta t$:

$$|\tilde{\psi}_{\alpha}(t + \delta t)\rangle = \frac{1 + \hat{H}_{\text{eff}} \delta t / i\hbar}{\sqrt{1 - \delta p_{\alpha}}} |\psi_{\alpha}(t)\rangle. \quad (6.17)$$

This normalized state corresponds the state of a system evolving solely under the influence of the first two terms in the master equation, i.e. a system which has never jumped into one of the $|\phi_{k,\alpha}\rangle$.

The “quantum jump” states $|\phi_{k,\alpha}\rangle$ are not normalized either, since

$$\langle\phi_{k,\alpha}|\phi_{k,\alpha}\rangle = \langle\psi_\alpha|\hat{c}_k^\dagger\hat{c}_k|\psi_\alpha\rangle = \frac{\delta p_{k,\alpha}}{\gamma_k\delta t}. \quad (6.18)$$

Again, we will define a normalized state

$$|\tilde{\phi}_{k,\alpha}\rangle = \sqrt{\frac{\gamma_k\delta t}{\delta p_{k,\alpha}}}|\phi_{k,\alpha}\rangle \quad (6.19)$$

to explicitly keep track of probability conservation.

Like the Schrodinger equation, the master equation may be written for discrete times δt ,

$$\hat{\rho}_S(t + \delta t) = \sum_\alpha p_\alpha \left(|\psi_\alpha(t + \delta t)\rangle\langle\psi_\alpha(t + \delta t)| + \delta t \sum_k \gamma_k |\phi_{k,\alpha}\rangle\langle\phi_{k,\alpha}| \right), \quad (6.20)$$

and expressed in terms of the normalized states $|\tilde{\psi}_\alpha(t + \delta t)\rangle$ and $|\tilde{\phi}_{k,\alpha}\rangle$,

$$\begin{aligned} \hat{\rho}_S(t + \delta t) &= \sum_\alpha p_\alpha \left((1 - \delta p_\alpha) |\tilde{\psi}_\alpha(t + \delta t)\rangle\langle\tilde{\psi}_\alpha(t + \delta t)| \right. \\ &\quad \left. + \sum_k \delta p_{k,\alpha} |\tilde{\phi}_{k,\alpha}\rangle\langle\tilde{\phi}_{k,\alpha}| \right). \end{aligned} \quad (6.21)$$

By rewriting the master equation in this form, we can use a probability interpretation to gain intuition – and develop numerics – for the resulting system dynamics. Eq. (6.21) has two terms, which lead to two possible outcomes after a time δt :

- (1) with probability $(1 - \delta p_\alpha)$, the system evolves according to \hat{H}_{eff} , and remains in state $|\tilde{\psi}_\alpha\rangle$.
- (2) with probability δp_α , the system jumps into another state; in particular it jumps into state $|\tilde{\phi}_{k,\alpha}\rangle$ with probability $\delta p_{k,\alpha}$.

This statistical picture of a state vector evolution provides a clear procedure for simulation which only requires computation of the state vector (rather than density matrix) elements. A sample algorithm is summarized in Table (6.1).

Table 6.1: Monte Carlo Procedure

- (1) Pick initial state $|\psi_\alpha\rangle$
- (2) Pick a random number r
- (3) For an appropriate time interval δt , calculate δp_α . If $\delta p_\alpha < r$, replace $|\psi_\alpha\rangle$ by $(1 - i\delta t \hat{H}_{\text{eff}}/\hbar)|\psi_\alpha\rangle / \sqrt{1 - \delta p_\alpha}$. If $\sum_{k=1}^K \delta p_{k,\alpha} \leq r < \sum_{k=1}^{K+1} \delta p_{k,\alpha}$, replace $|\psi_\alpha\rangle$ by $|\tilde{\phi}_{k,\alpha}\rangle$
- (4) Repeat steps (2) and (3) for the desired length of time.
- (5) Repeat steps (1-4) N times to generate a distribution of outcomes.
- (6) If necessary, repeat steps (1-5) for all possible initial states $|\psi_\alpha\rangle$.
- (7) Density matrix evolution: $\hat{\rho}_S(t) = \sum_\alpha p_\alpha |\psi_\alpha(t)\rangle\langle\psi_\alpha(t)|/N$.

6.2 Example: Decay of a two-level atom

As an example of the Monte Carlo Wavefunction method, consider a two level system which starts out in a pure state $|\psi(0)\rangle = a_1|1\rangle + a_2|2\rangle$, and decays at a rate γ so that $\hat{c} = |1\rangle\langle 2|$. In a time δt , the probability that the system jumps out of the superposition state is

$$\delta p = \delta t \gamma \langle \psi | \hat{c}^\dagger \hat{c} | \psi \rangle \quad (6.22)$$

$$= \delta t \gamma |a_2|^2. \quad (6.23)$$

Since δp is just the probability to emit a photon while decaying from $|2\rangle$ to $|1\rangle$, it makes sense that it is equal to the probability to be in the excited state multiplied by the probability for that excited state to decay. If the state does not decay, it evolves according to the effective Hamiltonian

$$\hat{H}_{\text{eff}} = \Delta |2\rangle\langle 2| + \frac{i\gamma}{2} \hat{c}^\dagger \hat{c}. \quad (6.24)$$

Solving the effective Schrodinger equation,

$$\frac{d}{dt} |\psi\rangle = - \left(\frac{\gamma}{2} + i\Delta \right) |2\rangle \quad (6.25)$$

we may easily find the time-dependent state,

$$|\tilde{\psi}(t)\rangle = \frac{1}{\sqrt{|a_1|^2 + |a_2|^2 e^{-\gamma t}}} \left(a_1 |1\rangle + a_2 e^{-(\gamma/2 + i\Delta)t} |2\rangle \right). \quad (6.26)$$

Due to the normalization terms in the denominator, the probability to be in state $|2\rangle$ decays more slowly than $e^{-\gamma t}$; however, at each step along the way, there is a finite probability to emit a photon and collapse definitely into the

ground state. If one averages over all such trajectories, following the Monte Carlo algorithm, one can show that the average population in the excited state does indeed decay as $e^{-\gamma t}$.

However, this picture has physical meaning beyond the statistical average, because it provides an answer to Carmichael's original question: What happens if the atom does not emit a photon? The above analysis shows that *not* detecting a photon is also a measurement on the system, because it causes the state to evolve in a certain way. Due to the normalization condition, at long times the system will always end up in $|1\rangle$ even if it never emits a photon.

Although the statistical wavefunction approach can provide some intuition and computational power, it is only useful in a small subset of calculations. In particular, it is advantageous to use the Monte Carlo method for simulations when

- (1) The Hilbert space is so large that density matrix calculations are impossible
- (2) One wishes to incorporate measurement-dependent feedback into the system. Feedback terms are difficult to incorporate into the master equation, but trivial to implement in the Monte Carlo Wavefunction algorithm. In general, however, this is a method of last resort, and should be employed only if other analytic and numerical techniques fail.

6.3 Non-Hermitian evolution: Summary

The stochastic wavefunction method has two fundamental parts: (1) evolution via the effective, non-Hermitian Hamiltonian, and (2) quantum jumps which occur randomly in time. Although the two parts are easily combined in numerical algorithms, only the first can be simply solved by hand. Nevertheless, in the limit that quantum jumps are very improbable, one might hope to accurately model a system using only the non-Hermitian Hamiltonian evolution. The non-Hermitian Hamiltonian has a simple intuitive interpretation: we just include by hand the imaginary parts to the energy, therefore accounting for a finite lifetime. We will often treat a system by solving a non-Hermitian Schrodinger equation and subsequently showing that the integrated probability for a quantum jump is negligible during the time interval under consideration.

For example, consider a two-level system initially in the ground state and illuminated by a weak field Ω . The probability of a quantum jump in this system is $\int dt \gamma \rho_{22} \propto |\Omega|^2$, so to lowest order in the applied field

we can neglect quantum jumps and treat the system using the effective Schrodinger equation. For this two-level system, the equations of motion obtained from the non-Hermitian Hamiltonian exactly mirror the master equation except for one term: the increase in ρ_{11} due to decay from the excited state is missing. By adding non-Hermitian terms to the Hamiltonian, we have effectively described loss from the system, but we cannot account for where the lost state ends up. In other words, probability slowly leaks from the system.

Chapter 7

Adiabatic Processes

Up to this point, our discussion has concentrated on understanding system dynamics for a Hamiltonian which is time-independent in an appropriate rotating frame. When we have encountered time-varying terms, such as the envelope shaping an applied laser pulse, we have argued that the system should be reasonably well described by a constant Hamiltonian containing the instantaneous value of the slowly changing parameter. In this chapter we will put this intuition on more formal footing, and discuss the limits to its applicability.

7.1 The adiabatic theorem for time-dependent Hamiltonians

Consider an N-dimensional Hilbert space spanned by an orthonormal basis, $\{|e_1\rangle \dots |e_N\rangle\}$ whose evolution is governed by a time-dependent Hamiltonian, $\hat{H}(t)$. At any given time $t = t_0$, we can always find the instantaneous eigenstates and eigenvalues of the Hamiltonian $\hat{H}(t_0)$,

$$\hat{H}(t_0)|\epsilon_k(t_0)\rangle = \epsilon_k(t_0)|\epsilon_k(t_0)\rangle. \quad (7.1)$$

An arbitrary state may be expanded in the basis of instantaneous eigenstates,

$$|\psi(t)\rangle = \sum_l c_l(t)|\epsilon_l(t)\rangle, \quad (7.2)$$

and it obeys the Schrödinger equation $i\hbar|\dot{\psi}(t)\rangle = \hat{H}(t)|\psi(t)\rangle$. For a constant Hamiltonian, a system prepared in an eigenstate will remain in that state; this is in general no longer true for time-dependent Hamiltonians.

Expanding the Schrödinger equation, we find that the time dependence of the eigenstates introduces new terms:

$$i\hbar \sum_l \left(\dot{c}_l(t) |\epsilon_l(t)\rangle + c_l(t) \frac{d}{dt} |\epsilon_l(t)\rangle \right) = \sum_l c_l(t) \epsilon_l(t) |\epsilon_l(t)\rangle. \quad (7.3)$$

To find the equations of motion for the probability amplitudes $c_k(t)$, we multiply Eq. (7.3) from the left by $\langle \epsilon_k(t) |$, yielding

$$i\hbar \dot{c}_k(t) = \epsilon_k(t) c_k(t) - i\hbar \sum_l c_l(t) \langle \epsilon_k(t) | \frac{d}{dt} |\epsilon_l(t)\rangle. \quad (7.4)$$

This set of N coupled differential equations may also be represented in matrix notation, with

$$\psi(t) = \begin{pmatrix} c_1(t) \\ c_2(t) \\ \vdots \\ c_N(t) \end{pmatrix} \quad \text{and} \quad \hat{H}(t) = \begin{pmatrix} \epsilon_1(t) & & & 0 \\ & \epsilon_2(t) & & \\ & & \ddots & \\ 0 & & & \epsilon_N(t) \end{pmatrix}, \quad (7.5)$$

whereby Eq. (7.4) becomes

$$i\hbar \frac{d}{dt} \begin{pmatrix} c_1 \\ c_2 \\ \vdots \\ c_N \end{pmatrix} = \begin{pmatrix} \epsilon_1 & -i\hbar \langle \epsilon_1 | \dot{\epsilon}_2 \rangle & \dots \\ -i\hbar \langle \epsilon_2 | \dot{\epsilon}_1 \rangle & \epsilon_2 & & \\ \vdots & & \ddots & \\ & & & \epsilon_N \end{pmatrix} \begin{pmatrix} c_1 \\ c_2 \\ \vdots \\ c_N \end{pmatrix}, \quad (7.6)$$

where the terms are implicitly time dependent for notational simplicity.¹

7.1.1 The condition for adiabaticity

Suppose the quantum state $|\psi\rangle$ is initially prepared at time $t = 0$ in one of the instantaneous eigenstates $|\epsilon_k(0)\rangle$. The off-diagonal couplings in Eqs. (7.4,7.6) indicate that $|\epsilon_k(t)\rangle$ is not an exact stationary state, but our intuition tells us that it should be approximately stationary for a Hamiltonian which changes very slowly. The situation where $|\epsilon_k(t)\rangle$ is essentially stationary is known as the “adiabatic” limit, and corresponds to off-diagonal terms sufficiently small that negligible population leaks to other states, i.e. $|c_k|^2 \approx 1$.

¹In general, the real part of $\langle \epsilon_k | \dot{\epsilon}_k \rangle$ vanishes, and we will neglect the Berry phase (imaginary component) in this treatment.

To estimate how small the off-diagonal couplings must be, we use perturbation theory to calculate how a weak coupling $\langle \epsilon_k | \dot{\epsilon}_l \rangle$ affects the state vector. In particular, for non-degenerate eigenstates and for $l \neq k$, the equation of motion for c_l is given by

$$\dot{c}_l \approx -i(\omega_l - \omega_k)c_l - \langle \epsilon_l | \dot{\epsilon}_k \rangle c_k(t) \quad (7.7)$$

$$\approx -i(\omega_l - \omega_k)c_l - \langle \epsilon_l | \dot{\epsilon}_k \rangle \cdot 1. \quad (7.8)$$

Here we have measured all the energies in reference to ϵ_k . The change induced in $|\psi\rangle$ by this coupling is

$$|\psi^{(1)}\rangle = -i\hbar \sum_l \frac{\langle \epsilon_l | \dot{\epsilon}_k \rangle | \epsilon_l \rangle}{\epsilon_k - \epsilon_l}. \quad (7.9)$$

The requirement that $|\epsilon_k(t)\rangle$ be stationary (or $|\psi^{(1)}\rangle = 0$) thus provides our adiabaticity condition,

$$\hbar \frac{|\langle \epsilon_l | \dot{\epsilon}_k \rangle|}{|\epsilon_k - \epsilon_l|} \ll 1. \quad (7.10)$$

A Hamiltonian which changes on a timescale τ will lead to couplings $|\langle \epsilon_l | \dot{\epsilon}_k \rangle| \propto 1/\tau$, so the system does indeed adiabatically follow the instantaneous eigenstates for a slowly varying Hamiltonian.

Note that the adiabatic theorem is formulated for coherent Hamiltonian evolution of the system. For systems which exhibit decay, the adiabatic requirement may be modified from the form exhibited in Eq. (7.10). Even when the adiabaticity condition is satisfied, the neglected diagonal terms may still introduce a phase factor known as a “geometric” or “Berry’s” phase. This geometric phase adds to the so-called “dynamical” phase (given by $e^{\{-i/\hbar \int_0^t d\tau \epsilon_k(\tau)\}}$) which comes from the diagonal part of the Schrodinger equation. A detailed discussion of such phases can be found in many modern quantum mechanics books (*e.g.* Sakurai); here we only note that in situations where the dynamical phase vanishes, there is frequently also no geometric phase.

7.2 Adiabaticity for the two-level system

Adiabatic evolution can be transparently illustrated by examining a two-level system with a time-dependent detuning $\Delta(t)$ and Rabi frequency $\Omega(t)$. Expressed in the time-independent (bare state) basis $\{|1\rangle, |2\rangle\}$, the Hamiltonian can be written

$$\hat{H}(t) = -\hbar\Delta(t)|2\rangle\langle 2| - \hbar\Omega(t)(|1\rangle\langle 2| + |2\rangle\langle 1|) \quad (7.11)$$

$$= -\hbar \begin{pmatrix} 0 & \Omega(t) \\ \Omega(t) & \Delta(t) \end{pmatrix}. \quad (7.12)$$

Diagonalizing the Hamiltonian gives us the instantaneous eigenstates $|\pm\rangle$ and eigenenergies ϵ_{\pm} ,

$$|+\rangle = \cos \theta(t)|1\rangle + \sin \theta(t)|2\rangle \quad (7.13)$$

$$|-\rangle = \sin \theta(t)|1\rangle - \cos \theta(t)|2\rangle \quad (7.14)$$

$$\epsilon_{\pm}(t) = \frac{\hbar}{2} \left(-\Delta(t) \pm \sqrt{\Delta(t)^2 + 4\Omega(t)^2} \right) \quad (7.15)$$

where the mixing angle is

$$\theta(t) = -\frac{1}{2} \arctan \frac{2\Omega(t)}{\Delta(t)}. \quad (7.16)$$

Note that $|\pm\rangle$ and $\epsilon_{\pm}(t)$ correspond exactly to a set of time-dependent dressed states and dressed energies.

We wish to examine this system in the adiabatic limit, so we will assume that Δ and Ω vary slowly enough that the adiabatic condition is fulfilled, or

$$\hbar \frac{|\dot{\Omega}\Delta - \Omega\dot{\Delta}|}{4\Omega^2 + \Delta^2} \ll \sqrt{4\Omega^2 + \Delta^2}. \quad (7.17)$$

7.2.1 Rapid adiabatic passage

Adiabatic passage represents an important application of the adiabatic theorem in a two-level system, because it provides a robust method for transferring population from one bare state to the other. For example, suppose the two-level system is initially in $|1\rangle$, and we seek to transfer all of the population into $|2\rangle$, but we cannot precisely control the values of Δ and Ω or the interaction time τ . With such imprecision, we will be unable to perform a given Rabi rotation, so we seek a more robust method.

Adiabatic return

Suppose that we tried keeping $\Delta \neq 0$ constant while sending in a pulse $\Omega(t)$. Initially, the dressed states would coincide with the bare states, and if the system adiabatically follows the ground state $|-\rangle$ it will evolve into a superposition of $|1\rangle$ and $|2\rangle$ for finite $\Omega(t)$. As $\Omega(t) \rightarrow 0$ at the end of the pulse, however, the system will return to its initial state $|1\rangle$ (see Fig. (9.3)).

Adiabatic passage

State transfer is possible when Ω/Δ changes from near $-\infty$ to near ∞ over the course of the experiment. One way to achieve this goal is to vary $\Delta(t)$ linearly in time, chirping the frequency through resonance while sending in a pulse $\Omega(t)$. The coupling between the levels leads to an avoided crossing, so an atom which starts out in $|1\rangle$ and adiabatically follows the ground state $|-\rangle$ will end up in $|2\rangle$ with near unit probability after a long time has passed.

7.2.2 Adiabaticity condition for the two-level system

For techniques like rapid adiabatic passage to work, the probability for the system to transition between eigenstates $|-\rangle$ and $|+\rangle$ must be small. In the two-level system, the adiabaticity condition requires that the coupling terms

$$\langle \dot{+} | - \rangle = \dot{\theta}(t) \quad (7.18)$$

be small compared to the energy splitting $\epsilon_+ - \epsilon_-$, or

$$\hbar \dot{\theta}(t) \ll |\epsilon_+(t) - \epsilon_-(t)|. \quad (7.19)$$

The minimum energy difference occurs when Δ sweeps through resonance, so $\epsilon_+(t) - \epsilon_-(t) \geq 2\Omega(t)$. Consequently the adiabaticity condition will be fulfilled whenever the total change in phase $\delta\theta$ is much less than the pulse area,

$$\int_{-\infty}^{\infty} dt \dot{\theta}(t) \ll \int_{-\infty}^{\infty} dt 2\Omega(t) = A. \quad (7.20)$$

Since adiabatic passage requires $\delta\theta = \mathcal{O}(1)$, the condition for adiabaticity can be simply stated as $A \gg 1$. The minimum time over which the system will adiabatically follow $|-\rangle$ is thus $\tau \approx 1/\Omega$. This time is not constrained by intrinsic atomic timescales; in particular it can be smaller than the excited state lifetime. Consequently, the technique may be considered “rapid” even while satisfying the adiabatic condition.

Exactly solvable system: the Landau-Zener model

This condition is a useful qualitative measure of the validity of the adiabatic approximation, but we would like to quantify any remaining corrections to the adiabatic result. Our discussion of adiabaticity has used perturbation theory, so it is tempting to extend the perturbative analysis to estimate

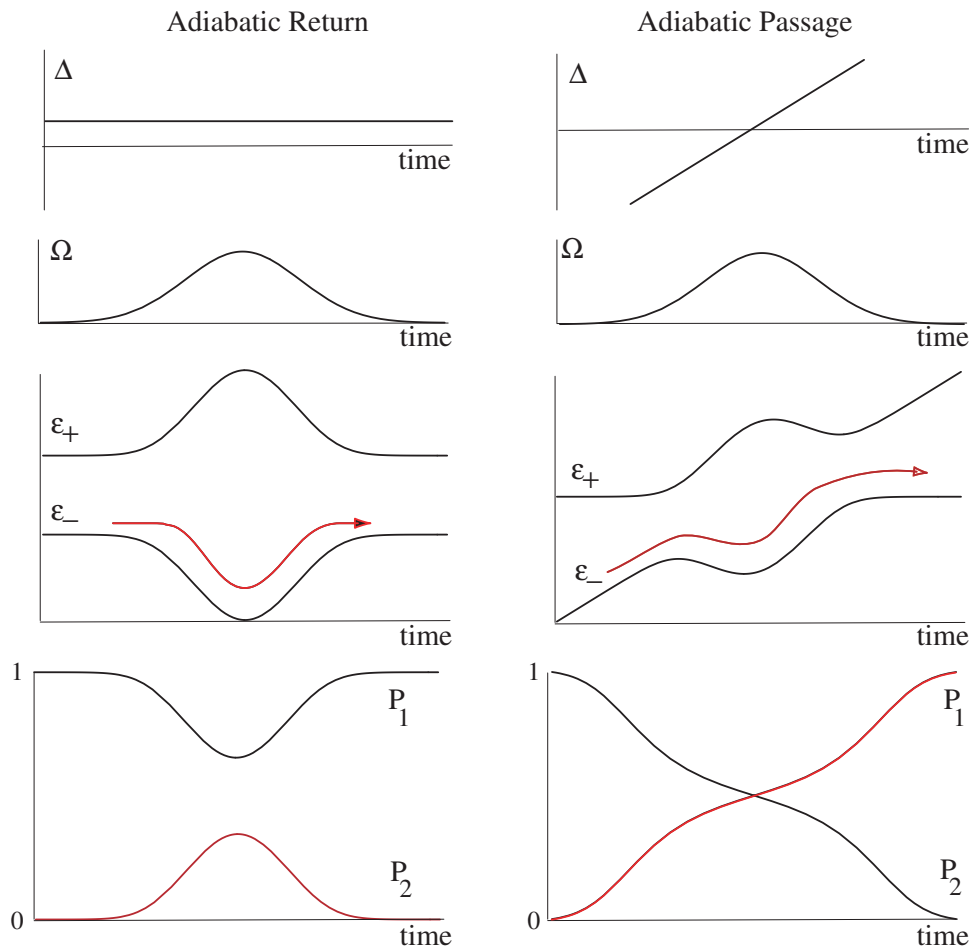


Figure 7.1: A comparison of adiabatic passage and adiabatic return. The time dependent parameters Δ and Ω lead to instantaneous eigenenergies ϵ_{\pm} . Assuming that the system follows the instantaneous ground state, it will be in a mixture of states $|1\rangle$ and $|2\rangle$ with occupation probabilities P_1 and P_2 respectively. Clearly, adiabatic passage can result in state transfer, whereas adiabatic return leaves the system in its initial state.

loss from the instantaneous eigenstates. For example, we might postulate a small parameter,

$$\epsilon = \frac{\dot{\theta}}{|\epsilon_+ - \epsilon_-|} \quad (7.21)$$

and try to expand the population loss in powers of ϵ . However, we have not verified that such an expansion is actually valid for this problem.

Examination of an exactly solvable problem provides a rather disturbing answer. For a system starting out at $t = -\infty$ in $|1\rangle$ with $\Omega = \Omega_0$ constant and $\Delta = \alpha t$, Landau and Zener showed that the probability of complete state transfer to $|2\rangle$ at large times is

$$P_{LZ} = 1 - e^{-2\pi \frac{|\Omega_0|^2}{|\alpha|}}. \quad (7.22)$$

Since $\dot{\theta} \sim \alpha/2\Omega_0$, the small parameter for this system is $\epsilon \approx \alpha/4\Omega_0^2$, which yields the non-adiabatic correction:

$$P_{LZ} - 1 \approx e^{-\frac{\pi}{2} \frac{1}{\epsilon}}. \quad (7.23)$$

This function is not analytic for small ϵ , and thus cannot be approximated by perturbation theory. Consequently more sophisticated methods are required to attempt a perturbative approach for this lossless system. Surprisingly, when loss from the excited state is included, the singularity at $\epsilon \rightarrow 0$ vanishes, and a perturbation series is possible.

7.3 Adiabatic processes in multi-level systems

In previous lectures we have seen how adiabatic processes can lead to interesting phenomena in three-level systems, in particular the adiabatic following of the dark state which leads to EIT. If we concentrate on the most interesting case of zero two-photon detuning, $\delta = 0$, and assume that the Rabi frequencies are real, the Hamiltonian for a three-level system coupled by two applied fields may be written (in the bare state basis)

$$\hat{H} = -\Delta|3\rangle\langle 3| - \Omega_1(|3\rangle\langle 1| + |1\rangle\langle 3|) - \Omega_2(|3\rangle\langle 2| + |2\rangle\langle 3|). \quad (7.24)$$

This Hamiltonian is diagonalized by the eigenbasis of dressed states

$$|\Phi_+\rangle = \sin \theta \sin \phi |1\rangle + \cos \theta \sin \phi |2\rangle + \cos \phi |3\rangle \quad (7.25)$$

$$|\Phi_0\rangle = \cos \theta |1\rangle - \sin \theta |2\rangle \quad (7.26)$$

$$|\Phi_-\rangle = \sin \theta \cos \phi |1\rangle + \cos \theta \cos \phi |2\rangle - \sin \phi |3\rangle, \quad (7.27)$$

where

$$\tan \theta = \frac{\Omega_1}{\Omega_2} \quad (7.28)$$

$$\tan 2\phi = -\frac{\sqrt{|\Omega_1|^2 + |\Omega_2|^2}}{\Delta} = -\frac{\Omega}{\Delta}. \quad (7.29)$$

The corresponding dressed energies are

$$\epsilon_+ = \frac{1}{2} \left(-\Delta + \sqrt{\Omega^2 + \Delta^2} \right) \quad (7.30)$$

$$\epsilon_0 = 0 \quad (7.31)$$

$$\epsilon_- = \frac{1}{2} \left(-\Delta - \sqrt{\Omega^2 + \Delta^2} \right). \quad (7.32)$$

The state $|\Phi_0\rangle$ corresponds to the dark state $|D\rangle$ of the system because it has no overlap with the excited state $|3\rangle$. By manipulating the system to adiabatically follow this dark state, we can have robust control over the population amplitudes in $|1\rangle$ and $|2\rangle$ while avoiding losses associated with spontaneous emission from $|3\rangle$.

7.3.1 Stimulated Raman adiabatic passage (STIRAP)

The instantaneous eigenstate $|\Phi_0\rangle$ is a superposition of the lower states $|1\rangle$ and $|2\rangle$ with probability amplitudes controlled by the mixing angle $\tan \theta = \Omega_1/\Omega_2$. As we noted earlier, the dark state approaches the two bare states when one of the applied fields vanishes,

$$\theta = 0 \Rightarrow |\Phi_0\rangle = |1\rangle \quad (7.33)$$

$$\theta = \frac{\pi}{2} \Rightarrow |\Phi_0\rangle = -|2\rangle. \quad (7.34)$$

If we change the two fields such that the mixing angle varies slowly from 0 to $\pi/2$, we can transfer population from $|1\rangle$ to $|2\rangle$ without ever populating the excited state $|3\rangle$. The appropriate pulse sequence begins with a pulse on the unoccupied transition, and is consequently referred to as a “counterintuitive” pulse sequence. More importantly, the precise shape and timing of the pulses is not terribly important; all that matters is that the mixing angle be slowly swept over $\pi/2$. Experiments have verified that STIRAP is an efficient and robust approach to state transfer, provided that the two-photon detuning can be kept small. Such adiabatic transfer techniques are particularly useful in molecular systems where the abundance of electronic, vibrational, and rotational decay channels makes dynamical control impossible.

Stimulated Raman Adiabatic Passage

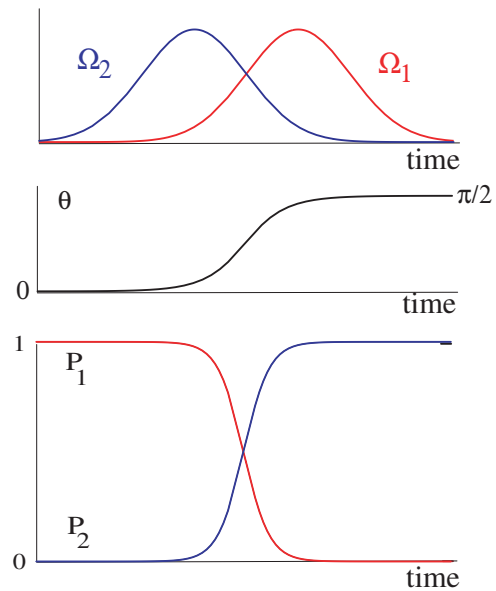


Figure 7.2: A possible pulse sequence to implement STIRAP in a three-level system. The two pulses are timed to smoothly change the mixing angle from 0 to $\pi/2$, resulting in a transfer of population between the lower metastable states.

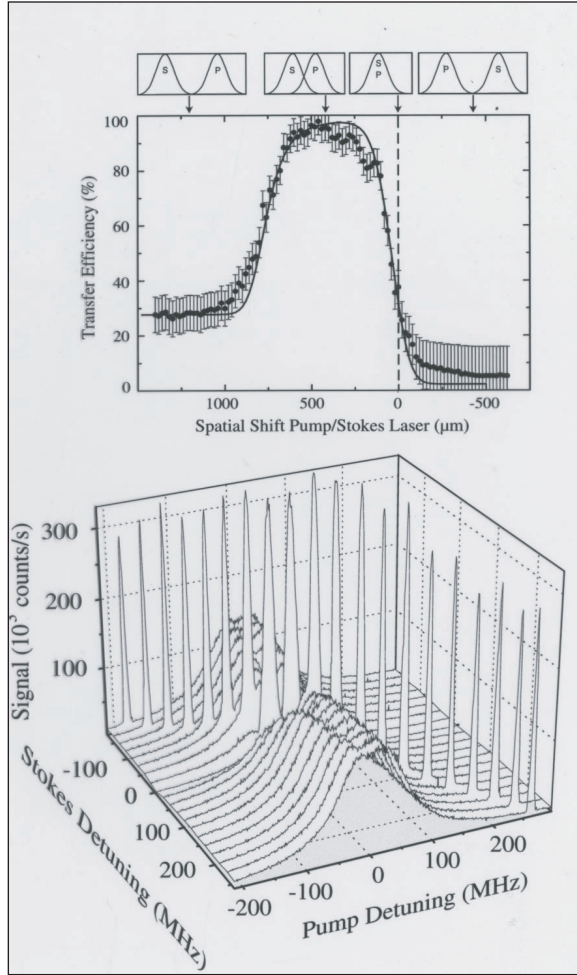


Figure 7.3: Experimental observation of STIRAP: (a) Transfer efficiency vs pulse overlap. In this experiment, atoms pass through a pump beam ($P = \Omega_1$) and a Stokes beam ($S = \Omega_2$). The percentage of atoms which are transferred from state $|1\rangle$ to $|2\rangle$ is subsequently measured. Note that the procedure only works for overlapping pulses in the counterintuitive order, but within those constraints it is robust to small changes in pulse shaping. (b) Transferred atoms vs detuning of the Stokes and pump beams. Our analysis was performed for precise $\delta = 0$ two photon resonance, which corresponds to the diagonal line of sharp peaks observed in the transfer efficiency. This shows that although adiabatic passage is insensitive to single-photon detuning, it is actually quite sensitive to the two-photon detuning.

7.3.2 Four-level systems

The three-level analysis can be generalized to higher dimensional Hilbert spaces with similar structure. For example, consider a system composed of three metastable states $\{|1\rangle, |3\rangle, |4\rangle\}$ resonantly coupled to an excited state $|2\rangle$ by applied fields $\{\Omega_1, \Omega_3, \Omega_4\}$. The Hamiltonian for such a system can

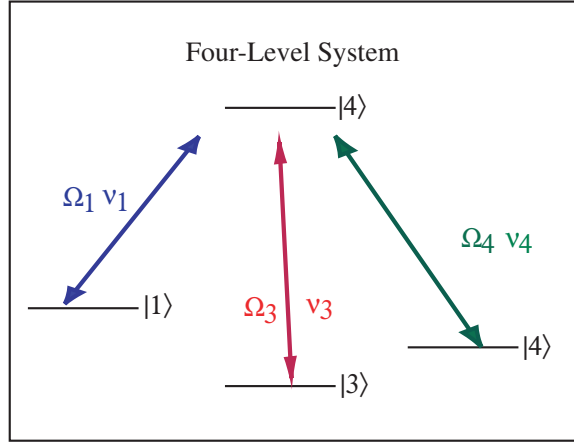


Figure 7.4: The four-level system under consideration. In our calculations we have assumed that all of the applied fields are resonant with the associated atomic transition.

be diagonalized, and has two degenerate dark states spanned by

$$|\Phi_1\rangle = \cos \theta |1\rangle - \sin \theta \cos \phi |3\rangle - \sin \theta \sin \phi |4\rangle \quad (7.35)$$

$$|\Phi_2\rangle = \sin \phi |3\rangle - \cos \phi |4\rangle, \quad (7.36)$$

where

$$\tan \theta = \frac{\Omega_1}{\sqrt{|\Omega_3|^2 + |\Omega_4|^2}} \quad (7.37)$$

$$\tan \phi = \frac{\Omega_3}{\Omega_4}. \quad (7.38)$$

The appearance of two dark states can be qualitatively understood by first considering $\Omega_1 = 0$. The remaining three-level system can be diagonalized, yielding a dark state $|D_{13}\rangle$ which is not coupled to the excited state.

Turning on Ω_4 does not affect $|D_{34}\rangle$, and it completes another three-level system (formed by $|1\rangle$ and the two bright states from the first three-level system) which also has a dark state $|D_1\rangle$. For resonant excitation, these two dark states will be degenerate since the Hamiltonian contains no detuning parameters and the dark states do not depend on the applied fields.

Because these two dark states are degenerate, we cannot ignore the non-adiabatic coupling between them. In fact, we can take advantage of the degeneracy to control mixing between $|\Phi_1\rangle$ and $|\Phi_2\rangle$, in the process preparing an arbitrary superposition of the two states. Suppose that initially $\theta = 0$ and the system starts out in $|1\rangle = |\Phi_1\rangle$. As $\theta \rightarrow \pi/2$, the system evolves into a superposition of $|3\rangle$ and $|4\rangle$ determined by the third field Ω_4 . By controlling the phase and amplitude of Ω_4 (and thus the mixing angle ϕ), one can control the final quantum state $c_3|3\rangle + c_4|4\rangle$.

Adiabatic manipulation of a four-level system has been used to experimentally construct a beamsplitter for atoms. As the atoms move through three spatially separated beams (which are thus pulsed in the frame moving with the atom), they are adiabatically transferred from their initial state $|1\rangle$ into a controllable mixture of $|3\rangle$ and $|4\rangle$. The momentum kicks imparted to an atom are determined by which state it ends up in, so the internal state of the atom is mapped onto its position. By changing the third field, one can control and detect which spatial path the atoms follow, verifying the adiabatic transfer.

7.4 Analysis of STIRAP: The condition for adiabatic following

We have argued qualitatively that the system adiabatically follows the dark state as a counter-intuitive pulse sequence is applied, and we have found the conditions for validity of the adiabatic theorem for coherent evolution. We have not yet quantified how slowly the probe pulse must change for this simple picture to remain valid in a system that exhibits dephasing and decay.

Analysis of the adiabaticity condition

To quantitatively analyze non-adiabatic losses, we assume a specific pulse profile that occurs on a characteristic timescale τ . For instance, suppose that the two pulses illuminating the atomic cloud have a time dependence

$$\Omega_1(t) = \Omega \sin \frac{t}{\tau} \quad (7.39)$$

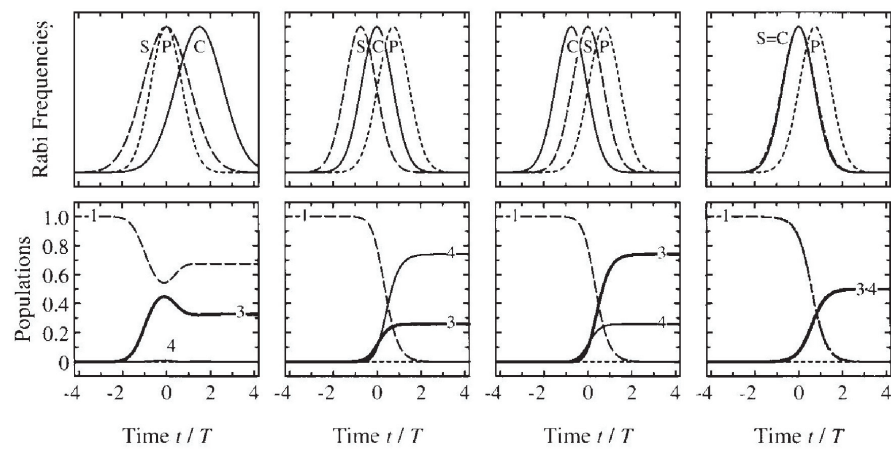


Figure 7.5: Pulse sequence for the four-level system. Three fields, $S = \Omega_3$, $C = \Omega_4$, and $P = \Omega_1$ are used to controllably transfer atoms from the initial state $|1\rangle$ to some superposition of $|3\rangle$ and $|4\rangle$. The probability amplitudes in the final state are determined by the timing, phase and power of the control pulse Ω_4 .

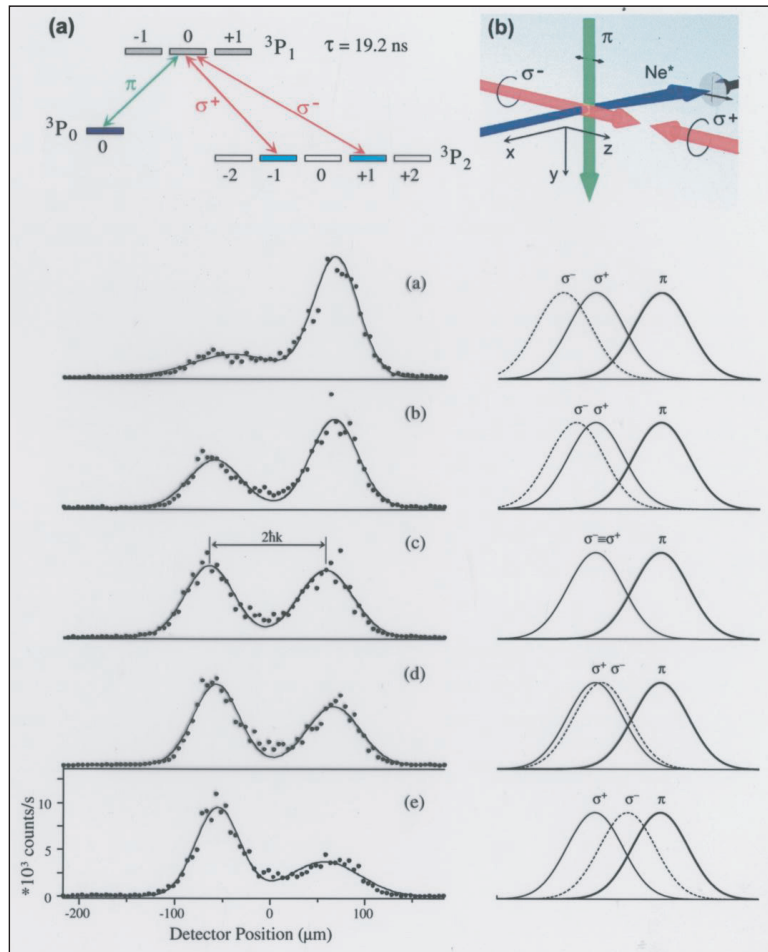


Figure 7.6: Beamsplitter for four-level atoms (metastable Neon) using adiabatic manipulation techniques. The relevant four levels are illustrated in (a), and the fields are named by their polarization: $\pi = \Omega_1$, $\sigma^+ = \Omega_3$, $\sigma^- = \Omega_4$. (b) The atoms travel through the three beams, which are offset by a variable distance. If the atoms end up in $|3\rangle$, they receive a momentum kick in the opposite direction than those which end up in $|4\rangle$. In the lower two graphs, the spatial distribution of atoms is shown for a variety of pulse sequences.

$$\Omega_2(t) = \Omega \cos \frac{t}{\tau}. \quad (7.40)$$

If the system starts out in $|1\rangle$ at $t = 0$, and adiabatically follows the dark state as the pulses change amplitude, then at $t = (\pi/2)\tau$, the system will be in $-|2\rangle$. We would like to find out the minimum time τ for which the atomic states can follow the evolution of the field without leaving the dark state.

In order to incorporate dephasing and decay into our description, we will use the stochastic wavefunction formulation. To keep things simple, we will neglect any decay out of $|2\rangle$ and also neglect any repopulation of lower states from decay out of $|3\rangle$.² The non-Hermitian Schrodinger equation for a generic state $|\psi(t)\rangle = c_1(t)|1\rangle + c_2(t)|2\rangle + c_3(t)|3\rangle$ yields the following equations of motion for the probability amplitudes:

$$\dot{c}_1 = i\Omega_1^*(t)c_3 \quad (7.41)$$

$$\dot{c}_2 = i\Omega_2^*(t)c_3 \quad (7.42)$$

$$\dot{c}_3 = -\gamma_{13}c_3 + i(\Omega_1(t)c_1 + \Omega_2(t)c_2). \quad (7.43)$$

We will look for a solution of these wave equations in the form

$$c_i = c_i^{(0)} + c_i^{(1)} + \dots \quad (7.44)$$

where each term in the sum represents a higher order correction in powers of a small parameter $\propto 1/\tau$. The lowest order solution $c_i^{(0)}$ is the stationary solution and can be found by neglecting all time derivatives in the equations of motion. The first two equations imply that $c_3^{(0)} = 0$, and by simultaneously solving the third equation and the normalization condition $\langle\psi|\psi\rangle = 1$ we can find the zeroth order amplitudes:

$$c_1^{(0)} = \frac{\Omega_2}{\sqrt{|\Omega_1|^2 + |\Omega_2|^2}} = \cos \frac{t}{\tau} \quad (7.45)$$

$$c_2^{(0)} = -\frac{\Omega_1}{\sqrt{|\Omega_1|^2 + |\Omega_2|^2}} = -\sin \frac{t}{\tau} \quad (7.46)$$

$$c_3^{(0)} = 0. \quad (7.47)$$

Note that neglecting time derivatives gives us precisely the dark state we found earlier.

²This is tantamount to assuming that all decay goes into a fourth state outside of the system we're considering.

Strictly speaking, however, $c_1^{(0)}$ and $c_2^{(0)}$ do not give an exact solution to the wave equations because their time derivatives are nonzero. To first nonvanishing order in $1/\tau$, we must include the effects of time variation in $c_1^{(0)}$ and $c_2^{(0)}$, yielding a set of equations for the first order corrections:

$$\dot{c}_1^{(0)} = i\Omega_1^* c_3^{(1)} \quad (7.48)$$

$$\dot{c}_2^{(0)} = i\Omega_2^* c_3^{(1)} \quad (7.49)$$

$$0 = -\gamma_{13} c_3^{(1)} + i(\Omega_1 c_1^{(1)} + \Omega_2 c_2^{(1)}). \quad (7.50)$$

The population amplitude for the excited state is no longer zero, since

$$c_3^{(1)} = \frac{\dot{c}_1^{(0)}}{i\Omega_1^*} = \frac{i}{\Omega\tau}. \quad (7.51)$$

Substituting the expression for $c_3^{(1)}$ into Eq. (7.50), we find

$$i(\Omega_1 c_1^{(1)} + \Omega_2 c_2^{(1)}) = \frac{i\gamma_{13}}{\Omega\tau}. \quad (7.52)$$

This equation cannot be solved³ for $c_1^{(1)}$ and $c_2^{(1)}$; however, we can immediately see that these first order corrections $c_1^{(1)}$ and $c_2^{(1)}$ are both proportional to $\gamma_{13}/\Omega^2\tau$. The evolution of the atomic state is approximately adiabatic when these corrections are small, so the adiabaticity condition becomes

$$\frac{\gamma_{13}}{\Omega^2\tau} \ll 1. \quad (7.53)$$

This result illustrates the importance of decay in adiabatic processes, since this result is quite different from what we found for adiabatic following of a coherently evolving system.

³Formally, we are seeking a solution to the vector differential equation

$$\dot{v} = M(t/\tau)v(t), \quad (7.54)$$

which we guess is of the form $v(t) = v^{(0)} + v^{(1)} + \dots$, where $v^{(0)}$ satisfies $M(t/\tau)v^{(0)} = 0$. Substituting this result into the differential equation above, we find that

$$\dot{v}^{(0)} \approx M(t/\tau)(v^{(0)} + v^{(1)}), \quad (7.55)$$

or $v^{(1)} = M^{-1}(t/\tau)\dot{v}^{(0)}$. Such an expansion fails for the system we are considering, however, because M is singular and cannot be inverted. Nonetheless, we see that the expansion does tell us some useful information about how the higher-order correction scales. To properly solve this system using some kind of adiabatic expansion, one should adiabatically eliminate the excited state, but solve the resulting equations of motion for $c_{1,2}$ exactly.

Error due to quantum jumps

In calculating the non-adiabatic corrections to dark state formation, we have neglected another source of error: quantum jumps. During the characteristic timescale τ , the probability for the system to undergo a quantum jump is

$$P_{\text{jump}} = \gamma_{13} \int_0^\tau |c_3|^2 = \frac{\gamma_{13}}{\Omega^2 \tau}. \quad (7.56)$$

The condition for the validity of the stochastic wavefunction approach us thus

$$P_{\text{jump}} \ll 1 \Rightarrow \frac{\gamma_{13}}{\Omega^2 \tau} \ll 1, \quad (7.57)$$

so the adiabatic approximation and the non-Hermitian evolution used to derive it are valid in the same situations.

Note that both non-adiabatic corrections to the non-Hermitian wave function and quantum jumps limit the fidelity of adiabatic passage from $|1\rangle$ to $-|2\rangle$. In particular, the probability to end up in the correct final state ($\Omega\tau = \pi/2$) can be explicitly calculated to be

$$\rho_{22} = e^{-\frac{\pi\gamma_{13}}{2|\Omega|^2\tau}}. \quad (7.58)$$

Unlike the Landau-Zener problem discussed above, this exact solution permits an expansion in the small parameter $\gamma_{13}/\Omega^2\tau$. While we cannot find a perturbative solution for coherent adiabatic processes, such an expansion can become possible in the presence of decay.

7.4.1 Remarks

The partially-diagonalized basis: an intuitive approach

Our analysis has been carried out using the bare state basis $|1\rangle$, $|2\rangle$ and $|3\rangle$. One could define a time-dependent dressed state basis by fully diagonalizing the Hamiltonian. In practice, however, this problem is most easily solved and understood in a partially diagonalized basis composed of the the dark state $|D\rangle$, the bright state $|B\rangle$, and the excited state $|E\rangle$:

$$|B\rangle = \frac{\Omega_1|1\rangle + \Omega_2|2\rangle}{\sqrt{|\Omega_1|^2 + |\Omega_2|^2}} \quad (7.59)$$

$$|D\rangle = \frac{\Omega_2|1\rangle - \Omega_1|2\rangle}{\sqrt{|\Omega_1|^2 + |\Omega_2|^2}} \quad (7.60)$$

$$|E\rangle = |3\rangle. \quad (7.61)$$

By choosing this hybrid basis we have achieved a considerable simplification of the interaction Hamiltonian,

$$\hat{H}_{\text{int}} = -\sqrt{|\Omega_1|^2 + |\Omega_2|^2} (|B\rangle\langle E| + |E\rangle\langle B|). \quad (7.62)$$

The dark state is not involved in the dynamics, since the excited state only couples to the bright state superposition of $|1\rangle$ and $|2\rangle$.

Working in this new basis provides us with an intuition for non-adiabatic corrections. States $|B\rangle$ and $|E\rangle$ are coupled by $\Omega = \sqrt{|\Omega_1|^2 + |\Omega_2|^2}$, while the finite pulse time induces a weak coupling between the dark and bright states. The strength of the $|D\rangle \rightarrow |B\rangle$ transition is given by

$$i\hbar\langle B| \frac{d}{dt}|D\rangle = -i\hbar \frac{1}{\tau}. \quad (7.63)$$

The nonadiabatic coupling acts like a weak field with Rabi frequency of $\Omega_{\text{NA}} = 1/\tau$ driving the $|D\rangle$ to $|B\rangle$ transition.⁴

This is precisely the kind of situation encountered for an atom excited by optical and microwave radiation in a double resonance experiment. The net effect of Ω and γ_{13} is to introduce a finite lifetime of $|B\rangle$, since $|B\rangle$ can be excited to $|E\rangle$ which then decays. The escape rate out of $|B\rangle$ is on the order of the optical excitation rate,

$$\gamma_B = \frac{\Omega^2}{\gamma_{13}}. \quad (7.64)$$

The atom will remain in the dark state provided that the mixing rate Ω_{NA} between $|D\rangle$ and $|B\rangle$ is weaker than the inverse lifetime of $|B\rangle$,

$$\frac{1}{\tau} \ll \frac{\Omega^2}{\gamma_{13}}. \quad (7.65)$$

Here, decay from the bright state helps to force the atoms into the dark state. By reasoning physically we have arrived at precisely the same adiabaticity condition we derived mathematically.

Adiabatic passage and EIT

There is an interesting relationship between the condition for adiabatic following and the condition for pulse propagation within an EIT medium. The

⁴Note that our choice of $\Omega_1(t), \Omega_2(t)$ as sines and cosines has led us to a constant non-adiabatic coupling, which makes the mathematics easier. Other functions would also lead to Ω_{NA} , but in general it would be a function of time.

spectral window for electromagnetically induced transparency allows a probe pulse to propagate without losses only if all of its spectral components fit within the dark resonance linewidth $\Delta\omega$, i.e. if the probe pulse duration is sufficiently long $\tau \gg 1/\Delta\omega$. Since $\Delta\omega = \Omega^2/\gamma_{13}$, the condition for EIT pulse transmission corresponds exactly to the adiabatic following condition.

This correspondence underscores the relationship between EIT and adiabatic processes. If the pulse enters slowly enough, the atomic system adiabatically follows the dark state into a superposition of $|1\rangle$ and $|2\rangle$ which propagates without loss through the medium. As the pulse exits, the atomic state adiabatically follows the dark state back to $|1\rangle$, transferring the atomic coherence to the transmitted light.

Non-adiabatic dark state preparation

The dark state can also be prepared without adiabatic processes. For example, suppose the system started in an incoherent mixture of states, $\rho_{11} = \rho_{22} = 1/2$. Since the desired final state is a pure state, no Hamiltonian evolution (adiabatic or not) could transform this mixed state into a dark state.

Nevertheless, the experimental discovery of dark states [Alzelter *et al.* Novvo Cirr. 36B, 5/76] was done by monitoring fluorescence from a thermal sodium vapor cell illuminated by two continuous-wave fields. A magnetic field gradient along the cell created a spatial gradient of detunings due to the Zeeman effect. At the precise location along the cell where the Zeeman-shifted two-photon detuning vanished, a dark stripe appeared in the fluorescence signal. This was interpreted as formation of a dark state – yet the thermal vapor had started out in a statistical mixture.

This puzzle is easily resolved by analyzing the experiment in the partially diagonalized basis of bright and dark states. The original mixed state is a statistical mixture of the bright state and the dark state. Consider the situation when the CW fields Ω_1 and Ω_2 are applied such that non-adiabatic coupling to $|B\rangle$ and $|D\rangle$ vanishes. Meanwhile, the pair of fields act as an optical pumping beam, exciting an atom in $|B\rangle$ to $|E\rangle$ where it either decays to $|D\rangle$ (where it then remains) or $|B\rangle$ (from which it gets pumped back to $|E\rangle$). Optical pumping in the partially diagonalized basis thus prepares the system in the dark state by purely incoherent processes.

Populations and coherences: The importance of basis

We see from the example of dark state formation that the preparation of atomic coherence is somehow related to optical pumping. This is not too surprising because coherence in one basis, (e.g. $\{|1\rangle, |2\rangle\}$) is just population difference in another basis, (e.g. $\{|B\rangle, |D\rangle\}$).

The relationship between populations and coherences can be illuminated by the simple example of an atom interacting with linearly polarized light on a $J = 1$ to $J' = 1$ transition. In the absence of an applied magnetic field, we are free to choose our axis of quantization either parallel or perpendicular to the light polarization.

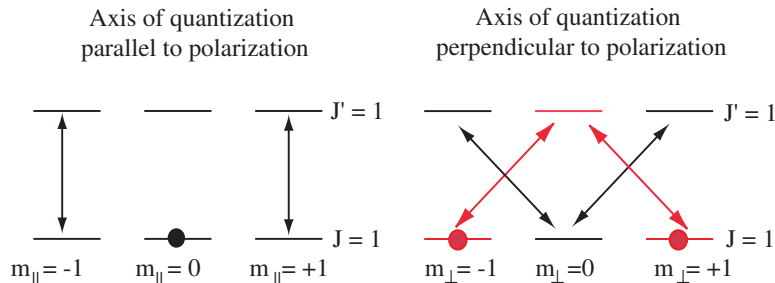


Figure 7.7: Linearly polarized light near resonant with a $J = 1$ to $J' = 1$ transition is most easily understood if the axis of quantization is chosen parallel to the axis of polarization. In this first case, the fields will clearly pump the atoms into the $m_{||} = 0$ state. If we choose to analyze the problem in the perpendicular basis, we must identify the Λ system highlighted in red. The light will pump the populations into the associated dark state superposition of $m_{\perp} = \pm 1$, which is exactly equal to the state $m_{||} = 0$.

Suppose that we choose to quantize the m_J sublevels parallel to the light polarization. Since symmetry considerations forbid transitions with $\Delta J = 0, \Delta m_J = 0$, the light will only couple $m_J = \pm 1 \rightarrow m'_J = \pm 1$, and any mixed state will be optically pumped into the lower $m_J = 0$ state.

Now suppose we choose to analyze the same problem with the light polarized perpendicularly to the axis of quantization. Any linear polarization can be decomposed into two circular polarizations, which couple the four $\Delta m_J = \pm 1$ transitions. In this mess of levels and transitions, we can identify a Λ configuration: the $m_J = 1$ state and the $m_J = -1$ state are now

both coupled to the same $m'_J = 0$ excited state. Consequently, the system has a dark state, and the atoms will be optically pumped into a dark superposition of $m_J = -1$ and $m_J = 1$ which precisely corresponds to the $m_J = 0$ state quantized along the polarization axis.

The bottom line of this discussion is that a coherence in one basis is a population distribution in another basis. Typically, the latter basis will provide the most physical insight into a complicated problem.

Applications of the dark state

The dark state is an important tool which has been used both to prepare and manipulate atomic states and to control pulses of light. In addition, a momentum transfer is associated with the formation of the dark state. Consequently dark state techniques can also be used to generate superpositions of momentum states or spatial states. For example, as noted in the previous lecture, adiabatic passage has been used to create a controllable atomic beamsplitter.

Chapter 8

Atomic motion in laser light

In addition to their internal level structure, atoms have external degrees of freedom corresponding to their center of mass motion. Since photons carry energy and momentum, interactions between atoms and light can affect the motional states of the atoms as well as their electronic states. Using a semi-classical picture of atomic motion, we will show how laser light can produce both dissipative and conservative forces on the atoms. The conservative force will be explained and interpreted in terms of dressed atomic energy levels, while the dissipative force can be understood in relation to incoherent pumping and damping rates.

8.1 Incorporating center of mass motion into atom-light interactions

In our discussion of atomic motion, we will focus for simplicity on an atom with only two relevant internal levels, $\{|1\rangle, |2\rangle\}$. Denoting the position and momentum of the atom by the operators $\hat{r} = \{\hat{x}, \hat{y}, \hat{z}\}$ and $\hat{p} = \{\hat{p}_x, \hat{p}_y, \hat{p}_z\}$, we can write down the Hamiltonian for a moving atom interacting with laser light with Rabi frequency Ω :

$$\hat{H} = \hat{H}_F + \hat{H}_{AF} + \frac{\hat{p}^2}{2m} + V(\hat{r}). \quad (8.1)$$

The free-field Hamiltonian \hat{H}_F accounts for electromagnetic energy density. The atom-field Hamiltonian \hat{H}_{AF} has two components: (1) the atom-reservoir interaction \hat{H}_{AR} leads to spontaneous emission and (2) the atom-laser interaction \hat{H}_{AL} causes transitions between the two atomic levels.

In the RWA, the atom-laser interaction may be written

$$\hat{H}_{AL} = -\hbar\Omega(\hat{r})|2\rangle\langle 1| - \hbar\Omega(\hat{r})^*|1\rangle\langle 2|, \quad (8.2)$$

where we have explicitly included spatial dependence of the laser amplitude and phase,

$$\Omega(\hat{r}) = |\Omega(\hat{r})|e^{i\phi(\hat{r})}. \quad (8.3)$$

Interactions with a plane wave

The force exerted on an atom by a plane wave furnishes an instructive example of momentum transfer between light and atoms. In the notation introduced above, a running wave has a constant amplitude $|\Omega|$ but spatially varying phase $\phi = \mathbf{k} \cdot \mathbf{r}$. For this analysis we will assume that the external potential $V(\hat{r})$ is negligible over a characteristic distance scale for the problem. The momentum \hat{p} is thus a good quantum number for the atomic motional state, and it is therefore advantageous to rewrite the laser phase operator $e^{i\mathbf{k} \cdot \mathbf{r}}$ in the momentum eigenbasis. Using two completeness relations, we find

$$e^{ik \cdot \hat{r}} = \int dp \int dp' |p\rangle \underbrace{\langle p| e^{ik \cdot \hat{r}} |p'\rangle}_{\delta(p-(p'+\hbar k))} \langle p'| \quad (8.4)$$

$$= \int dp' |p' + \hbar k\rangle \langle p'|. \quad (8.5)$$

Rewriting the atom-laser Hamiltonian,

$$\hat{H}_{AL} = -\hbar|\Omega(\hat{r})| \int (|2\rangle|p + \hbar k\rangle\langle p|\langle 1| + |1\rangle|p\rangle\langle p + \hbar k|\langle 2|) dp, \quad (8.6)$$

we see immediately that the interaction of light with the atom involves not only the internal state but also the center of mass momentum state. This momentum transfer is known as “atomic recoil.”

Suppose the atom starts out in the state $|p\rangle|1\rangle$. The plane wave light will promote it to the state $|p + \hbar k\rangle|2\rangle$, resulting in Rabi oscillations involving internal and momentum degrees of freedom. If we take into account the motional state of the atom, we find that the energy difference between these two states is not precisely equal to the internal transition energy $\hbar\omega_{12}$. In particular, the resonant frequency of this transition is

$$\omega_{\text{res}} = \omega_{12} + \frac{(p + \hbar k)^2}{2m\hbar} - \frac{p^2}{2m\hbar} \quad (8.7)$$

$$= \omega_{12} + \frac{pk}{m} + \frac{\hbar k^2}{2m}. \quad (8.8)$$

The two corrections have a simple physical interpretation: the first, $pk/m = vk$ is the Doppler shift, while the second is the recoil energy ω_R of the photon. Typically, the recoil shifts for alkali atoms are much smaller than the optical relaxation rate, with $\omega_R \sim \gamma/400 \sim 10 - 100$ kHz. However, the recoil shift is not so different from the linewidth of two-photon transitions, indicating that interesting effects might arise in laser cooling of multilevel atoms.

8.2 Semiclassical description

The interaction of an atom with a plane wave illustrated how the atom changes its momentum and energy in the process of coherently absorbing a photon. Incoherent processes will also have an effect on the motional state, since spontaneous emission will produce a random distribution of momentum kicks. Quantum treatment of the electromagnetic field and atomic momentum states would be required to truly describe such processes. That level of detail is unnecessary, however, to describe the center of mass motion in the classical regime. We will consequently use a semiclassical approach to understand the force the light exerts on the atoms.

The correspondence between classical and quantum dynamics is most easily seen in the Heisenberg picture, where the commutator of the momentum and the Hamiltonian gives the effective force¹:

$$\frac{d}{dt}\hat{p} = \frac{1}{i\hbar}[\hat{p}, \hat{H}] = \hat{F}. \quad (8.9)$$

In terms of the position operator, this force can be represented by

$$\hat{F} = -[\nabla, \hat{H}(\hat{r})] = \hbar\nabla\Omega|2\rangle\langle 1| + \hbar\nabla\Omega^*|1\rangle\langle 2|. \quad (8.10)$$

We now invoke the idea that our atom is very nearly a classically moving ball experiencing the average force

$$F = \langle \hat{F} \rangle = \hbar\nabla\Omega\rho_{12} + \hbar\nabla\Omega^*\rho_{21}. \quad (8.14)$$

¹In general, we can derive an identity to evaluate any commutator of the form $[\hat{p}, \hat{O}(\hat{r})]$. Working in the position basis, the action of this commutator on any state $|\psi(r)\rangle$ is given by

$$[\hat{p}, \hat{O}(r)]\psi(r) = [-i\hbar\nabla, \hat{O}(r)]\psi(r) \quad (8.11)$$

$$= -i\hbar\nabla(\hat{O}(r)\psi(r)) + i\hbar\hat{O}(r)\nabla\psi(r) \quad (8.12)$$

$$= -i\hbar(\nabla\hat{O}(r))\psi(r). \quad (8.13)$$

Thus we can write $[\hat{p}, \hat{O}(r)] = -i\hbar\nabla\hat{O}(r)$. One can use this identity, for example, to find the force operator above.

Note that the indices are counterintuitive but correct:

$$\langle|1\rangle\langle 2|\rangle = \text{Tr}[\rho|1\rangle\langle 2|] = \rho_{21}. \quad (8.15)$$

Since $\rho_{21}/\Omega \propto \chi$ is independent of the phase of Ω , it is convenient to write the force in terms of this ratio:

$$F = \hbar\Omega^*\nabla\Omega\left(\frac{\rho_{12}}{\Omega^*}\right) + \hbar\Omega\nabla\Omega^*\left(\frac{\rho_{21}}{\Omega}\right) \quad (8.16)$$

$$= \hbar\frac{1}{2}\nabla|\Omega|^2\left(\frac{\rho_{12}}{\Omega^*} + \frac{\rho_{21}}{\Omega}\right) + i\hbar|\Omega|^2\nabla\phi\left(\frac{\rho_{12}}{\Omega^*} - \frac{\rho_{21}}{\Omega}\right) \quad (8.17)$$

Separating out the real and imaginary parts of the susceptibility, we find that there are separate contributions from the reactive and dissipative components of the atomic response.

$$F = \underbrace{2\hbar|\Omega|^2\nabla\phi \text{Im}\left(\frac{\rho_{21}}{\Omega}\right)}_{\text{dissipative}} + \underbrace{\hbar\nabla|\Omega|^2\text{Re}\left(\frac{\rho_{21}}{\Omega}\right)}_{\text{reactive}}. \quad (8.18)$$

This force is particularly easy to calculate and understand when we can use the steady state solution of the density matrix equations to solve for ρ_{21} . The steady state solution will be valid for timescales t much greater than the dephasing time $1/\gamma_{12}$ or the inverse detuning $1/\delta$. For our description of the forces to be valid, the width of the atomic wave packet must be much less than the optical wavelength, $\Delta r(0)\ll\lambda$, such that the atom can resolve the phase of the field. At some later time, the center of mass motion is approximately given by $r(t)\sim r(0) + p(0)t/m$, which has an uncertainty $\Delta r(t)\sim\Delta r(0)+\Delta p(0)t/m$. For the force equation to still remain valid at time t , we must have that $\Delta p(0)t/m\ll\lambda$, or $k\Delta p(0)t/m\ll 1$. Using the uncertainty relationship $\Delta r(0)\Delta p(0)\sim\hbar$ and $\Delta r(0)\ll\lambda$, the limitation on time can be written $t\ll\omega_R$, where the recoil energy $\hbar\omega_R = (\hbar k)^2/2m$. This semiclassical force description is then valid in the regime

$$\omega_R\ll 1/t\ll \max(\gamma_{12}, \delta). \quad (8.19)$$

When this condition is satisfied, and when the light intensities are small, we can use $\rho_{21}/\Omega = i/(\gamma_{12} - i(\delta - kv))$ to find the light-induced force and analyze the physics behind it.

Large detuning: the dipole force

When the incident light is far detuned from atomic resonance, the real part of the susceptibility dominates and the response is almost purely reactive.

In this limit, $\rho_{21}/\Omega = -1/\delta$ and

$$F = -\hbar \nabla \left(\frac{|\Omega|^2}{\delta} \right). \quad (8.20)$$

This type of force is known as the “dipole force”, and it is conservative because it can be written as the gradient of a potential. Note that the potential $V_{\text{eff}} = \hbar|\Omega|^2/\delta$ corresponds to the AC Stark shift induced by the applied field. In fact, we can interpret the origin of the dipole force by examining the atomic energy levels in the dressed state picture. For a far-off resonance beam, the atoms remain in the ground state, but they can reduce their potential energy by moving to a region where the AC Stark shift lowers the ground state energy. The dipole force thus represents the attraction or repulsion of an atom in a dressed state potential.

The sign of the detuning determines the sign of the dipole force. In particular,

$$\begin{aligned} \delta < 0 &\Rightarrow \text{atoms attracted to field maxima} \\ \delta > 0 &\Rightarrow \text{atoms attracted to field minima.} \end{aligned}$$

Consequently the dipole force can be tailored to attract or repel atoms as needed. The sign dependence on detuning can also be found from a classical argument. If we consider the atom as a polarizable classical dipole d in a polarizing electric field E , its energy is $-E \cdot d$. Applied fields with frequencies below the resonance will induce a dipole which oscillates in phase with the field, yielding a decrease in energy. Excitation above resonance induces a dipole which is π out of phase with the applied field, yielding an increase in energy. Consequently, atoms in red-detuned fields will seek the field maximum, while atoms in blue-detuned fields will seek the field minimum.

The dipole force dominates only for large detunings, requiring similarly large powers $|\Omega|^2$ in order to create a tight trap. In this limit, the dipole force provides an effective method to confine atoms without introducing a lot of spontaneous emission.

Two important examples of the dipole force have found extensive application in atomic physics. The dipole trap is formed by tightly focussing a red-detuned beam which attracts atoms to the region of maximum intensity. This simple design has been used to manipulate and study cold atoms and Bose Einstein condensates. The second important application of the dipole force is known as the “optical lattice.” Atoms illuminated by a standing wave are attracted to the nodes or antinodes, spaced by $\sim \lambda/2$. A single standing wave will produce a one dimensional lattice, and by adding orthogonal beams higher dimensional lattices can be produced. These optical

lattices are approximately equivalent to “atomic crystals”, and can be used to study phenomena analogous to those in solid-state physics by building a model crystal out of atoms and lasers.

The dipole force can often be generalized to many states $\{|i\rangle\}$, with an effective potential associated with each state,

$$V_{\text{eff}} = \hbar \sum_i \frac{|\Omega_i|^2}{\delta_i} |i\rangle\langle i|. \quad (8.21)$$

This effective potential only incorporates the AC Stark shifts experienced by the multilevel atom; in general it may be important to take into account contributions (also of order $1/\delta$) due to two-photon processes between nearly degenerate atomic levels. In this situation, the internal states $\{|i\rangle\}$ are no longer good eigenstates, and we would need to rediagonalize the Hamiltonian to obtain the true dressed state potential.

Plane waves: the dissipative force

An atom illuminated by a plane wave does not experience a dipole force, since $\nabla|\Omega^2| = 0$. The dissipative force depends on $\text{Im}(\rho_{21}/\Omega)$, which for low intensities $|\Omega| \ll \gamma$ is given by

$$\text{Im}\left(\frac{\rho_{21}}{\Omega}\right) \approx \frac{\gamma_{12}}{\gamma_{12}^2 + (\delta - kv)^2}. \quad (8.22)$$

The kv term accounts for the fact that an atom moving with velocity v sees a Doppler-shifted laser frequency. The dissipative force is thus

$$\mathbf{F} \approx \hbar \mathbf{k} \frac{2\gamma_{12}|\Omega|^2}{\gamma_{12}^2 + (\delta - kv)^2} = \hbar \mathbf{k} R_{\text{opt}}, \quad (8.23)$$

where R_{opt} is the optical pumping rate. The expression above holds only in the weak field limit, when $R_{\text{opt}} \ll \gamma$.

The physical intuition behind the dissipative force is straightforward. The light directs a momentum kick $\hbar \mathbf{k}$ to the atom each time a photon is absorbed. When the atom relaxes incoherently to the ground state, it emits a photon into 4π , leading to no net change in momentum. Consequently the motional state changes on average by $\hbar \mathbf{k}$ every time a photon is absorbed and then spontaneously emitted. Absorption/re-emission occurs at the optical pumping rate, so the rate of momentum change must be $\mathbf{F} = \hbar \mathbf{k} R_{\text{opt}}$. More generally, following this line of reasoning, the dissipative force \mathbf{F} can also be

thought of as the change in momentum $\hbar\mathbf{k}$ per scattering event, multiplied by the rate of scattering, $\gamma\rho_{22}$,

$$\mathbf{F} = \hbar\mathbf{k}\gamma\rho_{22}. \quad (8.24)$$

This result can be confirmed directly with a bit of algebra, by rewriting ρ_{21}/Ω in terms of the excited state population.

How large can the dissipative force be? We have seen in previous lectures that the transition saturates as more and more power is applied. For large powers,

$$\text{Im}\left(\frac{\rho_{21}}{\Omega}\right) = \frac{\gamma_{12}}{\gamma_{12}^2 + (\delta - kv)^2} \frac{\gamma}{\gamma + 2R_{opt}}, \quad (8.25)$$

so the force becomes

$$\mathbf{F} = \hbar\mathbf{k} \frac{\gamma R_{opt}}{\gamma + 2R_{opt}} \quad (8.26)$$

In the limit of large powers, $\Omega \gg \gamma$, $R_{opt} \rightarrow \infty$, the maximum attainable dissipative force is set by the atomic spontaneous emission rate,

$$\mathbf{F}_{\max} = \hbar\mathbf{k} \frac{\gamma}{2}. \quad (8.27)$$

This limit makes intuitive sense given Eq. (8.24), because the atom cannot spend more than half of its time in the excited state, and thus achieves a maximum scattering rate given by $\gamma/2$.

It is instructive to consider typical orders of magnitude for the dissipative force. A single momentum kick $\hbar k$ will typically change the atomic velocity by a few centimeters per second. Compared to room temperature velocities $\sim 100 - 1000$ m/s, this recoil velocity is minuscule. A huge number of events $\sim 10^4$ are required to slow a room temperature atom down to the recoil velocity. For alkali atoms, $\gamma \sim 10^6$ Hz, so the slowing process will require a few milliseconds, during which the atom will travel about one meter. These kinds of considerations determine the physical scale of laser cooling experiments.

For practical experiments, it is important to consider the space and time dependent velocity of the atoms. In particular, as an atom is slowed by the dissipative force, it will be Doppler shifted out of resonance with the applied laser beam. In order to slow a beam of atoms, it is necessary to change the resonance condition so that a typical atom will always be in resonance with the applied light during the entire slowing process. In practice, this is accomplished in two ways: either the applied laser is chirped (its frequency is swept), or a spatially varying magnetic field adds a Zeeman shift to the atoms to keep them in resonance as they slow down.

8.3 Doppler Cooling

We have seen two ways in which photons can exert a force on atoms, in principle allowing deceleration of an atomic beam. However, the momentum kicks imparted to the atoms need not necessarily cool the atoms. Cooling requires the analogue of viscosity, so that the applied fields not only slow the atoms but also narrow their velocity distribution. In particular, an atomic ensemble will be cooled if the applied fields slow down hot atoms more efficiently than cool atoms. Consequently, a cooling force must depend on the velocity of the atom. The technique of Doppler cooling employs the velocity-dependent terms in the dissipative force to produce a viscous force on atoms.

Optical molasses

To understand where the viscosity arises, we will examine the dissipative force on slowly moving atoms, $\mathbf{k} \cdot \mathbf{v} \ll \delta, \gamma_{12}$. Expanding this force in small powers of the velocity, we find

$$F \approx \hbar \mathbf{k} \underbrace{\frac{2\gamma_{12}|\Omega|^2}{\gamma_{12}^2 + \delta^2}}_{R_{\text{opt}}^0} \left(1 + \frac{2\delta \mathbf{k} \cdot \mathbf{v}}{\gamma_{12}^2 + \delta^2} \right), \quad (8.28)$$

where we recognize R_{opt}^0 as the optical excitation rate for atoms with zero velocity. Two terms arise in Eq. (8.28): the first velocity-independent term gives a directed momentum kick to the atom while the second term provides the velocity dependent cooling force. Note that the first term is proportional to \mathbf{k} whereas the second $\propto k^2$, so that only the first term depends on the sign of \mathbf{k} . By applying counterpropagating beams, one might thus hope to cancel the effects of the first term while retaining the cooling force of the second term.

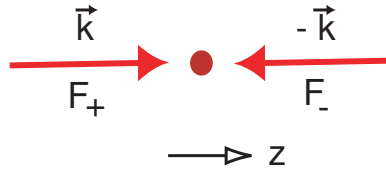


Figure 8.1: Counterpropagating beams used for Doppler cooling.

Consider an atom illuminated by two beams counterpropagating in the $\pm z$ direction. Provided that the optical pumping rate is small, the total

force on the atom is just the sum of the forces from each beam, $F = F_+ + F_-$. Indeed, the velocity-independent forces will precisely cancel, while the second term contributes a viscous force

$$F = F_+ + F_- = \eta m v_z \quad (8.29)$$

where m is the mass of the atom and η is the friction coefficient

$$\eta = \frac{8\hbar k^2}{m} \frac{\delta \gamma_{12} |\Omega|^2}{(\gamma_{12}^2 + \delta^2)^2}. \quad (8.30)$$

Note that the sign of η depends on the sign of the detuning: for $\delta < 0$, the viscous force will act to cool the atoms, whereas for $\delta > 0$ it will heat them.

The physics behind the Doppler cooling mechanism can be naively explained using energy conservation. For $\delta < 0$, the atom absorbs a red-detuned photon then spontaneously emits a photon resonant with the atomic transition, so that the atom loses energy with each cycle. Blue-detuned light increases the atom kinetic energy in a similar fashion. A more honest interpretation must include the Doppler shifts of the atoms, but the result is similar. When $\delta < 0$, faster atoms are Doppler shifted closer to resonance with one of the two counterpropagating beams, and thus absorb more light than slower atoms. When $\delta > 0$, the opposite is true, so the counterpropagating beams tend to heat the sample.

The reader will notice that the cooling force only works in one dimension. Cooling an atom in three dimensions requires three sets of orthogonal counterpropagating beams. For small optical pumping rates, the forces are independent and the above analysis holds in each direction. This three dimensional viscous cooling is known as optical molasses.

Maximum value of the friction coefficient

The friction coefficient η is largest when the detuning is close to the decoherence rate, *i.e.*, $\delta \sim \gamma_{12}$, such that

$$\eta = \frac{\hbar k^2}{m} \frac{R_{\text{opt}}^0(\delta = 0)}{\gamma_{12}}. \quad (8.31)$$

Here, $R_{\text{opt}}^0(\delta = 0) = 2|\Omega|^2/\gamma_{12}$ is the optical pumping rate on resonance. Although we have derived our previous results in the limit of small applied powers Ω , we can guess what will happen as the power is increased. The optical pumping rate will eventually saturate at a value close to the atomic

spontaneous emission rate γ . A more careful analysis reveals that the friction coefficient at large powers

$$\eta \rightarrow \frac{\hbar k^2}{8m} \frac{\gamma}{\gamma_{12}}. \quad (8.32)$$

The largest possible $\eta = \hbar k^2/4m$ is thus attained when the atomic transition is radiatively broadened. This maximal value can be rewritten in terms of the recoil frequency ω_R :

$$\eta_{\max} = \frac{1}{2}\omega_R. \quad (8.33)$$

Since $\frac{d}{dt}p = -\eta p$, we find that the atoms lose momentum at a rate $\sim \omega_R$. This discovery shows that the dynamical timescales for atomic motion are $\sim 1/\omega_R \gg 1/\gamma_{12}, 1/\delta$, justifying a posteriori the adiabatic approximation used to derive the light force. Since the typical timescale for cooling is $\omega_R \sim 10$ kHz, we see that Doppler cooling can be a fairly rapid process.

Behavior at finite velocity

Close to zero velocity, an atom in a red-detuned molasses experiences a nearly linear viscous force. As its velocity increases, the friction coefficient becomes velocity dependent, and we must resort to the full expression for the Doppler force. In fact, for $\mathbf{k} \cdot \mathbf{v} \gg \delta, \gamma_{12}$ the force vanishes. The range of velocities which are effectively cooled is known as the “capture range”, and is defined as $-v_c < v < v_c$ where the critical velocity corresponds to the maximum force $F_{\max} = |F(\pm v_c)|$.

The capture range depends on many parameters, but in certain limits it has a simple form. When the optical pumping rate is the same size as the detuning and the dephasing rate, the cooling force is maximized and the capture rate is $\sim \gamma_{12}/k$. A strongly driven system $R_{\text{opt}} \geq \gamma_{12}$ is power broadened, so $v_c \sim \Omega/k$. Finally, a far-detuned field $\delta \geq \gamma_{12}$ leads to a capture velocity $v_c \sim \delta/k$. In all of these situations, the capture velocity scales roughly as the wavelength multiplied by the dominant rate in the problem.

The magneto-optical trap (MOT)

Dissipative forces can be used to cool atoms, narrowing their velocity distribution, but they do not provide a confining potential. By combining optical molasses with a magnetic field gradient, it is possible to simultaneously cool and trap the atoms.

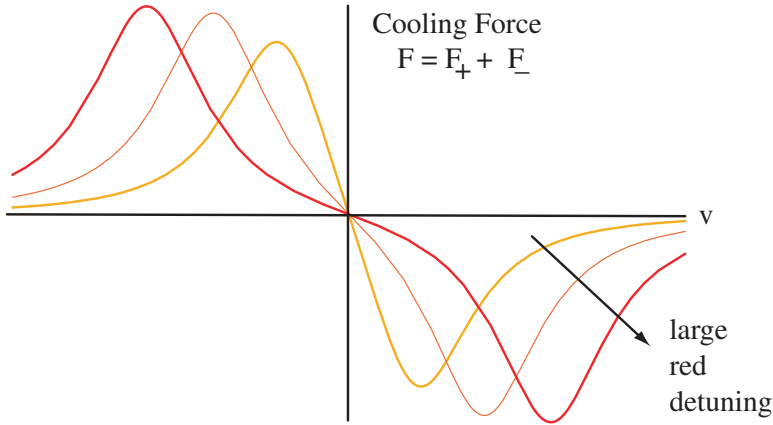


Figure 8.2: Doppler cooling force at finite velocity. For red-detuned beams, atoms with positive velocities experience a negative force and vice versa. The maximum force is experienced by atoms traveling at the critical velocity $\pm v_c$.

The magnetic field induces Zeeman shifts which can provide a position dependent detuning. By choosing the counterpropagating beams to have different circular polarizations, we can ensure that the position dependence causes atoms to be pushed back toward the center of the trap. Since we want the different polarizations to couple different atomic transitions, MOT operation requires a multilevel atom. The simplest possible configuration, shown in Figure 8.3, uses a $J = 0 \rightarrow J = 1$ atomic transition coupled by two counterpropagating, cross-circularly polarized beams. Applying a linear magnetic field shifts the three upper atomic levels, so that the dominant force pushes that atom back towards the center of the trap. Since the Doppler cooling technique is insensitive to polarization, the MOT simultaneously localizes and cools the atoms.

An excellent treatment of related subjects can be found in Bill Phillips' lecture notes from Les Houches LXXII (1999) or in "Laser Cooling and Trapping" by Metcalf and van der Straten.

The Doppler limit

We have shown how light forces can slow and cool an atomic ensemble, but we have not yet considered the final temperature attainable by Doppler

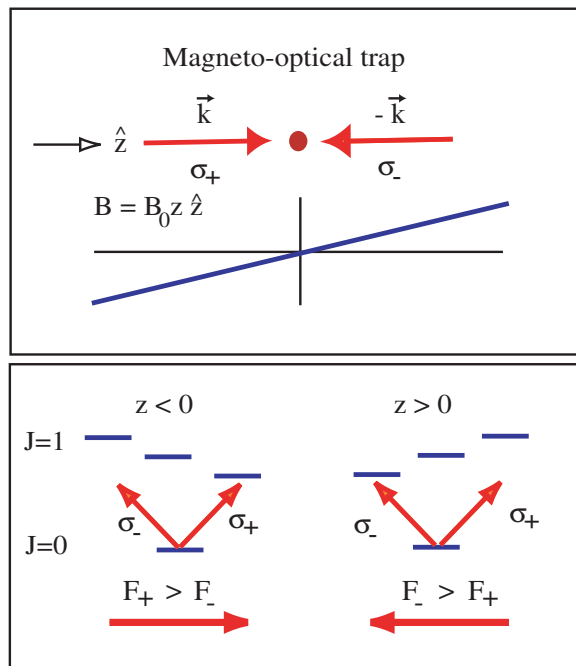


Figure 8.3: The magneto-optical trap. Top: A typical configuration of red-detuned laser beams and magnetic field. Bottom: Trapping forces for a $J=0 \rightarrow J = 1$ atomic transition.

cooling. Our analysis thus far indicates that the energy of the atom will decrease to zero. Clearly, we have missed something, because in practical situations one generally discovers a limit to any cooling method.

Qualitatively, we can understand this limit in terms of the momentum kicks imparted to atoms by spontaneous emission. As each atom radiates spontaneously into 4π , it receives a momentum kick in an arbitrary direction, heating the ensemble. Consequently, we expect that cooling will proceed until the spontaneous emission heating rate equals the Doppler cooling rate. Such considerations, however, are beyond the theory we have already developed, and they motivate a generalized Doppler cooling theory which includes the heating effects of spontaneous emission.

There are many ways to treat the heating effects of random processes; we will use the Heisenberg-Langevin approach. Before proceeding into a calculation of temperature, it is instructive to consider the basic theoretical ideas behind this approach, since they provide further intuition into atomic interactions with a coherent source and a radiation bath.

8.4 Dissipation and quantum noise: the Heisenberg-Langevin approach

The quantum description of random processes is closely related to the theory of random fluctuations in classical statistical mechanics. To motivate subsequent development of the quantum mechanical theory, we will briefly review the classic problem of Brownian motion.

8.4.1 Brownian motion

Consider a heavy particle surrounded by a bath of lighter particles. As the heavier particle moves through the cloud, its interactions with the lighter particles produce a viscous drag, slowing it down. However, the heavy particle never quite comes to rest because it is constantly bombarded by random momentum kicks inflicted by the lighter particles. At long times, the heavy particle will approach thermal equilibrium with its bath.

The Langevin equation

This classic problem of Brownian motion is described mathematically by the Langevin equation, which models the force on the heavy particle as a

viscous drag plus a fluctuating “Langevin force”,

$$\frac{d}{dt}p = -\eta p + f(t), \quad (8.34)$$

where η is the friction coefficient and $f(t)$ is the random force due to collisions between the heavy and light particles. On average, the Langevin force vanishes,

$$\langle f(t) \rangle = 0 \quad (8.35)$$

and we define its two-time expectation value

$$\langle f(t)f(t') \rangle = 2Dg(t-t') \quad (8.36)$$

in terms of a diffusion coefficient D and a second order correlation function $g(t-t')$ which satisfies the normalization condition

$$\int_{-\infty}^{\infty} g(t-t')dt = 1. \quad (8.37)$$

Note that the time dependence of $g(t-t')$ is determined by the collision frequency. We will be particularly interested in the situation where the lighter particles collide frequently with the heavy particle, but the effect of each collision is small. The heavy particle will thus lose momentum slowly, but the random force $f(t)$ will fluctuate very quickly. In this rapid-collision limit, we can separate out the two timescales, and the correlation function approaches a delta function

$$g(t-t') \rightarrow \delta(t-t'). \quad (8.38)$$

We can find a general solution to Langevin equation for arbitrary $f(t)$,

$$p(t) = p(0)e^{-\eta t} + \int_0^t dt' f(t')e^{-\eta(t-t')}. \quad (8.39)$$

If we average the momentum of the heavy particle over timescales large compared to the collision rate, we find

$$\overline{p(t)} = \overline{p(0)}e^{-\eta t}, \quad (8.40)$$

so the average momentum is unaffected by the Langevin force. However, its variance will have contributions from the stochastic momentum kicks. In

the rapid collision limit, we can calculate the mean square momentum:

$$\overline{p^2(t)} = \langle \left(p(0)e^{-\eta t} + \int_0^t dt' f(t') e^{-\eta(t-t')} \right)^2 \rangle \quad (8.41)$$

$$= \overline{p(0)^2} e^{-2\eta t} + \int_0^t \int_0^t dt' dt'' \langle f(t') f(t'') \rangle e^{-\eta(t-t')} e^{-\eta(t-t'')} \quad (8.42)$$

$$= \overline{p(0)^2} e^{-2\eta t} + \int_0^t \int_0^t dt' dt'' 2D \delta(t' - t'') e^{-\eta(t-t')} e^{-\eta(t-t'')} \quad (8.43)$$

$$= \overline{p(0)^2} e^{-2\eta t} + \frac{D}{\eta} (1 - e^{-2\eta t}). \quad (8.44)$$

Note that the terms linear in $\langle f(t) \rangle$ vanish because the average Langevin force is zero. This calculation shows that, unlike the average velocity, the mean square momentum is affected by the presence of the diffusion term. For very short times $\eta t \ll 1$, the square momentum simply decays exponentially,

$$\overline{p(t)^2} \approx \overline{p(0)^2} e^{-2\eta t}. \quad (8.45)$$

For long times $\eta t \gg 1$, however, the first viscous term is exponentially damped and the Langevin force determines the momentum,

$$\lim_{t \rightarrow \infty} \overline{p(t)^2} \rightarrow \frac{D}{\eta} \quad (8.46)$$

In this long-time limit, the kinetic energy

$$E_{\text{kinetic}} = \frac{\overline{p^2}}{2m} \rightarrow \frac{D}{2m\eta}. \quad (8.47)$$

The Einstein relation

If we can assume that the system approaches thermal equilibrium at such long times, then $E_{\text{kinetic}} = (1/2)k_B T$ for a one-dimensional system. The resulting equation for the diffusion constant in terms of the temperature and friction coefficient is known as the “Einstein relation”:

$$D = m\eta k_B T. \quad (8.48)$$

Physically, the finite equilibrium temperature T is determined by the balance of damping and diffusion. In particular, note that finite temperature dissipation (η) always leads to fluctuations (D). For our application to laser cooling, the Einstein relation will allow us to calculate the temperature which the atoms reach in equilibrium. Using a microscopic description to find a quantum analogue of the fluctuating force $f(t)$, we will be able to predict the lowest attainable temperature.

Random walks

If we make the unphysical assumption that the friction term vanishes $\eta \rightarrow 0$, the heavy particle only receives random kicks from the lighter particles with no dissipation. Its momentum will grow indefinitely,

$$\overline{p^2} = Dt, \quad (8.49)$$

and no thermal equilibrium is reached, so the Einstein relation does not hold. This so-called “random walk” problem shows that in the absence of damping a heavy particle will randomly diffuse through the cloud of lighter particles. A good reference for this subject is Cohen-Tannoudji, “Atom-Photon Interactions”.

8.4.2 The Heisenberg-Langevin approach

To apply an Langevin approach to the quantum mechanical description of Doppler cooling, we must determine the fluctuations in the system. Our semiclassical analysis averaged over the forces and atomic operators $\hat{F} \rightarrow \langle \hat{F} \rangle$, $\hat{\sigma}_{\alpha,\beta} \rightarrow \langle \hat{\sigma}_{\alpha,\beta} \rangle$ (where $\hat{\sigma}_{\alpha,\beta} = |\alpha\rangle\langle\beta|$), which immediately gets rid of any associated noise. Clearly, we need to do better.

In principle, we need only return to the Heisenberg equations of motion and avoid taking any expectation values:

$$\frac{d}{dt}\hat{\sigma}_{\alpha,\beta} = \frac{i}{\hbar}[\hat{H}, \hat{\sigma}_{\alpha,\beta}]. \quad (8.50)$$

There are two major contributions to the atomic evolution: the Hamiltonian evolution and the coupling to the reservoir operators. We have already accounted for the Hamiltonian contribution, and need only add in the effects of dissipation. In fact, these equations of motion look very similar to the density matrix equations, and it is tempting to account for dissipation by introducing dephasing terms $\dot{\hat{\sigma}}_{\alpha,\beta} \sim -\gamma_{\alpha,\beta}\hat{\sigma}_{\alpha,\beta}$. Unfortunately, this naive approach leads to unphysical results. In particular, such decoherence terms imply that $[\hat{\sigma}_{\beta,\alpha}, \hat{\sigma}_{\alpha,\beta}]$ decays exponentially in time:

$$\frac{d}{dt}[\hat{\sigma}_{\beta,\alpha}, \hat{\sigma}_{\alpha,\beta}] = [\frac{d}{dt}\hat{\sigma}_{\beta,\alpha}, \hat{\sigma}_{\alpha,\beta}] + [\hat{\sigma}_{\beta,\alpha}, \frac{d}{dt}\hat{\sigma}_{\alpha,\beta}] \quad (8.51)$$

$$= -\gamma_{\alpha,\beta}[\hat{\sigma}_{\beta,\alpha}, \hat{\sigma}_{\alpha,\beta}]. \quad (8.52)$$

Approaching the problem again more carefully, we will consider a generalized system and reservoir evolving according to the Hamiltonian

$$\hat{H} = \hat{H}_S + \hat{H}_R + \hat{H}_{SR} \quad (8.53)$$

where

$$\hat{H}_{SR} = -\hat{R}^\dagger \hat{S} - \hat{S}^\dagger \hat{R}. \quad (8.54)$$

In the case of a two-level atom interacting with modes \hat{a}_i of the radiation field with coupling coefficient g_i , the system and reservoir operators are given by

$$\hat{R} = \sum_j \hbar g_j \hat{a}_j \quad (8.55)$$

$$\hat{S} = \hat{\sigma}_{12} = |1\rangle\langle 2|, \quad (8.56)$$

but in general they may take any form.

We can write down the equation of motion for the evolution of an arbitrary system operator \hat{A} :

$$\frac{d}{dt} \hat{A} = \frac{i}{\hbar} [\hat{H}_S, \hat{A}] + \frac{i}{\hbar} \hat{R}^\dagger [\hat{A}, \hat{S}] + \frac{i}{\hbar} [\hat{A}, \hat{S}^\dagger] \hat{R}. \quad (8.57)$$

The first term describes the Hamiltonian evolution of the isolated system, while the remaining terms describe the system-bath interaction. For example, if we took $\hat{A} = \hat{\sigma}_{12}$,

$$\frac{d}{dt} \hat{\sigma}_{12} = \frac{i}{\hbar} [\hat{H}_S, \hat{\sigma}_{12}] + \frac{i}{\hbar} (\hat{\sigma}_{11} - \hat{\sigma}_{22}) \hat{R}, \quad (8.58)$$

the equation looks very similar to the density matrix equation for the atomic coherence, with the coherent field Ω replaced by the operator quantity \hat{R} . This is not so surprising, since \hat{R} acts as a quantum field operator. Note that the system and reservoir operators commute, so the ordering of the last two terms in Eq. (8.57) is arbitrary. Nevertheless, we have chosen this ordering because it highlights the action of \hat{R} on the vacuum state, and will prove useful when we write the reservoir operator \hat{R} in terms of the system operators which influence it.

We next consider the evolution equation for the reservoir operator \hat{R} itself. In the case of the radiation field, $\hat{R} = \sum_j \hbar g_j \hat{a}_j$ and each mode evolves according to

$$\dot{a}_j = \frac{i}{\hbar} [\hat{H}_R + \hat{H}_{SR}, \hat{a}_j] \quad (8.59)$$

$$= -i(\nu_i - \omega) \hat{a}_j + ig_j^* \hat{S}. \quad (8.60)$$

The first term represents the free field evolution in an appropriately chosen rotating frame of reference, whereas the system-reservoir coupling yields a

source term for the quantum field, which in turn drives the system. Formally integrating the equations for \hat{R} , we find

$$\hat{R}(t) = i\hbar \left(-i \sum_j g_j \hat{a}_j(0) e^{-i(\nu_j - \omega)t} + \int_0^t dt' \sum_j |g_j|^2 e^{-i(\nu_j - \omega)(t-t')} \hat{S}(t') \right). \quad (8.61)$$

This expression is very similar to the equation obeyed by the reservoir operators in Wigner-Weisskopf theory, and we will again make use of the Markov approximation to simplify the equation. If the atomic operator $\hat{S}(t)$ changes slowly in time, and the reservoir bandwidth is very broad, the source term can be approximated by a simple decay,

$$\int_0^t dt' \sum_j |g_j|^2 e^{-i(\nu_j - \omega)(t-t')} \hat{S}(t') \rightarrow \frac{\gamma}{2} \hat{S}(t). \quad (8.62)$$

In addition to the expected decay terms, however, we also need to consider the free-field evolution term. This so-called “quantum Langevin force,”

$$\hat{f}(t) = -i \sum_j g_j \hat{a}_j(0) e^{-i(\nu_j - \omega)t}, \quad (8.63)$$

was missing from our previous naive guess at the effects of the reservoir. The fluctuations associated with $\hat{f}(t)$ will protect the commutator $[\hat{\sigma}_{\beta,\alpha}, \hat{\sigma}_{\alpha,\beta}]$ from the unphysical exponential decay we found earlier.

The quantum Langevin operator: $\hat{f}(t)$

The physical meaning of the free-field evolution term can be understood by examining its moments. If the reservoir was initially in a thermal state, then $\langle \hat{f}(t) \rangle = 0$, so the average effect of $\hat{f}(t)$ vanishes. As in the case of the classical Langevin force, we find that the second moment does not vanish:

$$\langle \hat{f}(t)^\dagger \hat{f}(t') \rangle = \sum_{j,j'} g_j^* g_{j'}' \langle \hat{a}_j(0)^\dagger \hat{a}_{j'}(0) \rangle e^{i(\nu_j - \omega)t} e^{-i(\nu_{j'} - \omega)t'} \quad (8.64)$$

$$= \sum_j |g_j|^2 n(\nu_j) e^{-i(\nu_j - \omega)(t' - t)} \quad (8.65)$$

$$= n(\omega) \gamma \delta(t - t'), \quad (8.66)$$

where we have again made use of the Markov approximation in the last line. \hat{f} is an operator so the ordering matters, and a similar calculation yields the second moment for the opposite order:

$$\langle \hat{f}(t) \hat{f}(t')^\dagger \rangle = (n(\omega) + 1) \gamma \delta(t - t'). \quad (8.67)$$

Since \hat{f} is an operator with zero average and second-order moment given by a delta-function, we interpret \hat{f} as a quantum Langevin operator.

The Heisenberg-Langevin equation

Expressed in terms of the decay rate and Langevin force, the reservoir operator may be written

$$\hat{R}(t) = i\hbar \left(\frac{\gamma}{2} \hat{S}(t) + \hat{f}(t) \right). \quad (8.68)$$

Substituting back into the equation of motion for the system operator \hat{A} , we obtain a general result known as the Heisenberg-Langevin equation:

$$\frac{d}{dt} \hat{A} = \frac{i}{\hbar} [\hat{H}_S, \hat{A}] + \left(\frac{\gamma}{2} \hat{S}^\dagger + \hat{f}^\dagger \right) [\hat{A}, \hat{S}] - [\hat{A}, \hat{S}^\dagger] \left(\frac{\gamma}{2} \hat{S} + \hat{f} \right). \quad (8.69)$$

Physically, the Heisenberg-Langevin equation demonstrates that whenever a system has some dissipation $\gamma/2\hat{S}$, it will always be accompanied by fluctuations described by the Langevin noise operator \hat{f} .

Comparison to the Master Equation

The Heisenberg-Langevin equation was derived in the Heisenberg picture, whereas the density matrix approach uses the Schrodinger picture. The two descriptions, however, are entirely equivalent.

To illustrate the connection, suppose that we start out in the vacuum state $n(\omega) = 0$, so that $\hat{f}|vac\rangle = 0$. Taking the expectation value for \hat{A} yields

$$\frac{d}{dt} \langle \hat{A} \rangle = \frac{i}{\hbar} \langle [\hat{H}_S, \hat{A}] \rangle + \frac{\gamma}{2} \left(2 \langle \hat{S}^\dagger \hat{A} \hat{S} \rangle - \langle \hat{A} \hat{S}^\dagger \hat{S} \rangle - \langle \hat{S}^\dagger \hat{S} \hat{A} \rangle \right). \quad (8.70)$$

Since $\langle \sigma_{ij} \rangle = \rho_{ji}$, we can compare this equation term by term to the master equation for an atom in vacuum: they match exactly.

The quantum fluctuation-dissipation theorem

The Heisenberg-Langevin equations may be written in a compact form

$$\frac{d}{dt} \hat{A}_\mu = \hat{d}_\mu + \hat{\mathcal{F}}_\mu, \quad (8.71)$$

where μ denotes an arbitrary operator, \hat{d}_μ represents the coherent evolution and decay of that operator (such as one would predict from the density

matrix equations of motion), and $\hat{\mathcal{F}}_\mu$ is the quantum Langevin operator with $\langle \hat{\mathcal{F}}_\mu \rangle = 0$ and

$$\langle \hat{\mathcal{F}}_\mu(t) \hat{\mathcal{F}}_\nu(t') \rangle = 2D_{\mu\nu}\delta(t - t'). \quad (8.72)$$

As we found for the classical Langevin equation, there is a relationship between the noise force and the dissipation included in \hat{d}_μ . In particular, the generalized diffusion coefficient $D_{\mu\nu}$ is uniquely determined by the deterministic evolution of \hat{d}_μ :

$$2D_{\mu\nu} = \frac{d}{dt} \langle \hat{A}_\mu \hat{A}_\nu \rangle - \langle \hat{A}_\mu \hat{d}_\nu \rangle - \langle \hat{d}_\mu \hat{A}_\nu \rangle. \quad (8.73)$$

This “generalized Einstein relation” is the quantum analogue of the equation relating the diffusion coefficient to the temperature and the friction coefficient, and is valid for all systems coupled to Markovian reservoirs.

To prove the quantum fluctuation-dissipation theorem given in Eq. (8.73), consider the quantity

$$\langle \hat{A}_\mu(t) \hat{\mathcal{F}}_\nu(t) \rangle = \langle \hat{A}_\mu(t-\Delta t) \hat{\mathcal{F}}_\nu(t) \rangle + \int_{t-\Delta t}^t dt' \left(\langle \hat{d}_\mu(t') \hat{\mathcal{F}}_\nu(t) \rangle + \langle \hat{F}_\mu(t') \hat{\mathcal{F}}_\nu(t) \rangle \right). \quad (8.74)$$

Since $\hat{A}(t - \Delta t)$ is not correlated with $\hat{\mathcal{F}}_\mu(t)$ (by causality), and $\langle \hat{\mathcal{F}}_\nu(t) \rangle = 0$, the first term vanishes. The second term should be small because \hat{d}_μ is deterministic, so the second term is at most proportional to Δt . The third term is finite because $\langle \hat{\mathcal{F}}_\mu(t) \hat{\mathcal{F}}_\nu(t') \rangle = 2D_{\mu\nu}\delta(t - t')$; although the delta function argument appears at the endpoint of the region of integration, from our calculations of the Wigner-Weisskopf theory, we can account for the end effects with a factor of 1/2, so

$$\langle \hat{A}_\mu(t) \hat{\mathcal{F}}_\nu(t) \rangle = D_{\mu\nu}. \quad (8.75)$$

A similar calculation shows that

$$\langle \hat{\mathcal{F}}_\nu(t) \hat{A}_\mu(t) \rangle = D_{\nu\mu}. \quad (8.76)$$

We now calculate the time derivative of $\langle \hat{A}_\mu(t) \hat{A}_\nu(t) \rangle$,

$$\frac{d}{dt} \langle \hat{A}_\mu \hat{A}_\nu \rangle = \langle \hat{A}_\mu (d_\nu + \hat{\mathcal{F}}_\nu) \rangle + \langle (d_\mu + \hat{\mathcal{F}}_\mu) \hat{A}_\nu \rangle \quad (8.77)$$

which immediately gives us the generalized Einstein relation:

$$\frac{d}{dt} \langle \hat{A}_\mu \hat{A}_\nu \rangle - \langle \hat{A}_\mu \hat{d}_\nu \rangle - \langle \hat{d}_\mu \hat{A}_\nu \rangle = 2 \langle \hat{A}_\mu \hat{\mathcal{F}}_\nu \rangle = 2D_{\mu\nu}. \quad (8.78)$$

The generalized Einstein relation conveys a simple physical message: As soon as the deterministic part of the system evolution is given and the reservoir has no memory (i.e. quantum "white noise"), one can immediately calculate the associated noise terms. The fluctuation-dissipation theorem thus provides a convenient way to derive diffusion coefficients from known system decay and decoherence parameters.

8.5 The Heisenberg-Langevin formalism applied to Doppler cooling

8.5.1 Momentum diffusion in laser cooling of a two-level atom

We can now apply the Heisenberg-Langevin formalism to address momentum diffusion in the Doppler cooling model. Recall that a plane wave Ωe^{ikz} exerts a force on the atom which can be expressed as

$$\hat{F} = -i\hbar k \Omega^* \hat{\sigma}_{12} + h.c. \quad (8.79)$$

$$= \langle \hat{F} \rangle + \delta \hat{F}, \quad (8.80)$$

where we have broken the force down into the average force and the fluctuations about the mean. For the case of an atom in a radiation field bath, $\hat{A} = \hat{\sigma}_{12}$, $\hat{S} = \hat{\sigma}_{12}$, the Heisenberg-Langevin equation becomes

$$\frac{d}{dt} \hat{\sigma}_{12} = \frac{i}{\hbar} [\hat{H}_S, \hat{\sigma}_{12}] - (\hat{\sigma}_{11} - \hat{\sigma}_{22}) \left(\frac{\gamma}{2} \hat{\sigma}_{12} + \hat{f}(t) \right) \quad (8.81)$$

$$= \frac{i}{\hbar} [\hat{H}_S, \hat{\sigma}_{12}] - \frac{\gamma}{2} \hat{\sigma}_{12} + (\hat{\sigma}_{22} - \hat{\sigma}_{11}) \hat{f}(t). \quad (8.82)$$

The first term contributes only to the average force, which we have already calculated, so we will focus our attention on the second two terms. In particular, we identify the noise force we had previously been missing:

$$\hat{\mathcal{F}}_{12}(t) = (\hat{\sigma}_{22} - \hat{\sigma}_{11}) \hat{f}(t). \quad (8.83)$$

Clearly, the average noise force is zero. For optical transitions where $k_B T \ll \omega$, the radiation field is in a vacuum state $n(\omega) = 0$, and the only nonvanishing second moment of this noise force is

$$\langle \hat{\mathcal{F}}_{12}(t) \hat{\mathcal{F}}_{12}(t')^\dagger \rangle = \langle (\hat{\sigma}_{22} - \hat{\sigma}_{11})^2 \hat{f}(t) \hat{f}(t')^\dagger \rangle = \gamma \delta(t - t'). \quad (8.84)$$

Putting the component pieces together, and separating the detuning from the atom-laser interaction \hat{H}_{AL} , we find

$$\frac{d}{dt}\hat{\sigma}_{12} = \frac{i}{\hbar}[\hat{H}_{AL}, \hat{\sigma}_{12}] - (\frac{\gamma}{2} + i\delta)\hat{\sigma}_{12} + \hat{\mathcal{F}}_{12}(t). \quad (8.85)$$

Since we are interested in processes which are slow compared to γ , we can disregard the time derivative ², and easily solve for the atomic coherence

$$\hat{\sigma}_{12} = \frac{\hat{\mathcal{F}}_{12}(t)}{\gamma/2 + i\delta} + \frac{i}{\hbar(\gamma/2 + i\delta)}[\hat{H}_{AL}, \hat{\sigma}_{12}]. \quad (8.88)$$

Since the Hamiltonian terms were accounted for in the average force $\langle F \rangle$, the fluctuating force is simply

$$\delta\hat{F} = i\hbar k \Omega \frac{\hat{\mathcal{F}}_{12}(t)}{\gamma/2 + i\delta} + h.c., \quad (8.89)$$

Again, this force clearly has zero mean value, and its second moment is proportional to a delta function in time:

$$\langle \delta\hat{F}(t)\delta\hat{F}(t') \rangle = (\hbar k)^2 \frac{|\tilde{\Omega}|^2 \gamma}{(\gamma/2)^2 + \delta^2} \delta(t - t'), \quad (8.90)$$

where $\tilde{\Omega} = 2\Omega$ accounts for the two counterpropagating beams and for contributions to diffusion from absorption as well as spontaneous emission.³

²The validity of this approximation is most easily seen by solving exactly in the Fourier domain, where the relevant terms lead to a contribution to the coherence

$$\hat{\sigma}_{12}(\omega) = \frac{\hat{\mathcal{F}}_{12}(\omega)}{\gamma/2 - i(\omega - \delta)}. \quad (8.86)$$

The correlation function for the atomic operator (which appears in the expression for the force) is then

$$\langle \hat{\sigma}_{12}(\omega)\hat{\sigma}_{12}^\dagger(\omega') \rangle = \frac{2D\delta(\omega + \omega')}{(\gamma/2 - i(\omega - \delta))(\gamma/2 + i(\omega' - \delta))}. \quad (8.87)$$

Our approximation of neglecting the time derivative corresponds to neglecting the frequency in the denominator, which should have a negligible contribution at frequencies much lower than γ .

³There are two factors of two incorporated here: one comes from adding the force fluctuations from the two counterpropagating beams, neglecting any interference effects (for example by alternating the direction of the beam and considering only the average intensity of each beam.) The second factor of 2 comes from the fact that we have derived here only the diffusion associated with spontaneous emission, and there is an equivalent component associated with absorption. See Bill Phillip's notes http://cua.mit.edu/8.422/Reading%20Material/phill92_varenna.pdf for further details.

The diffusion constant

By analogy to the diffusion model of Brownian motion, we can identify the appropriate diffusion constant $2D\delta(t - t') = \langle \delta\hat{F}(t)\delta\hat{F}(t') \rangle$,

$$D = (\hbar k)^2 \frac{|\tilde{\Omega}|^2 \gamma / 2}{(\gamma/2)^2 + \delta^2} \quad (8.91)$$

$$= 2(\hbar k)^2 R_{\text{opt}}^0. \quad (8.92)$$

The physics behind the diffusion coefficient is quite simple. Momentum diffusion is caused by spontaneous emission events which occur at a rate $R_{\text{opt}}^0 = |\Omega|^2 \gamma / (\delta^2 + (\gamma/2)^2)$. This process is effectively like a random walk in momentum space, where the average step size is $\delta p = \hbar k$ and the steps occur at a rate R_{opt}^0 . Each event changes the momentum by $\hbar k = \delta p$, which has no effect on average, but increases the uncertainty in the momentum. The average root mean squared momentum grows as $\sqrt{\langle p^2 \rangle} = \sqrt{Dt}$.

8.5.2 The Doppler cooling limit

Since we now know both the diffusion coefficient and the viscosity associated with the dissipative force, we can estimate the final temperature T_D attainable by Doppler cooling by using the Einstein relation. Recall that the friction coefficient,

$$\eta = \frac{4R_{\text{opt}}}{m} \frac{\hbar k^2 \delta}{\delta^2 + \gamma_{12}^2}, \quad (8.93)$$

is proportional to the optical pumping rate, which consequently drops out of the expression for the temperature:

$$k_B T_D = \frac{D}{m\eta} \quad (8.94)$$

$$= \frac{\hbar(\delta^2 + \gamma_{12}^2)}{2\delta}. \quad (8.95)$$

At the optimal detuning $\delta \approx \gamma_{12}$, the final temperature is simply the linewidth of the excited state

$$k_B T_D = \hbar \gamma_{12}. \quad (8.96)$$

For a radiatively broadened system, the final temperature depends only on the spontaneous emission rate! This remarkable and intuitive result was believed for many years to represent the ultimate limit to laser cooling efforts. Typical values for the Doppler limit are around 10^{-3}K , e.g. 0.25 mK

for Na and 0.14 mK for Rb, which is low but still relatively warm compared to the temperatures required for many interesting applications.

From a practical point of view, it may seem strange that atoms in a room-temperature apparatus can be in thermal equilibrium at \sim mK temperatures. The resolution to this puzzle is that the atoms are interacting not only with the thermal reservoir of photons, but also with a (zero-temperature) laser. The atomic temperature is a result of interactions with both thermal and highly non-thermal reservoirs.

8.5.3 Corrections for a dense sample

The discussion thus far has implicitly assumed that the atoms in the sample are independent. This approximation will fail when the sample becomes dense enough that the atoms start to affect each other. To apply our calculations to such a dense sample, we would need to account for two effects.

Laser attenuation

An optically thick sample will attenuate any laser beam propagating through it, so the intensity of the cooling beams will diminish with distance into the sample. The associated forces will also acquire a spatial gradient, resulting in an additional dipole force as well as position-dependent cooling.

Spontaneous photon reabsorption

A more subtle effect emerges when we consider the effects of spontaneous emission from one atom on nearby atoms. If a nearby atom reabsorbs the spontaneously emitted photon, it will receive a momentum kick away from the first atom. Spontaneous photon reabsorption thus leads to an effective repulsive force between atoms. We have been able to neglect these effects in a dilute sample because the spontaneous photon field falls off with distance. The spontaneous photon creates an outgoing spherical wave with intensity $\propto \lambda^2/r^2$, and consequently has little effect on atoms more than a wavelength away. It is possible to derive the resulting force from this kind of qualitative consideration. Alternately, one might try to generalize the Heisenberg-Langevin approach to account for atom-atom scattering events. The source term for the reservoir operator \hat{R} would then involve a sum over all the atoms, so that the Langevin force on one atom depends on the other atoms. The result of this calculation will be a multi-atom Heisenberg-Langevin equation or, alternately, a multi-atom master equation (see, e.g.

Gross, Haroche PHYS REP 93 (5): 301-396 1982). Such a generalized theoretical approach is beyond the scope of this course, and the coupled atom dynamics in a dense sample remains a subject of current research (see e.g. Castin, Cirac, and Lewenstein, PRL 80 (24): 5305-5308 1998).

8.6 Sub-Doppler cooling

The final temperature for Doppler cooling, set by the balance of spontaneous emission heating and laser cooling forces, was long believed to represent the fundamental limit to all laser cooling schemes. In the early 1990's, however, a number of experiments with alkali metals (Na, Rb, Cs) measured temperatures which were ten times smaller than predictions of the Doppler cooling limit. This result was puzzling: the Doppler cooling limit is quite intuitive and reasonable. Moreover, it is based on an assumption of classical atomic motion which is valid for temperatures near $T_D = \hbar\gamma$. Since the deBroglie wavelength of an atom at $T_D \sim 10$ nm is much smaller than the wavelength of the radiation, the atoms do indeed act like classical point particles. However, there is one other assumption which is not necessarily valid: we neglected the multilevel structure of real atoms.

8.6.1 Experimental Observations

The explanation for sub-Doppler temperatures was motivated by two experimental observations.

Polarization gradients

First, it was found that the final temperature of the atomic ensemble depended sensitively on the polarizations of the applied laser beams. The cooling worked particularly well for linearly cross-polarized beams (the “lin \perp lin” configuration). In this configuration, the circular polarization of the electric field depends on the position, since

$$\mathbf{E} = E_0 e^{i\nu t} (\hat{x}e^{ikz} + i\hat{y}e^{-ikz}) + c.c. \quad (8.97)$$

$$= E_0 e^{i\nu t} \left(\underbrace{(\hat{x} + i\hat{y})}_{\sigma_+} \cos kz + i \underbrace{(\hat{x} - i\hat{y})}_{\sigma_-} \sin kz \right) + c.c. \quad (8.98)$$

The electric field is the sum of two cross-circularly polarized standing waves which are shifted by $\pi/2$ from one another. An atom moving through such

a field would experience a polarization gradient in the incident light. Since polarization gradients have little effect on a two-level atom, the importance of polarization in sub-Doppler cooling indicates that the multilevel atomic structure may play a crucial role.

Detuning

The second experimental observation concerned the detuning of the applied cooling beams. It was found that sub-Doppler temperatures were particularly easy to obtain in the limit of a large detuning $\delta \gg \gamma$. The main effect of a far-detuned laser beam is an AC Stark shift of the atomic levels, so this experimental result indicated that AC Stark shifts should also play an important role in sub-Doppler cooling.

8.6.2 Sisyphus Cooling

The theory underlying sub-Doppler cooling was worked out by Cohen-Tannoudji and collaborators. We will examine their explanation in the context of a specific atomic level configuration: a $J = 1/2 \rightarrow J' = 3/2$ transition.

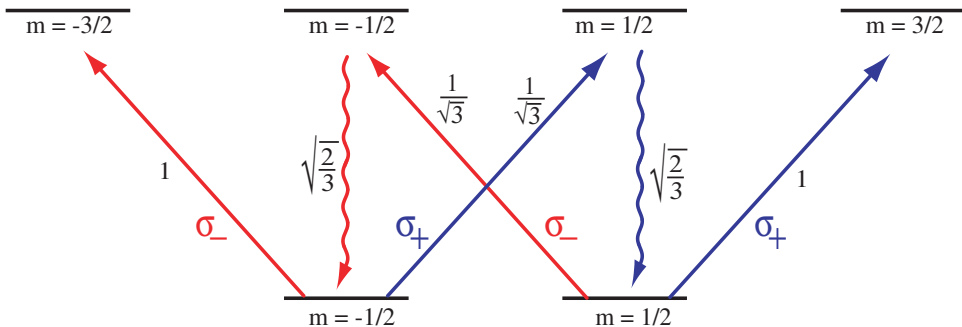


Figure 8.4: The level configuration used to explain sub-Doppler cooling. The Clebsch-Gordon coefficients for each transition are given. Note that the $m = \pm 1/2 \rightarrow m = \pm 1/2$ transitions are coupled only by spontaneous emission.

When such an atom is subject to circularly polarized σ_+ light with Rabi frequency Ω detuned by $|\delta| \gg |\Omega|$, the main effect it experiences is an AC Stark shift of the ground state levels. Since the Clebsch-Gordon coefficients for the two allowed transitions $m = -1/2 \rightarrow m = 1/2$, $m = 1/2 \rightarrow m = 3/2$

are not equal, the AC Stark shift is different for the two ground states:

$$\Delta_{1/2}^{\sigma_+} = \frac{|\Omega_+|^2}{\delta} \quad (8.99)$$

$$\Delta_{-1/2}^{\sigma_+} = \frac{|\Omega_+|^2}{3\delta}. \quad (8.100)$$

The other polarization σ_- has exactly the opposite effect,

$$\Delta_{1/2}^{\sigma_-} = \frac{|\Omega_-|^2}{3\delta} \quad (8.101)$$

$$\Delta_{-1/2}^{\sigma_-} = \frac{|\Omega_-|^2}{\delta}. \quad (8.102)$$

We found earlier that the lin \perp lin configuration leads to two cross-circularly polarized standing waves, so we are interested in spatially dependent Rabi frequencies

$$\Omega_+ = \Omega \cos kz \quad (8.103)$$

$$\Omega_- = \Omega \sin kz. \quad (8.104)$$

In the far-detuned regime, the effective atom-laser interaction Hamiltonian for the atom moving through such fields is

$$\hat{H}_{AL}^{\text{eff}} = \hbar \sum_{m=\pm\frac{1}{2}} (\Delta_m^{\sigma_+} + \Delta_m^{\sigma_-}) |m\rangle\langle m| \quad (8.105)$$

$$= \hbar \frac{|\Omega|^2}{\delta} \left(1 - \frac{2}{3} \sin^2 kz \right) \left| \frac{1}{2} \right\rangle \left\langle \frac{1}{2} \right| \quad (8.106)$$

$$= \hbar \frac{|\Omega|^2}{\delta} \left(1 - \frac{2}{3} \cos^2 kz \right) \left| -\frac{1}{2} \right\rangle \left\langle -\frac{1}{2} \right|, \quad (8.107)$$

where $\delta < 0$ will lead to cooling effects. Recall that in previous lectures we discussed that the applicability of such AC Stark shifted effective potentials is limited to situations where two-photon transitions can be neglected. By choosing our model system and polarizations carefully, we have eliminated any possible Λ -type configuration. Consequently the effective Hamiltonian provides an adequate description of the level configuration under consideration.

The effective dressed state potential gives rise to a conservative force analogous to the dipole force, which cannot provide cooling. To understand where the sub-Doppler cooling comes from, we must go beyond the AC

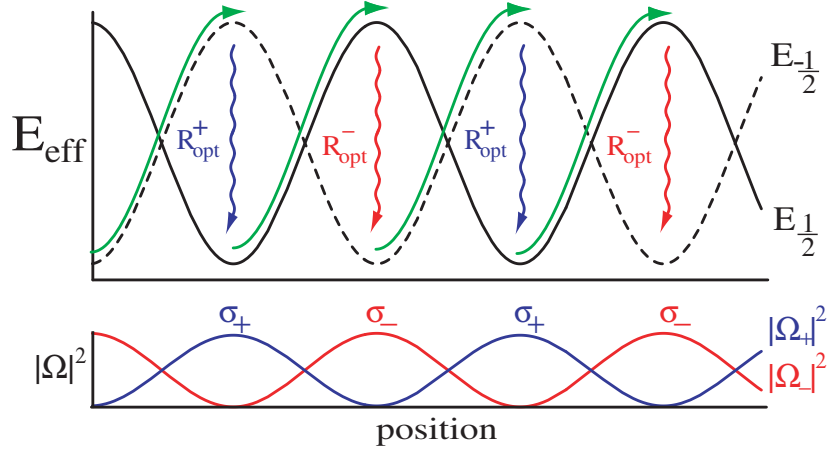


Figure 8.5: The Sisyphus cooling mechanism. As the atom moves through the polarization gradient fields, its internal energy level (illustrated in green) follows the Stark-shifted ground state. In regions where σ_{\pm} light dominates, the atom is optically pumped into the $m = \pm 1/2$ level. For a red-detuned beam, the atom is always optically pumped into the lower energy state, so it must lose kinetic energy with each cycle.

Stark effect and examine optical pumping. From Figure (8.4), we see that σ_+ light optically pumps the atom into the $m = 1/2$ state, whereas σ_- light pumps it into the $m = -1/2$ state. As the atom moves through the dressed state potential, it is also optically pumped between dressed states by the dominant field at its location. For red-detuned fields, the dominant polarization tends to optically pump the atom into the lower energy dressed state, so that the atom must continually climb up the potential energy curve between optical pumping cycles. Climbing the hills causes the atom to lose some kinetic energy while gaining potential energy; this potential energy is then dumped into the spontaneously emitted photon which pumps the atom into the lower state. This physical mechanism has earned the descriptive name “Sisyphus” cooling.

8.6.3 Quantitative analysis of sub-Doppler cooling

Although we now understand the physics behind Sisyphus cooling, to verify that it leads to sub-Doppler temperatures we must derive a more quantitative description.

The Sisyphus cooling force

In the limit of large detuning, the relevant motional dynamics must come from the reactive force

$$F_{\text{reactive}} = \sum_{m=\pm 1/2} \hbar \nabla (\Delta_m^{\sigma_+} + \Delta_m^{\sigma_-}) |m\rangle \langle m| \quad (8.108)$$

$$= \frac{2}{3} \hbar k \frac{|\Omega|^2}{\delta} \sin(2kz) \left(\left| \frac{1}{2} \right\rangle \langle \frac{1}{2} \right| - \left| -\frac{1}{2} \right\rangle \langle -\frac{1}{2} \right). \quad (8.109)$$

The only remaining unknown is the population difference $\Delta\rho = \left(\left| \frac{1}{2} \right\rangle \langle \frac{1}{2} \right| - \left| -\frac{1}{2} \right\rangle \langle -\frac{1}{2} \right)$.

The first step in finding $\Delta\rho$ is to calculate the relevant optical pumping rates. The Clebsch-Gordon coefficients for σ_+ light reveal that atoms are pumped out of the $m_g = -1/2$ ground state to the $m_e = 1/2$ excited state at a rate $R_{\text{opt}}^+ / 3$, while the probability for an atom to decay from $m_e = 1/2 \rightarrow m_g = 1/2$ is $2/3$. Consequently, the optical pumping rate from $m_g = -1/2$ to $m_g = 1/2$ is $(2/9)R_{\text{opt}}^+ = (2/9)R_{\text{opt}} \cos^2 kz$, where $R_{\text{opt}} = |\Omega^2| \gamma / ((\gamma/2)^2 + \delta^2)$. A similar calculation holds for σ_- light, which optically pumps the atom into the $m_g = -1/2$ state from $m_g = 1/2$ at a rate $(2/9)R_{\text{opt}} \sin^2 kz$.

Since we have chosen a level configuration which avoids Raman transitions, we can calculate the atomic population without also having to find the coherences. Furthermore, in the spirit of adiabatic elimination we can disregard the excited state population and write down a rate equation for the ground state populations:

$$\frac{d}{dt} \rho_{\frac{1}{2} \frac{1}{2}} = -\frac{2}{9} R_{\text{opt}} \sin^2(kz) \rho_{\frac{1}{2} \frac{1}{2}} + \frac{2}{9} R_{\text{opt}} \cos^2(kz) \rho_{-\frac{1}{2} -\frac{1}{2}} \quad (8.110)$$

$$\rho_{\frac{1}{2} \frac{1}{2}} + \rho_{-\frac{1}{2} -\frac{1}{2}} = 1. \quad (8.111)$$

From these two equations it is straightforward to find the evolution of the population difference,

$$\frac{d}{dt} \Delta\rho = -\frac{2}{9} R_{\text{opt}} (\Delta\rho - \cos(2kz)), \quad (8.112)$$

which describes a relaxation process at rate

$$\frac{1}{\tau_P} = \frac{2}{9} R_{\text{opt}} \quad (8.113)$$

towards a steady state value

$$\Delta\rho_{SS} = \cos(2kz). \quad (8.114)$$

It is tempting to use this steady state value to calculate the dissipative force:

$$F_{\text{reactive}}^{SS} = \frac{2}{3} \hbar k \frac{|\Omega|^2}{\delta} \sin(2kz) \Delta\rho_{SS} \quad (8.115)$$

$$= \frac{1}{3} \hbar k \frac{|\Omega|^2}{\delta} \sin(4kz). \quad (8.116)$$

The steady state force averages to zero over a few wavelengths, so we clearly have not yet found the dissipative effects we were after. Why didn't this work? In substituting the steady state population difference, we assumed that the optical pumping rate was much faster than typical timescales of atomic motional dynamics. Unlike Doppler cooling, where there is a well-defined hierarchy of timescales $\gamma \gg \omega_R$, the Sisyphus damping constant $1/\tau_P$ need not be large compared to the rate of momentum change.

In particular, we need to account for the change in atomic position with time $z = vt$. Modifying the rate equation for $\Delta\rho$ to incorporate atomic motion, we find

$$\frac{d}{dt} \Delta\rho = -\frac{1}{\tau_P} (\Delta\rho - \cos(2kvt)), \quad (8.117)$$

so that $\Delta\rho_{SS} = \cos(2kvt)$ is no longer an exact solution. For small velocities, we can solve Eq. (8.117) using an adiabatic expansion procedure, yielding

$$\Delta\rho \approx \cos(2kvt) - \tau_p \frac{d}{dt} \cos(2kvt) \quad (8.118)$$

$$= \cos(2kvt) + 2kv\tau_P \sin(2kvt) \quad (8.119)$$

$$\approx \cos 2k(z - vt\tau_P). \quad (8.120)$$

We see immediately that the population difference lags behind the instantaneous steady state value, which happens because it takes some time $\sim \tau_P$ for optical pumping to equilibrate the populations. Moreover, the time delay gives us a contribution to the force which will not average to zero and is proportional to the velocity:

$$\langle F \rangle = \frac{2}{3} \hbar k \frac{|\Omega|^2}{\delta} \langle \sin(2kz) (\cos(2kz) + 2kv\tau_P \sin(2kz)) \rangle \quad (8.121)$$

$$= \frac{2}{3} \hbar k^2 v \tau_P \frac{|\Omega|^2}{\delta}. \quad (8.122)$$

Assuming that the velocity does not change over the timescale defined by the optical pumping τ_P , it is possible to solve Eq. (8.117) exactly to find

$$\Delta\rho = \frac{1}{1 + (v/v_c)^2} \cos(2kz) + \frac{v/v_c}{1 + (v/v_c)^2} \sin(2kz), \quad (8.123)$$

where the capture velocity v_c is given by

$$v_c = \frac{1}{2k\tau_P} = \frac{\lambda}{18\pi} R_{\text{opt}}. \quad (8.124)$$

Substituting into the expression for the dissipative force, and averaging over several wavelengths, we find the average force

$$\langle F_{\text{reactive}} \rangle = \frac{1}{3} \hbar k \frac{|\Omega|^2}{\delta} \frac{v/v_c}{1 + (v/v_c)^2} = \eta_S v m. \quad (8.125)$$

It may appear that the force depends on the AC Stark shift, and indeed the energy lost in each optical pumping cycle is of order $|\Omega|^2/\delta$. Nevertheless, the optical pumping rate also determines the force through v_c , and since $v_c \propto R_{\text{opt}} \sim |\Omega|^2 \gamma / \delta^2$ (when $|\delta| \gg \gamma, \Omega$), for low powers the intensity of the applied fields exactly cancels, so

$$\eta_S = 3 \frac{\hbar k^2}{m} \frac{\delta}{\gamma} \left(\frac{1}{1 + (v/v_c)^2} \right). \quad (8.126)$$

In particular, for velocities much smaller than v_c , the Sisyphus friction coefficient approaches

$$\eta_S = 3 \frac{\hbar k^2}{m} \frac{\delta}{\gamma}. \quad (8.127)$$

The friction coefficient acts to cool the atoms when $\delta < 0$, whereas blue-detuned fields cause heating.

Comparison of Doppler and Sisyphus cooling

It is instructive to compare the friction coefficient for Sisyphus cooling η_S to that for Doppler cooling η_D in the limit of small powers and large detunings:

$$\eta_D = \frac{\hbar k^2}{m} \frac{\gamma_{12} |\Omega|^2}{\delta^3} \quad (8.128)$$

$$\eta_S = 3 \frac{\hbar k^2}{m \gamma} \delta. \quad (8.129)$$

The Doppler friction coefficient vanishes as the fields become weaker and farther detuned, whereas the Sisyphus cooling mechanism has no dependence on power, and increases as the applied field becomes farther red-detuned, so in this regime $\eta_S \gg \eta_D$. However, this increased viscosity comes at a cost: although the Sisyphus cooling can be much stronger near zero velocity, its capture velocity is also much smaller than the Doppler capture velocity.

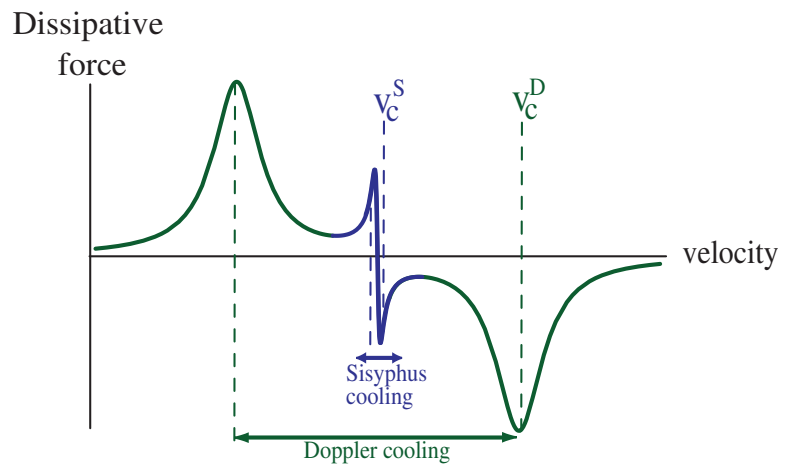


Figure 8.6: Comparison of Doppler force and Sisyphus force. The Doppler force can cool relatively hot atoms down to the Doppler limit. Only slowly-moving atoms can be cooled by the Sisyphus mechanism, but the Sisyphus friction coefficient (proportional to the slope of the curve at $v = 0$) is much larger, so much lower final temperatures can be reached.

Capture velocity

For relatively weak fields, the Doppler capture velocity is independent of the power $v_c^D \sim \gamma/k, \delta/k$. A careful calculation shows, however, that the Sisyphus capture velocity scales with the AC Stark shift: From Eq. (8.124), the large-detuning limit of the capture velocity is

$$v_c^S \sim \frac{\lambda}{18\pi} \frac{|\Omega|^2}{\delta}. \quad (8.130)$$

Thus we find that as $\delta \rightarrow \infty$, the friction coefficient grows, but the capture velocity vanishes.

Non-adiabaticity in Sisyphus cooling

From our quantitative analysis of Sisyphus cooling, we saw that the cooling force vanishes if the atom follows the instantaneous steady state solution to the density matrix equations. The friction force entered only when we accounted for a time lag, which therefore must be crucial to the Sisyphus mechanism. Physically, if the atomic populations were optically pumped much faster than the atomic velocity, then the atom would not have to lose potential energy to move through the dressed state potential. In particular, if the population distribution adiabatically follows the atomic position, then the atomic population moving uphill loses energy at precisely the same rate as the atomic population moving downhill gains it. Conversely, in the best case scenario for cooling the atom would climb the potential hill so quickly that none of its population could be optically pumped into the lower (accelerating) state.

8.6.4 The Sisyphus cooling limit

The limits to Sisyphus cooling are set by the same momentum diffusion process we encountered in Doppler cooling. We found that the momentum kicks caused by spontaneous emission lead to a diffusion rate

$$D_{sp} = (\hbar k)^2 \frac{|\Omega|^2 \gamma/2}{(\gamma/2)^2 + \delta^2}. \quad (8.131)$$

In addition, there is momentum diffusion from fluctuations of the instantaneous dipole force as the atom jumps between $m_s = \pm 1/2$ states, which occurs at the rate $1/\tau_p$. When the fluctuations are averaged over a

wavelength,⁴

$$\langle D_{dp} \rangle = \langle 2\hbar^2 k^2 \frac{\delta^2}{\gamma} \frac{\Omega^2/2}{\delta^2 + (\gamma/2)^2} \sin^4 2kz \rangle = \frac{3(\hbar k)^2 \delta^2}{4\gamma} \frac{\Omega^2/2}{\delta^2 + (\gamma/2)^2}. \quad (8.132)$$

In fact, this second diffusion coefficient dominates for large detuning. Using the Einstein relation and our result for the Sisyphus friction coefficient, we can find the final temperature attained by the atoms in the limit of large detuning:

$$k_B T_S = \frac{D_{sp} + D_{dp}}{m|\eta_S|} \approx \frac{\hbar|\Omega|^2}{8\delta} \quad (8.133)$$

This indicates that the lowest temperature corresponds to the depth of the dressed state potential. Once the kinetic energy of the atom becomes so small that the atom cannot make it up the hill, the Sisyphus cooling mechanism ceases to exist.

It may appear that T_S can be reduced to arbitrarily small values simply by letting $|\Omega|^2/\delta \rightarrow 0$. In fact, our analysis breaks down once the atom becomes slow enough that its motion can no longer be treated classically. When the atom is cold enough to be essentially localized within one potential well, its momentum has an uncertainty

$$\delta p \approx \frac{2\pi\hbar}{\lambda} \quad (8.134)$$

which sets a lower limit on the atomic energy equal to the recoil energy

$$E_{\min}^{\text{kinetic}} \sim \hbar\omega_R. \quad (8.135)$$

Typical values for the recoil energy $T_R \approx 2.4\mu\text{K}$ (Na) or $T_R \approx 0.37\mu\text{K}$ (Rb) are much smaller than the Doppler limit.

Other sub-Doppler cooling mechanisms

We have only discussed one of many sub-Doppler cooling schemes as applied to a particular atomic level configuration. The specific features vary, but this model gives a sense for the types of mechanisms employed to reach sub-Doppler temperatures. A good reference for other cooling techniques is “Laser Cooling and Trapping” by Metcalf and van der Straten or Cohen-Tannoudji’s lecture notes in Les Houches LXXII (1999).

Note that the recoil energy does not set an ultimate limit on laser cooling, but to proceed further, we would need to treat the atomic motion quantum

⁴see Dalibard and Cohen-Tannoudji, JOSA B, p2023 (1989) for further details.

mechanically. Laser cooling schemes which go beyond ω_R are known as “sub-recoil” mechanisms, and they require two-photon transitions or effects such as dark resonances.

Finally, note that we have only considered cooling of free neutral atoms. In many ways, cooling of confined atoms and ions can be much simpler, and will be addressed in subsequent lectures.

Chapter 9

Quantum properties of light interacting with matter

Until this point, we have only considered quantum fields as an environment leading to dissipation and fluctuations in the system of interest. Such analysis has its limitations, and we will now address a more complete situation where the quantum properties the electromagnetic field are explicitly included.

9.1 Basic properties of quantum fields

We saw earlier that the electric field can be represented in terms of a set of quantized harmonic oscillator modes,

$$\hat{\mathbf{E}} = \sum_{k,\alpha} \sqrt{\frac{\hbar\omega_k}{2\epsilon_0 V}} \hat{e}_\alpha \left(\hat{a}_{k,\alpha} e^{i(\mathbf{k}\cdot\mathbf{r}-\omega_k t)} + h.c. \right), \quad (9.1)$$

where ω_k and \hat{e}_α are the frequency and polarization of the mode $\{k, \alpha\}$. The Hamiltonian for such a field can also be expressed in terms of the creation and annihilation operators,

$$\hat{H} = \frac{1}{2} \int dV \left(\epsilon_0 E^2 + \frac{B^2}{\mu_0} \right) \quad (9.2)$$

$$= \sum_{k,\alpha} \hbar\omega_k \left(\hat{a}_{k,\alpha}^\dagger \hat{a}_{k,\alpha} + \frac{1}{2} \right), \quad (9.3)$$

and its eigenbasis is formed by the number states or “Fock” states $\{|n_{k,\alpha}\rangle\}$ obeying

$$\hat{n}_{k,\alpha} |n_{k,\alpha}\rangle = \hat{a}_{k,\alpha}^\dagger \hat{a}_{k,\alpha} |n_{k,\alpha}\rangle = n_{k,\alpha} |n_{k,\alpha}\rangle \quad (9.4)$$

where $n_{k,\alpha}$ is the number of photons in the mode $\{k, \alpha\}$.

Many properties of quantum fields can be understood by examining the evolution of a single mode. Such a description is also quantitatively appropriate for atoms interacting with the quantum field of a high finesse cavity, so we will frequently simplify our discussion by considering only a single mode.

9.1.1 Thermal states

A single mode field in thermal equilibrium with its environment at temperature T can be described by a density operator

$$\hat{\rho} = \frac{e^{-\hat{H}/k_B T}}{\text{Tr}[e^{-\hat{H}/k_B T}]} \quad (9.5)$$

Expressed in the Fock basis, the density matrix is purely diagonal with elements

$$\rho_{nn} = e^{-n\hbar\omega/k_B T} \cdot (1 - e^{-\hbar\omega/k_B T}) \quad (9.6)$$

corresponding to the probability to find n photons in the cavity.

The resulting probability distribution for photon number is known as the “photon distribution” or “photon statistics”. The thermal state is most likely to have zero photons in it, and the average number

$$\bar{n} = \sum_n n \rho_{nn} = \frac{1}{e^{\hbar\omega/k_B T} - 1} \quad (9.7)$$

reflects the fact that photons obey Bose-Einstein statistics with $\mu = 0$. The expectation value of the electric field vanishes

$$\langle \hat{E} \rangle \propto \langle \hat{a} \rangle = 0 \quad (9.8)$$

because the thermal field is incoherent, and thus has an undefined phase.

Note that photon statistics in a multimode thermal field look very different than this single mode example. Whereas each mode in a multimode field would most likely contain no photons, when one sums over all such modes, the most likely total photon number will be finite and the distribution looks more like a Poissonian. For example, sunlight corresponds to a multimode thermal field. In order to probe the photon statistics associated with the thermal nature of sunlight, it is necessary to design an experiment in which the sunlight acts as if it were a single-mode field. One way to do this would be to simultaneously filter the sunlight to a bandwidth $\Delta\omega$ and observe the photon arrival times using a detector which is gated for a time much shorter than $1/\Delta\omega$.

9.1.2 Coherent states

To understand the correspondence between our semi-classical description and the quantum mechanical approach, it is desirable to find a quantum state which corresponds to the classical coherent field of a laser. The defining characteristic of the laser field is a well defined, finite expectation value for the electric field, so we seek a state $|\psi\rangle$ satisfying

$$\langle\psi|\hat{E}|\psi\rangle = E. \quad (9.9)$$

We have seen that the thermal state does not have a finite electric field expectation value, and the Fock states likewise have vanishing electric field. Motivated by Eq. (9.9), we will consider an eigenstate $|\alpha\rangle$ of the photon annihilation operator,

$$\hat{a}|\alpha\rangle = \alpha|\alpha\rangle. \quad (9.10)$$

This so-called “coherent state” in fact corresponds to classical laser light.

As we hoped, the coherent state has a well-defined expectation value for the electric field

$$\langle\alpha|\hat{E}|\alpha\rangle = \sqrt{\frac{\hbar\omega}{2\epsilon_0V}} \left(\alpha e^{i(\mathbf{k}\cdot\mathbf{r}-i\omega t)} + c.c. \right), \quad (9.11)$$

and the average number of photons in the coherent state is

$$\langle\alpha|\hat{a}^\dagger\hat{a}|\alpha\rangle = |\alpha|^2. \quad (9.12)$$

The quadrature components

In analogy to the position and momentum operators of the simple harmonic oscillator, we can introduce the quadrature operators

$$\hat{x} = \frac{1}{\sqrt{2}} (\hat{a} + \hat{a}^\dagger) \quad (9.13)$$

$$\hat{p} = \frac{1}{i\sqrt{2}} (\hat{a} - \hat{a}^\dagger). \quad (9.14)$$

The uncertainty in these operators,

$$\langle\delta x^2\rangle = \frac{1}{2} \quad (9.15)$$

$$\langle\delta p^2\rangle = \frac{1}{2}, \quad (9.16)$$

is the “most classical” we could hope for, since the Heisenberg uncertainty principle limits $\delta x \delta p \geq 1/2$. The quadrature operators have a well defined physical meaning for the electromagnetic field. The electric field operator given by Eq. (9.1) can be re-written in terms of the two components

$$\hat{E} \propto \hat{x} \cos \omega t + \hat{p} \sin \omega t. \quad (9.17)$$

For example, if this electric field is mixed with some other field (referred to as a “local oscillator”)

$$E_{LO} \sim \cos \omega t, \quad (9.18)$$

then \hat{x} would yield the “in phase” component while \hat{p} gives the “out of phase” component.

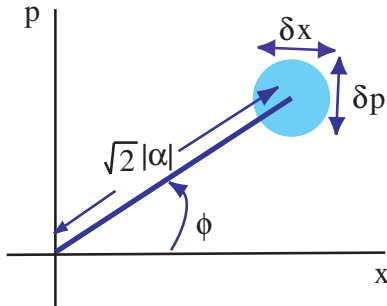


Figure 9.1: Any coherent state can be represented by an area in $\{\hat{x}, \hat{p}\}$ phase space. The distance to the origin is proportional to the absolute value of the coherent state $|\alpha|$, while the angle is the argument of α . The uncertainty in the quadrature operators is represented by a circle with a diameter of $\sqrt{2}$. Note that other textbooks choose to define $\hat{x} = \frac{1}{2} (\hat{a} + \hat{a}^\dagger)$, $\hat{p} = \frac{1}{2i} (\hat{a} - \hat{a}^\dagger)$, which gets rid of the $\sqrt{2}$ factors.

The shift operator

Coherent states can be generated from the vacuum state by the “shift operator”

$$\hat{D}(\alpha) = e^{\alpha \hat{a}^\dagger - \alpha^* \hat{a}}, \quad (9.19)$$

which shifts the state in the plane of \hat{x} and \hat{p} so that $\hat{D}(\alpha)|0\rangle = |\alpha\rangle$. Similarly,

$$\hat{D}^{-1}(\alpha)\hat{a}\hat{D}(\alpha) = \hat{a} + \alpha. \quad (9.20)$$

To prove Eq. 9.19, we will use the fact that if two operators satisfy $[\hat{A}, [\hat{A}, \hat{B}]] = [\hat{B}, [\hat{A}, \hat{B}]] = 0$, then

$$e^{\hat{A}+\hat{B}} = e^{\hat{A}} e^{\hat{B}} e^{-[\hat{A}, \hat{B}]/2}. \quad (9.21)$$

Consequently, when the shift operator acts on the vacuum, it generates a coherent state:

$$\hat{D}(\alpha)|0\rangle = e^{\alpha\hat{a}^\dagger - \alpha^*\hat{a}}|0\rangle \quad (9.22)$$

$$= e^{-|\alpha|^2/2} e^{\alpha\hat{a}^\dagger} e^{-\alpha^*\hat{a}}|0\rangle \quad (9.23)$$

$$= e^{-|\alpha|^2/2} \sum_n \frac{\alpha^n}{\sqrt{n!}} |n\rangle \quad (9.24)$$

$$= |\alpha\rangle. \quad (9.25)$$

Photon statistics in a coherent state

The probability to find n photons in a coherent state follows a Poisson distribution

$$\rho_{nn} = e^{-|\alpha|^2} \frac{\alpha^{2n}}{n!} \quad (9.26)$$

which has variance equal to its mean

$$\bar{n} = |\alpha|^2 \quad (9.27)$$

$$\langle \Delta n^2 \rangle = \bar{n} = |\alpha|^2. \quad (9.28)$$

For strong fields, $n \gg 1$, the standard deviation $\sqrt{\langle \Delta n^2 \rangle}$ is much smaller than the mean, so the intensity becomes better defined as the coherent field becomes larger.

Classical dipole radiation

The coherent state also corresponds to the field produced by a classical oscillating dipole. To see this, consider the Hamiltonian for such a dipole,

$$\hat{H} = -d\hat{E} = -d_0 \cos \omega t \hat{E}. \quad (9.29)$$

 In the RWA, the Hamiltonian becomes $-(d_0 E_0/2)\hat{a}^\dagger + h.c.$, so that after a time t the time evolution operator acts as the shift operator:

$$|\psi\rangle = e^{-i\hat{H}t/\hbar}|0\rangle = e^{\alpha\hat{a} - \alpha^*\hat{a}^\dagger}|0\rangle \quad (9.30)$$

where $\alpha = id_0 E_0 t / 2\hbar$.

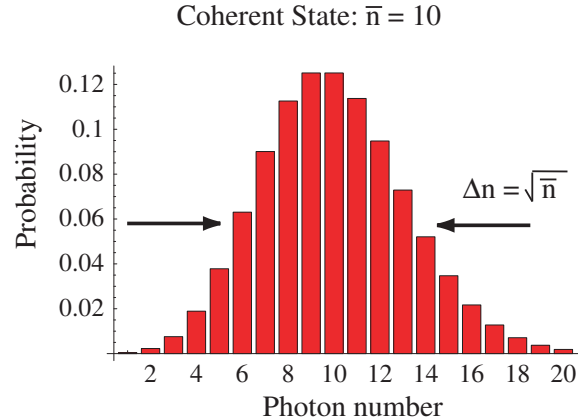


Figure 9.2: The photon number distribution for a coherent state with $|\alpha|^2 = 10$.

Generalization to multimode fields

These properties of the coherent state show that they do indeed provide a quantum description of classical laser light. The coherent states, however, can also be generalized to multimode situations by taking the direct product of a coherent state in each mode.

$$|\psi\rangle = \prod_k |\alpha_k\rangle. \quad (9.31)$$

The expectation value of the electric field in this multimode state is

$$E(r, t) = \langle \psi | \hat{E} | \psi \rangle \quad (9.32)$$

$$= \sum_k \underbrace{\sqrt{\frac{\hbar\omega_k}{2\epsilon_0 V}} \alpha_k}_{E_k} e^{i(\mathbf{k}\cdot\mathbf{r} - i\omega_k t)} + c.c. \quad (9.33)$$

where E_k is the Fourier component of the k^{th} mode of the classical field.

Quasi-probability distributions

Whereas the number states formed a basis for the electromagnetic field, the coherent states form an overcomplete set. We can prove completeness by

showing that the identity operator is proportional to the sum of all coherent states:

$$\int |\alpha\rangle\langle\alpha| d^2\alpha = \sum_{m,n} \int e^{-|\alpha|^2} \frac{\alpha^m \alpha^{*n}}{\sqrt{m!n!}} |m\rangle\langle n| d^2\alpha. \quad (9.34)$$

Writing $\alpha = |\alpha|e^{i\phi}$,

$$\begin{aligned} \int |\alpha\rangle\langle\alpha| d^2\alpha &= \sum_{m,n} \frac{1}{\sqrt{m!n!}} \int_0^\infty d|\alpha| e^{-|\alpha|^2} |\alpha|^{m+n+1} \times \\ &\quad \int_0^{2\pi} d\phi e^{i(m-n)\phi} |m\rangle\langle n| \end{aligned} \quad (9.35)$$

$$= \sum_{m,n} \pi n! \delta_{m,n} |m\rangle\langle n| \quad (9.36)$$

$$= \pi \sum_n |n\rangle\langle n|. \quad (9.37)$$

In other words,

$$1 = \frac{1}{\pi} \int d^2\alpha |\alpha\rangle\langle\alpha|. \quad (9.38)$$

However, using Eq. (9.24), we can directly verify that different coherent states are not orthogonal,

$$|\langle\alpha|\beta\rangle| = e^{-(1/2)|\alpha-\beta|^2}, \quad (9.39)$$

so they provide an unnecessarily large set of states for describing an arbitrary field. The coherent state representation of a density operator $\hat{\rho}$ nevertheless remains useful, and we define the quasi-probability distribution $P(\alpha)$ by

$$\hat{\rho} = \int P(\alpha) |\alpha\rangle\langle\alpha| d^2\alpha. \quad (9.40)$$

This quasi-probability distribution has some interesting properties. Firstly, it acts like a probability distribution when you consider the expectation value of any normally ordered operator \hat{O} :

$$\langle\hat{O}\rangle = \int P(\alpha) \langle\alpha|\hat{O}|\alpha\rangle d^2\alpha \quad (9.41)$$

$$= \int P(\alpha) O(\alpha) d^2\alpha \quad (9.42)$$

Second, it is worth noting that this distribution always exists, and can be found using the formula

$$P(\alpha) = \frac{e^{|\alpha|^2}}{\pi^2} \int \langle -\beta | \rho | \beta \rangle e^{|\beta|^2} e^{-\beta \alpha^* + \beta^* \alpha} d^2 \beta. \quad (9.43)$$

This relationship can be derived after a bit of algebra by calculating $\langle -\beta | \rho | \beta \rangle$ (see, e.g., Scully and Zubairy, p. 76).

The quasi-probability distribution $P(\alpha)$ is not a proper probability distribution because it can take on negative values. In particular, the negative values are associated with non-classical properties of the electromagnetic field, and mark a boundary between quantum and classical states.

Linear optical transformations of coherent states

Linear transformations are defined as effects independent of the incident light power, and a coherent state will remain a coherent state under a linear transformation. The simplest examples of linear transformations are phase shifts and beam splitters. As its name might imply, the phase shift only changes the phase of a coherent state

$$E \rightarrow E e^{i\phi} \Rightarrow \hat{a} \rightarrow \hat{a} e^{i\phi}. \quad (9.44)$$

A beamsplitter characterized by a transmission amplitude t and reflection amplitude r transforms two input electric fields $E_1^{\text{in}}, E_2^{\text{in}}$ into two output electric field¹

$$E_1^{\text{out}} = t E_1^{\text{in}} + i r E_2^{\text{in}} \quad (9.45)$$

$$E_2^{\text{out}} = t E_2^{\text{in}} + i r E_1^{\text{in}}. \quad (9.46)$$

Since these are linear relations, the same must hold true for the photon annihilation operators:

$$\hat{a}_1^{\text{out}} = t \hat{a}_1^{\text{in}} + i r \hat{a}_2^{\text{in}} \quad (9.48)$$

$$\hat{a}_2^{\text{out}} = t \hat{a}_2^{\text{in}} + i r \hat{a}_1^{\text{in}}. \quad (9.49)$$

¹Unitarity of this beamsplitter transformation requires that $|r|^2 + |t|^2 = 1$, which states that there are no losses due to the beamsplitter, and the less trivial relationship $r t^* - r^* t = 0$. This can be derived by letting

$$U = \begin{pmatrix} t & ir \\ ir & t \end{pmatrix}, \quad (9.47)$$

and solving $UU^\dagger = 1$.

Suppose that the inputs are $|\alpha_1\rangle|\alpha_2\rangle$. The resulting output field obeys

$$\hat{a}_1^{\text{out}}|\alpha_1\rangle|\alpha_2\rangle = (t\alpha_1^{\text{in}} + ir\alpha_2^{\text{in}})|\alpha_1\rangle|\alpha_2\rangle, \quad (9.50)$$

which is thus also a coherent state. The bottom line is that linear optical operations do not change the quantum statistical properties of coherent states.

Note that the beam splitter transformation can be viewed as resulting from a coupling of two simple harmonic oscillators, since

$$\begin{pmatrix} \hat{a}_1 \\ \hat{a}_2 \end{pmatrix}^{\text{out}} = \hat{U} \begin{pmatrix} \hat{a}_1 \\ \hat{a}_2 \end{pmatrix}^{\text{in}} \quad (9.51)$$

where the unitary operator

$$\hat{U} = e^{i\theta\hat{a}_1\hat{a}_2^\dagger + i\theta\hat{a}_2\hat{a}_1^\dagger} \quad (9.52)$$

can be written in terms of a parameter θ related to the transmission and reflection coefficients.

9.2 Interactions between a single-mode radiation field and a two level atom

We have seen that linear transformations preserve the properties of coherent classical fields. We will now consider several opposite examples in which nonlinear transformations can dramatically alter the properties of a single mode field. In particular, we will consider the interaction between a single mode of the radiation field and a single two-level atom. Although conceptually simple, the two-level atom provides an intrinsically anharmonic medium which will illustrate the nontrivial dynamics of the quantum field under nonlinear transformations.

Experimentally such a system is very difficult to realize. The single mode field must be isolated within a high finesse cavity (either optical or microwave), and a single atom must be confined within this cavity. This field is known as "cavity quantum electrodynamics", and recently experimentalists have begun to be able to probe the regime well described by a single mode and single atom.

9.2.1 The Jaynes-Cummings model

Initially, we will consider only the coherent interactions between the atom and cavity mode. This analysis neglects the dissipation and decoherence

associated with unconfined modes of the radiation bath or decay of the single mode field through the mirrors forming the cavity. The evolution of the atom and field can be solved exactly in this case.

If the atom is resonant with the cavity mode, the Hamiltonian in the rotating frame becomes

$$\hat{H} = -\hbar g \hat{a}|2\rangle\langle 1| - \hbar g^* \hat{a}^\dagger|1\rangle\langle 2|. \quad (9.53)$$

The first term in the Hamiltonian permits simultaneous excitation of the atom and absorption of a photon, while the second term describes atomic relaxation to the ground state and emission of a photon.

Suppose the atom starts off in the excited state, and the initial field is an arbitrary superposition of Fock states,

$$|\psi_0\rangle = |2\rangle_a \otimes \sum_n c_n(0)|n\rangle. \quad (9.54)$$

The Hamiltonian couples the state $|2\rangle_a|n\rangle$ to the state $|1\rangle_a|n+1\rangle$ and back, so after some time t , the system will be in the state

$$|\psi(t)\rangle = \sum_n c_n^{(1)}(t)|1\rangle_a \otimes |n\rangle + c_n^{(2)}(t)|2\rangle_a \otimes |n\rangle. \quad (9.55)$$

Since we are considering only coherent evolution, we can use the Schrodinger equation to find the evolution equations for the time-dependent probability amplitudes

$$\dot{c}_n^{(2)} = ig\sqrt{n+1}c_{n+1}^{(1)} \quad (9.56)$$

$$\dot{c}_{n+1}^{(1)} = ig\sqrt{n+1}c_n^{(2)}. \quad (9.57)$$

These equations hold independently for every pair $c_{n+1}^{(1)}, c_n^{(2)}$, so we can easily find the general solution for the probability amplitudes

$$c_{n+1}^{(1)}(t) = ic_n(0) \sin(g\sqrt{n+1}t) \quad (9.58)$$

$$c_n^{(2)}(t) = c_n(0) \cos(g\sqrt{n+1}t). \quad (9.59)$$

Note that even if the atom starts out in some superposition state, the same kinds of manipulations will again give a general solution.

9.2.2 Initial vacuum field: vacuum Rabi oscillations

The physics behind the Jaynes-Cummings model is particularly transparent when the radiation field initially starts out in the vacuum state,

$$|\psi_0\rangle = |2\rangle_a \otimes |0\rangle. \quad (9.60)$$

In this case, the system only couples to one other state, $|1\rangle_a \otimes |1\rangle$. We can project the Hamiltonian onto these two states to find an effective two-level system with coupling strength g :

$$\hat{H}_{\text{eff}} = -\hbar g|2\rangle_a|0\rangle\langle 1|_a\langle 1| - \hbar g^*|1\rangle_a|1\rangle\langle 2|_a\langle 0|. \quad (9.61)$$

Such a system exhibits oscillations at the vacuum Rabi frequency g , and its state is described by the wavefunction

$$|\psi(t)\rangle = \cos gt|2\rangle_a|0\rangle + i \sin gt|1\rangle_a|1\rangle. \quad (9.62)$$

Unlike classical Rabi oscillations induced by a coherent laser, these dynamics involve Fock states of the radiation field. In particular, after a time $t = \pi/2g$, the system is in an eigenstate of the number operator $\hat{a}^\dagger\hat{a}|\psi\rangle = i\hat{a}^\dagger\hat{a}|1\rangle_a|1\rangle = |\psi\rangle$. We emphasize that the Fock state with exactly one photon is very different coherent states created by a classical current; for example the classical coherence vanishes for the Fock state $\langle\hat{a}\rangle = 0$.

The state evolution may appear similar to the spontaneous emission of a single photon from an excited atom, but there is an important difference. Whereas spontaneous emission produces a single photon wavepacket distributed over an infinite number of free space modes, the vacuum Rabi oscillation produces a single photon in a well defined mode. The emission process is thus fully reversible, and the photon can be reabsorbed by the atom. Such reabsorption was impossible in the Wigner Wiesskopf theory, but it is predicted by this analysis because we have disregarded incoherent interactions. We have implicitly assumed that the vacuum Rabi frequency g is much greater than the rate of dissipation or decoherence. Achieving this so-called “strong coupling regime” presents a substantial challenge to experimentalists.

Initial coherent state field

The system behaves quite differently if the radiation field starts out in a coherent state,

$$|\psi_0\rangle = |2\rangle_a \otimes |\alpha\rangle. \quad (9.63)$$

Classically, we would expect to see Rabi oscillations, and we will now examine the quantum limit to such oscillations.

We can represent the coherent state in the general form

$$|\psi_0\rangle = |2\rangle_a \otimes \sum_n e^{-|\alpha|^2/2} \underbrace{\frac{\alpha^n}{\sqrt{n!}}}_{c_n(0)} |n\rangle, \quad (9.64)$$

and using the solution for $c_n^{(i)}(t)$ we can write down the general solution for $|\psi\rangle$:

$$|\psi(t)\rangle = \sum_n e^{-|\alpha|^2/2} \frac{\alpha^n}{\sqrt{n!}} (i \sin(g\sqrt{n+1}t) |1\rangle_a |n+1\rangle + \cos(g\sqrt{n+1}t) |2\rangle_a |n\rangle). \quad (9.65)$$

One might suppose that the atomic dynamics and field states represented by $|\psi(t)\rangle$ should be dominated by the most heavily weighted Fock states in the sum over n . The average photon number in the coherent state is given by $\bar{n} = |\alpha|^2$, and for large \bar{n} , the Poisson distribution centered around $n = \bar{n}$ has a narrow width $\Delta n/\bar{n} = 1/\sqrt{\bar{n}}$. The lowest order approximation we can make in Eq. (11.6) is to simply substitute $\sqrt{n+1} \approx \sqrt{\bar{n}}$, which should roughly produce the correct results in the sum above over the range $n \in [\bar{n} - \Delta n, \bar{n} + \Delta n]$. Such a substitution yields

$$\begin{aligned} |\psi(t)\rangle &\approx \sum_n e^{-|\alpha|^2/2} \frac{\alpha^n}{\sqrt{n!}} (i \sin(g\sqrt{\bar{n}}t) |1\rangle_a |n+1\rangle + \cos(g\sqrt{\bar{n}}t) |2\rangle_a |n\rangle) \\ &\approx \sum_n e^{-|\alpha|^2/2} \frac{\alpha^n}{\sqrt{n!}} (i \sin(g\sqrt{\bar{n}}t) |1\rangle_a |n\rangle + \cos(g\sqrt{\bar{n}}t) |2\rangle_a |n\rangle) \\ &= (i \sin(g\sqrt{\bar{n}}t) |1\rangle_a + \cos(g\sqrt{\bar{n}}t) |2\rangle_a) \otimes |\alpha\rangle. \end{aligned} \quad (9.66)$$

We find that the field remains in a coherent state while the atom cycles between the ground and excited states with period

$$\tau_{\text{Rabi}} \sim \frac{1}{g\sqrt{\bar{n}}} \sim \frac{1}{|\alpha|g}. \quad (9.67)$$

This naive analysis has thus only given us the classical Rabi oscillations, so a more careful treatment is required to find the quantum corrections.

The quantum limit to Rabi oscillations

Suppose we are interested in the probability for the atom to be in its excited state, which requires summation over all of the Fock states of the field. If

we still assume that \bar{n} is large, we can expand in terms of a small quantity $\delta n/\bar{n}$. The phase of the sine and cosine functions is then

$$\phi_n = g\sqrt{n+1}t \approx g\sqrt{\bar{n} + \delta n} t \quad (9.68)$$

$$\approx gt\sqrt{\bar{n}} \left(1 + \frac{\delta n}{2\bar{n}}\right) = gt\sqrt{\bar{n}} \left(\frac{\bar{n} + n}{2\bar{n}}\right). \quad (9.69)$$

To first order in $\delta n/n$, the phase depends linearly on n . This observation allows us to capture the main effect of photon number fluctuations, because it shows that at long times even small δn will have a non-negligible contribution to the phase. Qualitatively, these corrections introduce phases into the sum which depend on the precise value of δn , thereby dephasing the wavepacket.

The photon number fluctuations first become significant when the phase corrections $gt\delta n/\sqrt{\bar{n}}$ approach unity:

$$\tau_{\text{Collapse}} \sim \frac{\sqrt{\bar{n}}}{\delta n g} \sim \frac{1}{g}. \quad (9.70)$$

The different Fock states get out of phase with each other, so the Rabi oscillations damp out. If we evolve for even longer times, however, the Rabi oscillations revive. The revival time,

$$\tau_{\text{Revival}} \sim 2\pi \frac{\sqrt{\bar{n}}}{g} \sim 2\frac{\pi|\alpha|}{g}, \quad (9.71)$$

corresponds to the time required for the phase corrections $gt\sqrt{\bar{n}}\frac{\delta n}{2\bar{n}}$ to equal multiples of π for the dominant Fock states (it can be seen that multiples of π rather than 2π are sufficient since the sin and cos terms will cause at most just an overall phase shift). The collapse and revival phenomenon represents a generic feature of many quantum nonlinear systems which are isolated from their environments. In this case, the revival is imperfect, but there exist other nonlinear systems which exhibit complete revivals of oscillations.

The origin of the collapse and revival phenomenon lies in the field evolution. If we let a single-mode coherent field interact with a nonlinear medium (such as a two-level atom), at long times it will not remain in a coherent state. This situation is perhaps made most apparent by using our approximate value for ϕ_n to find the state at later times $t > 0$. Using

$$\phi_n \approx gt\sqrt{\bar{n}} \left(\frac{\bar{n} + n}{2\bar{n}}\right), \quad (9.72)$$

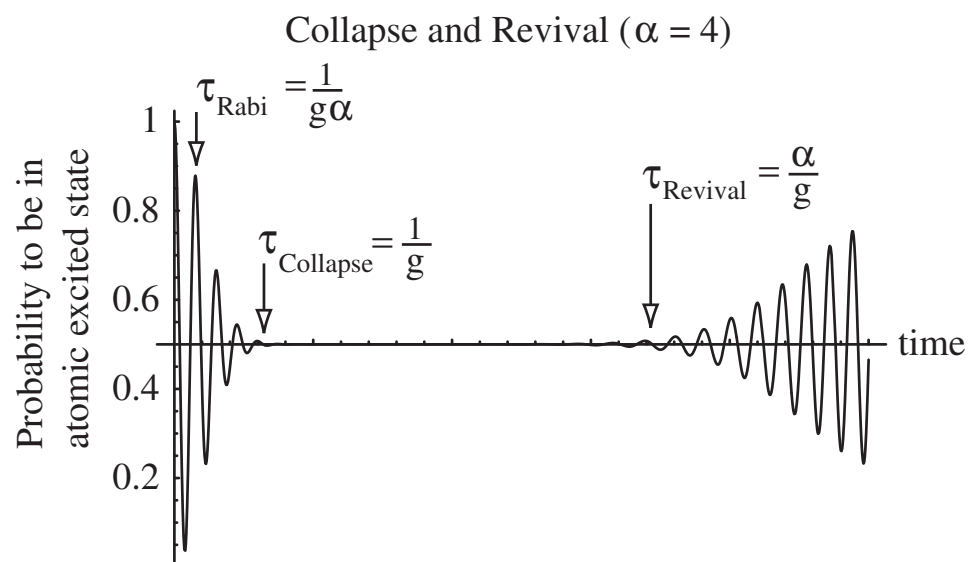


Figure 9.3: Collapse and revival of Rabi oscillations for a cavity field initially in a coherent state with $\alpha = 4$.

over the range of relevant n we can write

$$i \sin(g\sqrt{n+1}t) = \frac{1}{2} (e^{i\phi_n} - e^{-i\phi_n}) \quad (9.73)$$

$$\approx e^{ig\sqrt{\bar{n}}t/2} e^{ignt/2\sqrt{\bar{n}}} - e^{-ig\sqrt{\bar{n}}t/2} e^{-ignt/2\sqrt{\bar{n}}}. \quad (9.74)$$

The ground state contribution to Eq. (11.6) can then be written at arbitrary times as

$$\sum_n e^{-|\alpha|^2/2} \frac{\alpha^n}{\sqrt{n!}} i \sin g\sqrt{n+1}t |1\rangle_a |n+1\rangle \approx \quad (9.75)$$

$$\begin{aligned} & \frac{1}{2} |1\rangle_a \otimes \sum_n e^{-|\alpha|^2/2} \left(e^{ig\sqrt{\bar{n}}t/2} \frac{(\alpha e^{igt/2\sqrt{\bar{n}}})^n}{\sqrt{n!}} - e^{-ig\sqrt{\bar{n}}t/2} \frac{(\alpha e^{-igt/2\sqrt{\bar{n}}})^n}{\sqrt{n!}} \right) = \\ & \frac{1}{2} |1\rangle_a \otimes \sum_n \left(e^{ig\sqrt{\bar{n}}t/2} |\alpha e^{igt/2\sqrt{\bar{n}}}\rangle - e^{-ig\sqrt{\bar{n}}t/2} |\alpha e^{-igt/2\sqrt{\bar{n}}}\rangle \right). \end{aligned} \quad (9.76)$$

A similar calculation can be done with the excited state term of Eq. (11.6), and yields the total state

$$|\psi(t)\rangle = \frac{1}{\sqrt{2}} (|2\rangle_a |\alpha_+\rangle + |1\rangle_a |\alpha_-\rangle) \quad (9.77)$$

where

$$|\alpha_+\rangle = \frac{1}{\sqrt{2}} \left(e^{ig\sqrt{\bar{n}}t/2} |\alpha e^{igt/2\sqrt{\bar{n}}}\rangle + e^{-ig\sqrt{\bar{n}}t/2} |\alpha e^{-igt/2\sqrt{\bar{n}}}\rangle \right) \quad (9.78)$$

$$|\alpha_-\rangle = \frac{1}{\sqrt{2}} \left(e^{ig\sqrt{\bar{n}}t/2} |\alpha e^{igt/2\sqrt{\bar{n}}}\rangle - e^{-ig\sqrt{\bar{n}}t/2} |\alpha e^{-igt/2\sqrt{\bar{n}}}\rangle \right). \quad (9.79)$$

The atom and the field are in general no longer factorizable, and the field state is very different from a coherent state.

At time $gt = \pi\sqrt{\bar{n}} \sim g\tau_{Revival}/2$, suppose we measure the internal state of the atom, which in turn projects the field component into either the state $|\alpha_+\rangle$ or $|\alpha_-\rangle$, where $|\alpha_\pm\rangle \sim |\alpha e^{i\pi/2}\rangle \pm e^{-i\pi\bar{n}} |\alpha e^{-i\pi/2}\rangle$. Note that the classical coherence of this state $\langle \hat{a} \rangle \sim e^{-|\alpha|^2}$ is exponentially small for large α , but it possesses a higher order quantum coherence. This kind of superposition state is often called a “Schrodinger cat”: much like the infamous feline, the two superposed states $|\pm i\alpha\rangle$ are macroscopically distinguishable. Consequently this kind of state is very difficult to produce experimentally because it is easily destroyed by decoherence and dissipation. Nonetheless, such techniques have been demonstrated (see, *e.g.*, Phys. Rev. Lett. **94**, 010401 (2005)).

"Schrodinger cat" state of the radiation field

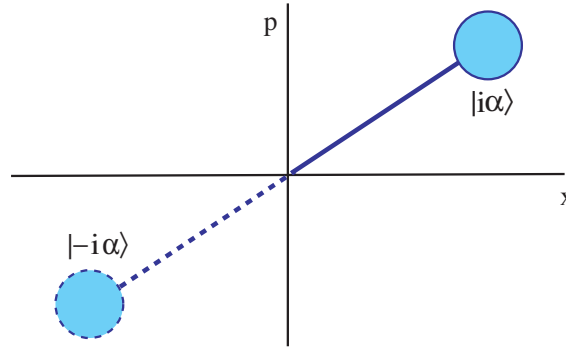


Figure 9.4: A phase space depiction of the field state $\sim |i\alpha\rangle - |-i\alpha\rangle$ near $\tau_{Revival}/2$.

9.3 The effects of dissipation on quantum fields

We have seen that linear transformations of coherent states retain their classical nature, but nonlinear interactions lead to highly nontrivial quantum states of the radiation field. Nevertheless, experience tells us that the real world is both nonlinear and classical. To understand how and why this happens, we will have to consider the effects of dissipation on quantum fields.

The beamsplitter provides an intuitive and simple model for loss. A signal incident on a beamsplitter is attenuated by its transmission amplitude t ; simultaneously, the vacuum field incident on the other port introduces fluctuations so that the output field is

$$\hat{a}_{\text{out}} = t\hat{a}_{\text{in}} + i\sqrt{1 - |t|^2}\hat{b}_{\text{vac}}. \quad (9.80)$$

If the signal starts out in a coherent state $|\alpha\rangle$, the transmitted field will also be a coherent state $|t\alpha\rangle$. But this is not true for arbitrary quantum states. For example, an incident Fock state will no longer be in a Fock state after interaction with the beamsplitter.

9.3.1 Dynamics of a single mode field in a lossy cavity

We now wish to consider the effects of dissipation on quantum fields in greater detail. For simplicity, we will focus here on single-mode fields such

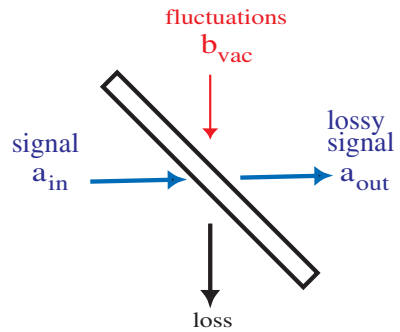


Figure 9.5: A beamsplitter model for loss.

as those in an optical cavity. However, we will treat a more realistic scenario in which the cavity is not perfect but is coupled to the outside world.

The beamsplitter model can be used to understand dissipation in a cavity formed by one partially transmitting mirror. Initially, we will consider only classical loss, and neglect the associated quantum noise.

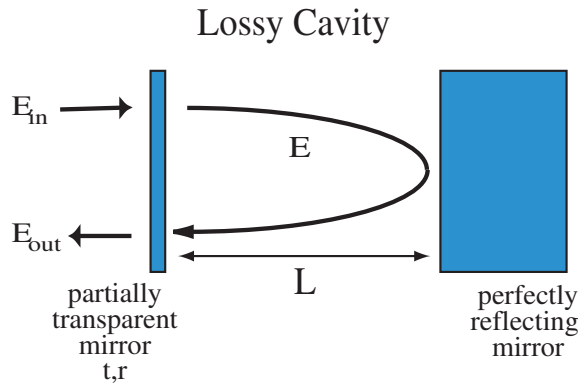


Figure 9.6: Model used to analyze dissipation in a lossy cavity.

Classical evolution

The classical evolution equation for the intra-cavity field can be found by calculating the change in E during one round trip,

$$E(t + \Delta t) = tE_{\text{in}}(t) + rE(t), \quad (9.81)$$

where t and r are the transmission and reflection coefficients for the left-hand mirror, and $\Delta t = 2L/c$ is the roundtrip time, and $E_{\text{in}}(t)$ is the field incident on the cavity. Converting this difference equation into a differential equation,

$$\frac{E(t + \Delta t) - E(t)}{\Delta t} \rightarrow \frac{d}{dt}E(t), \quad (9.82)$$

we find

$$\frac{d}{dt}E(t) = -\frac{(1-r)c}{2L}E(t) + \frac{tc}{2L}E_{\text{in}}(t). \quad (9.83)$$

For a perfect mirror, $r^2 + t^2 = 1$, so we can write the cavity loss rate in the limit $t \ll 1$ as

$$\kappa = \frac{2c(1-r)}{2L} \approx \frac{t^2 c}{2L}. \quad (9.84)$$

Here we have used $t^2 = 1 - r^2 \approx 2(1 - r)$. The evolution equation then becomes

$$\frac{d}{dt}E(t) = -\frac{\kappa}{2}E(t) + \sqrt{\frac{\kappa c}{2L}}E_{\text{in}}(t). \quad (9.85)$$

The cavity response function can be found by transforming the evolution equation into the Fourier domain. The cavity lineshape is Lorentzian, with width given by the cavity loss rate:

$$E(\omega) = \frac{\sqrt{\kappa c/2L}}{\kappa/2 - i\omega}E_{\text{in}}(\omega). \quad (9.86)$$

The field evolution will be modified by the atomic polarization induced if any medium is present inside the cavity. By projecting Maxwell's equations into the cavity mode (i.e. disregarding terms $\sim dE/dz$ for a slowly varying amplitude), we find that the cavity field evolves as

$$\frac{d}{dt}E(t) = -\frac{\kappa}{2}E(t) + \sqrt{\frac{\kappa c}{2L}}E_{\text{in}}(t) + \frac{i\bar{\nu}P}{2\epsilon_0}, \quad (9.87)$$

where $\bar{\nu}$ is the center frequency of the cavity resonance.

The output field is given by the sum of the reflected input field and the transmitted cavity field,

$$E_{\text{out}} = -rE_{\text{in}} + tE. \quad (9.88)$$

This equation is known as an “input-output relationship”, and a good reference on a semiclassical analysis of electromagnetic fields in a cavity can be found in Sargent, Scully, and Lamb, “Laser Physics”.

9.3.2 Quantum mechanical treatment of the cavity mode

We can adapt the classical evolution equation to a quantum description simply by replacing the cavity field E by the cavity photon annihilation operator \hat{a} and accounting for noise associated with the cavity decay rate κ . If the input field vanishes, then the evolution equation becomes

$$\frac{d}{dt}\hat{a} = \frac{-\kappa}{2}\hat{a} + \hat{\mathcal{F}}. \quad (9.89)$$

In principle, we could use the quantum fluctuation-dissipation theorem to determine the properties of the noise operator $\hat{\mathcal{F}}$. Instead, we proceed to highlight the physical origin of the fluctuations by introducing a microscopic model of noise. The noise we are adding in fact looks very much like the input field terms we neglected in Eq. (9.89), where we now account for the exterior vacuum field leaking into the cavity via the partially transmitting mirror.

Microscopic noise model

Our microscopic noise model will account for interactions between the quantum cavity field and its environment of continuum modes. Imperfect mirrors provide coupling between the cavity and reservoir, since cavity photons can leak out and reservoir photons can leak in. In the interaction picture, the effective Hamiltonian for the system-reservoir interaction can be written

$$\hat{V}_{SR} = i\hbar \sum_k t_k \hat{a} \hat{a}_k^\dagger e^{-i(\nu - \nu_k)t} + h.c., \quad (9.90)$$

where ν is the cavity frequency, \hat{a}_k is a continuum mode of frequency ν_k , and the coupling coefficient t_k between the cavity mode and \hat{a}_k is determined by the transmission properties of the mirrors forming the cavity. When the environment is large and has a broad bandwidth, this interaction Hamiltonian is mathematically equivalent to the model of atomic spontaneous emission

considered earlier. To make the connection with our formal approach, we identify the system and reservoir operators

$$\hat{S} = \hat{a} \quad (9.91)$$

$$\hat{R}^\dagger = i\hbar \sum_k t_k \hat{a}_k^\dagger. \quad (9.92)$$

Using the general reservoir theory we developed earlier, we can immediately write down the decay rate and noise operator in terms of microscopically defined quantities.² To review briefly, the equation of evolution of the reservoir field can be formally integrated to give, in a properly rotating frame,

$$a_k(t) = e^{i(\nu - \nu_k)t} a_k(0) + t_k \int_0^t dt' e^{i(\nu - \nu_k)(t-t')} a(t'), \quad (9.93)$$

while substituting this back into the equation of motion for $a(t)$ gives

$$\dot{a}(t) = - \sum_k t_k e^{i(\nu - \nu_k)t} a_k(0) - |t_k|^2 \int_0^t dt' a(t') e^{i(\nu - \nu_k)(t-t')}. \quad (9.94)$$

Making the Wigner-Weisskopf approximation, we find that

$$\dot{a}(t) \approx - \frac{\kappa}{2} a(t) + \hat{\mathcal{F}}(t), \quad (9.95)$$

where

$$\kappa = 2\pi \sum_k |t_k|^2 \delta(\nu - \nu_k) = 2\pi |t_k|^2 D(\nu) \quad (9.96)$$

$$\hat{\mathcal{F}} = - \sum_k t_k \hat{a}_k(0) e^{i(\nu - \nu_k)t}. \quad (9.97)$$

Armed with such expressions, we can easily calculate the relevant correlation functions for the noise operator. For example, if the environment is in a thermal state with photon number n at frequency ν ,

$$\langle \hat{\mathcal{F}}(t) \hat{\mathcal{F}}^\dagger(t') \rangle = (n+1)\kappa \delta(t-t') \quad (9.98)$$

$$\langle \hat{\mathcal{F}}^\dagger(t) \hat{\mathcal{F}}(t') \rangle = n\kappa \delta(t-t'). \quad (9.99)$$

The microscopic noise model provides a physical picture for the origin of fluctuations and dissipation. The partially transmitting mirrors allow

²For further details, the derivation of the cavity input/output relations was first given in Phys. Rev. A **31**, 3761 (1985) by Gardiner and Collett.

the cavity field to leak out (leading to decay), but also allow the continuum modes to leak in (leading to noise). Using the relationship $t_k = (\kappa/2\pi D(\nu))^{1/2}$, the noise operator is given by

$$\hat{\mathcal{F}}(t) = -\sqrt{\frac{\kappa}{D(\nu)}} \hat{E}_{\text{in}}(t), \quad (9.100)$$

where we have defined the input field

$$\hat{E}_{\text{in}}(t) = \sqrt{\frac{1}{2\pi}} \sum_k e^{i(\nu-\nu_k)t} a_k(0). \quad (9.101)$$

We used a Heisenberg-Langevin method to describe the quantum mechanical cavity evolution, but the master equation provides an equivalent alternative approach. If we again identify the system operator $\hat{S} = \hat{a}$, the system density operator obeys the master equation

$$\frac{d}{dt}\hat{\rho} = -\frac{\kappa}{2}(n+1) \left(\hat{a}^\dagger \hat{a} \rho - \hat{a} \rho \hat{a}^\dagger \right) - \frac{\kappa}{2} n \left(\rho \hat{a} \hat{a}^\dagger - \hat{a}^\dagger \rho \hat{a} \right) + h.c. \quad (9.102)$$

which can be used to describe the cavity loss and associated fluctuations.

Example: Coherent state

Suppose that the cavity field is initially in a coherent state $|\alpha\rangle$, and the radiation bath is initially in the vacuum state. Since a coherent cavity state corresponds to the quantum description of a classical field, one might expect it to remain a classical field as the cavity mode decays. Formally integrating the equation of motion, we find

$$\hat{a}(t) = e^{-\kappa t/2} \hat{a}(0) + \int_0^t \hat{\mathcal{F}}(t') e^{-\kappa(t-t')/2} dt'. \quad (9.103)$$

The classical coherence decays exponentially in time, following the electric field amplitude decay

$$\langle \hat{a}(t) \rangle = e^{-\kappa t/2} \langle \hat{a}(0) \rangle. \quad (9.104)$$

To verify that we are indeed in a coherent state, we should examine the quadrature components³

$$\hat{x}(t) = \hat{x}(0)e^{-\kappa t/2} + \int_0^t \left(\frac{\hat{\mathcal{F}}(t') + \hat{\mathcal{F}}^\dagger(t')}{\sqrt{2}} \right) e^{-\kappa(t-t')/2} dt. \quad (9.106)$$

³More directly, one can examine the initial state $|\alpha\rangle|0\rangle_r$, where $|0\rangle_r$ refers to the reservoir in the vacuum state. It can be readily seen that

$$\hat{a}(t)|\alpha\rangle|0\rangle_r = e^{-\kappa t/2} \alpha |\alpha\rangle|0\rangle_r, \quad (9.105)$$

such that the state at later times corresponds to a coherent state $|\alpha e^{-\kappa t/2}\rangle$.

$$\Rightarrow \langle \delta\hat{x}^2(t) \rangle = \langle \delta\hat{x}^2(0) \rangle e^{-\kappa t} + \frac{1}{2} (1 - e^{-\kappa t}). \quad (9.107)$$

Since the coherent state initially has $\langle \delta\hat{x}^2(0) \rangle = 1/2$, $\langle \delta\hat{x}^2(t) \rangle$ remains $1/2$ at all times. A similar calculation for the momentum quadrature component yields the same result, indicating that the cavity mode remains in a coherent state $\langle \delta\hat{x}^2(t) \rangle = \langle \delta\hat{p}^2(t) \rangle = 1/2$ as the system evolves, though the mean number of photons (and thus the coherent state amplitude α) decays with time.

Quantum field evolution

Whereas we found that coherent states retain their classical coherence despite cavity loss, a general quantum state will change character as the cavity field dissipates. Our derivation of the quadrature operators in Eq. (9.107) did not depend on the initial state, so at long times we obtain $\langle \delta\hat{x}^2(t) \rangle = \langle \delta\hat{p}^2(t) \rangle = 1/2$ no matter the initial quadrature components. Consequently initially squeezed quantum states lose their nonclassical coherence properties due to the cavity decay.

In general, a process for generating nonclassical states will have to compete with dissipation. We have seen, for example, that nonclassical states can arise from single-mode light interacting with a nonlinear medium (such as a two-level atom) when we neglect dissipation. When we include both the atom interaction with the unconfined radiation modes and the cavity mode interaction with the continuum, we will find that the resulting dissipation acts to wash out any non-classical correlations.

The appropriate theoretical approach depends on some details of the system under consideration. For example, in the limit of strong fields interacting with many atoms, the dynamics should be nearly classical. It thus makes sense to use the Heisenberg-Langevin approach, which explicitly shows the correspondence to classical dynamics. The interaction with the atoms gives us a driving term in the cavity mode evolution,

$$\frac{d}{dt}\hat{a} = -\frac{\kappa}{2}\hat{a} + \hat{\mathcal{F}} + i \sum_j g_j^* \hat{\sigma}_{\alpha,\beta}, \quad (9.108)$$

which describes the quantum mechanical analogue of the polarization of the medium. Such evolution equations are typically nonlinear, and are generally impossible to solve, except for some special cases. As an example, we will consider squeezed light generation.

At the same time, in the situation when only a few photons or a few atoms are present, the stochastic wavefunction approach or master equation

often prove more convenient. For example, these types of systems with few photons and atoms arise in quantum state engineering in cavity quantum electrodynamics or with trapped ions.

9.3.3 Cavity quantum electrodynamics

Cavity quantum electrodynamics (CQED) provides another important example of a system where dissipation and quantum effects both play an important role. Unlike squeezed light generation, which described properties of macroscopic fields interacting with many atoms, CQED typically represents a small system with few photons interacting with a single atom. Our discussion of CQED will thus provide an example of an exact approach to treat small systems.

The physical system under consideration consists of a single two-level atom with levels $|1\rangle$ and $|2\rangle$ coupled to a single-mode cavity at rate g . In addition to the coherent evolution we considered in previous lectures, we will also incorporate two dissipative rates: The atom emits into free space modes (other than the cavity mode) at rate γ , while photons leak out of the cavity at rate κ .

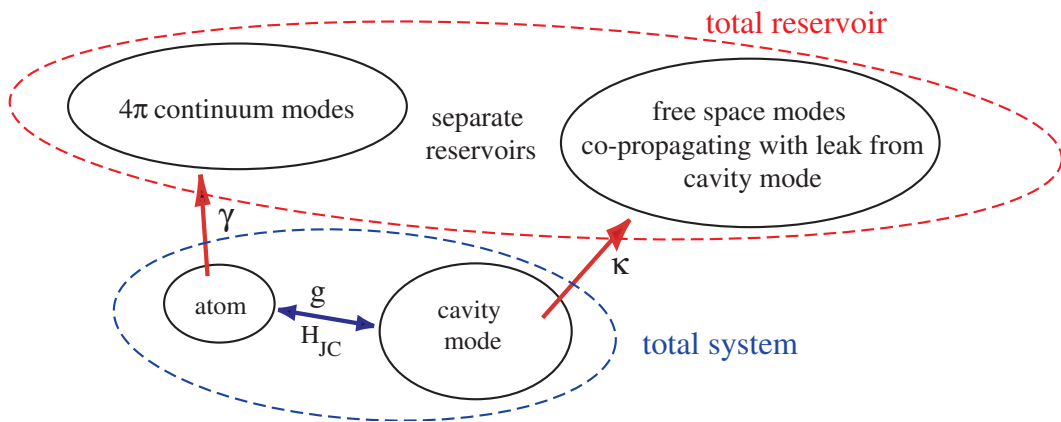


Figure 9.7: The system-reservoir division for cavity quantum electrodynamics. The quantum field in the cavity is treated as part of the total system, and it decays to a reservoir of modes corresponding to the leak out of the cavity. The atom reservoir corresponds to a different set of free space modes, into which the atom can decay directly.

Open vs closed cavities

In practice, it is useful to distinguish two situations. The open cavity regime describes a cavity mode confined in one dimension, with cavity length much greater than the wavelength $L \gg \lambda$. This regime typically occurs for CQED at optical frequencies, where a Fabry-Perot type cavity is employed to confine the light. The spontaneous emission rate γ for an atom in an open cavity is close to its free-space decay rate, since it can easily interact with free-space modes unconfined in the two directions orthogonal to the cavity mode.

The closed cavity confines the field in all three spatial dimensions, with length scales close to the wavelength $L \sim \lambda$. Such cavities can be constructed for microwave frequencies, with wavelengths on the order of millimeters to centimeters. An atom in a closed cavity can only interact with a small number of cavity modes, so its spontaneous emission rate can be strongly suppressed relative to the free space emission rate.

Theoretical formulation

To account for the two dissipation mechanisms κ, γ , we will need to incorporate both types of decay into the master equation

$$\begin{aligned}\hat{\rho} = & -\frac{i}{\hbar}[\hat{H}, \hat{\rho}] - \frac{\kappa}{2}(\hat{a}^\dagger \hat{a} \hat{\rho} + \hat{\rho} \hat{a}^\dagger \hat{a} - 2\hat{a} \hat{\rho} \hat{a}^\dagger) \\ & - \frac{\gamma}{2}(\hat{\sigma}_{21} \hat{\sigma}_{12} \hat{\rho} + \hat{\rho} \hat{\sigma}_{21} \hat{\sigma}_{12} - 2\hat{\sigma}_{12} \hat{\rho} \hat{\sigma}_{21}).\end{aligned}\quad (9.109)$$

Note that the density operator here includes both the atom and the cavity mode degrees of freedom since it represents the total system.

The coherent evolution is described by a Jaynes-Cummings Hamiltonian which couples the atomic operators $\hat{\sigma}_{ij}$ to the cavity mode \hat{a}

$$\hat{H} = \hbar\delta\hat{a}^\dagger\hat{a} + \hbar g\hat{a}^\dagger\hat{\sigma}_{12} + \hbar g^*\hat{a}\hat{\sigma}_{21}, \quad (9.110)$$

where we are working in the frame rotating with the atomic transition frequency ω , and δ is the detuning of the cavity mode $\delta = \nu - \omega$. Since we want to consider quantum states with few photons in the cavity, the natural basis states for the problem are Fock states of the cavity mode and the bare atomic states:

$$\{|1\rangle_a|n\rangle, |2\rangle_a|n\rangle\}. \quad (9.111)$$

Each pair of states $\{|1\rangle_a|n\rangle, |2\rangle_a|n-1\rangle\}$ is coupled with strength $g\sqrt{n}$. But when we add in dissipative mechanisms which couple $\{|1\rangle_a|n\rangle \rightarrow \{|1\rangle_a|n-1\rangle$ and $\{|2\rangle_a|n\rangle \rightarrow \{|1\rangle_a|n\rangle$, the dynamics will appear more complicated in this basis.

CQED in the dressed state basis

To gain intuition for the dissipative atom-cavity system, it is instructive to transform to the dressed state basis for the Jaynes-Cummings Hamiltonian. Each set of coupled states can be independently diagonalized as illustrated in Figure 9.8, and dissipation introduces coupling between each set.

The simplest experimental method for probing the dressed state manifold is to measure the reflectivity of the atom-cavity system as a function of detuning of the incident light. The external field will probe transitions between the ground state and the low-lying dressed states. Even when the atomic transition is precisely resonant with the cavity mode, the atom-field coupling g will show up as a splitting between peaks in reflectivity. Consequently the dressed-states splitting g is often referred to as the “vacuum Rabi splitting.” Note that the splitting will increase to $g\sqrt{N}$ if there are N atoms in the cavity antinode, an effect known as collective enhancement. Classically, this effect can be understood as a manifestation of atomic dispersion, which shifts the resonant frequency of the cavity by changing the phase shift the light picks up while it circulates.

Stochastic wavefunction analysis

Suppose that at time $t = 0$ the system starts out in the vacuum state of the cavity and the excited state of the atom, $|2\rangle_a|0\rangle$. As the system evolves, there are only a small number of states to which it can transition. In particular, the possible transitions are:

- (1) Free space emission couples $|2\rangle_a|0\rangle \rightarrow |1\rangle_a|0\rangle$
- (2) Coherent evolution couples $|2\rangle_a|0\rangle \rightarrow |1\rangle_a|1\rangle$
- (3) Cavity decay couples $|1\rangle_a|1\rangle \rightarrow |1\rangle_a|0\rangle$.

We therefore need only account for three states, and the master equation can in principle be solved exactly. We will use the stochastic wavefunction approach which will provide all of the essential elements we need to understand the physical processes involved in the no-jump regime.

In the case where quantum jumps are unimportant, we will consider a wavefunction which incorporates only those states coupled by the Hamiltonian evolution

$$|\psi\rangle = c_{1,1}|1\rangle_a|1\rangle + c_{2,0}|2\rangle_a|0\rangle. \quad (9.112)$$

The Hamiltonian evolution equations for the probability amplitudes are

$$\dot{c}_{1,1} = i\delta c_{1,1} + igc_{2,0} \quad (9.113)$$

$$\dot{c}_{2,0} = igc_{1,1}. \quad (9.114)$$

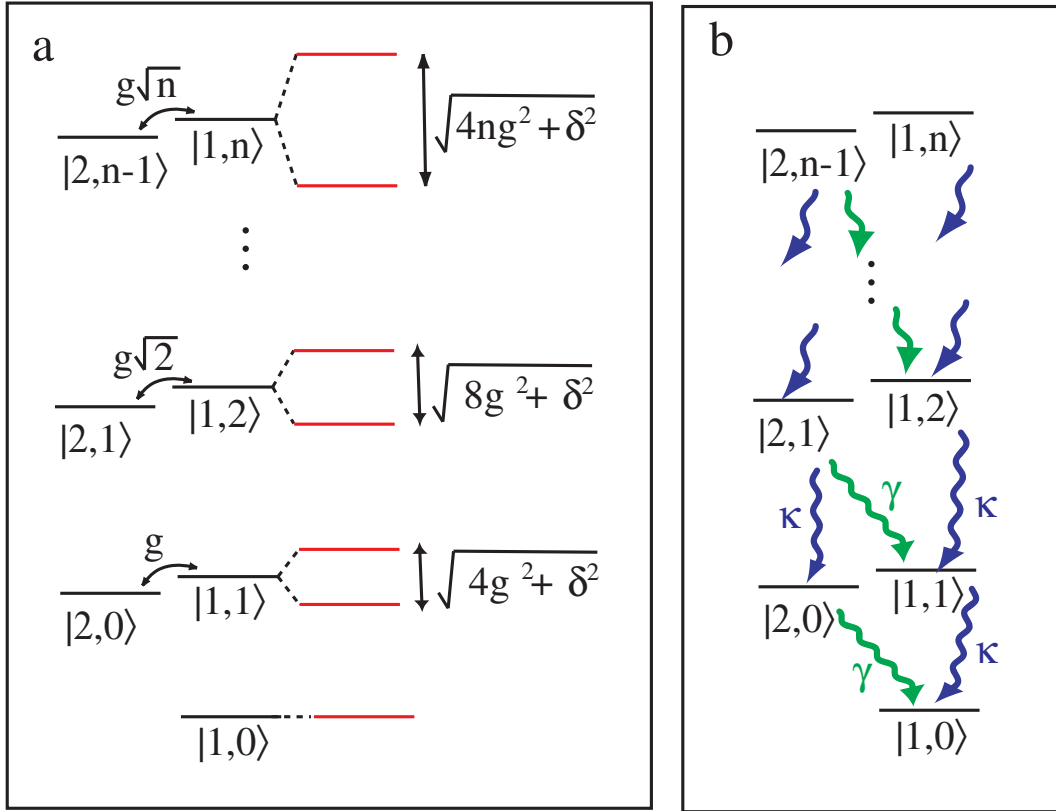


Figure 9.8: The dressed-state basis and dissipative couplings. (a) The natural basis corresponds to a ground state and an infinite ladder of independent two-level systems each coupled by $g\sqrt{n}$, where n is the maximum number of photons in the cavity for that pair of states. Each manifold can be exactly diagonalized, leading to the dressed state basis. (b) Atomic decay and cavity loss lead to couplings between the different manifolds, since they allow energy to leave the system. Consequently decays not only introduce an energy width to the dressed states, but also mix the independent dressed state manifolds.

Dissipation enters through the non-Hermitian effective Hamiltonian

$$\hat{H}_{eff} = -i\frac{\kappa}{2}\hat{a}^\dagger\hat{a} - i\frac{\gamma}{2}\hat{\sigma}_{21}\hat{\sigma}_{12}, \quad (9.115)$$

so the “no-jump” evolution equations become

$$\dot{c}_{1,1} = -(\frac{\kappa}{2} - i\delta)c_{1,1} + igc_{2,0} \quad (9.116)$$

$$\dot{c}_{2,0} = igc_{1,1} - \frac{\gamma}{2}c_{2,0}. \quad (9.117)$$

These equations are also what would be obtained through a Wigner Weis-skopf treatment - since $|1\rangle_a|0\rangle$ is uncoupled by coherent evolution, they are in fact exact. Examining these equations, we can see that in the limit of strong atom-field coupling $g \gg \gamma, \kappa$, the system exhibits weakly damped Rabi oscillations with the one-photon cavity state. However, many interesting effects can still be observed when g is smaller than one of the dissipative rates.

Open cavity: the Purcell effect

When the cavity decay rate overwhelms the atom-field coupling, $g < \kappa$, we can employ adiabatic elimination $\dot{c}_{1,1} \approx 0$ because the field mode is overdamped. The probability amplitude of the single-photon state is thus

$$c_{1,1} = \frac{ig}{\kappa/2 - i\delta}c_{2,0}. \quad (9.118)$$

The strongly damped cavity field affects the evolution of the atomic state

$$\dot{c}_{2,0} = -\left(\frac{\gamma}{2} + \frac{\kappa}{2} \frac{g^2}{\kappa^2/4 + \delta^2}\right)c_{2,0} + i\frac{g^2\delta}{\kappa^2/4 + \delta^2}c_{2,0}. \quad (9.119)$$

The first term shows that the atomic decay rate is modified by its coupling to the overdamped cavity mode, while the second term describes an energy shift which represents a modification of the Lamb shift by the cavity mode. The resulting atomic decay rate can be larger or smaller than the free space spontaneous emission rate depending on the type of cavity involved. For an open cavity, $\gamma \approx \gamma_{\text{free space}}$, so at zero detuning the atomic decay rate is enhanced

$$\gamma_{\text{eff}}^{\text{open}} = \gamma + 4\frac{g^2}{\kappa}. \quad (9.120)$$

This increase in the spontaneous emission rate is known as the “Purcell effect.”

The physical parameters governing this effect involve the cavity mode volume V and quality factor Q :

$$g = \mu \sqrt{\frac{\nu}{\epsilon_0 \hbar V}} \quad (9.121)$$

$$\kappa = \frac{\nu}{Q}, \quad (9.122)$$

where ν is the cavity mode angular frequency. The cavity decay rate can also be expressed in terms of the cavity finesse F , which is the number of times a photon circulates in the cavity on average before leaking out. The photon lifetime is the finesse multiplied by the round trip time in the cavity

$$\frac{1}{\kappa} = \frac{L}{\pi c} \cdot F. \quad (9.123)$$

The physics of strong coupling

In order to significantly alter the decay rate $\gamma_{\text{eff}}^{\text{open}}$ relative to γ , we need to have a sufficient atom-field coupling

$$g^2 > \gamma \kappa. \quad (9.124)$$

When this condition is satisfied, the system is said to be in the “strong coupling regime”. In fact, the figure of merit for strong coupling is independent of atomic parameters because the dipole moment appears both in g and γ :

$$\frac{g^2}{\kappa \gamma} \sim \frac{L \lambda^2}{V} \cdot F = \frac{\lambda^2}{d^2} \cdot F, \quad (9.125)$$

where d is the diameter of the cavity mode. The diffraction limit for a cavity of length L sets $d^2 \sim \lambda L$, so the figure of merit is maximized for small cavities with high reflectivity $r^2 = 1 - t^2$:

$$\frac{g^2}{\kappa \gamma} \sim \frac{\lambda}{L} \frac{1}{t^2} \quad (9.126)$$

Physically, when an open cavity is in the strong-coupling regime, an excited atom placed in the cavity transfers its energy to the cavity mode much faster than it emits into 4π , because $g > \gamma$. Since $g < \kappa$, the cavity mode then decays before the atom has time to reabsorb the photon. In effect, the excitation in the atom decays into the photon states leaking from the cavity.

We can see another physical picture of the strong-coupling regime if we recognize that the resonant cross-section for the atom is $\sim \lambda^2$. The probability for the atom to interact with a photon before the photon decays from the cavity is

$$P_{\text{interaction}} \sim \lambda^2 \cdot L \cdot \frac{1}{Ld^2} \cdot F, \quad (9.127)$$

where $1/Ld^2$ is the atomic density and F is the number of times the photon encounters the atom. This probability is greater than unity in the strong-coupling regime.

Closed cavity: suppressed decay

An atom confined to a closed cavity cannot emit spontaneously into unconfined modes, so $\gamma = 0$. The effective decay rate is then

$$\gamma_{\text{eff}}^{\text{closed}} = \frac{\kappa}{2} \frac{g^2}{\kappa^2/4 + \delta^2}. \quad (9.128)$$

When the cavity is far-detuned from the atomic resonance, $\delta \gg \kappa$, the atomic decay rate is strongly suppressed because there is no density of states at the atomic transition energy. This effect has been seen in microwave experiments where the cavity size is on the order of the wavelength $L \sim \lambda$ and the detuning is maximum $\delta = \omega/2$. The decay rate in this regime is

$$\gamma_{\text{eff}}^{\text{closed}} \sim \frac{g^2}{\kappa} \frac{\kappa^2}{\omega^2} \sim \frac{\lambda^3}{V} \frac{\gamma}{Q}. \quad (9.129)$$

For a closed cavity, $V \sim \lambda^3$, so the decay rate is suppressed by the cavity quality factor.

Microwave CQED with Rydberg atoms

Compared to optical CQED, microwave CQED offers several advantages. First, closed cavities can be constructed, and furthermore the atomic emission rate $\gamma \propto \omega^3$ is much smaller than at optical frequencies. Since the coupling strength $g \propto \sqrt{\omega}$, by going to lower frequencies one can get substantial improvement in g/γ . Finally, one can exploit the large dipole moment of Rydberg atoms to engineer a system with a large coupling constant g . The transition frequencies of highly excited Rydberg atoms $N \sim 50$ are in the microwave range $\sim 10\text{-}100$ GHz, so the appropriate cavities are about a centimeter in size. Furthermore, the atomic state can be measured by measuring the electric field required to ionize the atoms, providing a convenient mechanism to analyze final atomic states.

Lower frequencies also introduce potential problems. A typical Rydberg atom can decay at optical frequencies to a low-lying excited state, which will prevent microwave manipulation. Consequently experiments using Rydberg atoms have to pump them into so-called circular states of maximal angular momentum, where selection rules permit only a single microwave decay channel. The lifetime of circular Rydberg atoms can thus be very long, on the order of a second. Although exciting an atom into an N=50 L=50 state requires 50 microwave photons, groups in Paris and Munich routinely prepare circular Rydberg atoms.

A second problem arises at microwave frequencies because thermal photons cannot be neglected. Microwave cavities are therefore usually constructed from superconducting niobium and cooled to liquid helium temperatures. Additional tricks can also be employed to empty the thermal photons from the cavity by sending in atoms in the ground state to soak up the extra energy. With clever tricks and careful engineering, microwave CQED experiments have demonstrated the highest ratio between coherent evolution and decoherence in the field of quantum state engineering.

Application: single photons on demand

One potential application for CQED is creation of a source which can be triggered to emit exactly one photon into a wavepacket with well defined frequency, timing, direction, and shape. Such a device would be to Fock states what the laser is to coherent states, but the non-classical nature of Fock states makes its construction considerably more difficult.

One might envision placing a single, excited emitter inside a cavity, and monitoring the leak from the cavity. A single emitter would generically emit a photon into 4π , but the cavity can be used to improve directionality. In the strong-coupling regime, the excited emitter interacts primarily with the cavity mode \hat{a} , which subsequently interacts with the free-field modes \hat{a}_k via a the Hamiltonian

$$\hat{H}_{c-f} = -\hbar \sum_k t_k \hat{a}_k^\dagger \hat{a} e^{i\delta_k t} + h.c. \quad (9.130)$$

The state of the system, including the continuum modes can be expressed as

$$|\psi\rangle = c_{2,0}|2\rangle_a|0\rangle|vac\rangle + c_{1,1}|1\rangle_a|1\rangle|vac\rangle + \sum_k c_k|1\rangle_a|0\rangle|1_k\rangle. \quad (9.131)$$

The physics of this process is precisely that of the bound to free transition, so we can use our results from Wigner-Weisskopf theory find the probability

amplitudes for the free-space modes in the long-time limit and the strong-coupling regime:

$$c_k \sim \frac{t_k g / \kappa}{g^2 / \kappa + i \delta_k}. \quad (9.132)$$

A single-photon wavepacket will be emitted in the direction defined by the cavity mode, with electric field envelope $\sim e^{-(g^2/\kappa)t}$. This system is not yet the ideal single photon source because we cannot control the timing and shape of the pulse. By using a three-level atom, one can control the emitted wavepacket shape.

In principle, this single-photon emission process is coherent and thus reversible. For example, if the atom started out in a superposition of the ground and excited states, $(a|1\rangle + b|2\rangle) \otimes |\text{vac}\rangle$, the coherent superposition would be mapped onto the photon mode propagating away from the cavity, so the state would become $|1\rangle \otimes (a + b\hat{a}^\dagger) |\text{vac}\rangle$. By time reversing the pulse propagation, one could envision subsequently storing this quantum state (encoded in a superposition of orthogonal photon states) back into the atomic state. While ideas of this nature have received considerable theoretical attention, experiments have yet to implement coherent photon release and storage using cavity quantum electrodynamics.

Measurements of single photon fields

Experimental demonstration of a single photon on demand requires distinguishing small numbers of photons. There exist photo-detectors which can measure single optical photons with high efficiency via an avalanche process which generates a macroscopic pulse of photo-current. Due to dead-time effects, however, it is impossible to distinguish between short (< 100 ns) wavepackets containing multiple photons $|1\rangle, |2\rangle, |3\rangle \dots$

To study the nonclassical properties of short pulses, one can employ a Hanbury-Brown-Twiss setup, which splits the signal on a beamsplitter before sending it to two detectors. If a single photon is incident on the beamsplitter, the two detectors never register at the same time. This type of simultaneous detection is an example of a joint probability measurement. A full measurement of the correlations between the two detected signals can be used to obtain the second order correlation function

$$G^{(2)} = \langle \mathcal{E}^\dagger(r_1, t_1) \mathcal{E}^\dagger(r_2, t_2) \mathcal{E}(r_2, t_2) \mathcal{E}(r_1, t_1) \rangle. \quad (9.133)$$

$G^{(2)}$ factorizes for coherent states, but does not factorize for non-classical states. Consequently it is convenient to define a normalized correlation

function

$$g^{(2)}(t_1 - t_2) = \frac{G^{(2)}}{\langle \mathcal{E}^\dagger(r_1, t_1)\mathcal{E}(r_1, t_1)\langle \mathcal{E}^\dagger(r_2, t_2)\mathcal{E}(r_2, t_2)\rangle}. \quad (9.134)$$

For example, $g^{(2)}(0)$ is 1 for a coherent state, 2 for a thermal state (photon “bunching”), and 0 for a single photon state (photon “anti-bunching”). Measurements of the second order correlation function are clearly sensitive to a higher order quantum coherence than the classical coherence of a laser beam. Such measurements are useful because non-classical states can exhibit high order correlations, not just the classical coherence $\langle \mathcal{E}^\dagger(r_1, t_1)\mathcal{E}(r_2, t_2)\rangle$.

Reading

Further information on CQED can be obtained in texts by Meystre & Sargent or Yamamoto & Imamoglu or in a recent review by Mabuchi, Doherty Science 298 1372(2002). A discussion of correlation functions in quantum optics can be found in Scully and Zubairy, Quantum Optics, Chapter 4. Recent work on single-photon generation has been reported in Nature 419 594 (2002), PRL 89 067901 (2002) (see comments PRL 90 249801) and Science 290 2282 (2000).

9.4 Quantum dynamics in non-linear mixing processes

Linear amplification

We have seen how noise suppresses quantum correlations of a field mode subject to decay. Linear amplification likewise adds noise to the initial state of the field because it always involves spontaneous emission processes. The gain and associated noise of a linear amplifier can be modeled by a gas of inverted two-level atoms or inverted harmonic oscillators. For a gain coefficient $\sigma > 1$, one can derive a very general result:

$$\hat{a}_{\text{out}} = \sqrt{\sigma}\hat{a}_{\text{in}} + \sqrt{\sigma - 1}\hat{b}^\dagger, \quad (9.135)$$

where the noise operator \hat{b}^\dagger is analogous to vacuum noise, but acts rather differently because it comes from a spontaneous emission process. Like other noise operators, it ensures that the commutation relations for the field operators do not grow or decay with time. The additional noise is related to the quantum no cloning theorem, which states that an arbitrary quantum

state cannot be copied. Similarly, we find here that a quantum state cannot be amplified without losing some information due to added noise.

9.4.1 Nonlinear amplification

We have seen how nonlinear optical phenomena produce non-classical states of light whereas losses act to destroy non-classical correlations. The interplay of these two competing mechanisms can be illustrated by a specific example: the generation of squeezed light. We will first show how a squeezed state can be created by a lossless down-conversion process, and then discuss the effects of losses and noise.

Degenerate parametric down-conversion

Our semiclassical description of parametric down-conversion described the generation of a pair of fields \mathcal{E}_1 and \mathcal{E}_2 by a strong pump field \mathcal{E}_0 , where $\nu_1 + \nu_2 = \nu_0$ and $\Delta k = 0$. Away from atomic resonances, the polarizations which drive \mathcal{E}_1 and \mathcal{E}_2 include both the linear and nonlinear susceptibilities:

$$P_1 \sim \frac{\chi^{(2)}}{2} \mathcal{E}_0 \mathcal{E}_2^* + \frac{\chi_1}{2} \mathcal{E}_1 \quad (9.136)$$

$$P_2 \sim \frac{\chi^{(2)}}{2} \mathcal{E}_0 \mathcal{E}_1^* + \frac{\chi_2}{2} \mathcal{E}_2. \quad (9.137)$$

One method of squeezed light generation uses a degenerate version of parametric down-conversion for fields confined to a cavity. The pump field at frequency ν_0 drives a nonlinear medium inside a cavity whose frequency $\nu_c = \nu_0/2$ determines the frequencies of \mathcal{E}_1 and \mathcal{E}_2 , $\nu_1 = \nu_2 = \nu_c$. Assuming that the polarizations match, the two lower frequency fields are identical $\mathcal{E}_1 = \mathcal{E}_2$. This degenerate version of parametric down-conversion in a cavity is often called a “degenerate optical parametric oscillator” (OPO).

The polarization oscillating at the cavity frequency (which generates the fields $\mathcal{E}_1 = \mathcal{E}_2$) includes effects from both coherences

$$P = \mu_{13}\rho_{13} + \mu_{23}\rho_{23} \quad (9.138)$$

$$\sim \chi^{(2)} \mathcal{E}_0 \mathcal{E}_1^* + \frac{\chi_1 + \chi_2}{2} \mathcal{E}_1. \quad (9.139)$$

The evolution equation for the field \mathcal{E}_1 inside the cavity will contain a driving term from this polarization. Under phase-matching conditions,

$$\frac{\partial \mathcal{E}_1}{\partial t} = i\beta \mathcal{E}_1^* \quad (9.140)$$

$$\frac{\partial \mathcal{E}_1^*}{\partial t} = -i\beta^* \mathcal{E}_1, \quad (9.141)$$

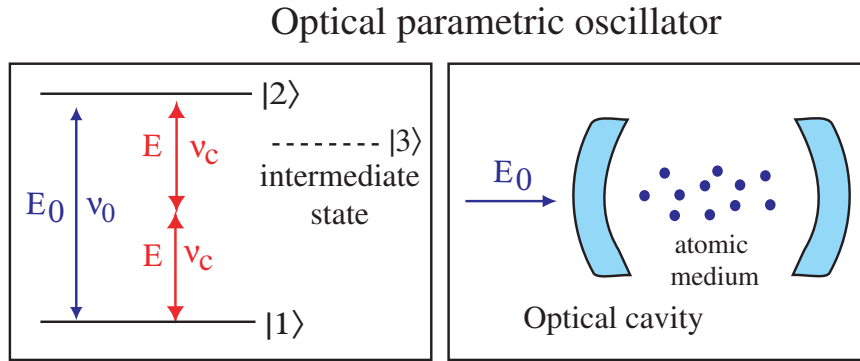


Figure 9.9: The optical parametric oscillator is formed by atoms with a cascade level configuration inside a cavity with resonance frequency $\nu_c = \nu_0/2$.

where β incorporates the pump power and nonlinear susceptibility into one constant. These equations may appear similar to the propagation of a field in a linear medium, where $\dot{\mathcal{E}} \sim \beta \mathcal{E}$. In this case, however, the field evolves differently than its complex conjugate, so we will need to keep careful track of the phases.

Phase-dependent amplification

Since the phase of β is arbitrary (only the relative phase of \mathcal{E}_1 and β matters), we are free to choose it to be purely imaginary, with $\beta = i\tilde{\beta}$. To decouple the evolution equations, we will work in the normal mode basis $\mathcal{E}_{\pm} = \mathcal{E}_1 \pm \mathcal{E}_1^*$ where they become

$$\frac{\partial \mathcal{E}_+}{\partial t} = -\tilde{\beta} \mathcal{E}_+ \quad (9.142)$$

$$\frac{\partial \mathcal{E}_-^*}{\partial t} = \tilde{\beta} \mathcal{E}_-. \quad (9.143)$$

One normal mode is amplified while the other is de-amplified, and the gain depends explicitly on the initial phase of \mathcal{E}_1 relative to $\beta \propto \mathcal{E}_0$. When \mathcal{E}_1 is real, the field is attenuated for $\tilde{\beta} > 0$ whereas if \mathcal{E}_1 is imaginary it is amplified.

Quantum mechanical approach

We would like to be able to convert our classical description of degenerate parametric down-conversion to a quantum mechanical version. The simplest approach would replace the cavity electric field values by the cavity photon annihilation operators $\mathcal{E} \rightarrow \hat{a}$. Such a naive substitution is in fact valid for lossless systems described by linear equations of motion, so in this case it turns out to work. However, it is not true in general, and we can use a more rigorous approach to show how the simple case arises.

Our quantum mechanical treatment will describe the generation of macroscopic fields. We will thus use the Heisenberg-Langevin approach, which provides a direct correspondence to the classical description we have already derived. The Hamiltonian governing interactions between the cavity mode and the atoms is

$$\hat{H} = -\hbar\hat{a}^\dagger \left(\sum_j g_j \sigma_{23}^{(j)} + g_j \sigma_{31}^{(j)} \right) + h.c. \quad (9.144)$$

In the absence of loss from the cavity, the Langevin equation of motion for the field mode \hat{a} is

$$\frac{d\hat{a}}{dt} = i \sum_j \left(g_j \sigma_{23}^{(j)} + g_j \sigma_{31}^{(j)} \right). \quad (9.145)$$

Corresponding equations can also be found for the atomic polarizations. For example, the atomic polarization $\sigma_{31}^{(j)}$ obeys

$$\dot{\sigma}_{31}^{(j)} = -(\gamma_{13} + i\delta)\sigma_{31}^{(j)} - ig_j \hat{a}^\dagger \sigma_{21}^{(j)} + ig_j \hat{a} (\hat{\sigma}_{11} - \hat{\sigma}_{33}) + \hat{\mathcal{F}}_{31}, \quad (9.146)$$

where δ is the detuning from the intermediate state. If the detunings are sufficiently large, we can neglect the decay of the atoms and the associated noise terms $\gamma_{13} \rightarrow 0, \hat{\mathcal{F}}_{31} \rightarrow 0$. Furthermore, if the pump field is assumed strong and classical then the operator $\hat{\sigma}_{21}$ is essentially equal to its classical expectation value $\hat{\sigma}_{21} = \Omega_0/\Delta$ (where Δ is the detuning of the classical pump field from the $|1\rangle \rightarrow |2\rangle$ transition). Using adiabatic elimination we obtain

$$\sigma_{31}^{(j)} = \frac{\Omega_0^*}{\Delta\delta} g_j \hat{a}^\dagger + \frac{g_j \hat{a}}{\delta}. \quad (9.147)$$

This atomic operator is analogous to the classical expression for the polarization, while $g_j \hat{a}^\dagger$ plays the role of the classical Rabi frequency of the generated fields \mathcal{E}_1 . Performing the same calculation for $\sigma_{23}^{(j)}$ yields an evolution equation involving only the cavity field operators. When the phase-matching

condition is fulfilled,

$$\frac{d\hat{a}}{dt} = 2i \sum_j \frac{\Omega_0}{\Delta\delta} g_j^2 \hat{a}^\dagger. \quad (9.148)$$

The Hermitian conjugate of the field operator appears on the right hand side of the equation, much as the complex conjugate appeared in the classical equations of motion. Note that our system involves a classical pump, linear operator equations, and large detunings, so the Heisenberg-Langevin approach gives precisely the same result we would have obtained from our naive substitution. If the system involved nonlinear operator terms, an ordering ambiguity would arise when going from the classical description to the quantum description.

Identifying the constant of proportionality $\beta^* = 2 \sum_j \frac{\Omega_0}{\Delta\delta} g_j$, we find

$$\frac{d\hat{a}}{dt} = -i\beta^* \hat{a}^\dagger \quad (9.149)$$

$$\frac{d\hat{a}^\dagger}{dt} = i\beta \hat{a}. \quad (9.150)$$

This set of equations could be derived from an effective Hamiltonian

$$\hat{H}_{\text{eff}} = \frac{\hbar}{2} \left(\beta \hat{a}^2 + \beta^* (\hat{a}^\dagger)^2 \right). \quad (9.151)$$

Physically, the effective Hamiltonian describes the absorption or emission of photon pairs, precisely as we would expect for a degenerate down-conversion process. Although we might have guessed its form, we have now derived it from microscopic considerations.

Non-degenerate parametric down-conversion

By a similar calculation, a non-degenerate parametric down-conversion process obeys the equations of motion

$$\frac{d\hat{a}_2}{dt} = -i\beta^* \hat{a}_1^\dagger \quad (9.152)$$

$$\frac{d\hat{a}_1^\dagger}{dt} = i\beta \hat{a}_2, \quad (9.153)$$

which can be described an effective Hamiltonian

$$\hat{H}_{\text{eff}} = \hbar \left(\beta \hat{a}_1 \hat{a}_2 + \beta^* \hat{a}_1^\dagger \hat{a}_2^\dagger \right). \quad (9.154)$$

Here, \hat{a}_1 and \hat{a}_2 are the two phase-matched field modes which are amplified by the process. As a vacuum field evolves under this effective Hamiltonian, it creates a state

$$|\psi\rangle = e^{-i\hat{H}_{\text{eff}}t/\hbar}|\text{vac}\rangle \quad (9.155)$$

$$= |\text{vac}\rangle + \xi|1, 1\rangle + \xi^2|2, 2\rangle + \dots, \quad (9.156)$$

where $|n, m\rangle = (\hat{a}_1^\dagger)^n(\hat{a}_2^\dagger)^m|\text{vac}\rangle$ and $\xi = \beta t$. It is useful to distinguish two limits in this process: $\xi < 1$ and $\xi \gg 1$. In the first case, the emission of photons is primarily a spontaneous process, which results in correlated generation of photon pairs. In the second case, stimulated emission plays an important role, and the system can be used as an optical parametric oscillator to generate squeezed states of light.

States generated by non-degenerate parametric down-conversion exhibit correlated photon statistics. While each mode (i.e. after tracing over the other mode) is in a thermal state, with a distribution function

$$p(n) = \frac{\xi^{2n}}{1 - \xi^2}, \quad (9.157)$$

the difference in photon numbers between the two modes is precisely zero:

$$\Delta\hat{n}|\psi\rangle = (\hat{n}_1 - \hat{n}_2)|\psi\rangle = 0. \quad (9.158)$$

This is an example of non-classical photon correlations: the photon number differences are suppressed far below the photon shot-noise limit of $\langle(\hat{n}_1 - \hat{n}_2)^2\rangle = n_1 + n_2$, which is what one would obtain by dividing a beam in half on a beamsplitter.

The correlated photons created in parametric down-conversion have a variety of applications. They can be used for heralded single photon generation by measuring only one of the two modes. Conditioned on a detection event in the first mode, there should be precisely one photon in the second mode. A slightly more complicated application uses some internal property of the modes – for example polarization – to encode an entangled state. In this situation, the resulting state could resemble

$$|\psi\rangle = |\text{vac}\rangle + \frac{\xi}{\sqrt{2}}(|1_H, 1_V\rangle + |1_V, 1_H\rangle) + \mathcal{O}(\xi^2). \quad (9.159)$$

Provided that the probability of photon generation $\sim \xi \ll 1$, the system is either in the vacuum or in an entangled two-photon state. As is the case with many single-photon processes, generation of this entangled state is probabilistic. Furthermore, losses inherent in any realistic system will destroy the

entangled state. However, by conditioning all subsequent measurements on detection of both photons (a process known as “post-selection”), we can use our state only in the situation where two photons were generated and neither was lost. In this manner one can devise few-photon experiments which tolerate probabilistic processes and are insensitive to loss.

9.4.2 Squeezed states

In the situation where $\xi \gg 1$, degenerate parametric down-conversion can lead to the generation of squeezed states. Returning to the situation where $\hat{a}_1 = \hat{a}_2 = \hat{a}$, we will now allow the driving field to have an arbitrary phase θ , so that the gain coefficient becomes

$$\beta = \tilde{\beta} e^{i(\theta - \pi/2)}. \quad (9.160)$$

Using this phase to weight the field operators, we define quadrature components of the cavity mode

$$\hat{x} = \frac{1}{\sqrt{2}} (\hat{a} e^{i\theta/2} + \hat{a}^\dagger e^{-i\theta/2}) \quad (9.161)$$

$$\hat{p} = \frac{1}{\sqrt{2}i} (\hat{a} e^{i\theta/2} - \hat{a}^\dagger e^{-i\theta/2}), \quad (9.162)$$

which are “normal modes” of the operator equations of motion

$$\frac{d\hat{x}}{dt} = \tilde{\beta} \hat{x} \quad (9.163)$$

$$\frac{d\hat{p}}{dt} = -\tilde{\beta} \hat{p}. \quad (9.164)$$

The x quadrature component is amplified for $\tilde{\beta} > 0$, whereas the p component is attenuated:

$$\hat{x}(t) = \hat{x}(0)e^{\tilde{\beta}t} \quad (9.165)$$

$$\hat{p}(t) = \hat{p}(0)e^{-\tilde{\beta}t}. \quad (9.166)$$

Hence, if the cavity mode starts out in a coherent state, the variance of the quadrature components will change in opposite directions.

$$\langle \Delta \hat{x}^2 \rangle = \frac{1}{2} e^{2\tilde{\beta}t} \rightarrow \infty \quad (9.167)$$

$$\langle \Delta \hat{p}^2 \rangle = \frac{1}{2} e^{-2\tilde{\beta}t} \rightarrow 0 \quad (9.168)$$

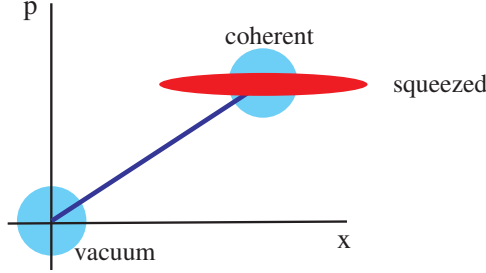


Figure 9.10: Phase space representation of the noise in the vacuum state, a coherent state, and a squeezed state.

Note that the field is still in a minimum-uncertainty state, since $\langle \Delta \hat{p}^2 \rangle \langle \Delta \hat{x}^2 \rangle = 1/4$, but its noise properties are “squeezed” relative to the initial coherent state.

Mathematically, the squeezed state can be represented by the time evolution operator for the effective Hamiltonian acting on the initial coherent state $|\alpha\rangle$:

$$|\psi\rangle_{Sq} = e^{-i(\beta^*(\hat{a}^\dagger)^2 + \beta\hat{a}^2)t/2} |\alpha\rangle. \quad (9.169)$$

This formal definition of a squeezed state allows all of its properties to be calculated. Note that if we started out in the vacuum $\alpha = 0$, the effective Hamiltonian would add and subtract photons in pairs, so the final squeezed state would only contain superpositions of even numbers of photons. Clearly such a state is very different from a coherent state.

9.4.3 Effects of loss

Our analysis predicts that as time progresses, one quadrature component of the squeezed state will vanish while the other will diverge. From a practical perspective, we would expect such divergences to be damped out, so it is important to account for decay processes to obtain a realistic description of squeezed light generation.

Squeezed light generation in a damped cavity

We will consider only losses from the cavity, which are the simplest type of noise to incorporate into our analysis. The Langevin equations for the field

operators are modified by a decay rate κ and an associated noise operator $\hat{\mathcal{F}}$,

$$\frac{d\hat{a}}{dt} = -i\beta^*\hat{a}^\dagger - \frac{\kappa}{2}\hat{a} + \hat{\mathcal{F}} \quad (9.170)$$

$$\frac{d\hat{a}^\dagger}{dt} = i\beta\hat{a} - \frac{\kappa}{2}\hat{a}^\dagger + \hat{\mathcal{F}}^\dagger. \quad (9.171)$$

The cavity decay corresponds to leakage of photons in and out of the cavity to the outside world through a semi-transparent mirror. The field modes outside the cavity (many modes) now act as the reservoir for the single cavity mode we considered. When the field outside the cavity is initially in the vacuum state $\bar{n} = 0$, the noise operator correlation function is

$$\langle \hat{\mathcal{F}}(t)\hat{\mathcal{F}}^\dagger(t') \rangle = \kappa\delta(t-t'). \quad (9.172)$$

Using the normal modes defined in Eq. (9.161) and Eq. (9.162), we can rewrite the Langevin equations

$$\frac{d\hat{x}}{dt} = -\left(\frac{\kappa}{2} - \tilde{\beta}\right)\hat{x} + \hat{\mathcal{F}}_x \quad (9.173)$$

$$\frac{d\hat{p}}{dt} = -\left(\frac{\kappa}{2} + \tilde{\beta}\right)\hat{p} + \hat{\mathcal{F}}_p. \quad (9.174)$$

where the Hermitian noise operators $\hat{\mathcal{F}}_{x,p}$ are linear combinations of $\hat{\mathcal{F}}$ and $\hat{\mathcal{F}}^\dagger$ analogous to the quadrature operators:

$$\hat{\mathcal{F}}_x = \frac{1}{\sqrt{2}}\left(\hat{\mathcal{F}}e^{i\theta/2} + \hat{\mathcal{F}}^\dagger e^{-i\theta/2}\right) \quad (9.175)$$

$$\hat{\mathcal{F}}_p = \frac{1}{\sqrt{2}i}\left(\hat{\mathcal{F}}e^{i\theta/2} - \hat{\mathcal{F}}^\dagger e^{-i\theta/2}\right), \quad (9.176)$$

and their correlation functions follow directly from those of $\hat{\mathcal{F}}$, i.e.

$$\langle \hat{\mathcal{F}}_x(t)\hat{\mathcal{F}}_x(t') \rangle = \langle \hat{\mathcal{F}}_p(t)\hat{\mathcal{F}}_p(t') \rangle = \frac{\kappa}{2}\delta(t-t'). \quad (9.177)$$

We can formally solve for the time dependent quadrature components

$$\hat{x}(t) = e^{-(\kappa/2-\tilde{\beta})t}\hat{x}(0) + \int_0^t dt' e^{-(\kappa/2-\tilde{\beta})(t-t')}\hat{\mathcal{F}}_x(t') \quad (9.178)$$

$$\hat{p}(t) = e^{-(\kappa/2+\tilde{\beta})t}\hat{p}(0) + \int_0^t dt' e^{-(\kappa/2+\tilde{\beta})(t-t')}\hat{\mathcal{F}}_p(t'). \quad (9.179)$$

Using the correlation function identities for the noise operators, we can also find the variances

$$\langle \Delta \hat{x}^2(t) \rangle = \frac{1}{2} e^{-(\kappa/2 - \tilde{\beta})t} + \frac{\kappa}{2} \frac{1 - e^{-(\kappa/2 - \tilde{\beta})t}}{\kappa - 2\tilde{\beta}} \quad (9.180)$$

$$\langle \Delta \hat{p}^2(t) \rangle = \frac{1}{2} e^{-(\kappa/2 + \tilde{\beta})t} + \frac{\kappa}{2} \frac{1 - e^{-(\kappa/2 + \tilde{\beta})t}}{\kappa + 2\tilde{\beta}}. \quad (9.181)$$

In the large-time limit, the uncertainty in \hat{p} approaches an asymptotic but nonzero value

$$\langle \Delta \hat{p}^2 \rangle \rightarrow \frac{\kappa}{2(\kappa + 2\tilde{\beta})}, \quad (9.182)$$

which shows that losses reduce the quantum correlations of the squeezed state.

Steady state squeezing

When the cavity damping rate far exceeds the squeezing coefficient $\kappa \gg \beta$, both variances approach the classical value of 1/2. Such strong losses collapse the squeezed state into a classical coherent state. In general, quantum correlations emerge from a balance between nonlinear coherent interactions and dissipation. We would like to identify the steady state result of this competition.

In the strongly pumped regime $\beta > \kappa/2$, however, we run into nonphysical results, because the predicted number of cavity photons grows indefinitely $\langle \hat{a}^\dagger \hat{a} \rangle \rightarrow \infty$. Our analysis is inadequate to describe the steady state behavior in this regime, because we have made an undepleted pump approximation. For finite interaction times, this approximation might suffice, but a steady-state solution requires a full treatment which accounts for these corrections using nonlinear operator equations.

Our solution is well-behaved in the intermediate regime $\beta < \kappa/2$, where

$$\langle \Delta \hat{x}^2 \rangle \rightarrow \frac{\kappa}{2(\kappa - 2\tilde{\beta})} \quad (9.183)$$

$$\langle \Delta \hat{p}^2 \rangle \rightarrow \frac{\kappa}{2(\kappa + 2\tilde{\beta})}. \quad (9.184)$$

Note in particular that at the threshold pumping rate $\beta = \kappa/2$, the maximum squeezing is only 50%. This limit arises from the exterior vacuum field which leaks into the cavity at rate κ , contaminating the non-classical states.

Squeezing in the output field

It might appear from our results thus far that one could only expect to see 50% squeezing in the steady state. Nevertheless, this limitation is not the end of the story. In an experiment, one looks not at the field inside the cavity but at the component which leaks out into the continuum. The output field can be found using the quantum mechanical version of the input-output relations

$$\text{Classical : } E_{\text{out}} = -rE_{\text{in}} + tE_{\text{cavity}} \quad (9.185)$$

$$\text{Quantum : } \hat{E}_{\text{out}} = -\frac{\hat{\mathcal{F}}}{\sqrt{\kappa}} + \sqrt{\kappa}\hat{a}. \quad (9.186)$$

Here we clearly see that the noise operator is due to leakage of photons in and out of the cavity. Since the output field is the sum of the reflected portion of the input field as well as the transmitted cavity field, we need to account for interference terms between the two components. We are interested in the continuous-wave regime, so it is convenient to work in the Fourier domain, in which the input-output relation gives us

$$\hat{E}_{\text{out}}(\omega) = -\frac{\hat{\mathcal{F}}(\omega)}{\sqrt{\kappa}} + \sqrt{\kappa}\hat{a}(\omega). \quad (9.187)$$

The momentum quadrature component obeys a similar equation

$$\hat{P}_{\text{out}}(\omega) = -\frac{\hat{\mathcal{F}}_p(\omega)}{\sqrt{\kappa}} + \sqrt{\kappa}\hat{P}(\omega). \quad (9.188)$$

From Eq. (9.174), we know the quadrature component inside the cavity

$$\hat{P}(\omega) = \frac{\hat{\mathcal{F}}_p(\omega)}{i\omega + (\kappa/2 + \tilde{\beta})}, \quad (9.189)$$

so we can solve for the external field

$$\hat{P}_{\text{out}}(\omega) = \frac{\hat{\mathcal{F}}_p(\omega)}{\sqrt{\kappa}} \left(\frac{\kappa}{i\omega + (\kappa/2 + \tilde{\beta})} - 1 \right). \quad (9.190)$$

In particular, when $\beta \rightarrow \kappa/2$ and $\omega \rightarrow 0$, the two components interfere destructively and $\hat{P}_{\text{out}}(0) \rightarrow 0$. The output field can thus be perfectly squeezed!

For finite detuning between a Fourier component of the output field and the cavity frequency, the output only partially squeezed. The squeezing has a Lorentzian lineshape with width $\sim \kappa$ (see Figure 9.11). In practical experiments one would look at intermediate frequencies where classical noise can be suppressed and yet finite squeezing is present.

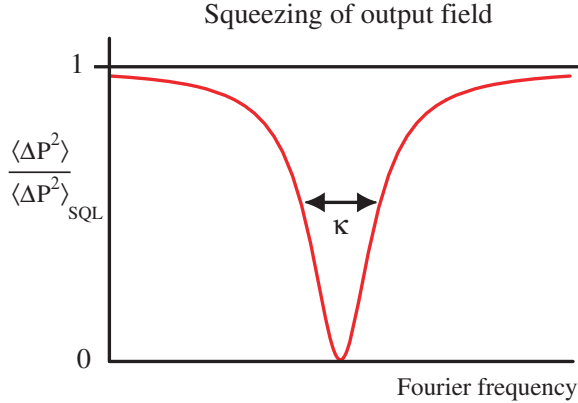


Figure 9.11: Squeezing in the momentum quadrature component of the output field, relative to the noise of a coherent state (known as the “standard quantum limit”).

Homodyne detection

Generation of a squeezed state can be assessed only if there is some means for measuring the squeezing. Since the quadrature components oscillate at optical frequencies, direct detection of squeezing is an extremely difficult task. Instead, a technique known as “homodyne detection” is used to transform the signal to lower frequencies where standard electronics can be used.

Homodyne detection employs a strong classical field \hat{b}_{LO} in a coherent state $\bar{\beta}e^{i\phi}$ with the same central frequency as the signal. When this so-called “local oscillator” field is mixed with the signal on a 50/50 beamsplitter, the two output fields are

$$\hat{a}_{\text{out}}^{(1)} = \frac{1}{\sqrt{2}} (\hat{a} + i\hat{b}_{LO}) \quad (9.191)$$

$$\hat{a}_{\text{out}}^{(2)} = \frac{1}{\sqrt{2}} (i\hat{a} + \hat{b}_{LO}). \quad (9.192)$$

Photodetectors measure the intensity of the two fields, which is proportional to the number of photons in each arm of the beamsplitter:

$$(\hat{a}_{\text{out}}^{(1)})^\dagger \hat{a}_{\text{out}}^{(1)} = \frac{1}{2} (\hat{a}^\dagger \hat{a} + \hat{b}_{LO}^\dagger \hat{b}_{LO}) + \frac{i}{2} (\hat{a}^\dagger \hat{b}_{LO} - \hat{b}_{LO}^\dagger \hat{a}) \quad (9.193)$$

$$(\hat{a}_{\text{out}}^{(2)})^\dagger \hat{a}_{\text{out}}^{(2)} = \frac{1}{2} (\hat{a}^\dagger \hat{a} + \hat{b}_{LO}^\dagger \hat{b}_{LO}) - \frac{i}{2} (\hat{a}^\dagger \hat{b}_{LO} - \hat{b}_{LO}^\dagger \hat{a}). \quad (9.194)$$

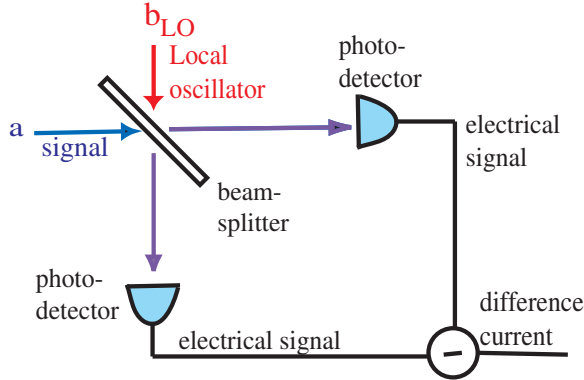


Figure 9.12: Schematic for homodyne detection of the quantum field \hat{a} . A local oscillator \hat{b}_{LO} is mixed with the signal on a beamsplitter, and the two output fields are subtracted to provide a phase-sensitive measurement of the quadrature components of \hat{a} .

By measuring the difference current, which is proportional to the difference in photon number, one can eliminate the average number of photons and detect only the beatnote between the signal and the local oscillator:

$$\hat{n}_- = (\hat{a}_{out}^{(1)\dagger}\hat{a}_{out}^{(1)} - \hat{a}_{out}^{(2)\dagger}\hat{a}_{out}^{(2)}) \quad (9.195)$$

$$= i(\hat{a}^\dagger\hat{b}_{LO} - \hat{b}_{LO}^\dagger\hat{a}). \quad (9.196)$$

For an initial state of the signal and local oscillator $|\psi\rangle = |\psi\rangle_a|\beta\rangle$, this difference current provides a measure of the quadrature components of the signal

$$\langle \hat{n}_- \rangle = \bar{\beta} \langle i(\hat{a}^\dagger e^{i\phi} - \hat{a} e^{-i\phi}) \rangle = \bar{\beta} \langle P_\phi \rangle \quad (9.197)$$

$$\langle \Delta \hat{n}_-^2 \rangle \approx \bar{\beta}^2 \langle \Delta P_\phi^2 \rangle \quad (9.198)$$

provided that $\bar{\beta} \gg 1$ is large.

Application to precision measurements

Precision measurements can be quantum mechanically limited by fluctuations in classical laser light. Replacing the laser beam with squeezed light

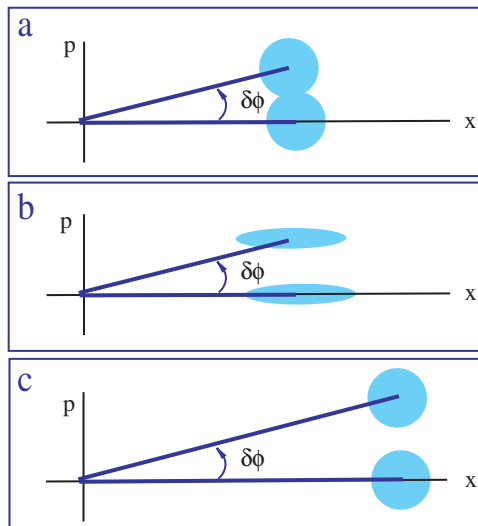


Figure 9.13: Three methods for measuring a phase shift ϕ . (a) Using a coherent state, the quadrature variance in \hat{p} sets a minimum value of ϕ which can be measured. (b) Using a squeezed state with $\langle \Delta P^2 \rangle < 1/2$, a more precise measurement can be made. (c) A similar improvement in precision can be obtained simply by using a larger coherent field, which is considerably easier to create than a squeezed state.

can improve certain measurements, and the potential gain in precision provided the original motivation for investigation of squeezing.

Suppose an interferometric measurement required finding the difference in phase between two fields (see Figure 9.13 and Figure 9.14). If the fields have a squeezing parameter r , the signal

$$\Delta P = \langle x \rangle \delta\phi \quad (9.199)$$

can only be measured to within the noise

$$\langle \Delta P^2 \rangle = \frac{1}{2} e^{-2r}. \quad (9.200)$$

The minimum phase which can be measured is

$$\delta\phi_{\min} \sim \frac{1}{\langle \hat{x} \rangle} e^{-r} \sim \frac{1}{\sqrt{n}} e^{-r}. \quad (9.201)$$

Clearly a nonzero squeezing parameter offers improvement in the sensitivity of this measurement.

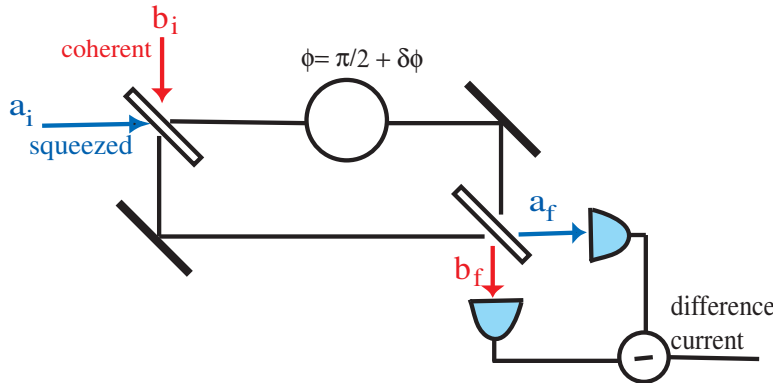


Figure 9.14: An experimental configuration for measuring a phase shift $\delta\phi$ using squeezed light to improve the precision (see PRL 59 278 (1987) and PRL 59 2153 (1987)).

For example, consider the interferometer illustrated in Figure 9.14. The initial states \hat{b}_i and \hat{a}_i are a coherent state $|\beta\rangle$ and a squeezed vacuum $e^{r/2(\hat{a}^2 - (\hat{a}^\dagger)^2)}|0\rangle$ respectively. After mixing these fields on a beam splitter, a phase shift $\phi = \pi/2 + \delta\phi$ is induced in one of the arms before recombination

on a second beamsplitter. Photodetectors measure the difference in photon number in the two output beams of the second beamsplitter,

$$\hat{n}_- = \hat{b}_f^\dagger \hat{b}_f - \hat{a}_f^\dagger \hat{a}_f \quad (9.202)$$

$$= \cos \phi (\hat{b}_i^\dagger \hat{b}_i - \hat{a}_i^\dagger \hat{a}_i) - i \sin \phi (\hat{a}_i^\dagger \hat{b}_i - \hat{b}_i^\dagger \hat{a}_i). \quad (9.203)$$

The mean and variance of this quantity give the phase difference $\delta\phi$ and the precision of the measurement

$$\langle \hat{n}_- \rangle \sim \bar{\beta} \delta\phi \langle \hat{b}_i^\dagger \hat{b}_i \rangle \quad (9.204)$$

$$\langle \Delta \hat{n}_-^2 \rangle_{(\delta\phi \approx 0)} \sim \bar{\beta}^2 \langle \Delta P^2 \rangle_a \rightarrow 0. \quad (9.205)$$

Experiments in the late 1980's demonstrated enhancement of interferometric sensitivity using squeezed light. Nevertheless, these ideas never found practical application because (roughly speaking) similar improvements can be made simply by increasing the strength of the coherent input field (see Figure 9.13c). Increasing laser power is considerably easier than generating squeezed light, so the original motivation for squeezed light generation has not proved useful in practice. Note however that highly squeezed states may still find applications, for example in the field of quantum information or for gravity wave detection, where increasing the number of photons is not an option.

Squeezing in atoms

Many of the concepts we have considered in the context of photonic excitations will translate directly to atomic physics. In particular, it is possible to consider spin squeezing in an atomic ensemble, where the total or "collective" spin is defined as the vector sum of the N individual spins

$$\mathbf{S} = \sum_i^N S_i. \quad (9.206)$$

If we consider a spin-polarized sample of $S_i = 1/2$ atoms, the collective spin projection we find $\mathbf{S}_z = N/2$. Although the expectation values of the orthogonal projections vanish, $\langle \mathbf{S}_x \rangle = \langle \mathbf{S}_y \rangle = 0$, their fluctuations do not, since

$$\langle \mathbf{S}_x^2 \rangle = \langle \mathbf{S}_y^2 \rangle = \frac{N}{2}. \quad (9.207)$$

This uncertainty in the orthogonal projections is known as the “atom shot noise.” In analogy to squeezed light, however, it is possible to use effective interactions between atoms to squeeze one of the spin projections below this shot noise limit at the expense of increasing fluctuations in the other projection:

$$\langle \mathbf{S}_x^2 \rangle < \frac{N}{2} \quad (9.208)$$

$$\langle \mathbf{S}_y^2 \rangle > \frac{N}{2}. \quad (9.209)$$

Atom-photon correlations

The ideas of probabilistic entanglement generation and post-selection (which we first encountered for parametric downconversion) can also be applied to atom-photon entanglement. As a concrete example, consider the case of N-atom Raman scattering, where

$$\hat{H} = g\hat{a}^\dagger \sum_i^N S_i^\dagger + g^*\hat{a} \sum_i^N S_i \quad (9.210)$$

$$= g\hat{a}^\dagger \mathbf{S}^\dagger + g^*\hat{a} \mathbf{S}. \quad (9.211)$$

This Hamiltonian bears a remarkable resemblance to the effective Hamiltonian for non-degenerate parametric down-conversion, and it leads to precisely the same sort of probabilistically entangled state. By conditioning on detection of the entangled photon, one can project out the vacuum state and photon loss. This technique could potentially permit entanglement of different atomic ensembles, which has bearing on a number of applications in quantum information science.

Chapter 10

Trapped ions: quantum state engineering

Although our discussion has concentrated on interactions between photons and neutral atoms, similar techniques and physical processes arise with trapped ions. Unlike neutral atoms, charged ions can be confined in traps so tight that the quantization of motional states becomes very important. This leads to rather different processes which bear a remarkable similarity to the dynamics of atoms and photons in cavity quantum electrodynamics.

10.1 Ion traps

Unlike neutral atoms, ions respond very strongly to applied electric fields via the Coulomb force. This allows creation of extremely tight traps. However, because one cannot create a static electric field minimum, an ion cannot be confined using static electric fields. To get around this problem, two solutions have been found, one using magnetic fields and the other using RF electric fields to provide 3D confinement.

The Penning trap uses the cyclotron motion of a charged particle in a magnetic field to confine the ion in two dimensions. The third dimension is confined using charged endcaps as shown in Figure 10.1. The ion orbits the magnetic field lines following the usual cyclotron motion; in addition, the axial confinement associated with the electric field produces motion along the magnetic field; finally, the crossed electric and magnetic fields produce a larger-scale magnetron motion.

The Paul trap provides 3D confinement using high-frequency electric fields to simulate an electric field minimum. To understand how this works,

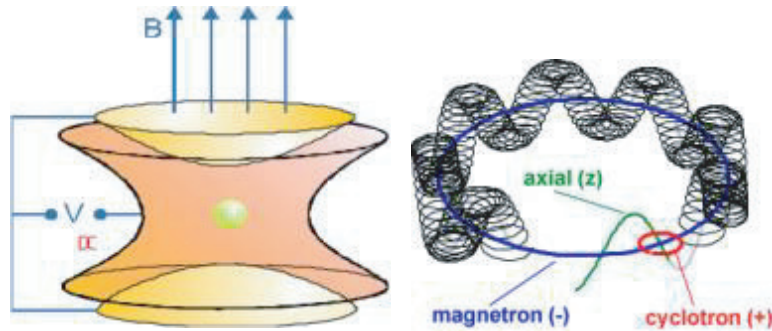


Figure 10.1: The Penning trap, with cyclotron and magentron motion of the ion illustrated below.

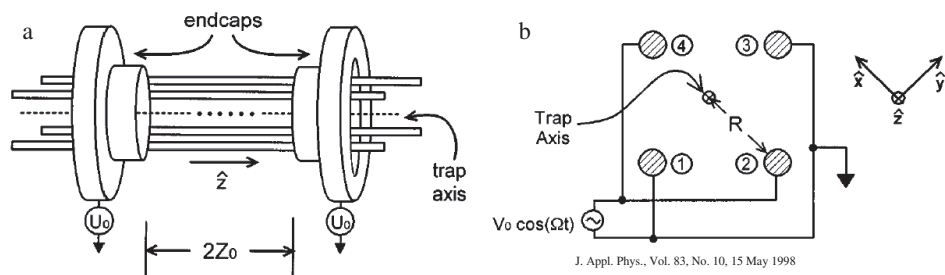


FIG. 1. Linear Paul trap (a) side view and (b) axial view. A string of trapped ions is shown schematically in (a). For clarity, the endcaps are not shown in (b). The trap electrodes are labeled 1, 2, 3, and 4. The trap axis defines the z -axis, and the origin of the z axis is centered between the two endcaps.

Figure 10.2: The Paul trap.

consider a quadrupole electric field with potential

$$\Phi = \phi_0 (\alpha x^2 + \beta y^2 + \gamma z^2). \quad (10.1)$$

From LaPlace's equation, $\alpha + \beta + \gamma = 0$, so choosing $\alpha = -\beta, \gamma = 0$, one can generate a 2D potential which is confining in one direction and repulsive in the other direction. If one now rotates this potential in time, the ion will follow the motion of the trap (the so-called "micromotion" of the ion). In particular, the position of the atom will be 180 degrees out of phase with the trap, so that when the atom is near the center of the trap it will experience the repulsive potential and when the atom is far from the center of the trap it will experience the confining potential. Averaging over many cycles, the net effect of this oscillating trap is to confine the ion in both dimensions. This effect can be used in three dimensions by adding charged endcaps as illustrated in Figure 10.2.

10.2 Model: An ion in a harmonic trap

For our purposes, the physics of an ion trap can be understood by approximating the trap by a harmonic oscillator potential.

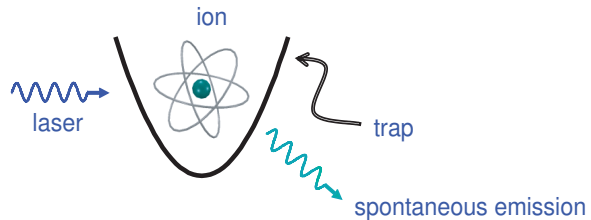


Figure 10.3: Model of an ion confined to a 1D harmonic oscillator trap, subject to laser excitation and spontaneous emission.

The ion can interact with a laser beam, which will couple transitions between internal electronic degrees of freedom. If the internal transition is dipole allowed, the ion will quickly relax, spontaneously emitting a photon. Such transitions can be used for laser cooling the ion into its motional ground state and also for reading out the state of the qubit by observing whether or not it fluoresces. For quantum state engineering, however, it is desirable to have a long-lived metastable state which can be driven on a quadrupole transition. Ions have such metastable states with lifetimes of around a second,

and we will focus on these dipole-forbidden transitions where spontaneous emission is negligible. These internal levels are illustrated in Figure 10.4.

Since the ion is tightly bound by its trap, its motional state also has quantized energy levels. The Hilbert space of the ion can then be understood as a two level system with a harmonic oscillator ladder of Fock states describing its motion. Since we are concerned primarily with quantum state engineering, we will neglect phonon heating effects and assume that the ion can be prepared in its motional ground state. Consequently we are considering a trapped ion which is isolated both from the radiation bath and the phonon reservoir which constitute its environment.

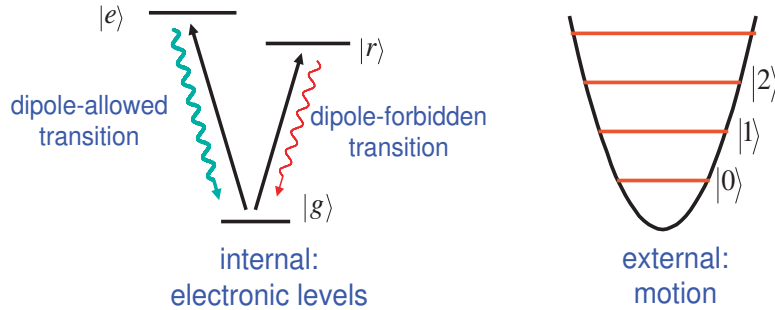


Figure 10.4: The internal and external degrees of freedom of an ion in a harmonic oscillator trap. Note that the dipole allowed transition is used for cooling the ion, whereas the dipole forbidden transition is used for encoding information in the ion.

10.2.1 The harmonic oscillator potential

The strong Coulomb interaction allows ions to be confined in traps with harmonic oscillator frequency $\nu \sim 10$ MHz. The position and momentum of the ion can be represented in terms of the creation and annihilation operators for a quantum of vibrational energy:

$$\hat{x} = \sqrt{\frac{\hbar}{2m\nu}} (\hat{a} + \hat{a}^\dagger) \quad (10.2)$$

$$\hat{p} = i\sqrt{\frac{\hbar m\nu}{2}} (\hat{a}^\dagger - \hat{a}), \quad (10.3)$$

and the Hamiltonian for the ionic motion is simply

$$\hat{H}_{\text{motion}} = \hbar\nu\hat{a}^\dagger\hat{a}. \quad (10.4)$$

The characteristic size of the ion wave function in its motional ground state is

$$a_0 = \sqrt{\frac{\hbar}{2m\nu}}, \quad (10.5)$$

and for tightly trapped ions this harmonic oscillator length is significantly smaller than optical wavelengths.

10.2.2 Internal energy levels

The electronic energy structure can be simply represented by a two-level system with ground state $|g\rangle$ and excited state $|e\rangle$. If we neglect spontaneous emission processes, the Hamiltonian is just

$$\hat{H}_{\text{electronic}} = \hbar\omega_{eg}|e\rangle\langle e|. \quad (10.6)$$

In order to neglect decay from the excited state, we require that the decay rate γ be small compared to the inverse of the timescale τ over which we wish to manipulate the ion. There are two commonly used methods to achieve $\gamma\tau \ll 1$:

- (1) Use a metastable state which can be driven on a quadrupole transition.
- (2) Use a far-detuned Raman transition to reduce the effective linewidth by $(\Omega/\Delta)^2 \ll 1$.

10.2.3 Ion-laser interactions

When the ion absorbs a photon, the associated momentum kick can excite higher vibrational states in the trap. To understand quantitatively where this comes from, consider the electric field associated with a running wave

$$E_{\text{running}} = \mathcal{E}e^{i(kx-\omega t)} + c.c. \quad (10.7)$$

or a standing wave

$$E_{\text{standing}} = \mathcal{E} \sin(kx + \phi)e^{-i\omega t} + c.c. \quad (10.8)$$

The interaction of this electric field with the ion occurs at the position of the ion, so we will replace the classical quantity x by the operator quantity

\hat{x} . The resulting interaction Hamiltonians (in the RWA) are then

$$\hat{H}_{\text{running}} = -\hbar \left(\Omega |e\rangle\langle g| e^{i(k\hat{x}-\omega t)} + h.c \right) \quad (10.9)$$

$$\hat{H}_{\text{standing}} = -\hbar \left(\Omega |e\rangle\langle g| \sin(k\hat{x} + \phi) e^{-i\omega t} + h.c \right). \quad (10.10)$$

The momentum kick imparted to the atom can be seen explicitly if we write the state in the momentum basis, in which the Hamiltonian can induce the transition

$$|g\rangle|p\rangle \rightarrow |e\rangle e^{ik\hat{x}}|p\rangle = |e\rangle|p + \hbar k\rangle. \quad (10.11)$$

Consequently we can manipulate the center of mass motion of the ion via laser excitation.

The Lamb-Dicke parameter

As we have alluded to previously, there are different length scales associated with the laser wavelength and the ion spatial extent. For tight traps, the ratio between them provides a small parameter

$$\eta = \frac{2\pi a_0}{\lambda} \sim 0.1, \quad (10.12)$$

and by expanding in this parameter we can highlight the physical processes allowed by the interaction Hamiltonian in the so-called “Lamb-Dicke regime”. We can also interpret the Lamb-Dicke parameter η in terms of the recoil energy $\omega_R = \hbar k^2/2m$

$$\eta = \sqrt{\frac{\omega_R}{\nu}}. \quad (10.13)$$

Since $\omega_R \sim \text{kHz}$ and $\nu \sim 10 \text{ MHz}$, we can see that η can be quite small. Physically, the Lamb-Dicke regime corresponds to the limit when the ion is so tightly bound that the recoil energy of a photon is insufficient to excite a higher vibrational state, so the photon momentum is absorbed by the trap rather than the ion.

In terms of the Lamb-Dicke parameter, the total Hamiltonian in the rotating frame for the running wave is

$$\hat{H}_r = \hbar\nu\hat{a}^\dagger\hat{a} - \hbar\Delta|e\rangle\langle e| - \hbar \left(\Omega |e\rangle\langle g| e^{i\eta(\hat{a}+\hat{a}^\dagger)} + h.c \right) \quad (10.14)$$

while the standing wave Hamiltonian is

$$\hat{H}_s = \hbar\nu\hat{a}^\dagger\hat{a} - \hbar\Delta|e\rangle\langle e| - \hbar \left(\Omega |e\rangle\langle g| \sin(\eta(\hat{a} + \hat{a}^\dagger) + \phi) + h.c \right). \quad (10.15)$$

Note that η appears in the exponent or the sine, so expanding in the Lamb-Dicke parameter can provide a significant simplification of these Hamiltonians. In particular, we will see that the resulting dynamics bear a remarkable resemblance to the Jaynes-Cummings Hamiltonian in cavity quantum electrodynamics, with cavity photons replaced by quantized excitations of the ion motional state.

The bare energy spectrum

Before analyzing the effects of the laser-ion interaction, we should understand the structure of the bare energy levels, which are eigenstates of

$$\hat{H}_0 = \hbar\nu\hat{a}^\dagger\hat{a} - \hbar\omega_{ge}|e\rangle\langle e|. \quad (10.16)$$

Since $\omega_{eg} \gg \nu$, the ground and excited states of the electronic structure are well separated, but subdivided into different motional states. In particular, the bare states take the form

$$\hat{H}_0|g\rangle|n\rangle = \hbar n \nu |g\rangle|n\rangle \quad (10.17)$$

$$\hat{H}_0|e\rangle|n\rangle = \hbar(n\nu + \omega_{eg})|e\rangle|n\rangle. \quad (10.18)$$

Laser-induced couplings: Running waves

The ion-laser interaction couples the bare energy states of the trapped ion. In the case of a running wave, the matrix elements between the states $|g\rangle|n\rangle$ and $|e\rangle|m\rangle$ are

$$\langle g| \langle n | \hat{H} | e \rangle | m \rangle = -\hbar\Omega \langle n | e^{i\eta(\hat{a} + \hat{a}^\dagger)} | m \rangle. \quad (10.19)$$

Expanding the exponent to lowest order in η , the only nonvanishing matrix elements couple n to $m = n, n+1, n-1$:

$$\langle g | \langle n | \hat{H} | e \rangle | n \rangle = -\hbar\Omega (1 + \mathcal{O}(\eta^2)) \quad (10.20)$$

$$\langle g | \langle n | \hat{H} | e \rangle | n+1 \rangle = -\hbar\Omega (\eta\sqrt{n+1} + \mathcal{O}(\eta^3)) \quad (10.21)$$

$$\langle g | \langle n | \hat{H} | e \rangle | n-1 \rangle = -\hbar\Omega (\eta\sqrt{n} + \mathcal{O}(\eta^3)). \quad (10.22)$$

Note that in fact the real expansion parameter is $\eta\sqrt{n}$, since we are expanding an exponent of $\eta(\hat{a} + \hat{a}^\dagger)$, and \hat{a} scales as \sqrt{n} .

These three matrix elements induce couplings between the internal states and motional states as illustrated in Figure 10.5. By tuning the laser frequency, these three transitions can be addressed individually.

Suppose the laser frequency is tuned to resonance with the bare atomic transition frequency $\omega = \omega_{eg}$. If the power is sufficiently small $\Omega \ll \nu/\eta$,

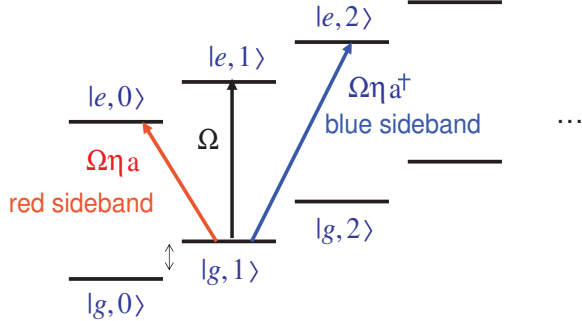


Figure 10.5: When the laser is tuned to the bare atomic resonance, the atom cycles between internal states without changing its motional state. By tuning the laser to the blue or the red sideband, different motional states can also be addressed.

excitation of the sideband transitions is strongly suppressed, so the internal and external degrees of freedom decouple. In this limit, the system is well described by a two-level Hamiltonian

$$\hat{H} = \hbar\nu\hat{a}^\dagger\hat{a} - \hbar\Delta|e\rangle\langle e| - \hbar\Omega(|e\rangle\langle g| + |g\rangle\langle e|). \quad (10.23)$$

Physically, this limit corresponds to a well-localized ion whose momentum distribution is far greater than the recoil momentum imparted by the laser excitation. When the ion absorbs a photon, its energy is insufficient to excite the ion to a higher motional state, and its momentum is imparted to the trap.

If the laser is tuned to the red sideband, the effective dynamics can be described by a Jaynes-Cummings model

$$\hat{H} = \hbar\nu\hat{a}^\dagger\hat{a} - \hbar\Delta|e\rangle\langle e| - i\hbar\eta\Omega\left(|e\rangle\langle g|\hat{a} + |g\rangle\langle e|\hat{a}^\dagger\right), \quad (10.24)$$

where the internal transitions are accompanied by creation or annihilation of a phonon. Precisely the same Hamiltonian appears in cavity quantum electrodynamics, so we can apply our intuition from cavity quantum electrodynamics to understand how the trapped ion evolves. Nevertheless, there are some important physical differences between the two systems. The frequency scales for optical photons \sim THz are far greater than those for ion

motion \sim MHz. In addition, the vacuum Rabi coupling is replaced by the effective Rabi frequency $g \rightarrow \eta\Omega$. Consequently, the strong coupling regime is significantly easier to attain for ion traps, since one only needs to increase the laser power to increase the coupling strength. Furthermore, the coupling parameter can be switched on and off using the laser, enabling controlled manipulation of the ion internal and motional state.

Similar considerations apply for blue sideband transitions. In this case, the system obeys an “anti-Jaynes Cummings” Hamiltonian

$$\hat{H} = \hbar\nu\hat{a}^\dagger\hat{a} - \hbar\Delta|e\rangle\langle e| - i\hbar\eta\Omega(|e\rangle\langle g|\hat{a}^\dagger + |g\rangle\langle e|\hat{a}), \quad (10.25)$$

where internal state excitation is accompanied by emission of a phonon and vice versa.

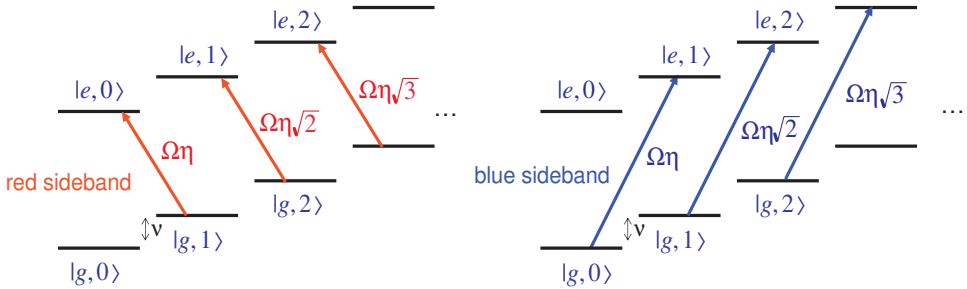


Figure 10.6: The transitions induced by a laser tuned to the red or blue sideband. Note that, unlike the vertical transitions, the Rabi frequency for sideband transitions changes as a function of the number of phonons $\sim \eta\Omega\sqrt{n}$.

Laser-induced couplings: Standing waves

When the ion is illuminated by a standing wave, the phase of the standing wave relative to the ion trap minimum provides another means to manipulate the system. Performing the Lamb-Dicke expansion on the Hamiltonian yields

$$\hat{H}_s = \hbar\nu\hat{a}^\dagger\hat{a} - \hbar\Delta|e\rangle\langle e| - \hbar\left(\Omega|e\rangle\langle g|\left(\sin\phi + \eta(\hat{a} + \hat{a}^\dagger)\cos\phi + \mathcal{O}(\eta^2)\right) + h.c\right). \quad (10.26)$$

Similar transitions occur between the bare energy levels, but by setting the phase $\phi = 0$, one can eliminate vertical transitions of the ion.

10.2.4 Sideband cooling

By optically addressing transitions between motional states, it is possible to cool ions into the ground state of the trap. Typically, this is done by applying a laser resonant with the red sideband of an allowed transition. Every excitation cycle decreases the motional energy, while the emission happens into all three possible transitions; on average, this pumps the ions into the ground state of the trap, which is dark to the red-detuned laser.

The rate at which the cooling takes place is set by the fluorescence rate of the ionic excited state γ . Initially, one would like to have a large fluorescence rate to increase the cooling rate; however, to cool into the ground state requires $\gamma \ll \nu$ so that off-resonant excitation of the direct and blue sideband transitions can be neglected. In practice, the decay rate is often adjusted by choosing a cooling transition which is nominally forbidden. By applying another laser to couple the (forbidden) excited state to a different excited state which has an allowed transition to the ground state, one can control the effective spontaneous emission rate. Using such techniques, experimentalists have cooled ions in to the trap ground state with in excess of 99% efficiency.

10.3 Quantum state engineering

We have seen how the internal and motional state of a trapped ion can be manipulated by applied lasers with a remarkable level of control. As a potential application for this system, one might inquire whether these techniques permit one to engineer an arbitrary motional state

$$|\psi\rangle = |g\rangle \otimes \sum_{n=0}^{\infty} c_n |n\rangle. \quad (10.27)$$

While the coefficients c_n are in principle arbitrary, they could correspond to a variety of interesting or useful quantum states such as Fock states, coherent states, squeezed states, or Schrodinger cat states. The ability to engineer such quantum states is crucial to developing quantum gates based on an ion trap architecture.

10.3.1 Preparation of an arbitrary motional quantum state

Suppose that we start out with the system in an initial state $|i\rangle$, and we would like to end up in a state $|f\rangle$. Using laser pulses tuned to the bare and sideband transitions, we hope to find a series of unitary transformations

linking these two states

$$|f\rangle = U_N U_{N-1} \dots U_2 U_1 |i\rangle. \quad (10.28)$$

Two simple examples

For example, if the ion started out in the ground state $|i\rangle = |g\rangle \otimes |0\rangle$, and we wanted to end up with the ion in state $|f\rangle = (\alpha|g\rangle + \beta|e\rangle) \otimes |0\rangle$, we need only apply a laser pulse at the bare resonance frequency for an appropriate time.

A slightly more complicated transformation involves swapping information between the internal and external degrees of freedom

$$|i\rangle = (\alpha|g\rangle + \beta|e\rangle) \otimes |0\rangle \quad (10.29)$$

$$|f\rangle = |g\rangle \otimes (\alpha|0\rangle + \beta|1\rangle). \quad (10.30)$$

This transformation can be implemented by tuning the laser to the red sideband and applying a π pulse.

Procedure

Ultimately, we would like to be able to prepare an arbitrary motional quantum state from, for example, the ground state $|i\rangle = |g\rangle \otimes |0\rangle$. If our desired final state is $|f\rangle = |\psi\rangle$ (where the coefficients c_n are specified), we claim that it is possible to find a series of unitary transformations linking $|i\rangle$ and $|f\rangle$. To prove this statement, it is convenient to work backwards. Since unitary transformations are invertible, if we can show how to start in $|f\rangle$ and end up in $|i\rangle$, then the inverse transformation will accomplish the desired task.

Suppose that our initial state has coefficients satisfying $c_n = 0$ for all $n > N$, where N is arbitrary but finite. Our procedure works by systematically emptying population from the N^{th} rung of the harmonic oscillator, then iterating until the entire ionic population is in the ground state. The required steps are:

- (1) Apply the laser on the red sideband, coupling $|g\rangle|N\rangle \rightarrow |e\rangle|N-1\rangle$. Using our knowledge of the c_n , we can apply the laser for the appropriate time to implement a π -pulse, emptying the population amplitude of $|g\rangle|N\rangle$ into the initially empty state $|e\rangle|N-1\rangle$.
- (2) Apply the laser on the bare atomic frequency. From the specified c_n we can again determine the pulse length which will empty $|e\rangle|N-1\rangle$ into $|g\rangle|N-1\rangle$.
- (3) Repeat steps (1) and (2) until the entire population is in the ground

state.

The inverse of this procedure can then be used to construct an arbitrary motional quantum state.

10.4 Ion trap quantum computation

In previous sections we have seen how it is possible to control both the motional and electronic states of an ion, allowing us to write an arbitrary quantum state. In order to perform nontrivial calculations using ions, we will need a mechanism to link up different ions, and the motional degree of freedom provides a convenient tool.

Multiple ions confined to the same anisotropic trap $\nu_x \ll \nu_y, \nu_z$ repel each other, so in the motional ground state they form a string of ions with each ion spaced by $5\text{-}10\mu\text{m}$. The Coulomb repulsion thus provides sufficient separation to spatially resolve individual ions with a focussed laser beam. In addition, the Coulomb interaction couples their motional degrees of freedom. Vibrational modes of the ions can be interpreted as phonons with different frequencies and spatial modes.

10.4.1 Two ions in a linear trap

To understand the physics of the linear ion trap, it is instructive to analyze the evolution of two ions at positions r_1, r_2 and momenta p_1, p_2 confined to the same trap. If the equilibrium positions are $\langle r_1 \rangle = -a/2$ and $\langle r_2 \rangle = a/2$, and $r_i = \langle r_i \rangle + x_i$, then the Hamiltonian for the system can be written

$$\hat{H} = \sum_i \left(\frac{p_i^2}{2m} + \frac{m}{2} \nu^2 x_i^2 - \hbar \Delta_i |e\rangle_{ii} \langle e| - \hbar \Omega_i (|e\rangle_{ii} \langle g| e^{ikx_i} + h.c.) \right) + \frac{e^2}{4\pi\epsilon_0 |r_1 - r_2|}. \quad (10.31)$$

Rewriting the Hamiltonian in the center of mass and relative coordinates

$$X = \frac{1}{2} (x_1 + x_2) \quad (10.32)$$

$$x = x_2 - x_1 \quad (10.33)$$

$$P = \frac{1}{2} (p_1 + p_2) \quad (10.34)$$

$$p = p_2 - p_1, \quad (10.35)$$

we find

$$\hat{H} = \left(\frac{P^2}{2(2m)} + \frac{2m}{2} \nu^2 X^2 \right) \quad (10.36)$$

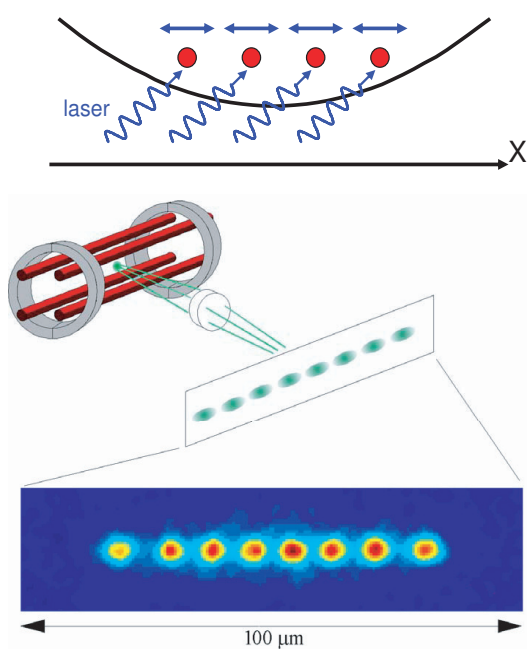


Figure 10.7: Many ions can be trapped in the same harmonic potential, and they can communicate through collective motional modes.

$$+ \left(\frac{p^2}{2(m/2)} + \frac{m/2}{2} 3\nu^2 x^2 \right) \quad (10.37)$$

$$+ \frac{e^2}{4\pi\epsilon_0|a+x|} \quad (10.38)$$

$$- \sum_i \left(\hbar\Delta_i |e\rangle_{ii}\langle e| + \hbar\Omega_i \left(|e\rangle_{ii}\langle g|e^{ikx_i} + h.c.\right) \right). \quad (10.39)$$

We find from the first two terms that the two ions vibrate in a center of mass mode at frequency ν and in a stretch mode at frequency $\sqrt{3}\nu$. Denoting these phonon modes by the annihilation operators \hat{a}_{cm} and \hat{a}_s respectively, the Hamiltonian may be expressed as

$$\hat{H} = \hbar\nu\hat{a}_{cm}^\dagger\hat{a}_{cm} + \hbar\sqrt{3}\nu\hat{a}_s^\dagger\hat{a}_s - \sum_i \hbar\Delta_i |e\rangle_{ii}\langle e| \quad (10.40)$$

$$- \sum_i \hbar\Omega_i \left(|e\rangle_{ii}\langle g|e^{i\eta_{cm}(\hat{a}_{cm}+\hat{a}_{cm}^\dagger)}e^{-i\eta_s(\hat{a}_s+\hat{a}_s^\dagger)} + h.c.\right). \quad (10.41)$$

Note that the two phonon modes may be separately addressed by choosing the appropriate laser detuning.

10.4.2 Quantum gates

A quantum computer uses two-level quantum systems to store information. The internal states are interpreted as bit values, $|g\rangle = |0\rangle$ and $|e\rangle = |1\rangle$, and information is encoded in the state $\alpha|0\rangle + \beta|1\rangle$ of the so-called ‘‘qubit’’. These qubits form the backbone for the quantum computer, providing a memory for quantum states.

By manipulating the qubits, one can perform calculations. In fact, it can be shown that one need only be able to perform a very small number of manipulations to be able to perform all calculations. If one can address each qubit and perform any rotation of its state, then to have universal computation ability one only needs a non-trivial gate which couples any two-qubit pair. One such two-qubit gate is the π phase gate, which maps two qubits according to the table

$$|0\rangle|0\rangle \rightarrow |0\rangle|0\rangle \quad (10.42)$$

$$|0\rangle|1\rangle \rightarrow |0\rangle|1\rangle \quad (10.43)$$

$$|1\rangle|0\rangle \rightarrow |1\rangle|0\rangle \quad (10.44)$$

$$|1\rangle|1\rangle \rightarrow -|1\rangle|1\rangle. \quad (10.45)$$

The sign of one qubit's excited state is flipped only if the other qubit is also in the excited state.

Trapped ions provide a possible architecture for a quantum computer. We have seen that single-qubit rotations can be performed by applying laser light resonant with the bare atomic frequency. Furthermore, collective motion of the ions in the trap provides the interaction required to implement a two-qubit gate. We will now show how the phase gate can be implemented between any two ions in a linear ion trap.

Requirements for the phase gate

As we present it here, the phase gate for trapped ions requires cooling the vibrational modes down to the ground state where no phonons are present. If a product state of the internal states of N ions in the trap is represented by $|x_{N-1} \dots x_0\rangle_{\text{ion}}$, then the overall initial state of the system can be written as a superposition of such states

$$|\psi\rangle = \sum_x c_x |x_{N-1} \dots x_0\rangle_{\text{ion}} \otimes |0\rangle_{\text{phonon}}. \quad (10.46)$$

In addition to the excited and ground states considered previously, we will also need access to an auxiliary ionic level which is degenerate with the excited state and coupled to the ground state by an orthogonal laser polarization (see Figure 10.8).

Phase gate procedure

Suppose that we wish to perform the phase gate on the m^{th} and n^{th} ions in the trap. By transferring the quantum state of the m^{th} ion onto the vibrational mode, the bare levels of the n^{th} atom are affected. A single-qubit rotation of the n^{th} atom is then performed conditional on the vibrational state of the trap. Finally, the information stored in the collective mode is transferred back to the state of the m^{th} ion.

The precise sequence for the phase gate implementation is described and illustrated in Figure 10.9.

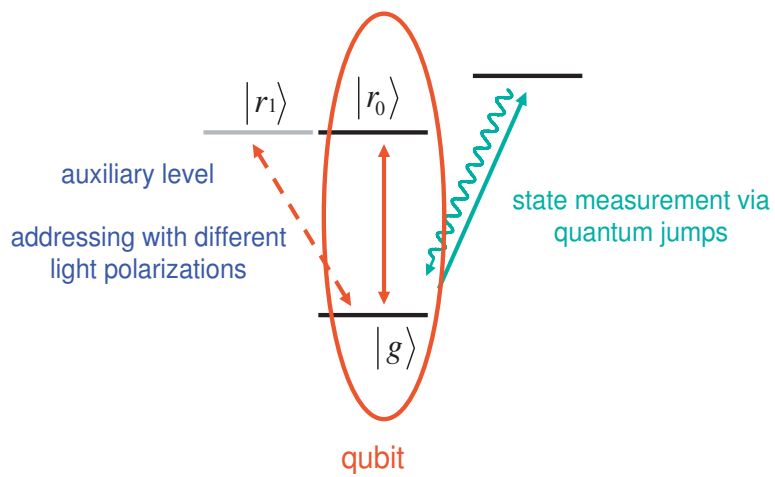


Figure 10.8: The four levels used to implement the phase gate. A dipole allowed transition is used to cool the ion, while an auxiliary state is used to implement the phase shift of the qubit states.

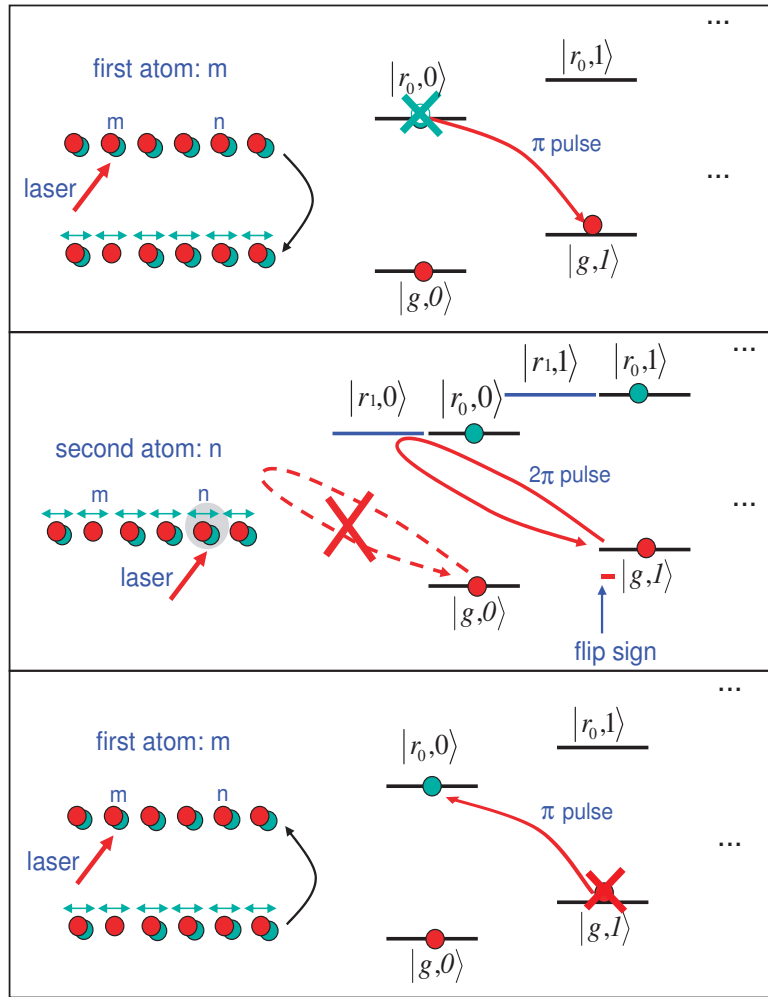


Figure 10.9: A conditional phase gate is implemented in three steps. The first step writes the state of qubit m onto the collective motion of the ions. The second step conditionally changes the phase of the qubit n by applying a 2π pulse to the auxiliary level, which changes the sign only if the qubit m is in the excited state and qubit n is in the ground state. The third step writes the collective motion back onto qubit m, inducing an overall sign change due to two consecutive π pulses. The final state is unchanged unless both qubits were in their excited state, in which case it is multiplied by an overall negative sign.

Chapter 11

Quantum dynamics of atomic matter waves

Our previous lectures have focussed on the quantum properties of light waves; we now turn to the quantum properties of matter fields. In our treatment of atomic physics, we have discussed techniques for cooling atoms using light forces. As the atomic temperature approaches zero, however, the quantum statistics of the atoms become increasingly important. As an ensemble of non-interacting, unconfined bosons is cooled $T \rightarrow 0$, a macroscopic number of atoms occupy the ground state. Advances in laser cooling and trapping techniques have allowed experiments to probe this quantum degenerate state of an atomic gas. In the case of bosonic atoms, the most prominent example of such a state is a Bose-Einstein condensate (BEC).

11.1 Introduction

Qualitatively, a gas at high temperature should behave classically, with each atom behaving like a point particle with a well-defined position and momentum. At low temperature, the atoms are best described as matter wavepackets, whose size is set by the deBroglie wavelength

$$\lambda_{dB} = \sqrt{\frac{2\pi\hbar^2}{mk_B T}}. \quad (11.1)$$

When the atomic wavepackets start to overlap in position, the quantum statistics of the atoms becomes important. A quantitative calculation shows

that the transition between primarily classical and primarily quantum mechanical behaviour occurs when the density n and the temperature T_c satisfy

$$n \lambda_{dB}(T_c)^3 = \zeta(3/2) \approx 2.612, \quad (11.2)$$

or

$$k_B T_c = \frac{2\pi\hbar^2}{m\lambda_{dB}^2} = \frac{2\pi\hbar^2}{m} \left(\frac{n}{2.612}\right)^{2/3}. \quad (11.3)$$

For Bose atoms below this critical temperature, $0 < T < T_c$, a macroscopic number of atoms will occupy the lowest energy state—even at finite temperature. This so-called Bose condensation will occur only if the atom cloud is both dense and cold, which means that the phase space density must be large.

11.1.1 Bose-Einstein statistics

Bose-Einstein statistics describe the behaviour of indistinguishable particles with integer spin, and thus determine how an ensemble of N identical Bose atoms with some total energy E will distribute themselves among the possible energy states.

It is worth noting the role that distinguishability plays in determining this distribution. From statistical mechanics, we know that the weight of a certain arrangement of atoms is given by the number of ways that arrangement can be formed – or, in some sense, how random that arrangement is. The distinguishability of particles plays a crucial role in determining this weight. For example, consider 10 particles distributing themselves between two states. When the particles are distinguishable, the statistical weight of the $\{5, 5\}$ arrangement is 252 times greater than the statistical weight of the $\{10, 0\}$ arrangement. When the particles are indistinguishable, the two configurations have equal weight. This illustrates the huge change in statistics obtained upon losing the ability to distinguish particles.

In the grand canonical ensemble, N Bose particles with total energy E will distribute themselves among a set of energy levels ϵ_i according to the Bose-Einstein distribution,

$$n_i = \frac{1}{e^{(\epsilon_i - \mu)/k_B T} - 1}, \quad (11.4)$$

where n_i is the number of particles occupying energy level ϵ_i , and

$$N = \sum_i n_i \quad (11.5)$$

$$E = \sum_i \epsilon_i n_i. \quad (11.6)$$

This set $\{n_i\}$ represents the most random way to distribute the energy E among N atoms occupying the energy states $\{\epsilon_i\}$. At sufficiently low temperature, the most random distribution is obtained by putting a large fraction of the atoms into the ground state ϵ_0 and letting the remaining atoms occupy higher energy states. When converting these summations into integrals, it is therefore important to keep track of the atoms occupying the ground state ϵ_0 , so that

$$N = \frac{1}{e^{(\epsilon_0 - \mu)/k_B T} - 1} + \int \frac{g(\epsilon)}{e^{(\epsilon_i - \mu)/k_B T} - 1} d\epsilon \quad (11.7)$$

$$E = \frac{\epsilon_0}{e^{(\epsilon_0 - \mu)/k_B T} - 1} + \int \epsilon \frac{g(\epsilon)}{e^{(\epsilon_i - \mu)/k_B T} - 1} d\epsilon, \quad (11.8)$$

where $g(\epsilon)$ is the density of states appropriate to the geometry of the problem.

11.1.2 BEC in an ideal gas

For non-interacting and unconfined bosons, the textbook treatment outlined above results in a macroscopic ground state occupation number

$$N_{g.s.} = N \left(1 - \left(\frac{T}{T_c} \right)^{3/2} \right), \quad (11.9)$$

where N is the total number of atoms and T_c is the condensation temperature. One can also find the temperature dependence for a slightly more realistic scenario when the atoms are confined to a three-dimensional harmonic oscillator trap:

$$N_{g.s.} = N \left(1 - \left(\frac{T}{T_c} \right)^3 \right). \quad (11.10)$$

In reality, however, even the dilute atomic gases interact, and even weak interactions can have a large effect on the dynamics of the condensate.

11.2 Experimental History

Superfluid helium was discovered and explored many decades before the recent advent of Bose condensation in atomic gases, and in some sense represents the first experimental evidence for BEC. However, the extent to which superfluid helium can be described as a Bose condensate was a subject of

great debate: Liquid helium is a strongly correlated fluid, and bears little resemblance to the non-interacting ideal gas for which Bose condensation was first envisioned. Only about 10% of the helium atoms are in the ground state in superfluid helium; the rest compose coherent excitations which nevertheless exhibit superfluid behaviour. One can thus consider superfluid helium to be a Bose condensate with a strong quantum depletion imposed by the strong interactions between atoms.

For many years it was believed that Bose condensation in a gas was impossible (see Figure 11.1). The constraints of temperature and density required to reach the critical temperature for condensation cannot be attained for gaseous material in thermodynamic equilibrium, because all materials become solid or liquid long before they are cold and dense enough to Bose condense.

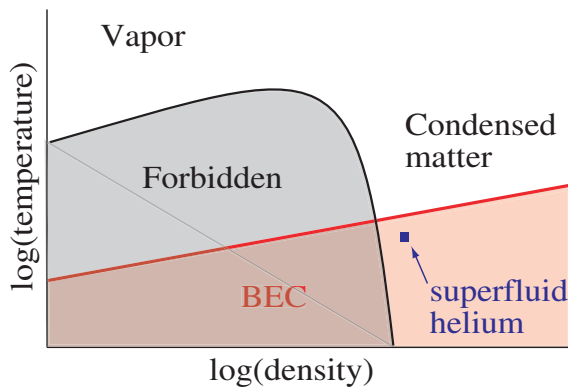


Figure 11.1: Allowed and forbidden regions of temperature and density, shown with the BEC critical temperature $T = T_c(n)$ (qualitative).

While there is no stable regime for BEC in a gas, one might hope to use a metastable state to realize condensation which would last long enough to measure. Spin-polarized hydrogen was the first candidate proposed, because the metastable triplet state of hydrogen has no bound state. Spin-polarized hydrogen therefore cannot recombine into H_2 , and left undisturbed remains polarized for days. Early contributors to this field included Isaac Silvera, Walraven, Dave Pritchard, and Dan Kleppner. They and others cryogenically cooled hydrogen atoms by coating the chamber walls with superfluid helium; the spin polarization was maintained by applying a magnetic field.

The hydrogen could be trapped with magnetic fields and – at least in principle – evaporatively cooled below the condensation temperature. However, at low temperatures, the hydrogen BEC experiments ran into a problem: whereas collisions with the walls typically did not flip the H spin at high temperatures, at low temperatures the density of H on the walls was high enough that spin-flip collisions became inevitable.

Following the advent of laser cooling, many of the techniques pioneered by proponents of hydrogen BEC were adopted and adapted for use with the alkali atoms. Rather than using an initial cryogenic cooling stage, the atoms could be cooled and trapped using a magneto-optical trap and optical molasses before transfer to a magnetic or off-resonant optical trap for evaporative cooling. As we will soon see more quantitatively, this evaporative cooling step could only succeed for atoms whose elastic scattering rate far exceeds their inelastic scattering rate. By working at very low densities – and pursuing very low temperatures in the nano-Kelvin regime – researchers were able to find a stability window for the alkali gases, where recombination into bound states was extremely unlikely. In this regime, recombination requires a three-particle collision to satisfy energy and momentum conservation. For very low densities the three-body recombination rate is small compared to the two-body elastic scattering rate, allowing effective evaporative cooling.

11.3 Experimental techniques used in Bose condensation of atoms

There is an intimate relationship between trapping and cooling in atomic physics. In order to trap atoms, they must be sufficiently cold; once they are trapped, it is possible to cool them still further since the trap breaks their thermal contact with the outside world. Consequently we will begin by discussing some of the basic considerations behind atom trapping.

11.3.1 Atom-surface interactions

Experiments use magnetic, electric, or gravitational traps to isolate atoms from their environment. In particular, traps prevent atoms from coming into contact with solid or liquid surfaces. Atom loss is the primary problem associated with atom-surface collisions, because atoms have a tendency to stick to a solid. However, this tendency can vary depending on the type of atom and the type of surface under consideration.

The effective potential for an atom above a surface will generally support

Table 11.1: Typical surface binding energies

He-NaCl	$\sim 60K$
Ne-LiF	$\sim 130K$
Kr-graphite	$\sim 1000K$
$^3\text{He}-\text{H}_2$	$\sim 10K$
H- ^4He	$\sim 1K$
Cs- ^4He	$\sim 1.5K$

many bound states which can trap the atom. Moreover, solids and liquids have a huge number of vibrational and rotational modes, so once trapped near the surface the atom will quickly relax to the ground state of the potential. At high temperatures $> 1 \text{ mK}$, the probability for an atom to stick is essentially unity. Typical binding energies for different atom-solid pairs are listed in Table 11.1.

Once the atom sticks to the surface, it thermalizes with the solid, and remains stuck to the surface for some characteristic resonance time τ_R . To find this resonance time, we will consider the condition for equilibrium: the number of atoms attaching to the surface must equal the number of atoms leaving.

If the sticking probability is s , the atomic density is n , and the average atomic velocity is \bar{v} , the flux onto the surface $\Phi = (1/4)n\bar{v}s$ must match the rate at which atoms leave the surface σ/τ_R , where σ is the areal density. Assuming that the gas and surface are in thermal equilibrium, their chemical potentials must be equal, and

$$\frac{\sigma}{n} = \lambda_{DB} e^{E_B/(k_B T)}, \quad (11.11)$$

where λ_{DB} is the DeBroglie wavelength of the atom, E_B is the binding energy to the surface, and T is the temperature of the surface. Substituting this value for σ , we find the resonance time

$$\tau_R = \frac{4\lambda_{DB}}{\bar{v}s} e^{E_B/(k_B T)}. \quad (11.12)$$

The resonance time is exponentially sensitive to the binding energy, so only those atom-solid pairs with binding energies smaller than or close to the temperature will have reasonably small resonance times. As the temperature of the wall is lowered beneath the binding energy, τ_R grows. Eventually the

Table 11.2: Typical surface densities for $n \sim 10^{13} \text{ cm}^{-3}$ using the lowest binding energy $E_B \sim 1K$. Note that the areal density saturates around 10^{14} ; above that, the atoms pile up on themselves.

T	$\sigma(\text{cm})^{-2}$	$\mathcal{L}(d)$
$10K$	10^{11}	> 100
$1K$	$3 \cdot 10^{13}$	$2 - 20$
$0.1K$	$2 \cdot 10^{16}$	< 1

atoms begin to pile up on top of the surface, which dramatically changes its properties. If \mathcal{L} is the distance between atoms, in units of the atom diameter d , then pile-up occurs at temperatures low enough that $\mathcal{L} < 1$.

At high areal densities, chemically active atoms will begin to react with each other, forming molecules which are then permanently lost from the ensemble of chemically metastable atoms.

If the atoms are not reactive, the material will collect in multiple monolayers, and the atom density in the gas phase will be in thermal equilibrium with the solid phase. The density of gaseous non-reactive atoms is then simply the vapor pressure of the atomic species at the temperature of the surface. This observation explains why vacuum chambers attain much lower pressures after bakeout. Bakeout produces a low "effective vapor pressure" because the binding energy of the surface becomes visible to other atoms impinging on the chamber walls, so they will stick regardless of the vapor pressure at the chamber temperature.

In principle, it should be possible to use cold chamber walls to cool atoms, provided that the resonance time is reasonably short at the desired temperature. In practice, however, there are hardly any species (H on He is one example) which can be cooled to useful temperatures $\sim 1K$, and only a few special pairs which can be cooled below $\sim 100K$. Consequently, surface cooling techniques have only ever been employed for the hydrogen atom.

11.3.2 Trap depths

In order to trap an atomic ensemble, the atoms must be sufficiently cold that they cannot climb up the potential barrier forming the atomic trap. How cold must they be? The depth of a trap can be expressed in terms of the highest temperature atoms it can confine, and typical trap depths are given in Table 11.3.

Table 11.3: Trap depths for realistic laboratory conditions.

Trap type	Lab field strengths	Trap depth for atoms	Trap depth for molecules
Magnetic	$0.1 - 4T$	$60\text{mK} - 15\text{K}$	$60\text{mK}-10\text{K}$
Electric	$1-100\text{MV/cm}$	$1\mu\text{K}-1\text{mK}$	$1\mu\text{K}-1\text{K}$
Gravitational	980cm/s^2	$0.1 \text{ mK/m}-10\text{mK/m}$	$0.1 \text{ mK/m}-10\text{mK/m}$

11.3.3 Initial Cooling

A variety of methods may be employed to cool the atoms below the trap depth. From Table 11.3, one can see that it is indeed possible to cool hydrogen using a cold He surface to $\sim 1\text{K}$ and capture it directly in a magnetic trap. This method, however, is inapplicable to just about every other atom. Consequently, most experiments which trap cold atoms use a laser cooling stage prior to switching on the trap.

Laser cooling

We have considered in detail the mechanisms behind Doppler and sub-Doppler cooling. Experimentally, these are usually implemented in order: first a combination of Doppler cooling techniques is used to capture atoms in a magneto-optical trap, then the magnetic trap is switched off to enable polarization gradient cooling. Using these techniques, atom densities of $\sim 10^{11}\text{cm}^{-3}$ and temperatures $\sim 50\mu\text{K}$ can be achieved in typical alkali atoms. Nevertheless, to reach Bose condensation, the phase space density must still be increased by many orders of magnitude. Further cooling is done by transferring the atoms to a trap without any resonant light fields, for example a magnetic trap or a far-off-resonant optical dipole force trap.

Buffer gas cooling

Laser cooling has its limitations, since it only works well for atoms with a cycling transition (and doesn't work for molecules), and can only produce cold clouds of at most $\sim 10^{10}$ atoms. For every other species of atom and molecule, one can actually use a slightly different type of surface cooling. We have seen that typically an atom will bind to a cold surface for very long times. Nevertheless, if the chamber contains sufficient cold buffer gas, the atom can be cooled to the temperature of the buffer gas before it reaches the

walls of the chamber. Experimentally, this temperature is set by the required vapor pressure. For example, a helium buffer gas can cool atoms from 1000K to $\sim 1\text{K}$ while maintaining sufficient vapor pressure that the atomic mean free path is much less than a typical chamber size. Once the atoms have been cooled, the buffer gas can be pumped away, and the atoms can be thermally isolated from the chamber walls by trapping them magnetically. We note in passing that there also exist pulsed cooling mechanisms, which slow a pulse of atoms or molecules by timing a series of electrodes so that the pulse is always travelling up a potential gradient.

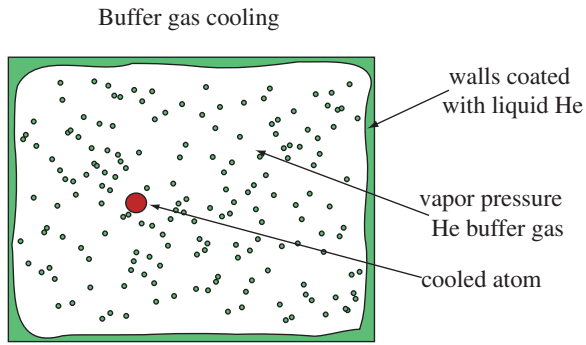


Figure 11.2: Buffer gas cooling can be used to prepare any atom or molecule near 1K, sufficiently cold to trap nearly all paramagnetic atoms and molecules.

11.3.4 Optical and Magnetic traps

The final cooling step must be done in a trap which does not excite atomic transitions. One possible solution uses the atomic dipole force to confine the atoms to the focus of a red-detuned laser beam. Experimentally, a powerful CO₂ laser is often employed for this task, as its wavelength $\sim 10\mu\text{m}$ is far detuned from most optical transitions.

Magnetic traps use the magnetic dipole interaction to confine atoms with nonzero angular momentum. Quantum mechanically, the energy of an atomic state with magnetic quantum number m_F along the axis of a magnetic field B_z is given by

$$H = g_F \mu_B m_F B_z. \quad (11.13)$$

Since Maxwell's equations forbid static magnetic field maxima, this dipole force can only be employed for weak-field-seeking states.

In order for atoms to remain confined by a magnetic trap, their spin must adiabatically follow the magnetic field direction as they move around the trap. Provided that the angle θ of the magnetic field changes sufficiently slowly that

$$\frac{d\theta}{dt} \ll \frac{\mu_B B_z}{\hbar} = \omega_{\text{Larmor}}, \quad (11.14)$$

the atoms will remain in the weak-field seeking state. If the angle of the magnetic field changes too quickly, spin flips (or "Majorana flops") will result, ejecting the atom from the trapped state.

The simplest magnetic trap one might imagine is a quadrupole trap, in which anti-Helmholtz coils create a magnetic field minimum at their center. The magnetic field in each direction $i = x, y, z$ is linear: $B_i = \tilde{B}_i x_i$, with $\sum |\tilde{B}_i| = 0$. However, such a trap has a vanishing magnetic field at its center, for which the adiabatic following criterion cannot be satisfied. Consequently this trap acts as if it had a hole in the center! By changing the location of the magnetic field zero with time, the hole in the quadrupole trap can be plugged. The time-orbiting potential (TOP) trap uses a time-averaged quadrupole field to simulate harmonic confinement for the atoms.

Alternately, one can build a magnetic trap with a nonzero magnetic field minimum by combining a two-dimensional quadrupole trap with Helmholtz coils to provide axial confinement. This so-called "Ioffe-Pritchard" trap is named after the researchers who first employed it to confine plasmas and atoms, respectively. Near the center of the trap the potential is nearly harmonic, with a magnetic field given by

$$\mathbf{B} = B_0 \begin{pmatrix} 0 \\ 0 \\ 1 \end{pmatrix} + B_1 \begin{pmatrix} x \\ -y \\ 0 \end{pmatrix} + \frac{B_2}{2} \begin{pmatrix} -xz \\ -yz \\ z^2 - \frac{1}{2}(x^2 + y^2) \end{pmatrix}. \quad (11.15)$$

11.3.5 Evaporative cooling

Once atoms are confined within a trap, further cooling techniques can be applied to them. Evaporative cooling has provided the most effective method for reaching ultracold temperatures, and the only technique for creating quantum degenerate gases. The physical mechanism behind evaporative cooling is very simple: those atoms which "boil off" the top of the trap must have more energy than the atoms remaining behind. Once the remaining atoms re-thermalize, their temperature should go down.

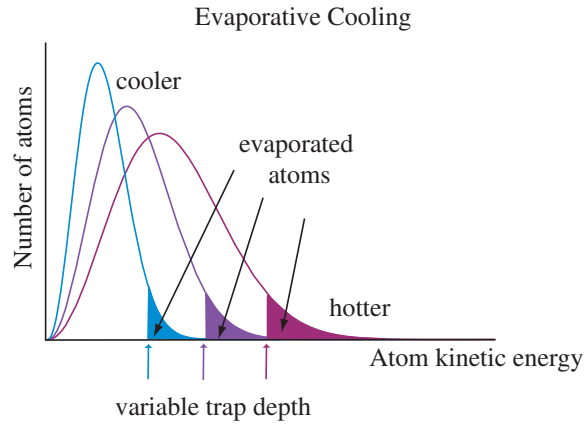


Figure 11.3: Evaporative cooling. Only the hottest atoms have enough energy to escape the confining potential of the trap and stick to the walls. When the remaining atoms rethermalize, they attain a lower temperature. By lowering the trap potential, successively colder temperatures can be reached without a significant slowdown in the cooling rate.

History

Evaporative cooling was invented by Harald Hess in the 1980s while working in the groups of Tom Greytak and Dan Kleppner. The method was first demonstrated and developed using atomic hydrogen. Around five years later, it was applied to the alkali metals, and eventually became the standard method for production of quantum degenerate matter.

Idealized evaporative cooling

In a perfect world where evaporation was the only process affecting the trapped atoms, evaporative cooling could be used to cool atoms to indefinitely low temperatures simply by waiting long enough. However, the rate of cooling would decrease with time, so a more effective cooling mechanism would slowly lower the potential barrier of the atom trap, so that the cooling rate remains reasonably large (see Figure 11.4).

Alternatively, one can resonantly excite atoms into an untrapped, thus selecting the hottest atoms to be removed from the trap. By slowly changing the resonance energy, one can start off ejecting the hottest atoms from

the trap, and cut out successively colder and colder atoms until the desired temperature is reached. Typically this technique is accomplished using RF coupling between hyperfine levels of the atom. In a magnetic trap, only weak-field seeking states will be trapped, so resonant excitation of strong-field seeking states can be used to selectively remove certain atoms. Although all of the atoms have the same hyperfine structure regardless of their kinetic energy, the magnetic trap induces spatially dependent Zeeman splittings. Consequently this so-called “RF knife” can be used to cut out atoms on the edges of the trap, and a slow change in the RF frequency can sweep the knife closer to the trap center where the colder atoms remain.

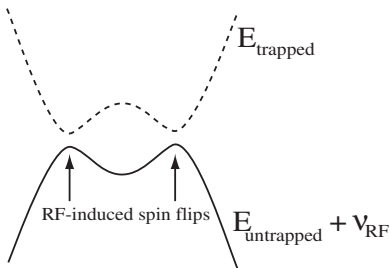


Figure 11.4: One can envision the RF knife as a Landau-Zener process, in which the frequency of the RF field sets the location of the avoided crossing and the magnitude of the RF field sets its width. The RF knife thus effectively acts to limit the trap depth.

Competing processes

Evaporative cooling is not the only process affecting trapped atoms. Three-body recombination, inelastic scattering, and collisions with background gas conspire to limit the lifetime of trapped atoms. Evaporative cooling must therefore be performed quickly enough that the atoms remain in the trap throughout the process, but slowly enough that they have time to rethermalize after the hot atoms have been ejected.

Three-body recombination

Nearly every atom used in trapping experiments is in a metastable state. Given sufficient time, the alkali atoms will form molecules and eventually

metal crystals, and the noble gases are typically trapped in a metastable hyperfine state. On first sight, this observation is very worrisome, since it means we are trapping an inherently unstable object. There is, however, a loophole: In order to relax to their ground (molecular) state, two atoms require a third body to take away the excess energy and momentum. If the atom densities are sufficiently low, the probability for three atoms to interact simultaneously can be quite small. Nevertheless, these considerations limit usable atomic densities to $\sim 10^{15} \text{ cm}^{-3}$.

Inelastic collisions

A magnetic trap only confines certain spin species, so any collision process which flips the spin of an atom will lead to loss. These so-called “dipolar” or “inelastic” processes require only two atoms. Luckily, for the alkali metals, two-body processes do not present much of a problem at low temperatures.

Background gas

Finally, atoms can be lost from the trap due to collisions with background gas in the vacuum chamber. Any material adsorbed on the walls of the chamber can evaporate and knock atoms out of the trap. The alkali atoms are very sensitive to these processes, and as a result ultra-high vacuum $\sim 10^{-11} - 10^{-12}$ torr is required for successful evaporative cooling to quantum degeneracy.

11.3.6 The theory of evaporative cooling

To quantitatively examine how evaporative cooling works, we will assume a specific model for a magnetic trap, and account for two-body inelastic processes. If the magnetic trap is built from anti-Helmholtz coils, near the center we can approximate the trap as a spherical linear potential

$$B(\rho) = \frac{B_0}{\rho_0} \rho, \quad (11.16)$$

where ρ is the distance from the center of the trap, ρ_0 is the size of the trap, and B_0 is the maximum field of the trap. If the atom density at the center of the trap is n_0 , the density distribution in thermal equilibrium is

$$n(\rho) = n_0 e^{-\mu|B(\rho)|/k_B T}, \quad (11.17)$$

where μ is the magnetic moment of the trapped atom. The total number of atoms in the trap is thus

$$N = \int d^3\mathbf{r} n_0 e^{-\mu|B(\rho)|/k_B T} \quad (11.18)$$

$$= \int_0^{\rho_0} d\rho 4\pi \rho^2 n_0 e^{-\overbrace{(\mu B_0/k_B T)}^{\eta}(\rho/\rho_0)} \quad (11.19)$$

$$\approx \frac{4\pi\rho_0^3}{\eta^3} n_0 \int_0^{\infty} du u^2 e^{-u} \quad (11.20)$$

$$= 6 \underbrace{\frac{4\pi\rho_0^3}{3}}_{V_0} \frac{1}{\eta^3}, \quad (11.21)$$

where we have set the upper limit of the integral to ∞ rather than ρ_0 because the density of atoms near the edge of the trap is negligibly small when $\eta > 5$. The quantity V_0 represents the geometric volume of the trap, while η^3 is a compression factor for the density referenced to the density at the bottom of the trap.

Including two-body processes

Two-body losses must happen at a rate proportional to the square of the atomic density,

$$\dot{n} = -g_{in} n^2, \quad (11.22)$$

where g_{in} is a rate constant for inelastic processes. In principle g_{in} could depend on the magnetic field, temperature and so on, but for purposes of our discussion we shall assume it to be constant. The total loss rate from the trap due to dipolar relaxation is

$$\dot{N}_d = - \int d^3\mathbf{r} g_{in} n_0^2 e^{-2\eta\rho/\rho_0} \quad (11.23)$$

$$= -g_{in} 4\pi n_0^2 \int_0^{\rho_0} \rho^2 d\rho e^{-2\eta\rho/\rho_0} \quad (11.24)$$

$$= -g_{in} 4\pi n_0^2 \frac{\rho_0^3}{4\eta^3} \quad (11.25)$$

$$= -6g_{in} n_0^2 \frac{V_0}{\eta^3} \cdot \frac{1}{8}. \quad (11.26)$$

Note that a factor of $1/8$ (relative to Eq. (11.21)) appears in this expression because of the nonlinear dependence on density.

Evaporation itself

The basic idea behind evaporation is that the atoms at the edge of the trap leave the system and stick to the chamber walls. The flux of atoms hitting the chamber walls is thus approximately

$$\Phi = \frac{1}{4}n\bar{v}s \quad (11.27)$$

$$= \frac{1}{4}n_0 e^{-\mu B_0/(k_B T)} \bar{v}s, \quad (11.28)$$

where \bar{v} is the average atomic velocity at the edge of the trap and s is the sticking probability.

We must also account for the thermalization rate Γ of the remaining atoms, which is governed by the rate of elastic collisions σ_{el} within the atom cloud

$$\Gamma \propto n_0^2 \bar{v} \sigma_{el}. \quad (11.29)$$

The rate at which atoms evaporate from the cloud is then set by the rate at which thermalization can refill the pool of hot atoms (which subsequently evaporate). The evaporation rate is approximately

$$\dot{N}_v = -n_0^2 \bar{v} \sigma_{el} e^{-\eta} V_0 \eta^{\sim 1.5}. \quad (11.30)$$

An important dimensionless quantity is the ratio of the evaporative loss to the inelastic loss,

$$\frac{\dot{N}_v}{\dot{N}_d} \approx e^{-\eta} \eta^{4.5} \frac{g_{el}}{g_{in}}. \quad (11.31)$$

To assemble a full model, we must now consider the average energy of atoms lost by the trap. The initial average energy is

$$\bar{E} = \bar{K} + \bar{U} = \frac{9}{2} k_B T \quad (11.32)$$

Evaporating atoms will typically have an energy of order the trap threshold energy plus the thermal energy, or

$$E_v = \bar{K} + \bar{U}_v \sim E_{th} + (3/2)k_B T, \quad (11.33)$$

while atoms lost due to inelastic collisions will have

$$E_d = \bar{K} + \bar{U}_d \sim 6/2k_B T. \quad (11.34)$$

Clearly, atoms lost to dipolar relaxation act to heat rather than cool the sample, and in steady state one expects that the dipolar heating rate should

match the evaporative cooling rate, or $\frac{\dot{N}_v}{\dot{N}_d} \sim 1$. The ratio of the elastic to inelastic scattering rate therefore becomes crucially important to the success of evaporative cooling. In many systems, most notably the alkali metals, a favorable ratio $g_{in} \ll g_{el}$ makes evaporative cooling to quantum degeneracy possible.

11.3.7 Probing atomic ensembles

The spatial and momentum distribution of cold atomic ensembles can be probed using near-resonant laser light. By imaging the shadow that the atom cloud leaves in a resonant laser beam, one can measure the temperature and number of atoms without having to collect fluorescence photons.

The atom cloud affects the incident laser beam via its complex index of refraction,

$$n = \sqrt{1 + 4\pi \frac{N}{V} \alpha} \quad (11.35)$$

$$, \quad (11.36)$$

where α is the polarizability of the atom. Typically, one either measures the real (refractive) or imaginary (absorptive) parts of the refractive index, with the latter measurement more common.

Absorptive imaging measures the spatially dependent transmission coefficient for the atomic ensemble,

$$t = e^{-d/2} \quad (11.37)$$

which scales as the exponential of the optical depth d ,

$$d = \frac{n_c \sigma_0}{1 + \delta^2}, \quad (11.38)$$

where $n_c = \int \frac{N}{V} dz$ is the column density integrated over the line of sight, σ_0 is the cross-section, and $\delta = (\omega - \omega_0)/(\Gamma/2)$ is the normalized detuning. Absorptive imaging is typically done on resonance, where there are no refractive effects to distort the image. One problem with absorptive imaging is that the optical depth of a Bose condensate is huge, of order $d \sim 300$, so a trapped condensate will completely absorb resonant light. Instead, time-of-flight imaging is used. The atom cloud is released from the trap and allowed to expand and fall. After a few milliseconds, the atom cloud has mapped its initial velocity (or momentum) distribution onto the position of the particles, allowing absorption imaging of the in-trap momentum

distribution. The shape of this momentum distribution allows one to distinguish the parabolic condensate from the gaussian thermal component of the atomic cloud.

Off-resonant imaging can be accomplished by measuring the phase

$$\phi = -\delta \frac{d}{2}, \quad (11.39)$$

that the atom cloud imprints on the laser beam by interfering the image with a reference beam (or, in practice, putting an appropriate phase plate in the beam path). Since the laser is not resonant with the atom cloud, such imaging can be done in trap; furthermore, very few atoms are excited by the laser, so “phase-contrast imaging” can be used to take multiple images of a single condensate.

These imaging techniques provide a quantitative measurement of the atomic distribution. Recently, it has even been shown that such pictures can be shot noise limited, with noise set by the finite number of atoms contributing to each camera pixel.

11.4 Atomic interactions

We have seen how trapping and cooling can be combined to bring an atomic ensemble to quantum degeneracy, where an ideal gas would exhibit Bose condensation. Real atoms, however, are not an ideal gas, and their interactions play an important role in determining how atomic Bose condensates behave.

In principle, including atomic interactions in our theory could prove problematic. However, dilute atomic gases offer an appealing opportunity to work with extremely low densities $n \sim 10^{12} - 10^{15} \text{ cm}^{-3}$ where the atoms are separated by distances $n^{-1/3} \sim 100\text{nm} - 1\mu\text{m}$. In contrast, liquids typically have a density $n \sim 10^{21} \text{ cm}^{-3}$ so high that the interatomic spacing $n \sim 1\text{nm}$ is hardly larger than the size of the atoms $r_0 \sim 1\text{nm}$ set by the tail of the van der Waals interaction. As a result, the theory for dilute gases is much simpler than that for liquids because we can identify a small parameter $n^{-1/3}r_0$ in which to perturbatively expand. For example, the alkali atoms have typical size $r_0 \sim 1 - 10\text{nm}$, so $n^{-1/3}r_0 < 0.1$.

The small parameter $n^{-1/3}r_0$ is not, however, quite what we want. In order to effectively describe scattering processes in a low-density limit, it is desirable to expand in a different small parameter $\mathbf{k} \cdot \mathbf{r}_0 \ll 1$. Nevertheless, if the gas is sufficiently cold $T < T_c$, where $T_c \sim \hbar^2 n^{2/3}/m$ corresponds

to the condensation temperature for bosons or the degeneracy temperature for fermions, then $n^{-1/3}r_0 \ll 1$ implies $\mathbf{k} \cdot \mathbf{r}_0 \ll 1$. These so-called dilute quantum gases provide a theoretically tractable system in which to study atomic interactions.

11.4.1 The van der Waals potential

Interactions between well-separated, neutral, ground-state atoms are dominated by the van der Waals potential. Consider two such atoms separated by a distance much larger than the Bohr radius of the atom $r \gg a_0$. At these large distances, the electrostatic interaction between the atom can be written as a multipole expansion

$$U(r) = \frac{c_1}{r} + \frac{c_2}{r^2} + \frac{c_3}{r^3} + \frac{c_4}{r^4} + \frac{c_5}{r^5} + \frac{c_6}{r^6} + \dots \quad (11.40)$$

The first term corresponds to the Coulomb potential, is nonzero only if the atoms are charged. The second term represents charge-dipole interactions, with higher orders in r representing higher order interactions. For the alkali atoms, all of these terms are zero in first order perturbation theory because the diagonal matrix elements of the dipole, quadrupole, etc... operators vanish. Second order perturbation theory is required to find the leading order potential, and the main contribution (for neutral atoms in their ground states) comes from the dipole-dipole interaction

$$\hat{V}_d(r) = \frac{\mathbf{d}_1 \cdot \mathbf{d}_2}{r^3} - 3 \frac{(\mathbf{d}_1 \cdot \mathbf{r})(\mathbf{d}_2 \cdot \mathbf{r})}{r^5}. \quad (11.41)$$

If the energy of the atom in state $|n\rangle$ is E_n , then to leading order in $1/r$, the resulting potential is

$$U(r) = \frac{6}{r^6} \sum_{n,n'} \frac{|\langle 0 | d_z | n \rangle|^2 |\langle 0 | d_z | n' \rangle|^2}{2E_0 - E_{n'} - E_n} \quad (11.42)$$

$$= -\frac{\hbar r_0^4}{2\mu r^6}, \quad (11.43)$$

where $\mu = m_1 m_2 / (m_1 + m_2)$ is the atomic reduced mass. Note that $E_0 < E_{n \neq 0}$, so the second order correction is always negative, so at large distances the van der Waals potential is attractive. Typical values of r_0 for the alkalis are between 1 nm and 10 nm, which is substantially larger than their physical sizes ~ 0.1 nm. If the interatomic distance becomes of the order of r_0 , the multipole expansion breaks down, and the potential is no longer necessarily attractive. At short distances, electronic exchange dominates the atomic interactions, producing a strong short-range repulsive potential.

11.4.2 Basic scattering theory

Our analysis of two-body scattering theory will consider only relative motion between two atoms. This assumption is valid when the center of mass motion decouples from the relative motion, for instance if the two atoms collide in a uniform background potential or are confined in a parabolic external potential. By focussing on relative motion, we can reformulate interatomic collisions as a single body scattering off a fixed potential $U(r)$, where r is the interatomic distance. The only important difference is a change in the mass from the bare atomic masses m_1, m_2 to the reduced mass of the single body $\mu = m_1 m_2 / (m_1 + m_2)$.

The wavefunction for a single body impinging on the potential from direction \hat{z} can be written in the form

$$\psi_k(\mathbf{r}) = e^{ikz} + \psi_{sc}(\mathbf{r}), \quad (11.44)$$

where ψ_k satisfies the Schroedinger equation

$$-\frac{\hbar^2 \nabla^2}{2\mu} \psi_k + U(\mathbf{r}) \psi_k = \frac{\hbar^2 k^2}{2\mu} \psi_k. \quad (11.45)$$

In the limit that $r \rightarrow \infty$, the scattered wave approaches an outgoing wave with some angular dependence

$$\lim_{r \rightarrow \infty} \psi_k(\mathbf{r}) = e^{ikz} + f_k(\theta) \frac{e^{ikr}}{r} \quad (11.46)$$

The incoming plane wave portion of the wavefunction can be written in terms of the spherical harmonics with help from the following useful formula:

$$e^{ikz} = \sum_{l=0}^{\infty} i^l (2l+1) P_l(\cos \theta) j_l(kr), \quad (11.47)$$

where $j_l(kr)$ is the spherical Bessel function of order l . In the limit $kr \gg 1$, i.e. far away from the scatterer, the Bessel function approaches a sinusoidal function, so that

$$e^{ikz} \approx \sum_{l=0}^{\infty} \frac{2l+1}{2ik} P_l(\cos \theta) \frac{1}{r} \left((-1)^{l+1} e^{-ikr} + e^{ikr} \right). \quad (11.48)$$

The entire wavefunction can thereby be written as a coherent superposition of incoming and outgoing spherical waves.

Scattering cross-sections

Experiments involving scattering typically measure quantities like the number of atoms scattered in a certain direction. Consequently it is convenient to identify the partial scattering cross-section

$$\frac{d\sigma}{d\Omega} = \frac{\text{scattering rate into solid angle } d\Omega}{\text{intensity of incoming beam}}. \quad (11.49)$$

Since the numerator has units of 1/time, and the denominator has units of 1/(area·time), the cross-section has units of area, which can be interpreted as the size of the scattering potential. Expressed in terms of the scattered wavefunction defined in Eq. (11.46), the partial cross-section is

$$\frac{d\sigma}{d\Omega} = |f_k(\theta)|^2 \frac{v_{\text{final}}}{v_{\text{initial}}}, \quad (11.50)$$

where v_{final} and v_{initial} are the final and initial velocities of the atom. We will focus on elastic collisions, where $v_{\text{final}} = v_{\text{initial}}$.

The total cross-section is found by integrating the partial scattering cross-section over all solid angles

$$\sigma = \int d\Omega \frac{d\sigma}{d\Omega} = 2\pi \int_0^\pi |f_k(\theta)|^2 \sin \theta d\theta. \quad (11.51)$$

The Born approximation

In order to calculate useful quantities like the cross-section, we need to know how to write $f_k(\theta)$ in terms of the scattering potential $U(r)$. If we knew the scattered wavefunction $\psi_k(\mathbf{r})$, we could integrate the Schrödinger equation to obtain

$$f_k(\theta) = \frac{-\mu}{2\pi\hbar^2} \int d^3\mathbf{r}' e^{-i\mathbf{k}' \cdot \mathbf{r}'} U(\mathbf{r}') \psi_k(\mathbf{r}'), \quad (11.52)$$

where θ is the angle between the incident wave k and the scattered wave k' . The Born approximation corresponds to a perturbative expansion in the potential. In the Born approximation, the incident wave is not much affected by the scatterer, so that

$$\psi_k(\mathbf{r}) \approx e^{ikz}, \quad (11.53)$$

and the partial scattering cross-section is given by the Fourier transform of the potential:

$$f_k(\theta) = \frac{-\mu}{2\pi\hbar^2} \int d^3\mathbf{r}' e^{-i(\mathbf{k}' - \mathbf{k}) \cdot \mathbf{r}'} U(\mathbf{r}'). \quad (11.54)$$

$$(11.55)$$

While the Born approximation does not provide a good solution for most situations, it does provide some useful intuition for cold collisions. In particular, when the incident particles have low energy, so that k is small relative to the effective size of the potential r_0 , it is valid to expand the exponential in the first Born approximation,

$$f_k(\theta) \approx \frac{-\mu}{2\pi\hbar^2} \int d^3\mathbf{r}' (1 - i(\mathbf{k}' - \mathbf{k}) \cdot \mathbf{r}' + \dots) U(\mathbf{r}'). \quad (11.56)$$

At low energies, only the first term will contribute, so that there is no angular dependence in the partial scattering amplitude $f_k(\theta)$. In other words, at low temperatures the outgoing scattered wave is isotropic.

The partial wave expansion

To arrive at a quantitative description of low-energy scattering, we will make use of partial wave analysis. Assuming a spherical interatomic potential $U(r)$, we can expand the wavefunction in terms of the spherical harmonics,

$$\psi = \sum_{l=0}^{\infty} A_l P_l(\cos \theta) R_l(r), \quad (11.57)$$

where P_l is the l^{th} Legendre polynomial. Substituting ψ into the Schrodinger equation

$$-\frac{\hbar^2 \nabla^2}{2\mu} \psi_k + U(\mathbf{r}) \psi_k = \frac{\hbar^2 k^2}{2\mu} \psi_k. \quad (11.58)$$

and using $U(\mathbf{r}) = U(r)$, we get a set of uncoupled equations, one for each $R_l(r)$:

$$\frac{d^2}{dr^2} R_l(r) + \frac{2}{r} R_l(r) - \frac{l(l+1)}{r^2} R_l(r) - \frac{2\mu}{\hbar^2} U(r) R_l(r) = -k^2 R_l(r). \quad (11.59)$$

Due to the short range character of $U(r)$ (since $\mathbf{k} \cdot \mathbf{r}_0 \ll 1$), we can divide space into two regions where different approximations are valid (see Figure 11.5). Provided we are working in the ultracold limit $\mathbf{k} \cdot \mathbf{r}_0 \ll 1$, the two regions overlap, and we can match the solutions to find the scattering amplitude.

In region A, $k \ll 1/r$ so we can neglect the energy term in the Schrodinger equation. In principle, we can solve this equation to find $R_l^{(A)}(r < r_0)$, and this solution will depend on the details of the short-range potential, but not on the energy k .

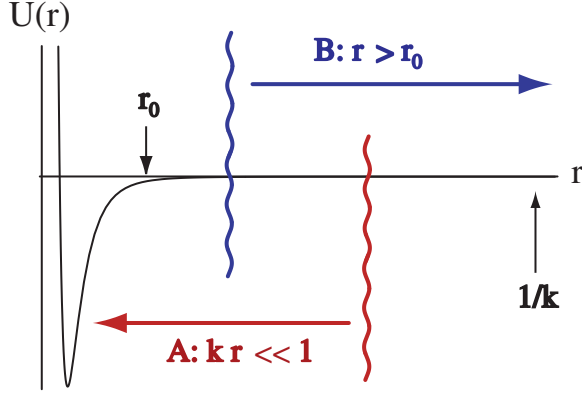


Figure 11.5: The Schrodinger equation can be approximately solved for small r in region A and for large r in region B. In the ultracold limit $\mathbf{k} \cdot \mathbf{r}_0 \ll 1$ the regions of validity overlap, the two solutions can be matched for $r_0 < r < 1/k$.

In region B , where $r > r_0$, the effect of the potential is negligible, and the Schrodinger equation reduces to a free-space Schrodinger equation in spherical coordinates. The solutions in this region are thus spherical Bessel functions, and for small distances $1 > kr > kr_0$

$$R_l^{(B)}(r) = c_1 r^l + c_2 r^{-(l+1)}. \quad (11.60)$$

By matching $R_l^{(B)}(r)$ with $R_l^{(A)}(r)$ in their simultaneous region of validity, we can obtain the two coefficients c_1 and c_2 . Furthermore, since $R_l^{(A)}(r)$ and $R_l^{(B)}(r < 1/k)$ are independent of k , we find that the two coefficients c_1 and c_2 also do not depend on k . The ratio between the two coefficients can be estimated qualitatively by arguing that for $r \sim r_0$ the two terms should be comparable, so

$$\frac{c_2}{c_1} \propto r_0^{2l+1}. \quad (11.61)$$

The constant of proportionality is usually of order unity, but in special situations it can be dramatically enhanced.

The spherical Bessel function solutions $R_l^{(B)}(r)$ have a different asymptotic behavior at large $kr \gg 1$:

$$R_l^{(B)}(r) \propto \frac{\sin\left(kr - \frac{\pi l}{2} + \delta_l\right)}{r} \sim \frac{(-1)^{l+1} e^{-ikr} + e^{ikr+2i\delta_l}}{r}, \quad (11.62)$$

where the phase shift δ_l is determined by the coefficients c_1 and c_2 :

$$\tan \delta_l = \frac{c_2}{c_1} \frac{k^{2l+1}}{(2l-1)!!(2l+1)!!}. \quad (11.63)$$

The double factorial symbol !! is defined by $n!! = n(n-2)(n-4)\dots$. Note from the definition that in the limit of zero energy $k \rightarrow 0$, the phase shift vanishes. This is a kinematic effect, which is a consequence of the short range potential.

We have seen how to calculate c_1 and c_2 using the short range potential, and from that derive the phase shift δ_l . If we can represent $f_k(\theta)$ in terms of the phase shift, then at least in principle we can derive the scattering cross section from the interatomic potential energy. Examine Eq. (11.62) and Eq. (11.46), noting that the plane wave can be written as in Eq. (11.48). By comparing the coefficients in front of e^{ikr} and e^{-ikr} , we see that the scattering amplitude may be written

$$f_k(\theta) = \sum_{l=0}^{\infty} P_l(\cos \theta) \frac{2l+1}{2ik} (e^{2i\delta_l} - 1). \quad (11.64)$$

In the ultracold limit $\mathbf{k} \cdot \mathbf{r}_0 \ll 1$, the phase shift is small, so $\tan \delta_l \approx \delta_l \approx c(r_0 k)^{2l+1}$ where c is a constant of order unity. The scattering amplitude for partial wave l is then

$$f_l = \frac{(e^{2i\delta_l} - 1)}{2ik} \approx \frac{\delta_l}{k} \approx c r_0 (r_0 k)^{2l}. \quad (11.65)$$

At low temperatures, $f_{l \neq 0} \ll f_0$ unless there is a resonance which increases the value of c . Since such resonances are highly improbable, in the ultracold limit we may safely neglect all but the s-wave scattering amplitude f_0 .

11.4.3 S-wave scattering

S-wave ($l = 0$) scattering dominates at low temperatures, so we will discuss its properties in some detail. In particular, its properties can be entirely characterized by a single parameter, the s-wave scattering length.

The $l = 0$ radial wavefunction has a particularly simple form for $r_0 < r < 1/k$:

$$R_0^{(B)}(r) = c_1 + \frac{c_2}{r} \propto 1 - \frac{a}{r}, \quad (11.66)$$

where we identify the s-wave scattering length

$$a = -\frac{c_2}{c_1}. \quad (11.67)$$

The *s*-wave phase shift can likewise be written in terms of the scattering length

$$\tan \delta_0 = -ka \quad (11.68)$$

as can the *s*-wave scattering amplitude

$$f_0 = -\frac{a}{1 + ika}. \quad (11.69)$$

Note that in the low-energy limit, $f_0 \approx -a$; this furnishes an alternate definition of the scattering length:

$$\lim_{k \rightarrow 0} f_0 = -a. \quad (11.70)$$

However, it is important to remember that when $ka \sim 1$ the scattering amplitude will differ from the scattering length.

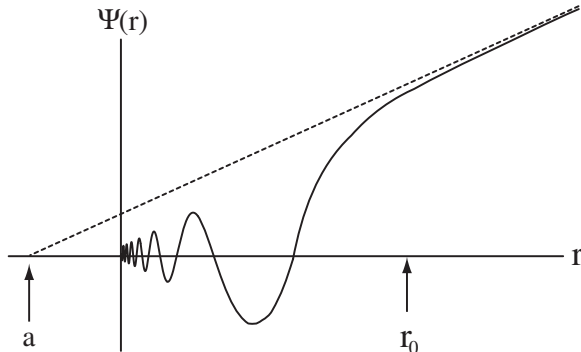


Figure 11.6: The scattering length can be visualized as the intercept of the asymptote to the wavefunction in the region $r_0 \ll r \ll 1/k$.

Physical interpretation

To obtain some physical intuition for the *s*-wave scattering length, we will consider three examples: a hard sphere, a generic repulsive potential, and a generic attractive potential. A hard sphere is characterized by a potential

$$U_H = \left\{ \begin{array}{ll} \infty & r < r_0 \\ 0 & r > r_0 \end{array} \right\}. \quad (11.71)$$

Clearly, the radial wavefunction must vanish at the boundary, so the intercept of the wavefunction asymptote must be

$$a_H = r_0. \quad (11.72)$$

At low energies, any potential with a positive scattering length therefore acts like a hard sphere of radius a . For example, a repulsive potential with a finite height

$$U_R = \begin{cases} |V_0| & r < r_0 \\ 0 & r > r_0 \end{cases}, \quad (11.73)$$

will have a scattering length which is positive but less than r_0 :

$$0 < a_R < r_0. \quad (11.74)$$

The behaviour of an attractive potential is less obvious. A generic attractive

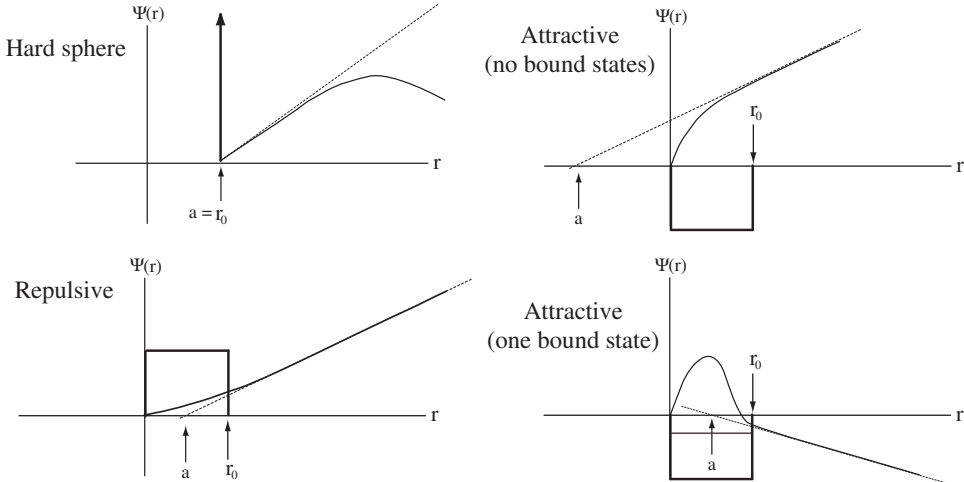


Figure 11.7: The wavefunction and scattering length for the hard sphere, the repulsive potential, and the attractive potential

potential such as

$$U_A = \begin{cases} -|V_0| & r < r_0 \\ 0 & r > r_0 \end{cases} \quad (11.75)$$

can either have a positive or a negative scattering length depending on the proximity of the highest energy bound state. For a sufficiently shallow potential that no bound state exists, the scattering length will be negative

$$a_A^{(0)} < 0. \quad (11.76)$$

As the attractive potential gets deeper, eventually a bound state will enter, bringing a node from $r = \infty$ into the wavefunction, and changing the sign of the scattering length. As we will see, the bound state resonances lead to an enhancement of the scattering length which can be exploited to experimentally manipulate the strength of atomic interactions.

The s-wave pseudopotential

In the ultracold limit $\mathbf{k} \cdot \mathbf{r}_0 \ll 1$, all interatomic potentials with the same scattering length a are equivalent to the pseudopotential $U(r)$ where

$$U(r)\psi(r) = \frac{4\pi\hbar^2 a}{2\mu}\delta^3(\mathbf{r})\frac{\partial}{\partial r}(r \cdot \psi(r)). \quad (11.77)$$

In turn, this potential is equivalent to setting a boundary condition on the wavefunction

$$\lim_{r \rightarrow 0} \psi(r) \propto \left(1 - \frac{a}{r}\right). \quad (11.78)$$

The Schrodinger equation for the pseudopotential is

$$-\frac{\hbar^2 \nabla^2}{2\mu}\psi(r) + \frac{4\pi\hbar^2 a}{2\mu}\delta^3(\mathbf{r})\frac{\partial}{\partial r}(r \cdot \psi(r)) = 0, \quad (11.79)$$

and it is simple to verify that $\psi(r) = 1 - a/r$ satisfies this equation.

The pseudopotential is useful because it only acts on the regular part of the wavefunction, ignoring the $1/r$ singularity. For smooth functions (without any singularities) it acts like a simple delta-function potential

$$U(r) = \frac{4\pi\hbar^2 a}{2\mu}\delta^3(\mathbf{r}). \quad (11.80)$$

This is important for first order perturbation theories, where the change in ground state energy due to interatomic interactions is

$$\Delta E_0 = \langle \phi_0 | \sum_{\langle i,j \rangle} U(r_{ij}) | \phi_0 \rangle = \frac{N(N-1)}{2} \frac{1}{V} \frac{4\pi\hbar^2 a}{m}. \quad (11.81)$$

This allows one to calculate the chemical potential

$$\mu = \frac{\partial E_0}{\partial N} \approx \frac{4\pi\hbar^2 a}{m} \frac{N}{V}. \quad (11.82)$$

11.4.4 Particle statistics

Our analysis thus far has assumed that the colliding particles were distinguishable, for example different atomic species or atoms of the same species in different electronic states. In order to apply our analysis to indistinguishable particles, we must consider the fact that scattering of identical particles by angle θ produces the same result as scattering by angle $\pi + \theta$. We will consequently need to sum over both possibilities:

$$\psi_k(r) = \frac{e^{ikz} + \epsilon e^{-ikz}}{\sqrt{2}} + \frac{f_k(\theta) + \epsilon f_k(\pi + \theta)}{\sqrt{2}} \frac{e^{ikr}}{r} \quad (11.83)$$

Since the two-particle wavefunction must be symmetric or antisymmetric under particle exchange, $\epsilon = +1$ for bosons and -1 for fermions.

Using this expression, we can find the scattering cross-section for identical particles:

$$\frac{d\sigma}{d\Omega} = \left| \frac{f_k(\theta) + \epsilon f_k(\pi + \theta)}{\sqrt{2}} \right|^2. \quad (11.84)$$

For even l partial waves, the two amplitudes add for bosons and subtract for fermions; for odd l partial waves, the amplitudes cancel for bosons and add for fermions. In particular, identical bosons will see a factor of 2 enhancement in their s-wave interaction cross-section, while identical fermions do not interact at all via the s-wave channel.

11.4.5 Scattering off an atomic ensemble

The formalism for treating two-particle scattering events can be compared to the quantum-optical problem of light scattering off a single atom. In both cases, the incident light or matter wave is modified by an outgoing radial (or dipole) wave. Likewise, both situations can be extended to include effects of many coherent scatterers: each emitted wave adds up in phase to produce a plane wave, modified from the incident wave by absorption and refraction.

To illustrate this analogy, we will consider a cold particle (or matter wave) incident on a slab of width L containing a dilute cloud of N cold atoms, such that their density n satisfies $na^3 \ll 1$. We will assume that the incident particle has wavevector $\mathbf{K} = K_z$ and position \mathbf{r}_0 , and we will label the positions of the j^{th} scatterer by \mathbf{r}_j . For this ensemble, $f_k(\theta) = -a$, so the many-body wavefunction may be written as

$$\psi_{\mathbf{K}}(\mathbf{r}_0, \mathbf{r}_1, \mathbf{r}_2, \dots, \mathbf{r}_N) = e^{iK_z x_0} - \sum_j \frac{a}{|\mathbf{r}_0 - \mathbf{r}_j|} e^{i|K||\mathbf{r}_0 - \mathbf{r}_j|} \quad (11.85)$$

$$= e^{iKz_0} - \sum_j \frac{a}{|\mathbf{r}_0 - \mathbf{r}_j|} e^{iK(r_0 - r_j)/2} e^{iK(z_0 + z_j)/2}.$$

By tracing over the positions of the scattering particles $\mathbf{r}_1, \mathbf{r}_2, \dots, \mathbf{r}_N$, we can obtain the transmitted matter wave

$$\psi_K(\mathbf{r}_0) = e^{iKz_0} - n \int d^3 r_j \frac{a}{|\mathbf{r}_0 - \mathbf{r}_j|} e^{iK(r_0 - r_j)/2} e^{iK(z_0 + z_j)/2} \quad (11.86)$$

Far beyond the slab of scatterers, $z_0 \gg L$, the wave is of the form

$$\psi_k(z_0) = A e^{iKz_0}, \quad (11.87)$$

where

$$A \approx e^{i4\pi a n L / K}. \quad (11.88)$$

The slab has produced a phase shift

$$\delta K = \frac{-4\pi a n}{K}, \quad (11.89)$$

which corresponds to the effective potential energy shift caused by interactions with atoms in the slab. In particular, the change in kinetic energy while the particle is in the slab is

$$\delta \left(\frac{\hbar^2 K^2}{2m} \right) = \frac{4\pi \hbar^2 a n}{m}. \quad (11.90)$$

This change in kinetic energy corresponds energy cost associated with the mean-field potential energy in the slab.

11.4.6 Resonances

In quantum dilute gases, it is possible to find situations where the scattering length far exceeds the size of the van der Waals tail $a \gg r_0$. In this regime,

$$ka \sim 1 \quad (11.91)$$

$$kr_0 \ll 1, \quad (11.92)$$

so the gas is cold and dilute, but strongly interacting. Liquids are strongly interacting, but because they are not dilute $kr_0 \sim 1$, the perturbative expansion in partial waves is invalid, so we must take into account p-wave, d-wave, etc... scattering amplitudes in addition to the s-wave channel. The

cold dilute, strongly interacting gases thus provide a novel system for studying purely s-wave, strong interactions.

One particularly interesting feature of the dilute gases is that it is possible to find situations where $a \gg r_0$. This limit corresponds to the s-wave resonance, where $ka \sim 1$ but a small parameter $kr_0 \ll 1$ still exists. For large and positive a , the resonance in the scattering length is connected to the appearance of a peculiar weakly bound state with radial wavefunction

$$R_0^{(0)}(r) = \frac{e^{-r/a}}{\sqrt{2\pi ar}}, \quad (11.93)$$

and energy

$$E_0 = -\frac{\hbar^2}{2\mu a^2}. \quad (11.94)$$

This corresponds to a bound state of the attractive van der Waals tail with energy very close to zero.

A number of interesting phenomena arise near this resonance, and it is possible to form molecules in these weakly bound states. There are two methods for molecule formation:

- (1) Cool a gas with positive scattering length $a > 0$ to temperatures below the binding energy $k_B T < E_0$
- (2) Prepare a cold gas with negative scattering length $a < 0$ and sweep through the resonance $a \rightarrow -\infty \rightarrow \infty \rightarrow a > 0$.

The second method can only be accomplished if we can somehow controllably manipulate the interatomic potential $U(r)$ to change the scattering length. Feshbach resonances provide one technique for controlling the scattering length.

Feshbach Resonances

Until this point, we have considered scattering of atoms in their ground state, and have neglected any effects associated with internal states of the atoms. In reality, we have to take into account other scattering channels, for example singlet or triplet states of the two atoms. For example, suppose there are two channels, each with their own effective interatomic potential $U_o(r)$ and $U_c(r)$. The higher energy channel is referred to as the “closed” channel because it presents a higher potential barrier for quasibound states.

Both channels obey a Schrodinger equation, and if there is some small interaction g between the two channels, their Schrodinger equations are

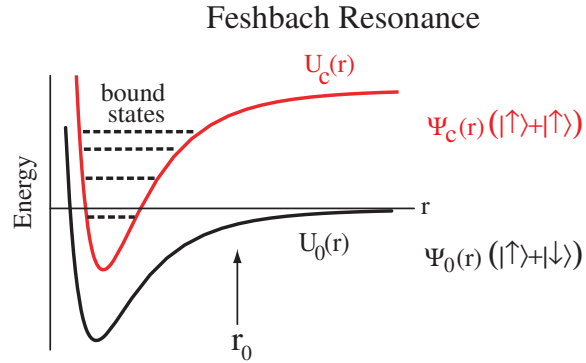


Figure 11.8: The upper potential corresponds to a “closed” channel, with many unoccupied bound states. The lower or “open” channel corresponds to the initial internal state of the atoms. When a bound state in the closed channel approaches the threshold energy in the open channel, any small coupling between the two channels can have a large effect, leading to dramatic changes in the scattering length in the open channel.

coupled:

$$\left(\hat{\xi} + U_o(r) - E \right) \psi_o + g \psi_c = 0 \quad (11.95)$$

$$\left(\hat{\xi} + U_c(r) - E \right) \psi_c + g \psi_o = 0, \quad (11.96)$$

where $\hat{\xi}$ is the kinetic energy operator. Let ψ_c^m be a complete set of orthonormal eigenfunctions of

$$\left(\hat{\xi} + U_c(r) - E_m \right) \psi_c^m = 0, \quad (11.97)$$

and expand ψ_c in terms of them:

$$\psi_c = \sum_{m=1}^{\infty} \alpha_m \psi_c^m. \quad (11.98)$$

Substituting into Eq. (11.96) and taking the inner product with ψ_c^n yields the coefficients

$$\alpha_n = - \frac{\langle \psi_c^n | g | \psi_o \rangle}{E_n - E}. \quad (11.99)$$

Close to resonance, only one of these coefficients α_{res} will have an appreciable physical effect, so the closed channel wavefunction is approximately given by

$$\psi_c(r) \approx -\frac{\langle \psi_c^{res} | g | \psi_o \rangle}{E_{res} - E} \psi_c^{res}(r). \quad (11.100)$$

We now substitute this expression into Eq. (11.96) to find the effect of the nearly resonant closed channel on the Schrodinger equation for the open channel

$$\left(\hat{\xi} + U_o(r) - E \right) \psi_o(r) = g(r) \frac{\langle \psi_c^{res} | g | \psi_o \rangle}{E_{res} - E} \psi_c^{res}(r). \quad (11.101)$$

To solve this equation, we can make use of the homogeneous solution

$$\left(\hat{\xi} + U_o(r) - E \right) \chi = 0 \rightarrow \chi = 1 - \frac{a_{bg}}{r}, \quad (11.102)$$

where a_{bg} is the background scattering length of the open channel in the absence of any effects from the closed channel. There are many possible solutions to the inhomogenous equation

$$\left(\hat{\xi} + U_o(r) - E \right) \eta = g(r) \psi_c^{res}(r), \quad (11.103)$$

and we will choose the one which behaves as

$$\eta = A \left(1 - \frac{b}{r} \right), \quad (11.104)$$

where the constants A and b are determined by the potential energy curve and coupling constant. The complete solution is a superposition of the homogeneous and inhomogeneous solution

$$\psi_o = \alpha \chi + \beta \eta = (\alpha + \beta A) - \frac{\alpha a_{bg} + \beta A b}{r}, \quad (11.105)$$

which corresponds to an effective scattering length

$$a = a_{bg} + A \frac{b - abg}{\frac{\alpha}{\beta} + A}, \quad (11.106)$$

where all of the parameters are known with the exception of α/β . Again substituting $\psi_o = \alpha \chi + \beta \eta$ into the second Schrodinger equation Eq. (11.101),

a bit of algebra allows one to solve for the unknown ratio, yielding the scattering length:

$$a = a_{bg} \left(1 + \frac{\overbrace{(A/a_{bg})(b - a_{bg})\langle\psi_c^{res}|g|\eta\rangle}^{\Delta}}{\underbrace{E_{res} + \langle\psi_c^{res}|g|A\chi - \eta\rangle - E}_{E_{res}^*}} \right), \quad (11.107)$$

where the denominator can be rewritten in terms of a shifted resonance energy. If the different channels correspond to atomic states with different magnetic moments, the resonance energy can be shifted by tuning the magnetic field $E_{res}^* \propto \mu_B(B - B_0^*)$. For low-energy collisions, as expected in ultracold atomic gases,

$$a = a_{bg} \left(1 + \frac{\Delta}{E_{res}^* - E} \right) \quad (11.108)$$

$$\approx a_{bg} \left(1 + \frac{\Delta}{E_{res}^*} \right), \quad (11.109)$$

$$(11.110)$$

the scattering length diverges near the critical magnetic field where the closed channel bound state is resonant with the threshold energy of the open channel.

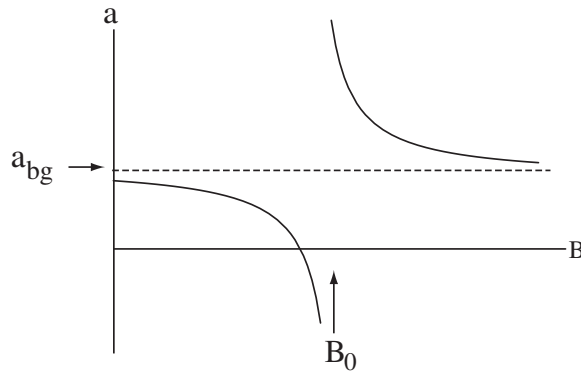


Figure 11.9: The form of the scattering length in the vicinity of a Feshbach resonance

Feshbach resonances are typically extremely narrow, with a typical width of a few Gauss. For the ultracold atoms, the scattering length is well defined $\Delta B \sim 10G \Rightarrow \Delta \sim 500\mu\text{K}$, since the resonance width is much greater than typical atomic temperatures $\sim 1\mu\text{K}$.

One should note that the binding energy of the weakly bound level is not equal to the energy of the resonance level. Near resonance, this binding energy takes the form

$$|E_0| = \frac{\hbar^2}{2\mu a^2} \approx \frac{\hbar^2}{2\mu} \frac{(E_{res}^*)^2}{a_{bg}^2 \Delta^2} \neq E_{res}. \quad (11.111)$$

11.4.7 Quantum theory of an interacting Bose gas

A weakly interacting, dilute atomic gas can be well described by a Hamiltonian which incorporates single-particle terms and two-body interactions,

$$\hat{H} = \sum_{i=1}^N \left(\frac{p_i^2}{2m} + V_{\text{trap}(r_i)} \right) + \sum_{\langle ij \rangle} V_{\text{int}}(r_i - r_j), \quad (11.112)$$

where r_0 is the typical range of the interaction potential. In cold, dilute atomic gases where $\mathbf{k} \cdot \mathbf{r}_0 \ll 1$, the interaction potential can be replaced by the s-wave pseudopotential

$$V_{\text{int}}(r) \approx \underbrace{\frac{4\pi\hbar^2 a}{m}}_{U_0} \delta(r), \quad (11.113)$$

where all of the properties of the interatomic potential are represented by one parameter, the scattering length a . In principle, we could now begin to calculate the ground state and dynamics of the N atoms in the ensemble. Since the atoms are indistinguishable, however, we would have to be careful to symmetrize (for bosons) or antisymmetrize (for fermions) our wavefunctions, which becomes quite inconvenient for large numbers of atoms. Instead, we will rewrite this Hamiltonian in the language of second quantization, which implicitly incorporates the indistinguishability of the atoms.

Second quantization

The second quantization formalism for matter waves resembles closely the methods used to quantize the electromagnetic field. As for photons, we will consider a complete set of single-atom states $\{|\zeta\rangle\}$, and define creation and

annihilation operators $\hat{b}_\zeta, \hat{b}_\zeta^\dagger$ which can add or remove an atom from those states

$$\hat{b}_\zeta |\zeta\rangle = |\text{vac}\rangle \quad (11.114)$$

$$\hat{b}_\zeta^\dagger |\text{vac}\rangle = |\zeta\rangle. \quad (11.115)$$

The statistics of the atoms determine the commutation properties of these operators.

$$\text{Bosons: } [\hat{b}_\zeta, \hat{b}_{\zeta'}^\dagger] = \delta_{\zeta, \zeta'} \quad (11.116)$$

$$\text{Fermions: } \{\hat{b}_\zeta, \hat{b}_{\zeta'}^\dagger\} = \delta_{\zeta, \zeta'}, \quad (11.117)$$

where $[A, B] = AB - BA$ is the commutator and $\{A, B\} = AB + BA$ is the anticommutator. Since the commutation relations guarantee the symmetry or anti-symmetry of the resulting wave-functions, this formalism provides a convenient tool for treating indistinguishable particles.

Many-body states are easily represented in terms of these creation and annihilation operators acting on the vacuum state. For example, a state $|\phi\rangle$ with n_i atoms in the single-particle state $|\zeta_i\rangle$ can be represented by

$$|\phi\rangle = |n_1, n_2 \dots\rangle = \prod_i (\hat{b}_i^\dagger)^{n_i} |\text{vac}\rangle. \quad (11.118)$$

For example, in the case of bosons, field operators are analogous to the creation and annihilation operators for the electromagnetic field modes:

$$\hat{b}_\zeta |\phi\rangle = \sqrt{n_\zeta + 1} |n_1, n_2 \dots n_\zeta + 1, \dots\rangle \quad (11.119)$$

$$\hat{b}_\zeta^\dagger |\phi\rangle = \sqrt{n_\zeta} |n_1, n_2 \dots n_\zeta - 1, \dots\rangle. \quad (11.120)$$

Although we will concentrate on bosons here, it is worth noting that the rules for raising and lowering fermion number are similar, but one must keep track of the negative signs which arise from anticommutation.

One particularly useful basis is the momentum basis, $|k\rangle$, with its associated creation and annihilation operators \hat{b}_k and \hat{b}_k^\dagger . In this case, there is an exact analogy between bosonic atoms and photons. Moreover, we can take the Fourier transform of these operators to define a real-space operator for the matter field

$$\hat{\psi}(\mathbf{r}) = \frac{1}{\sqrt{V}} \sum_{\mathbf{k}} e^{i\mathbf{k}\cdot\mathbf{r}} \hat{b}_{\mathbf{k}}, \quad (11.121)$$

where the allowed \mathbf{k} -vectors are determined by the boundary conditions at the edges of the quantization volume V . Using the commutation relation

$[\hat{b}_k, \hat{b}_{k'}^\dagger] = \delta_{k,k'}$ and the identity $\sum_k e^{i(\mathbf{k} \cdot (\mathbf{r} - \mathbf{r}'))} = V\delta(\mathbf{r} - \mathbf{r}')$, we can find the commutation rules for $\hat{\psi}(r)$:

$$[\hat{\psi}(\mathbf{r}), \hat{\psi}(\mathbf{r}')^\dagger] = \delta(\mathbf{r} - \mathbf{r}'). \quad (11.122)$$

Physically, $\hat{\psi}(\mathbf{r})$ can be interpreted as an operator which annihilates a particle at position \mathbf{r} .

Operators in the second quantization representation

Every atomic observable can be represented in terms of the matter field creation and annihilation operators. For example, the number operator is

$$\hat{N} = \sum_\zeta \hat{b}_\zeta^\dagger \hat{b}_\zeta = \int d^3\mathbf{r} \hat{\psi}(\mathbf{r})^\dagger \hat{\psi}(\mathbf{r}). \quad (11.123)$$

The Hamiltonian in Eq. (11.112) can also be written in terms of $\hat{\psi}(\mathbf{r})$:

$$\hat{H} = \int d^3\mathbf{r} \hat{\psi}(\mathbf{r})^\dagger \left(\frac{\hat{p}^2}{2m} + V_{\text{trap}}(\mathbf{r}) \right) \hat{\psi}(\mathbf{r}) \quad (11.124)$$

$$+ \frac{1}{2} \int d^3\mathbf{r} \int d^3\mathbf{r}' \hat{\psi}(\mathbf{r})^\dagger \hat{\psi}(\mathbf{r}')^\dagger \hat{V}(\mathbf{r} - \mathbf{r}') \hat{\psi}(\mathbf{r}') \hat{\psi}(\mathbf{r}). \quad (11.125)$$

When the interatomic potential can be replaced by the s-wave pseudopotential, the second term can be considerably simplified, so that the Hamiltonian becomes

$$\hat{H} = \int d^3\mathbf{r} \hat{\psi}(\mathbf{r})^\dagger \left(\frac{\hat{p}^2}{2m} + V_{\text{trap}}(\mathbf{r}) + \frac{U_0}{2} \hat{\psi}(\mathbf{r})^\dagger \hat{\psi}(\mathbf{r}) \right) \hat{\psi}(\mathbf{r}). \quad (11.126)$$

Zero temperature non-interacting BEC

It is instructive to consider the ground state at zero temperature in two types of potentials:

- (1) Homogeneous potential
- (2) Harmonic oscillator potential

The single particle states for these potentials are well known, and at zero temperature we expect all of the atoms to pile into the ground state. In the case of the infinite wall square well,

$$\psi_0(r) \sim \sin \pi x/L \sin \pi y/L \sin \pi z/L. \quad (11.127)$$

The harmonic oscillator ground state wavefunction is a Gaussian

$$\phi_0(r) = \frac{e^{-\left(\frac{x^2}{2a_x^2} + \frac{y^2}{2a_y^2} + \frac{z^2}{2a_z^2}\right)}}{\pi^{3/4}(a_x a_y a_z)^{1/2}}, \quad (11.128)$$

where $\{a_x, a_y, a_z\}$ are the harmonic oscillator lengths associated with the trapping frequencies $\{\omega_x, \omega_y, \omega_z\}$ in each dimension: $a_j^2 = \frac{\hbar}{m\omega_j^2}$. If the atoms do not interact, then the many-body state can be written as

$$|\Psi\rangle = (\hat{b}_0^\dagger)^N |\text{vac}\rangle, \quad (11.129)$$

where \hat{b}_0 annihilates an atom in the ground state of the appropriate potential.

Weak interactions: the Gross-Pitaevski equation

If the interactions are sufficiently weak, then we qualitatively expect that Bose condensation should still occur, with most of the atoms occupying one quantum state. We now need to determine which state will be macroscopically occupied.

Using the Hamiltonian given in Eq. (11.126), we can find the Heisenberg equations of motion for the matter field operator

$$i\hbar \frac{\partial}{\partial t} \hat{\psi} = [\hat{\psi}, \hat{H}] = \left(-\frac{\hbar^2 \nabla^2}{2m} + V_{\text{trap}} + U_0 \hat{\psi}^\dagger \hat{\psi} \right) \hat{\psi}. \quad (11.130)$$

This type of nonlinear operator equation is in general quite difficult to solve, but we can use our physical intuition to find an appropriate approximation. In particular, since we expect macroscopic occupation of one state, the field operator should be close to a classical coherent field

$$\hat{\psi} = \psi + \hat{\delta\psi}, \quad (11.131)$$

where $\langle \hat{\delta\psi} \rangle = 0$. When these fluctuations around the mean value are small

$$\langle \hat{\delta\psi}^\dagger \hat{\delta\psi} \rangle \ll \langle \hat{\psi}^\dagger \hat{\psi} \rangle, \quad (11.132)$$

the Bose condensate can be well described by a classical nonlinear equation for ψ , known as the Gross-Pitaevski equation:

$$i\hbar \frac{\partial \psi}{\partial t} = -\frac{\hbar^2}{2m} \nabla^2 \psi + V_{\text{trap}} \psi + U_0 |\psi|^2 \psi. \quad (11.133)$$

The Gross-Pitaevski equation resembles a Schrodinger equation with a nonlinear term, where ψ acts like the wavefunction for the Bose condensate.

Since ψ acts like a wavefunction, we should be careful about its normalization, which is set by the total number of particles

$$N = \int d^3r |\psi|^2. \quad (11.134)$$

This normalization condition motivates us to interpret $|\psi(r)|^2$ as the condensate spatial density.

Before proceeding, we note that replacing the operator quantity $\hat{\psi}$ by the c-number quantity ψ is strictly speaking only valid if the atom field is in a coherent state $\hat{\psi}|\psi\rangle = \psi|\psi\rangle$. The matter-wave coherent state is analogous to the electromagnetic coherent state in the sense that it has a non-vanishing classical coherence $\langle\hat{\psi}\rangle = \psi$, a well-defined phase $\propto \psi$, and a distribution of possible atom numbers centered at $\langle\int dV \hat{\psi}^\dagger \hat{\psi}\rangle = \int dV |\psi|^2$. Our derivation of the Gross-Pitaevski equation implicitly assumes that the condensate is in a coherent state with an arbitrary phase (this represents a so-called symmetry breaking description). The validity of this assumption is not obvious, but for large atom numbers it provides an excellent description of condensate dynamics.

The Gross-Pitaevski equation provides an adequate description of most properties of zero temperature Bose condensates, and it bears a strong resemblance to the evolution of the electromagnetic field in a Kerr medium. The relevant questions for a matter field, however, are rather different than those for light.

The ground state of a condensate at T=0

The ground state of the electromagnetic field is the vacuum, but matter behaves rather differently because the total number of atoms is conserved, resulting in a finite chemical potential. The ground state is a stationary solution of the Gross-Pitaevski equation with phase evolution

$$\psi = \tilde{\psi} e^{-i\mu t/\hbar}, \quad (11.135)$$

where $\tilde{\psi}$ obeys

$$\mu\tilde{\psi} = \underbrace{\left(-\frac{\hbar^2}{2m}\nabla^2 + V(r)\right)}_{\sim\hbar\omega_t} \underbrace{U_0|\tilde{\psi}|^2}_{E_{mf}} \tilde{\psi}. \quad (11.136)$$

The character of the solution $\tilde{\psi}$ is determined by the relative importance of the kinetic energy terms and the interaction terms. The ratio of the trap frequency $\hbar\omega_t$ to the mean-field interaction energy $E_{mf} \sim U_0 N/V$ is

$$\frac{E_{mf}}{\hbar\omega_t} \approx \frac{4\pi N a a_t^2}{V} \sim \frac{Na}{a_t}, \quad (11.137)$$

where a is the scattering length and a_t is the characteristic size of the harmonic oscillator trap. Note that the number of condensed atoms appears in the numerator of this expression, so even when the gas is weakly interacting ($a \ll a_t$) the interactions can still have important effects on the condensate behaviour. When $\hbar\omega_t \gg E_{mf}$, the condensate behaves essentially as a non-interacting gas. In the opposite limit $\hbar\omega_t \ll E_{mf}$ (known as the Thomas-Fermi regime for $U_0 > 0$) the interactions dominate.

The Thomas-Fermi approximation

When the interactions between atoms are strong and repulsive $U_0 > 0$, we can neglect the kinetic energy term. The resulting solution for the mean field is

$$|\tilde{\psi}|^2 = \begin{cases} \frac{\mu - V(r)}{U_0} & \text{for } r \text{ such that } V(r) < \mu \\ 0 & \text{for larger } r. \end{cases} \quad (11.138)$$

The chemical potential μ is set by the normalization condition

$$N = \int \frac{\mu - V(r)}{U_0} d^3r = N. \quad (11.139)$$

For example, a BEC confined by a harmonic trap has a chemical potential given by

$$\mu = \frac{\hbar\omega_t}{2} \left(\frac{15Na}{a_t} \right)^{2/5}. \quad (11.140)$$

Since we are in the regime of strong interactions, the factor $Na/a_t \gg 1$ increases the chemical potential significantly. The size \bar{a} of the condensate also increases due to interactions,

$$\bar{a} = a_t \cdot \left(\frac{15Na}{a_t} \right)^{2/5}. \quad (11.141)$$

This expansion makes physical sense because it lowers the energy cost of the repulsive interactions.

The healing length

The Thomas-Fermi approximation works poorly in regions where the atom density is insufficient to satisfy the assumption that the mean-field energy overwhelms kinetic energy. In particular, in the vicinity of the walls of the traps, the kinetic energy can no longer be neglected. For example, consider a condensate in a box with infinite potential walls. The Thomas-Fermi approximation would predict that $\tilde{\psi} = N/V$ is constant, dropping off suddenly to zero right at the edges of the box. Physically, this makes no sense: the wavefunction must be smooth even at the walls because sharp variations in $\tilde{\psi}(r)$ exact a high kinetic energy cost. We expect the wavefunction to fall off smoothly over some characteristic length ξ . This so-called “healing length” can be estimated by equating the kinetic energy associated with variation on length ξ with the interaction energy $\sim U_0 N/V$, which results in

$$\xi^2 = \frac{1}{8\pi a N/V} = \frac{1}{8\pi n_0 a}. \quad (11.142)$$

As long as the gas is sufficiently dilute $n_0 a^2 \ll 1$, the healing length extends over many atoms

$$\xi \gg \frac{1}{n_0^{3/2}}. \quad (11.143)$$

When this dilute gas assumption breaks down, the Gross-Pitaevski equation can no longer provide an adequate description of the condensate. We also note that the above discussion is valid only for repulsive atoms; we will find that problems arise for attractive interactions when the kinetic energy approaches the mean-field energy.

11.5 Excitations in a Bose condensate

We have developed a basic understanding of the ground state wavefunction for a Bose-Einstein condensate; a more complete picture of condensate behaviour requires knowledge of the elementary excitations in a BEC. A description of such excitations will allow us to account for the spectrum of the condensate, thermal effects at finite temperatures, and possible non-classical effects analogous to squeezing of a photon field.

11.5.1 The Bogoliubov approximation

Our approach is motivated by an analogy to classical coherent beams, where the electric field operator $\hat{\mathcal{E}}$ is well approximated by a c-number \mathcal{E} and

some small operator deviation $\delta\hat{\mathcal{E}}$. For matter waves, we will replace the field operator with its average value and some small fluctuations about that average

$$\hat{\psi} = \psi + \delta\hat{\psi}. \quad (11.144)$$

We can then linearize the Heisenberg equation for $\hat{\psi}$ in the small quantity $\delta\hat{\psi}$, obtaining a set of linear coupled equations for $\delta\hat{\psi}$ and $\delta\hat{\psi}^\dagger$:

$$i\hbar\frac{\partial}{\partial t}\delta\hat{\psi} = \left(-\frac{\hbar^2}{2m}\nabla^2 + V(r)\right)\delta\hat{\psi} + U_0\delta\hat{\psi}^\dagger\psi^2 + 2U_0|\psi|^2\delta\hat{\psi}, \quad (11.145)$$

and similar for the hermitian conjugate.

Since these coupled equations are linear, we can solve them by looking for normal mode solutions. We will define operators \hat{a}_j and \hat{a}_j^\dagger which annihilate and create bosonic excitations in the normal mode with frequency ω_j ; since the excitations are bosons, their creation and annihilation operators obey Bose statistics $[\hat{a}_j, \hat{a}_k^\dagger] = \delta_{jk}$. We can expand $\delta\hat{\psi}$ in terms of the normal modes

$$\delta\hat{\psi} = e^{-i\mu t/\hbar} \sum_j \left(u_j(r) \hat{a}_j e^{-i\omega_j t} + v_j^*(r) \hat{a}_j^\dagger e^{i\omega_j t} \right), \quad (11.146)$$

and the field operator will be properly normalized if

$$|u_j|^2 - |v_j|^2 = 1. \quad (11.147)$$

When we substitute our expansion for $\delta\hat{\psi}$ Eq. (11.145), we find that the coefficients for each normal mode are independent, so we obtain a set of equations for each mode j . Equating terms $\propto e^{i\omega_j t}$ and $\propto e^{-i\omega_j t}$, we find

$$\left(-\mu - \omega_j(r) - \frac{\hbar^2\nabla^2}{2m} + V(r) + 2U_0\tilde{\psi}^2 \right) u_j(r) = U_0\tilde{\psi}^2 v_j(r) \quad (11.148)$$

$$\left(-\mu + \omega_j(r) - \frac{\hbar^2\nabla^2}{2m} + V(r) + 2U_0\tilde{\psi}^2 \right) v_j(r) = U_0\tilde{\psi}^2 u_j(r) \quad (11.149)$$

where $\psi = \tilde{\psi}e^{-i\mu t/\hbar}$ and $\tilde{\psi} \in \mathbb{R}$. These time independent equations give the eigenfrequencies ω_j and eigenmodes $\{u_j, v_j\}$ of excitations in the condensate, and are known as the “Bogoliubov equations”.

Example: homogeneous potential

The Bogoliubov equations are particularly transparent for a condensate in a uniform potential $V(x) = 0$. The Thomas-Fermi approximation gives

$\tilde{\psi} = \sqrt{n_0}$, where n_0 is the condensate density and $\mu = n_0 U_0$ is the chemical potential. Since there is no explicit dependence on position anywhere in the problem, the eigenmodes are most easily obtained in the Fourier domain,

$$u_j(r) = u_q e^{iqr} \quad (11.150)$$

$$v_j(r) = v_q e^{iqr}. \quad (11.151)$$

The Bogoliubov equations become

$$\begin{pmatrix} \epsilon_q + n_0 U_0 - \hbar\omega_q & -n_0 U_0 \\ -n_0 U_0 & \epsilon_q + n_0 U_0 + \hbar\omega_q \end{pmatrix} \begin{pmatrix} u_q \\ v_q \end{pmatrix} = 0, \quad (11.152)$$

where $\epsilon_q = \hbar^2 q^2 / 2m$. To find the eigenvalues and eigenmodes associated with excitations in the homogenous condensate, we need only solve this matrix equation. The frequencies $\omega_q(q)$ follow from setting the determinant of the matrix to zero, yielding the dispersion relation

$$\hbar\omega_q = \sqrt{\epsilon_q^2 + 2n_0 U_0 \epsilon_q}. \quad (11.153)$$

Due to the presence of interactions, the dispersion relation is qualitatively different from that of a free particle $\hbar\omega_q = \epsilon_q$. In the large-wavenumber and small-wavenumber regimes, the frequency is

$$\hbar\omega_q = \begin{cases} \epsilon_q + n_0 U_0 & \text{large } q \\ \hbar q s & \text{small } q, \end{cases} \quad (11.154)$$

which correspond to particle-like and sound-like excitations respectively. The sound-like spectrum has an associated sound velocity

$$s = \sqrt{\frac{n_0 U_0}{m}}, \quad (11.155)$$

and the cross-over between the two regimes occurs near a critical wave-vector

$$q_c \sim \hbar \sqrt{2mn_0 U_0} \sim \frac{1}{\xi} \sim \frac{ms}{\sqrt{2}\hbar}. \quad (11.156)$$

Physically, the long-wavelength excitations correspond to collective excitations of the condensate, and are responsible for the phenomenon of superfluidity. Once the wavelength approaches the inverse healing length, the condensate ceases to behave as a continuum, and single-particle-like excitations dominate.

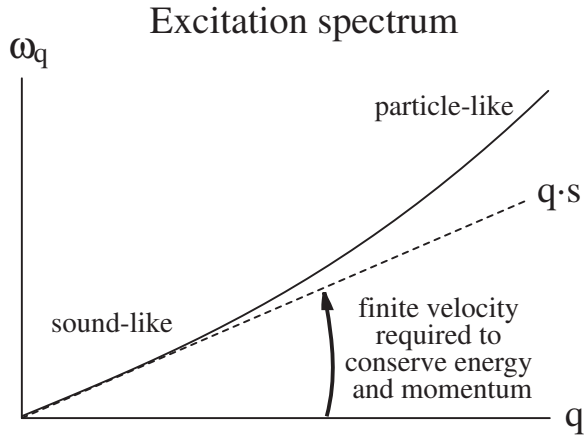


Figure 11.10: The Bogoliubov excitation spectrum for a condensate confined in a homogeneous potential. Note that in the presence of interactions, a critical velocity must be reached in order to excite the condensate while conserving energy and momentum.

Probing the excitation spectrum

Experiments have measured the excitation spectrum in a gaseous Bose condensate using a Bragg scattering technique. Two lasers with frequencies ω_1, ω_2 and wavevectors k_1 and k_2 interact with the condensate via a Hamiltonian

$$\hat{H} = \int d^3 p \hat{b}_p \hat{b}_{p+q}^\dagger \hbar \Omega_q + h.c. \quad (11.157)$$

transferring momentum $q = k_1 - k_2$ to excitations within the cloud. When the energy difference $\omega_1 - \omega_2$ is resonant with the energy of the excitation ω_q , the lasers create a collective excitation. By measuring the spectrum of such resonances, one can determine the sound velocity in the condensate.

Superfluidity of repulsive atoms

Superfluidity requires that an object can move slowly through the fluid without experiencing any drag. Since drag is the macroscopic manifestation of excitations in a medium, we will see that the excitation spectrum of a repulsive Bose condensate implies superfluidity. In particular, consider an object moving at velocity v through a Bose condensate. It will only create

an excitation if it can resonantly impart its momentum and energy to an elementary excitation:

$$\Delta p_{\text{object}} = \hbar q \quad (11.158)$$

$$\Delta \epsilon_{\text{object}} = \epsilon_q. \quad (11.159)$$

Kinematics require that $\Delta \epsilon_{\text{object}} \leq \Delta p v$, so the object can only create an excitation if it is moving faster than some critical velocity

$$v > v_c = \frac{\epsilon_q}{\hbar q}. \quad (11.160)$$

This represents the so-called Landau criterion for superfluidity, which states that objects moving slower than the speed of sound do not produce excitations.

11.5.2 BEC with attractive interactions

If the interatomic potential is attractive $U_0 < 0$, long-wavelength excitations $q \rightarrow 0$ have an imaginary frequency $\hbar\omega_q$. This implies that the condensate is unstable! Experimentally, however, stable condensates with attractive interactions have been observed. The explanation for the stability lies in the finite number of atoms confined to the trap.

If an atomic cloud is localized within a characteristic trap length a_t , the minimum wave-vector allowed by the system is of order

$$q_{\min} \approx \frac{1}{a_t}, \quad (11.161)$$

so the excitations in the system have a minimum energy

$$\hbar\omega_{\min} = \sqrt{\epsilon_{q_{\min}}^2 - 2n_0|U_0|\epsilon_{q_{\min}}}. \quad (11.162)$$

When this minimum energy is real,

$$\frac{\hbar^2}{a_t^2 m} \geq 4n_0 U_0 = \frac{16\pi\hbar^2 N}{mV} |a|, \quad (11.163)$$

the condensate will be stable despite the attractive interactions. In particular, this implies a maximum number of atoms in the cloud

$$N_{\max} \sim \frac{a_t}{|a|}. \quad (11.164)$$

If condensate size exceeds N_{\max} , the attractive interactions will destabilize it and it will collapse.

11.5.3 Observation of BEC

As we mentioned earlier in the chapter, typical experiments probe the cold atom cloud using absorption imaging with near-resonant light. In certain cases, one could image the condensate in the trap, obtaining a spatial profile of the atom cloud. Alternately, by releasing the cold atom cloud from the trap and allowing it to expand for a time τ , the momentum distribution of the atoms p is mapped onto the spatial distribution $r = p\tau/m$. Such expansion images provide a means for distinguishing a cold, thermal atom cloud from a condensate. In a condensate, the momentum distribution follows from the size of the atom cloud a_c and the uncertainty principle,

$$p_{\text{BEC}} \sim \frac{\hbar}{a_c}, \quad (11.165)$$

resulting in a post-expansion spatial distribution

$$R_{\text{BEC}} \sim \frac{\hbar t}{a_c m} \quad (11.166)$$

In contrast, a thermal cloud of atoms will have a gaussian distribution of momenta in the trap

$$P_{\text{thermal}}(p) \sim e^{-p^2/p_T^2} \quad (11.167)$$

leading to a gaussian spatial distribution

$$P_{\text{thermal}}(R) \sim e^{-R^2/R_T^2}, \quad (11.168)$$

where R_T and p_T are the distance and momentum scale for an atom cloud at temperature T . The two momentum distributions are qualitatively different. By fitting the observed image to a bimodal distribution corresponding to a gaussian thermal cloud and a parabolic condensate, one can accurately calculate the proportion of condensed atoms.

11.6 First-order coherence of Bose condensates

Before delving into quantum states of a BEC, we will consider the classical coherence properties of the condensate, and discuss how they are measured experimentally.

11.6.1 Interference of two atomic clouds

Using expansion techniques, one can probe the classical coherence of an atomic cloud. Since the condensate wavefunction ψ has a well-defined (though arbitrary) phase, interference between two such condensates will result in observable fringes in the atom number distribution. These interference fringes are precisely analogous to the interference fringes seen for laser light split into two beams and then recombined, and they correspond to first-order coherence of the atomic matter wave.

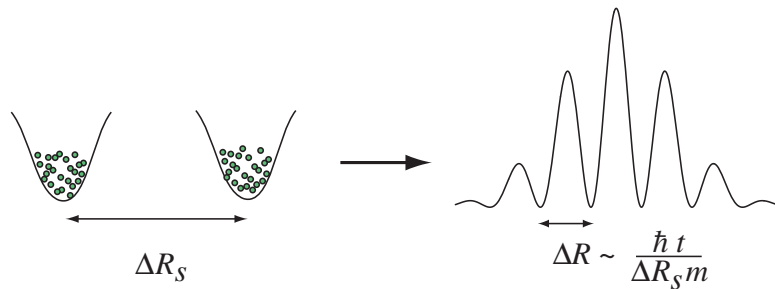


Figure 11.11: By allowing two classically coherent condensates separated by a distance ΔR_s to expand and interfere, one can observe fringes spaced by $\Delta R \sim \hbar\tau/\Delta R_s m$. Experiments at MIT (c.f. Andrews *et al.*, Science 275, p637 (2000)) observed these fringes. Two BECs, imaged in trap using phase-contrast imaging, were allowed to expand and interfere, producing interference fringes in the time-of-flight absorption image.

Just as incoherent light can exhibit limited interference fringes, first-order coherence can also occur in cold ensembles of uncondensed, thermal atoms. However, in thermal atoms the first-order coherence is only maintained over a distance of roughly the deBroglie wavelength, which corresponds to the size of the thermal atom wavepacket. In contrast, a condensate will exhibit long-range coherence, which extends over the entire condensed atom cloud.

To probe the transition from short-range thermal atom coherence to long range condensate coherence, a series of experiments were carried out using the atomic equivalent of a laser beam (see I. Bloch *et al.*, Nature 403 p166 (2000) for more details). The atom laser beam was created by outcoupling atoms from the trapped hyperfine state into an untrapped state

which experiences a magnetic field gradient¹. The frequency of the RF required to drive the atoms from the trapped to untrapped states includes the untrapped state Zeeman shift, and therefore depends on the atoms' position. Application of two RF frequencies thus outcouples atoms from two locations; the two outcoupled beams then interfere as they fall away from the cloud under the influence of gravity. The visibility of the interference fringes provides a measure of the first order coherence between the two outcoupled regions of the cloud. By varying the frequency of the RF fields, one can measure the first order coherence as a function of the distance between the two outcoupled regions. As shown in Figure 11.12, the thermal atom coherence dies off quickly with distance, whereas the coherence of the condensate fraction approaches a flat plateau as the distance increases.

11.6.2 Spontaneous symmetry breaking

Experimental observations clearly indicate that two independently prepared Bose condensates will interfere with one another. However, for a long time this was a subject of controversy: if the numbers of atoms in the two condensates, N_1 and N_2 , were precisely known, then how could the two clouds have a well-defined relative phase?

The establishment of a well-defined relative phase comes about through spontaneous symmetry breaking in the measurement process. As an example, suppose that an atom laser beam is outcoupled from each of the two condensates, and interference of the two atom lasers is measured to determine the relative phase of the two condensates. In order to build up statistics necessary to measure the interference pattern, one must measure atoms without knowing which condensate they came from. When one has detected enough atoms n to measure the phase of the interference pattern, one no longer knows the number of atoms remaining in the two condensates, $N_1 - n_1$ and $N_2 - n_2$, such that $n_1 + n_2 = n$. By projecting the relative phase onto the measured value, one introduces number uncertainty between the condensates.

11.7 Higher-order coherence of atomic matter waves

Quantum states of light often exhibit no first order coherence, but can have higher order coherences. We would like to know whether similar non-classical

¹The magnetic field gradient arises because the center of the trap is shifted from the magnetic field minimum by gravity, so the untrapped states have a position-dependent Zeeman energy.

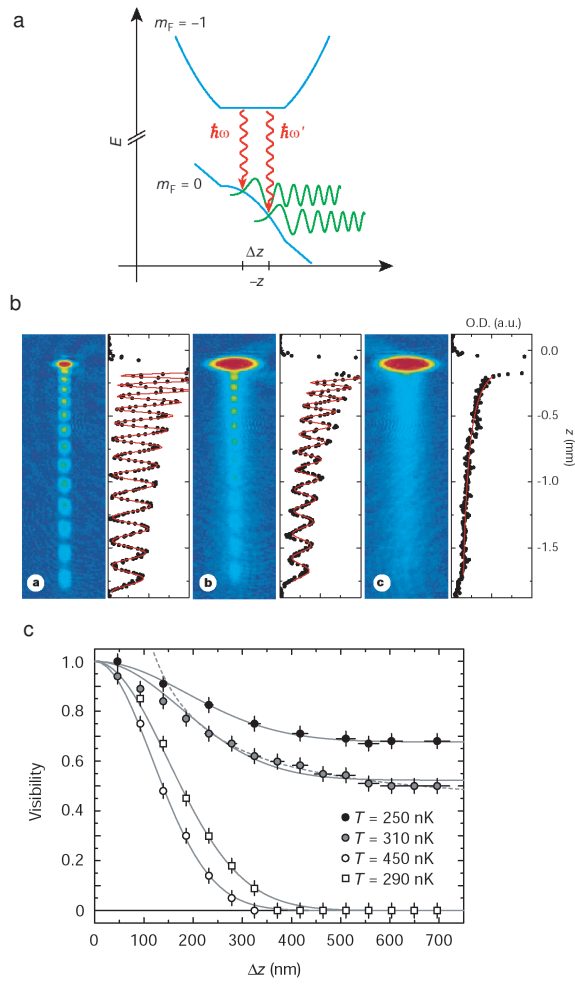


Figure 11.12: Measurement of the spatial coherence of a trapped Bose gas [figure taken from Nature 403 p166 (2000) without permission]. (a) Position-dependent Zeeman shifts are used to outcouple atoms from two regions in the cloud. (b) The outcoupled atoms interfere as they fall away from the cloud, and the visibility of the interference pattern reveals the degree of first-order coherence between the atomic wavefunctions at the two outcoupled positions. (c) The visibility of the interference fringes as a function of distance for four realizations. A true condensate maintains its coherence to long distances (upper two traces), whereas the thermal atom coherence dies off on a length scale set by the deBroglie wavelength (lower two traces).

states can appear in a BEC. In particular, one could inquire whether two condensates must always produce an interference pattern, or whether there are physically important effects which cannot be described by the Gross-Pitaevski equation. Since the atomic interactions introduce nonlinearity into the matter-wave field, it seems possible that such nonlinearities might indeed give rise to non-classical states.

11.7.1 Toy model: cold, interacting atoms in a double-well potential

As an example of how non-classical states of matter can arise from atomic interactions, we will consider N cold atoms confined to the double-well potential illustrated in Figure 11.13.

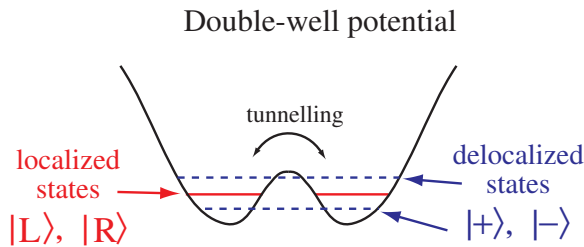


Figure 11.13: A double-well potential for cold atoms. A finite barrier separates the two localized states, so atoms can tunnel between them at rate t . This tunnelling produces two delocalized states: the ground state is a symmetric combination of left and right $|+\rangle = (1/\sqrt{2})(|L\rangle + |R\rangle)$, and the excited state $|-\rangle = (1/\sqrt{2})(|L\rangle - |R\rangle)$ is higher in energy by $2t$.

Noninteracting atoms

If the atoms do not interact, the Hamiltonian for the system includes only the kinetic energy or tunnelling terms:

$$\hat{H}_{\text{kin}} = -t\hat{a}_R^\dagger \hat{a}_L - t^* \hat{a}_L^\dagger \hat{a}_R \quad (11.169)$$

The ground state of the system $|\phi_N\rangle$ has all N atoms in the single-particle symmetric superposition state $|+\rangle$. Defining the annihilation operators for

the left and right potential well by $\{\hat{a}_L, \hat{a}_R\}$ respectively, we can write this ground state in second quantization notation

$$|\phi_N\rangle = \frac{(\hat{a}_L^\dagger + \hat{a}_R^\dagger)^N}{\sqrt{N!} \cdot 2^{N/2}} |\text{vac}\rangle. \quad (11.170)$$

This state has a well-defined phase between the particles on the left and the particles on the right, so $\langle \hat{a}_L^\dagger \hat{a}_R \rangle \neq 0$.

In fact, for large N this ground state is very close to a coherent state satisfying

$$\hat{a}_R |\alpha\rangle = \alpha |\alpha\rangle \quad (11.171)$$

$$\hat{a}_L |\alpha\rangle = \alpha |\alpha\rangle, \quad (11.172)$$

with $|\alpha_R|^2 = |\alpha|^2 = N/2$. This similarity arises because the number uncertainty for the coherent state goes as $1/\sqrt{N}$, and for large N the coherent state will give us an intuitive picture of the system behavior. In particular, if we indeed had two coherent states in the two wells with phases ϕ_R and ϕ_L , this device would correspond to a classical Josephson device, with a kinetic energy given by $E = -(Nt/2) \cos(\phi_R - \phi_L)$. It is worth emphasizing that the correspondence between the classical Josephson device and the quantum double well potential emerges only in the limit of large occupation number N .

Strongly interacting atoms

We now consider the opposite limit, where strong repulsive interactions dominate. We can thus neglect the tunnelling terms, so the Hamiltonian can be written as

$$\hat{H}_{\text{int}} = U_0 \left(\hat{a}_L^\dagger \hat{a}_L^\dagger \hat{a}_L \hat{a}_L + \hat{a}_R^\dagger \hat{a}_R^\dagger \hat{a}_R \hat{a}_R \right), \quad (11.173)$$

or, in terms of the number occupancy,

$$\hat{H}_{\text{int}} = U_0 (\hat{n}_L (\hat{n}_L - 1) + \hat{n}_R (\hat{n}_R - 1)). \quad (11.174)$$

If $U_0 \gg t$, then $|\phi_N\rangle$ is not a ground state of the multiparticle system, because the potential energy cost associated with the repulsive interaction overwhelms the kinetic energy benefit conferred on the delocalized states. For example, consider two strongly repulsive atoms in the double well potential. The best way to avoid interactions is for each atom to occupy its own well, so the ground state is

$$|\psi_2\rangle = \hat{a}_L^\dagger \hat{a}_R^\dagger |\text{vac}\rangle. \quad (11.175)$$

Although each atom pays an energy price of $\sim t$, the huge gain $\sim U_0$ from avoiding interaction more than compensates for the associated increase in kinetic energy. Similarly, in the ground state of the N -particle system, the atoms pile up evenly in the two wells, generating a highly non-classical Fock state

$$|\psi_N\rangle = (\hat{a}_L^\dagger \hat{a}_R^\dagger)^N |\text{vac}\rangle. \quad (11.176)$$

Such states do not display a first-order interference pattern, and cannot be described by the Gross-Pitaevski equation.

This example shows that creating non-classical states of matter requires a system where interactions are stronger than kinetic energy. However, it is also important to keep losses low, since these act to destroy non-classical coherences. In practice, there are two methods currently employed to produce Fock states of atoms. First, by confining atoms more tightly, for example in an optical lattice, one can decrease the tunnelling rate between different sites, thus decreasing the kinetic energy scale. Second, one can increase the scattering length a using, for example, a Feshbach resonance, to enhance the interactions.

11.7.2 Optical lattice potentials

A variety of experiments have used an optical lattice potential to confine atoms or other polarizable objects in one, two, or three-dimensional arrays. The optical lattice is based on the optical dipole force associated with the AC Stark shift from a red-detuned light source, which attracts the polarizable particles to the intensity maxima. Counterpropagating beams produce a standing wave with a period of $\lambda/2$, where λ is the wavelength of the red-detuned light source. By combining standing waves in multiple dimensions, one can create a simple cubic lattice with a potential

$$V(x) \propto \sin^2\left(\frac{2\pi x}{\lambda}\right) + \sin^2\left(\frac{2\pi y}{\lambda}\right) + \sin^2\left(\frac{2\pi z}{\lambda}\right), \quad (11.177)$$

plus a confining harmonic potential. The optical lattice potential resembles the double-well potential discussed above in that it can be parameterized by two quantities: the tunnelling rate between lattice sites, and the interaction strength for atoms occupying the same lattice site.

11.8 Cold atoms in an optical lattice

Before we discuss recent experimental advances in studying cold atoms in an optical lattice, we will begin by formulating a general theoretical framework

for analyzing indistinguishable atoms in a periodic potential. Our system of N atoms at positions $\{x_i\}$ is governed by a general Hamiltonian including two-particle interactions,

$$\hat{H} = \sum_{i=1}^N \frac{p_i^2}{2m} + V(x_i) + \sum_{j \neq i} \frac{1}{2} U(x_i - x_j), \quad (11.178)$$

where for sufficiently cold atoms the interaction potential may be replaced by the s-wave pseudopotential,

$$U(x_i - x_j) = \frac{4\pi\hbar^2 a_s}{m} \delta(x_i - x_j). \quad (11.179)$$

In the language of second quantization, where $\hat{\psi}^\dagger(\mathbf{r})$ creates a boson or fermion at position \mathbf{r} , the Hamiltonian may be written

$$\begin{aligned} \hat{H} = & \int \hat{\psi}^\dagger(\mathbf{r}) \left(\frac{p^2}{2m} + V(x) \right) \hat{\psi}(\mathbf{r}) d^3\mathbf{r} \\ & + \frac{1}{2} \frac{4\pi\hbar^2 a_s}{m} \int \hat{\psi}^\dagger(\mathbf{r}) \hat{\psi}^\dagger(\mathbf{r}) \hat{\psi}(\mathbf{r}) \hat{\psi}(\mathbf{r}) d^3\mathbf{r}. \end{aligned} \quad (11.180)$$

For bosons, the field operators obey commutation relations

$$[\hat{\psi}(\mathbf{r}), \hat{\psi}^\dagger(\mathbf{r}')] = \delta(\mathbf{r} - \mathbf{r}') \quad (11.181)$$

$$(11.182)$$

whereas for fermions they obey anticommutation relations

$$\{\hat{\psi}(\mathbf{r}), \hat{\psi}^\dagger(\mathbf{r}')\} = \delta(\mathbf{r} - \mathbf{r}'). \quad (11.183)$$

Our previous analysis of Bose condensates replaced the operator $\hat{\psi}$ by a c-number representing the macroscopic wavefunction of the condensate. This analysis was valid provided that the interactions were not too strong, i.e. the first term in the Hamiltonian dominated over the second. In an optical lattice, however, this hierarchy need not be obeyed, and we will need to go beyond the Gross-Pitaevskii equation to understand how the system behaves.

11.8.1 Atoms in a periodic potential

Atoms confined to an optical lattice will experience a potential $V(\mathbf{r})$ which is periodic. Under the assumption of a strong periodic potential, we can

find an approximate form for the Hamiltonian Eq. 11.180 which gives us a simpler formalism and greater physical intuition for the system.

First, we simplify the periodic potential itself. If the antinodes of the lattice occur at positions $\{\mathbf{r}_i\}$, then we can write the potential as

$$V(\mathbf{r}) = \sum_i \tilde{V}(\mathbf{r} - \mathbf{r}_i). \quad (11.184)$$

Near the intensity maxima (or potential energy minima), the atomic motion will approach that of a harmonic oscillator, so we can approximate the potential by

$$\tilde{V}(\mathbf{r} - \mathbf{r}_i) = V_0 K_L^2 (\mathbf{r} - \mathbf{r}_i)^2. \quad (11.185)$$

Each lattice site is a harmonic potential with a characteristic frequency

$$\nu_T = \sqrt{\frac{2V_0 K_L^2}{m}} = \sqrt{\frac{4V_0 E_R}{\hbar^2}}, \quad (11.186)$$

where $E_R = \frac{\hbar^2 K_L^2}{2m}$ is the recoil energy of the lattice. For sufficiently large trap depths $V_0 \gg E_R$, the atoms will be localized near the potential minima (this condition is analogous to the Lamb-Dicke limit for ion traps). Each site will have a set of harmonic oscillator wavefunctions $\phi_n(\mathbf{r} - \mathbf{r}_i)$ associated with it, and for sufficiently strong potentials $V_0 \gg E_R$ there will be very little overlap between wavefunctions in different wells. Finally, for sufficiently cold atoms only the ground state ϕ_0 will be occupied.

If there were no interactions between the lattice sites, then the atomic wavefunction could be expanded in terms of an orthonormal set of harmonic oscillator wavefunctions on each site, $\phi_n(\mathbf{r} - \mathbf{r}_i)$. Much as we saw in the case of the double-well potential, a tunnelling term will hybridize the harmonic oscillator levels, producing Bloch bands with a width given by the tunnelling strength and a separation given by the harmonic oscillator energy levels.

To derive the Bloch bands for atoms in a periodic potential, we will express the field operator as a sum over localized states

$$\hat{\psi} = \sum_i \hat{b}_i W(\mathbf{r} - \mathbf{r}_i), \quad (11.187)$$

where \hat{b}_i annihilates a particle at the i^{th} site, and satisfies

$$[\hat{b}_i, \hat{b}_j] = \delta_{ij} \quad (\text{bosons}) \quad (11.188)$$

$$\{\hat{b}_i, \hat{b}_j\} = \delta_{ij} \quad (\text{fermions}). \quad (11.189)$$

Strictly speaking, the expansion in terms of Wannier functions W requires that they be orthogonal to one another. For our purposes, however, it will be a good approximation to replace the Wannier functions by the harmonic oscillator ground state at site \mathbf{r}_i ,

$$\hat{\psi} \approx \sum_i \hat{b}_i \phi(\mathbf{r} - \mathbf{r}_i). \quad (11.190)$$

Taking this as a trial wavefunction and substituting it into the Hamiltonian yields

$$\begin{aligned} H &= \sum_{i,j} \hat{b}_i^\dagger \hat{b}_j \int \phi^*(\mathbf{r} - \mathbf{r}_i) \left(\frac{p^2}{2m} + V(\mathbf{r}) \right) \phi(\mathbf{r} - \mathbf{r}_j) d^3\mathbf{r} \\ &\quad + \frac{1}{2} \frac{4\pi\hbar^2 a_s}{m} \sum_{i,j,k,l} \int \hat{b}_i^\dagger \hat{b}_j^\dagger \hat{b}_k \hat{b}_l \phi^*(\mathbf{r} - \mathbf{r}_i) \phi^*(\mathbf{r} - \mathbf{r}_j) \phi(\mathbf{r} - \mathbf{r}_k) \phi(\mathbf{r} - \mathbf{r}_l) d^3\mathbf{r}. \end{aligned}$$

Since the overlap between wavefunctions at different sites is very small, we can calculate the Hamiltonian to leading order in this small parameter.

The leading order for the interaction term occurs for $i = j = k = l$, which means that we are only accounting for interactions between particles localized to the same site. This so-called “on-site” interaction term is

$$\begin{aligned} \hat{H}_{\text{int}} &= \frac{1}{2} \frac{4\pi\hbar^2 a_s}{m} \sum_i \int |\phi(\mathbf{r} - \mathbf{r}_i)|^4 \cdot \hat{b}_i^\dagger \hat{b}_i^\dagger \hat{b}_i \hat{b}_i \\ &= U_0 \sum_i \hat{n}_i (\hat{n}_i - 1). \end{aligned} \quad (11.191)$$

The strength of the onsite interaction is approximately given by the interaction energy associated with having two atoms confined to a volume the size of the harmonic oscillator ground state,

$$U_0 \sim \frac{2\pi a_s \hbar^2}{m a_{HO}^3}. \quad (11.192)$$

This calculation gives us a simple and physical form for the interaction term in the Hamiltonian Eq. 11.180.

There are both diagonal (involving only a single site i) and off-diagonal (involving two sites i and j) contributions to the kinetic energy term. The lattice site potential leads to a harmonic oscillator energy associated with the i^{th} site occupation, and any additional external potential $V_{\text{trap}}(\mathbf{r})$ will add to the energy of that site. In addition, we will need to keep track of

the lowest order overlap integrals. These occur for nearest-neighbor terms where $i = j \pm 1$, so that the kinetic energy term becomes

$$\begin{aligned}\hat{H}_{\text{kin}} &= \sum_i \left(V_{\text{trap}}(\mathbf{r}_i) + \frac{\hbar\nu_T}{2} \right) \hat{b}_i^\dagger \hat{b}_i \\ &\quad - \sum_{\langle i,j \rangle} \left(V_0 \int \phi^*(\mathbf{r} - \mathbf{r}_i) \phi(\mathbf{r} - \mathbf{r}_j) d^3\mathbf{r} \right) \hat{b}_i^\dagger \hat{b}_j \quad (11.193)\end{aligned}$$

$$= \sum_i \epsilon_i \hat{b}_i^\dagger \hat{b}_i - \sum_{\langle i,j \rangle} t_{i,j} \hat{b}_i^\dagger \hat{b}_j, \quad (11.194)$$

where $\langle i, j \rangle$ denotes a sum over all nearest neighbors. The first term is the energy associated with having a particle on lattice site i , whereas the second term allows atoms to hop from one lattice site to a nearest-neighbor site at a rate t . Note that the sign of the hopping term is negative. This occurs because the actual potential for any given lattice site is reduced from its bare value by the potentials for nearby lattice sites. Treating this difference in energy in perturbation theory allows tunnelling and reduces the overall energy of the system.

Putting the kinetic energy and interaction terms together yields a simple form for the Hamiltonian in terms of creation and annihilation operators for atoms on each lattice site:

$$\hat{H} = \sum_i \epsilon_i \hat{b}_i^\dagger \hat{b}_i - \sum_{\langle i,j \rangle} t_{i,j} \hat{b}_i^\dagger \hat{b}_j + U_0 \sum_i \hat{n}_i (\hat{n}_i - 1). \quad (11.195)$$

This Hamiltonian is known as the “Hubbard model,” and has been extensively studied in the context of condensed-matter physics.

11.8.2 The physics of the Bose-Hubbard model

By loading an Bose condensate into an optical lattice, one can create a physical implementation of the Bose-Hubbard model where the parameters U and t can be experimentally adjusted by changing the atomic scattering length or lattice depth respectively. As we shall see, changing the relative size of these parameters results in qualitative changes in the ground state of the system. To elucidate this transition, we will consider the two limiting cases: $t \gg U_0$ and $U_0 \gg t$.

The weak lattice: $t \gg U_0$

When the laser beams forming the optical lattice are weak, the condensate state is dominated by the hopping term in the Bose-Hubbard Hamiltonian,

$$\hat{H}_{\text{kin}} = -t \sum_{\langle ij \rangle} \hat{b}_i^\dagger \hat{b}_j, \quad (11.196)$$

and the effect of the interaction term is negligible. This kinetic part of the Hamiltonian can be easily diagonalized by defining annihilation operators in momentum space,

$$\hat{b}_{\mathbf{k}} = \frac{1}{\sqrt{N}} \sum_i e^{-i\mathbf{k} \cdot \mathbf{x}_i} \hat{b}_i \quad (11.197)$$

$$\hat{b}_i = \frac{1}{\sqrt{N}} \sum_{\mathbf{k}} e^{i\mathbf{k} \cdot \mathbf{x}_i} \hat{b}_{\mathbf{k}} \quad (11.198)$$

where N is the total number of sites in the lattice. For example, in one dimension the Hamiltonian would take the form

$$\hat{H}_{\text{kin}} = -\frac{t}{N} \sum_i \sum_{k,q} \hat{b}_k^\dagger \hat{b}_q e^{-ikx_i} (e^{iqx_{i-1}} + e^{iqx_{i+1}}) \quad (11.199)$$

$$= -2t \sum_k \hat{b}_k^\dagger \hat{b}_k \cos 2ka, \quad (11.200)$$

where a is the spacing between lattice sites. The ground state of the Hamiltonian is clearly obtained by putting all of the atoms into the $k = 0$ state:

$$|\psi_0\rangle = \frac{1}{\sqrt{N!}} \left(\hat{b}_{k=0}^\dagger \right)^N |\text{vac}\rangle \quad (11.201)$$

$$= \frac{1}{\sqrt{N!}} \left(\frac{1}{\sqrt{N}} \sum_i \hat{b}_i^\dagger \right)^N |\text{vac}\rangle. \quad (11.202)$$

As was the case for the double-well potential, the coherence between neighboring lattice sites is finite, and in the limit of large N the ground state approaches a coherent state. This state exhibits superfluidity because the atoms can freely tunnel between lattice sites. However, since the relative phase between lattice sites is well defined, the atom number fluctuates.

The strong lattice: $t \ll U_0$

In the opposite limit of a strong optical lattice, atomic hopping between lattice sites is very weak and the Hamiltonian is dominated by the interaction

term

$$\hat{H}_{\text{int}} = U_0 \sum_i \hat{n}_i (\hat{n}_i - 1). \quad (11.203)$$

When the lattice is perfectly occupied, i.e. N atoms occupy N lattice sites, the lowest energy eigenstate of the system must have one atom in each lattice site:

$$|\psi_0\rangle = \prod_i \hat{b}_i |\text{vac}\rangle \quad (11.204)$$

To lowest order in perturbation theory, the effect of hopping is an overall energy shift arising from virtual processes. This so-called “exchange energy” reduces the overall energy of each atom by $\Delta E = -t^2/U_0$, but does not affect the ground state of the system. This ground state is known as a “Mott insulator” because there is no movement of atoms around the lattice; they are frozen in place. Unlike the $k = 0$ ground state in the weak lattice, the number of particles in each lattice site is well defined, so the phase between them is not.

The Mott insulator to superfluid transition

The ground state of the strong lattice, the Mott insulator, is qualitatively different from the ground state of the weak lattice, the superfluid. By changing the parameter t/U_0 , it is possible to move between these two limits, effecting a phase transition of the system. This phase transition can happen even at $T = 0$ because the state change is driven by quantum (rather than thermal) fluctuations, so it is known as a “quantum phase transition.”

In order to analyze this phase transition, we will make a number of assumptions. First, we will assume that we are working with a homogeneous system, thus disregarding the effect of a harmonic confining potential. Second, we will assume “commensurate” filling

$$\nu = \frac{N_{\text{atoms}}}{N_{\text{sites}}} = 1. \quad (11.205)$$

Note that with incommensurate filling $\nu \neq$ integer, strictly speaking there is no phase transition, since the extra atoms or holes will delocalize to minimize their kinetic energy. Finally, we will use a mean-field approach in which we assume that the state vector is factorizable into a product of lattice site

states, each with an integer number of atoms:

$$\begin{aligned}
|\psi_0\rangle &= \prod_i |\phi\rangle_i \\
&= \prod_i \left(\sum_{n=0}^{\infty} c_n \frac{(\hat{b}_i^\dagger)^n}{\sqrt{n!}} \right) |\text{vac}\rangle \\
&= \prod_i \left(\sum_{n=0}^{\infty} c_n |n_i\rangle \right).
\end{aligned} \tag{11.206}$$

This assumption is not quite valid, since the superfluid ground state is not quite a product of coherent states, but it will provide a useful qualitative description of the phase transition.

With this ansatz wavefunction, we can identify two limits: in the Mott insulator state, each site is singly occupied

$$|\phi\rangle_i^{(\text{MI})} = |1\rangle_i, \tag{11.207}$$

whereas in the superfluid limit, each site occupation corresponds to a coherent state

$$|\phi\rangle_i^{(\text{SF})} = e^{-1/2} \sum_n \frac{1}{\sqrt{n!}} |n\rangle_i, \tag{11.208}$$

with mean occupancy $|\alpha|^2 = 1$. This state, $|\phi\rangle_i^{(\text{SF})}$ corresponds to the Gross-Pitaevskii wavefunction, which approaches a superfluid state in the large-N limit, similar to the situation with the double-well system. To understand where the phase transition between superfluid and Mott insulator occurs, we can examine the energies for the two limiting wavefunctions and see which is lower in energy. In this simple model, the superfluid state has an energy

$$E_{\text{SF}} = -t \cdot z \cdot 2 + U_0, \tag{11.209}$$

where z is the number of nearest neighbors, whereas the Mott insulator state has an energy

$$E_{\text{MI}} = -\frac{t^2}{U_0}. \tag{11.210}$$

From this simple analysis, we would predict a phase transition to occur when

$$t \cdot z \cdot 2 \sim U_0. \tag{11.211}$$

Although this model captures the qualitative features of the phase transition, it underestimates the critical ratio $U_0/(t \cdot z)$. A more careful analysis takes a variational wavefunction which includes both limits as well as a transition between them, for example

$$|\text{phi}\rangle_i = \frac{\sin \theta}{\sqrt{2}} |0\rangle_i + \cos \theta |1\rangle_i + \frac{\sin \theta}{\sqrt{2}} |2\rangle_i. \quad (11.212)$$

This trial wavefunction works well near the phase transition, and gives

$$t \cdot z \cdot 5 \sim U_0 \quad (11.213)$$

as the condition for $\theta = 0$ to be the ground state, which compares well to the exact value of $U_0/(t \cdot z) = 5.8$. For $\nu > 1$, the criticality condition scales as $U_0 \sim t\nu$, since tunnelling is enhanced when several particles are in a single site.

We have seen how the ground state of the system changes as we cross from a superfluid to Mott insulator state. In addition, the excitations of the system are qualitatively different on either side of the quantum phase transition. In the superfluid state, the system exhibits a Bogoliubov spectrum of excitations; in the Mott insulator state, the excitation spectrum is gapped because it costs an energy $\Delta\epsilon \sim U_0 - t$ to delocalize a single particle. The vanishing excitation gap is one distinguishing feature of the quantum phase transition.

In real experiments, our assumption of commensurate filling requires re-examination. Since there is an overall harmonic trapping potential holding the atoms in the optical lattice, the center of the trap should hold a higher density of atoms than the outer edges. In fact, what happens is that in the Mott insulator phase the density takes on a "wedding-cake" structure, with filling factors ν increasing in steps towards the center of the trap, see Fig. 11.14.

A series of experiments have observed the superfluid to Mott insulator transition by observing the interference or lack thereof between atoms in different sites of the lattice potential. The superfluid phase has first order coherence, so as the atoms expand they interfere, producing an interference pattern which shows the reciprocal lattice of their periodic trapping potential. The Mott insulator phase, however, has no first order coherence, so no periodic pattern is visible in the expansion image. By increasing and then decreasing U_0/t , experiments have shown that one can reversibly ramp into and out of the Mott insulator phase, as shown in Fig. 11.15.

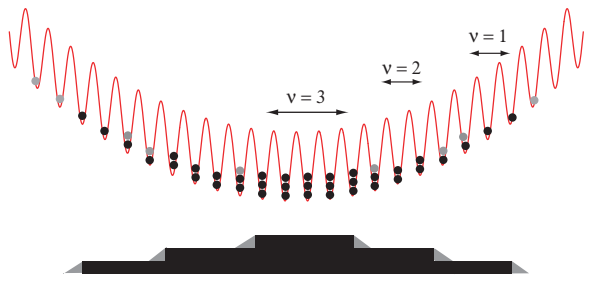


Figure 11.14: Experimental realizations of an optical lattice potential always include an additional harmonic confining potential. In a strongly-interacting system, Mott insulator phases with different filling factor ν occur in different portions of the lattice, with a small region of superfluid (non-integer ν) phase between them.

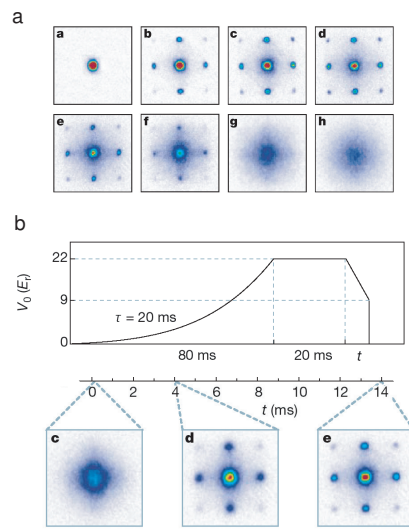


Figure 11.15: Experimental observation of the superfluid to Mott insulator transition [taken from Nature 415, 39 without permission]. (a) Expansion images for different values of t/U_0 , with the lattice potential ranging from $0E_r$ (a) to $20E_r$ (g). The superfluid phase is associated with the reciprocal lattice pattern forming in the expansion image, while the Mott insulator phase shows no first order coherence. (b) Demonstration that the Mott insulator transition is reversible. The lattice depth is ramped well into the Mott insulator phase and then decreased over a time t . For slow ramp times t , the superfluid phase is regained.